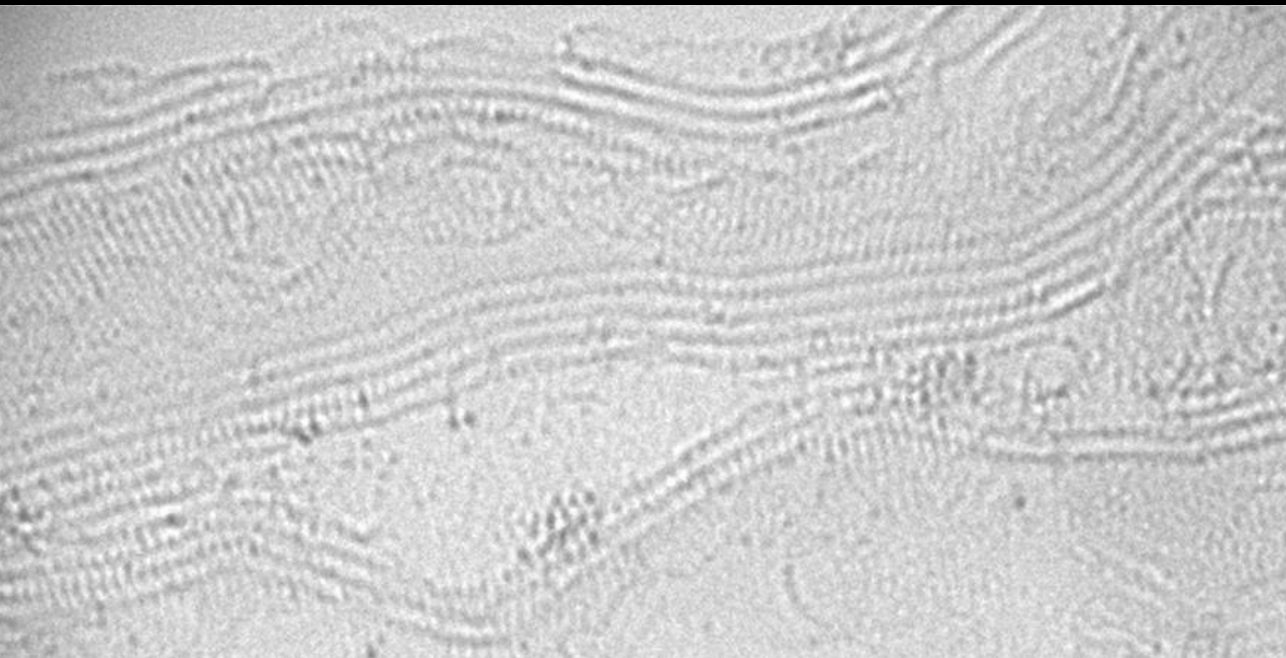


**SYNTHESIS AND CHARACTERISATION
OF GOLD NANOCCLUSERS
FOR CATALYSIS APPLICATIONS**



Maria Leonor Rodrigues Alves

UNIVERSITAT AUTÒNOMA DE BARCELONA
DEPARTAMENT DE FÍSICA

**SYNTHESIS AND CHARACTERISATION
OF GOLD NANOCCLUSERS
FOR CATALYSIS APPLICATIONS**

PhD Thesis

Maria Leonor Rodrigues Alves

Directors:

Dr. Ernest Mendoza Gómez

Dr. Jordi Llorca Piqué

Tutor:

Dr. Jordi Pascual Gainza

Barcelona, 2014

UNIVERSITAT AUTÒNOMA DE BARCELONA
DEPARTAMENT DE FÍSICA

**SYNTHESIS AND CHARACTERISATION
OF GOLD NANOCCLUSERS
FOR CATALYSIS APPLICATIONS**

Thesis submitted by
Maria Leonor Rodrigues Alves
for the degree of Doctor in Materials Science

Barcelona, 2014

Maria Leonor Rodrigues Alves

Barcelona, Març 2014

El Dr. Ernest Mendoza Gómez, Professor Agregat del Departament de Física i Enginyeria Nuclear de la Universitat Politècnica de Catalunya, el Dr. Jordi Llorca Piqué, Professor Agregat de l'Institut de Tècniques Energètiques de la Universitat Politècnica de Catalunya, i el Dr. Jordi Pascual Gainza, Catedràtic del Departament de Física de la Universitat Autònoma de Barcelona.

CERTIFIQUEN:

La present tesis titulada: **“Synthesis and characterisation of gold nanoclusters for catalysis applications”** presentada per Maria Leonor Rodrigues Alves per optar al grau de Doctora en Ciència de Materials per la Universitat Autònoma de Barcelona ha estat realitzada sota la seva direcció en el Centre de Recerca en Nanoenginyeria de la Universitat Politècnica de Catalunya, i trobant-se concloua, autoritzen la seva presentació perquè sigui avaluada pel tribunal corresponent.

Dr. Ernest Mendoza Gómez
(Director)

Dr. Jordi Llorca Piqué
(Director)

Dr. Jordi Pascual Gainza
(Tutor)

To my mother, father,
brothers and sister.

ACKNOWLEDGEMENTS

Firstly, I would like to thank Ernest Mendoza for many reasons. For always supporting me from the beginning and for always being available and believing in my work over the past four years. I am grateful for his enthusiasm, imparting knowledge in different fields, advice on how to improve my work and for having always closely followed my PhD research. I thank him for his kindness and humanity.

Then, I thank Jordi Llorca, who contributed a lot since the second year of my PhD. I also thank him for his kindness and humanity, sharing his knowledge in different fields, for always being available and following the work closely.

I thank Marta Santiago, for all her help, teaching, sharing of ideas and her kindness.

I thank Belén Ballesteros for having taught me during the first year how to operate an HRTEM microscope; for all her patience, kindness, good teaching and help.

I thank César Fernández, for all the help in the first year.

I thank Trifon Trifonov, for all the help and for teaching me how to operate the SEM microscope.

I thank Zaira Blazquez, Edurne Galindo, Nahikari Zuasti, Meritxell Molmeneu, Montserrat Domínguez, Alvaro Mayoral and Gemma Guilera, for their contributions to this thesis.

I thank Lucília Salbany, for the help improving the language of this thesis.

I thank *Fundação para a Ciência e a Tecnologia*, for the SFRH/BD/75925/2011 fellowship assigned to me.

I thank Carlos, Sérgio, Arnau, Sunny, Neus and Jesús, for making my integration during my first year in Barcelona so much easier.

I thank Núria, Cristian, Elena, Edu, Albert, Vanessa, Reinhold, David and César, for the time and moments that we shared every day at work.

I thank Kasia, Magda, Pablito, Joa, Miriam, Sara, Fer, Francisco, Majo, Juan, Rox, Sebastián, Anita and Marcelo, for the good moments that we had during the time we were together in Barcelona.

I thank Catarina, Cátia, Joana and João, for the friendship which we have maintained for nine years and for the mutual support even when we were living in three different continents and five different cities.

I thank Filipe, Clara, Nuno and Susana, for the good moments that we always share each time we get together in Portugal. For the contact that we keep, the care and for being such good listeners.

I thank David for always having the right words.

I thank Maria, for being such a good example of courage and determination.

I thank Raúl, Esteban, Felipe and Robert, for their support, friendship, help and mutual trust.

I thank Diana and Rosa, for their support, care and for always being there to listen whenever I needed.

I thank Ana, my sister, for having so much patience with me, for her help in improving my work and for always taking care of me.

I thank Pedro, my brother, for the care, help and support, never judging me.

I thank Zé, my brother, for the care.

I thank my father, for the education and values that he has instilled in me during all these years. For the help in everything that I needed wherever I would be.

I thank my mother, especially, because she is the one who suffered the most with my absence over the last four years. Thank you for being so kind, a good educator and for always supporting me. Because in the end, family is the only thing that is always present to defend and support you during the difficult moments.

NOMENCLATURE AND ABBREVIATIONS

SYNTHESISED CATALYSTS NOMENCLATURE

Au(xwt%)/support	Catalyst of Au synthesised in-situ with a x wt% nominal gold content
ncAu(xwt%)/support	Catalyst of Au synthesised ex-situ with a x wt% nominal gold content

ABBREVIATIONS

AFM	Atomic Force Microscopy
BE	Binding Energy
BET	Brunauer-Emmett-Teller
CB	Carbon Black
CN	Coordination Number
CNTs	Carbon Nanotubes
Co-P	Co-Precipitation
d	Metal particle diameter
DI	Distilled water
DOM	Dimensionally Ordered Macroporous
DP	Deposition-Precipitation
EXAFS	Extended X-ray Absorption Fine Structure
fcc	face-centered cubic
FT	Fourier Transform
HRTEM	High Resolution Transmission Electron Microscopy
ICP-OES	Inductively Coupled Plasma-Optical Emission Spectroscopy

MWCNTs	Multiwalled Carbon Nanotubes
NPs	Nanoparticles
SEM	Scanning Electron Microscopy
STEM	Scanning Transmission Electron Microscopy
SWCNTs	Singlewalled Carbon Nanotubes
T	Temperature
TEM	Transmission Electron Microscopy
TG	Thermogravimetric
TGA	Thermogravimetric Analysis
TPO	Temperature Programmed Oxidation
T₅₀	Temperature at which 50% of the carbon material is converted
T_i	Initial temperature of combustion of the carbon material
T_m	Temperature of the maximum combustion rate of the carbon material
T_s	Temperature of the inflection point of the TG curve of the carbon material
XANES	X-ray Absorption Near Edge Structure
XAS	X-ray Absorption Spectroscopy

INDEX

SUMMARY.....	1
CHAPTER 1:.....	5
INTRODUCTION.....	5
1.1 CATALYSIS BY GOLD.....	7
1.2 THE IMPORTANCE OF SMALL GOLD NANOPARTICLES (GOLD CLUSTERS).....	8
1.2.1 GOLD NANOPARTICLES STRUCTURAL AND ELECTRONIC PROPERTIES DEPENDENCE ON THEIR SIZE.....	10
1.2.2 METAL-SUPPORT INTERACTIONS.....	13
1.3 SYNTHESIS OF SUPPORTED Au NANOPARTICLES/NANOCLUSTERS..	16
1.3.1 IMPREGNATION.....	18
1.3.2 CO-PRECIPITATION.....	20
1.3.3 DEPOSITION-PRECIPITATION.....	21
1.3.4 ANION ADSORPTION.....	23
1.3.5 COLLOIDAL GOLD.....	23
1.3.6 SONOCHEMICAL SYNTHESIS.....	25
1.3.7 OTHER METHODS.....	28
1.4 HETEROGENEOUS CATALYSIS WITH GOLD ATOMS (SYNTHESIS OF ISOLATED GOLD ATOMS).....	29
1.5 CATALYSTS SUPPORTS.....	31
1.6 GOLD CATALYSTS' PRACTICAL APLICATIONS.....	35
1.6.1 CO OXIDATION.....	35
1.6.2 CATALYTIC OXIDATION OF CARBONACEOUS MATERIALS.....	41
1.8 OBJECTIVES.....	57
1.9 REFERENCES.....	59
CHAPTER 2:.....	71
CHARACTERISATION TECHNIQUES AND METHODS.....	71
2.1 TRANSMISSION ELECTRON MICROSCOPY (TEM).....	73

2.2	SCANNING ELECTRON MICROSCOPY (SEM).....	76
2.3	ATOMIC FORCE MICROSCOPY (AFM).....	77
2.4	X-RAY PHOTOELECTRON SPECTROSCOPY (XPS)	79
2.5	X-RAY ABSORPTION SPECTROSCOPY (XAS).....	80
2.7	THERMOGRAVIMETRIC MEASUREMENTS (TGA).....	82
2.8	SURFACE AREA MEASUREMENTS	83
2.9	INDUCTIVELY COUPLED PLASMA-OPTICAL EMISSION SPECTROSCOPY (ICP-OES).....	85
2.10	REACTION SYSTEMS.....	86
2.10.1	SONOCHEMICAL SYNTHESIS OF Au NANOCCLUSERS.....	86
2.10.2	CO OXIDATION.....	88
2.10.3	CARBONACEOUS MATERIALS OXIDATION	90
2.11	REFERENCES.....	92
CHAPTER 3:.....		93
IN-SITU SYNTHESIS OF GOLD CLUSTERS AND CATALYTIC ACTIVITY STUDY .		93
3.1	SYNTHETIC PROTOCOL.....	95
3.2	ICP-OES CHEMICAL ANALYSES.....	103
3.3	Au CLUSTERS SIZE DISTRIBUTION DEPENDENCE PARAMETERS.....	104
3.3.1	NOMINAL GOLD CONTENT	104
3.3.2	SUPPORT SURFACE AREA.....	107
3.3.3	STABILITY	123
3.3.4	SYNTHESIS TEMPERATURE.....	126
3.4	ATOMIC RESOLUTION OF Au/MWCNTs CATALYSTS	128
3.4.1	ABERRATION-CORRECTED HRTEM.....	128
3.4.2	XAS	139
3.5	X-RAY PHOTOELECTRON SPECTROSCOPY	141
3.6	CATALYTIC ACTIVITY	146
3.6.1	Au/MWCNTs CATALYSTS	146
3.6.2	Au/CeO ₂ CATALYSTS.....	147
3.7	CONCLUSIONS.....	154
3.8	REFERENCES.....	156

CHAPTER 4:.....	159
EX-SITU SYNTHESIS OF GOLD NANOCCLUSERS AND CATALYTIC ACTIVITY STUDY	159
4.1 SYNTHETIC PROTOCOL – Au NANOCCLUSERS.....	161
4.2 RCO_2^- /Au MOLAR RATIO INFLUENCE IN THE Au PARTICLE SIZE ...	163
4.3 SYNTHESIS OF SUPPORTED Au NANOCCLUSERS CATALYSTS	169
4.3.1 HIGH RESOLUTION TRANSMISSION ELECTRON MICROSCOPY.	170
4.3.2 X-RAY PHOTOELECTRON SPECTROSCOPY	172
4.4 CATALYTIC ACTIVITY	175
4.5 CONCLUSIONS.....	185
4.6 REFERENCES.....	187
 CHAPTER 5:.....	 189
OXIDATION OF CARBONACEOUS MATERIALS	189
5.1 CATALYSTS SYNTHESIS	191
5.2 CATALYTIC ACTIVITY	195
5.2.1 COMBUSTION TEMPERATURE OF Au DECORATED MWNCTs (in- situ).....	197
5.2.2 COMBUSTION TEMPERATURE OF Au DECORATED CARBON BLACK (ex-situ)	208
5.2.3 SOOT OXIDATION	212
5.3 CONCLUSIONS.....	222
5.4 REFERENCES.....	225
 CHAPTER 6:.....	 227
GENERAL CONCLUSIONS.....	227
 ANNEXES.....	 233
A.1 DETERMINATION OF THE NOMINAL NUMBER OF Au CLUSTERS PER MWNCT	235
A.2 IN-SITU CATALYSTS ACTIVITY: CO OXIDATION – EXPERIMENTAL PROTOCOL	237

A.3	EX-SITU CATALYSTS ACTIVITY: CO OXIDATION – EXPERIMENTAL PROTOCOL	242
A.4	REFERENCES	246

SUMMARY

This doctoral thesis is about the synthesis and the catalytic activity study of gold particles with a diameter lower than 2 nm, gold nanoclusters. The interest is due to the catalytic activity that gold has at room temperature when its size is less than approximately 5 nm.

In this thesis, two distinct synthesis' methods that allow stable gold clusters with a well defined particle size to be obtained have been developed. In one method, gold clusters with a narrow size distribution and a particle diameter less than 2 nm are firstly synthesised and then deposited on a support. In the other method, gold clusters are directly synthesised on the selected support. In the latter method, the size of gold can be easily varied by simply altering the gold precursor quantity during the synthesis process. Thus, uniformly dispersed isolated gold atoms, 2 nm Au clusters or nanoparticles larger than 10 nm can be obtained on the material support surface.

The synthesised catalysts were characterised using distinct physico-chemical techniques: HRTEM, SEM, AFM, XPS and XAS. Additionally, their catalytic activity was investigated for the oxidation of CO and carbonaceous materials. Finally, the particle size was related with the catalytic activity of the material.

This thesis is organised in 6 chapters. It starts, in Chapter 1, with an introduction to gold catalysis, including the description of various developed gold catalysts synthetic protocols. This chapter also emphasises the importance of the gold clusters and its structural and electronic properties that confer them an exceptional activity, thus the importance of the metal-support interaction on the catalysts activity. It refers also to the interest and the actual state in the study of the activity and synthesis of Au atoms. Finally, the catalysts supports used and the catalytic reactions studied in this work are also described in

detail. The last section of this chapter summarises the objectives of this PhD thesis.

In Chapter 2, a brief description of the mode of operation of the characterisation techniques used in this work can be found. The equipments used to perform the analyses, the operating conditions and the properties determined with each technique are also presented. In addition, the reaction systems used for the catalytic activity tests are also described in this chapter.

In Chapter 3 a synthetic protocol (in-situ) that allows obtaining gold clusters ($d < 2$ nm) or even isolated gold atoms supported on different surfaces (MWCNTs, TiO_2 and CeO_2) covered with amine groups is presented. In this method gold is directly reduced on the different support surfaces. An intensive characterisation of the factors that might influence the gold nanoparticle size such as gold content, support surface area and synthesis temperature is presented. Finally, the results obtained for the catalytic activity of Au/ CeO_2 catalysts in the CO oxidation reaction are presented. Its activity is compared with the one obtained by other authors using Au/ CeO_2 catalysts synthesised by deposition-precipitation and co-precipitation protocols. Calcination observations of a Au/MWCNTs catalyst are discussed leading to the experiments carried out in Chapter 5.

Chapter 4 focuses on the presentation of an alternative synthetic protocol of gold clusters. In this ex-situ synthetic protocol gold nanoclusters ($d < 2$ nm) were firstly synthesised and then supported on the referred support surfaces covered by amine groups. A discussion about how the RCO_2^-/Au ratio influences the Au nanocluster size is presented. Finally, the catalytic activity of these catalysts for the CO oxidation reaction is presented. A discussion about the differences observed in the catalytic activity of the catalysts obtained by both synthetic protocols is carried out. The activity of these catalysts is also

compared with the activity of the commonly synthesised by deposition-precipitation and co-precipitation Au/CeO₂ catalysts.

The activity and selectivity of the synthesised gold catalysts (in-situ and ex-situ synthetic protocols) for the oxidation of carbonaceous materials such as MWCNTs and carbon black is presented in Chapter 5. The effect of the Au content/Au particle size on the catalytic activity is discussed. The ability of in-situ Au/CeO₂ catalysts to decrease the oxidation temperature of soot is also investigated.

Finally, the general conclusions of this PhD thesis are presented in Chapter 6.

CHAPTER 1:

INTRODUCTION

1.1 CATALYSIS BY GOLD

Gold has been considered for many years as chemically inert and it was often regarded to be poorly active as a catalyst. Nevertheless, in the late 1980s, Haruta *et al.* discovered that specifically supported gold particles (those with a mean diameter smaller than 5 nm) show unique catalytic properties at the low temperature CO oxidation^[1-3]. Further studies also showed a high activity of these catalysts in several other reactions, such as the selective oxidation of propene to propene oxide, the water gas-shift reaction, the NO reduction and the selective hydrogenation of acetylene or butadiene^[2]. Since then, catalysis with gold has gained a huge interest and, as consequence, the publications in this field, essentially in heterogeneous gold catalysis, have grown significantly (Figure 1).

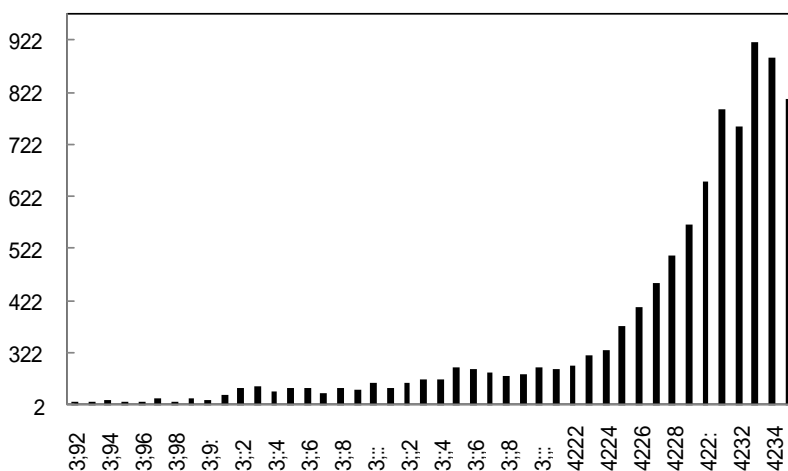


Figure 1. Number of publications on gold catalysis per year from 1970 until 2013. Data extracted from ISI web of knowledge. Search: gold cat* (title)^[4].

Moreover, in the catalysis field, gold presents several advantages over other typical catalytic metals. Indeed, when compared with platinum which is extensively used in catalysis, important advantages can be named. Au catalysts are able to convert CO at a much lower temperature than Pt catalysts and, since

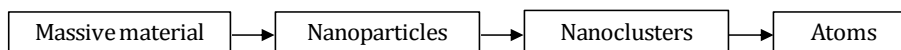
it is more resistant to poisoning in the presence of CO it is not deactivated as easily^[5].

The low temperature CO oxidation reaction has a particular importance on finding applications in indoor air quality control and as a guard bed catalyst to prevent CO poisoning of proton exchange membrane fuel cells^[2]. Further study revealed that, indeed, the catalytic performance of gold in the CO oxidation reaction strongly depends on the gold nanoparticle size. In addition, finding how the support might also affect the catalytic activity is also a target of study and interest, as well as the interaction between gold and the support or the gold nanoparticle's structure. Thus, the need for understanding and explaining this exceptional catalytic activity is responsible for a significant increase noticed in the research on this subject. Nevertheless, much more investigation is still required in order to clarify several key questions about gold catalysis, particularly heterogeneous gold catalysis.

Finally, it is important to state that gold nanoparticles (Au/Fe₂O₃ on a zeolite wash-coated honeycomb) first commercial application took place in 1992. Gold containing systems were used to reduce the odours in toilets in Japan^[6].

1.2 THE IMPORTANCE OF SMALL GOLD NANOPARTICLES (GOLD CLUSTERS)

The properties of a metal vary significantly with its size. These are separated in three groups: nanoparticles (NPs, from around 2 nm up to 100 nm, i.e. more than around 200 atoms), nanoclusters (less than 2 nm, i.e., less than approximately 200 atoms) and finally isolated atoms^[7].



A nanoparticle is defined as any metal particle whose diameter is in the nanoscale. These particles are usually structurally composed by a metal nucleus surrounded with a shell of disordered atoms.

The interest in nanoclusters resides in the fact that these species fill the “gap” between atomic and nanoparticle behaviour in metals. A subnanometric or atomic cluster is characterised by its size which is comparable to the Fermi wavelength of an electron (~ 0.52 nm for Au). It consists in a group of atoms with a well defined composition and one or very few stable geometric structures. Due to their reduced size they present quantum effects which are responsible for the appearance of new chemical, optical or electronic properties such as the magnetism, photoluminescence or catalytic activity (Section 1.2.1)^[2].

In this thesis, Au particles with a diameter larger than 2 nm are named as nanoparticles (NPs). When the diameter of Au is lower than 2 nm the term cluster or nanocluster is used.

When the gold nanoparticle size is decreased to around 1 nm – 1.5 nm an unexpected activity is observed^[8]. This activity, among other factors, results from the number of atoms at the surface of gold available. The degree of dispersion can be calculated considering the particles, as spheres, all of the same size^[9, 10]. Notice, however, that this approximation is not valid for very small gold clusters once that the approximation to a sphere is no longer valid. In this case, it is interesting to investigate the relation between the coordination number of surface atoms and the size of particles with a specific shape^[9, 11]. Both models mentioned have been intensively used in order to try to understand the dependence of the catalytic activity on the particle size^[9-11]. Nevertheless, these models are applied to particles that have exactly the required number of electrons to complete the outer layer and, therefore, are a rough approximation.

In this context, in order to understand the origin of the previously described unexpected activity of the gold clusters, it is essential to investigate how their physical properties vary with their size. Moreover, it is also important to distinguish between unsupported and supported gold clusters, since the metal-support interactions will also affect the catalyst activity^[5].

1.2.1 GOLD NANOPARTICLES STRUCTURAL AND ELECTRONIC PROPERTIES DEPENDENCE ON THEIR SIZE

Bulk gold ($d > 100$ nm) is known as a shiny yellow inert noble metal. Decreasing its size metallic reddish inert nanoparticles ($d > 2$ nm) are obtained. Decreasing even more the size, fluorescent and active in catalysis gold clusters ($d < 2$ nm) are obtained. One of the factors responsible for the development of these new properties is the appearance of a band gap between the conduction and valence bands inexistent for bulk gold (Figure 2).

The atomic orbitals of an atom, depending on the extent of overlap in a solid, might remain practically unchanged as in noble gases or they might combine to form continuous bands, as in metals or semiconductors^[12]. Each atom contributes with its atomic orbitals to a band whose density increases, slightly, when more atoms are added to the structure. These bands are characterised by the density of states (DOS). Thus, for the massive material, the DOS is continuous. Nevertheless, when reducing significantly the number of atoms of a particle, this continuous band is gradually replaced by discrete energy levels. Furthermore, the quasi-molecular behaviour of the clusters is also evidenced by the fact that, unlike nanoparticles, very small clusters are characterised by delocalised molecular orbitals instead of bands and that the bandgap is large enough to remember the highest occupied molecular orbital-lowest unoccupied molecular orbital (HOMO-LUMO) molecular gap^[12, 13]. Figure 2 shows how the band gap and the DOS vary with the number of atoms of a particle.

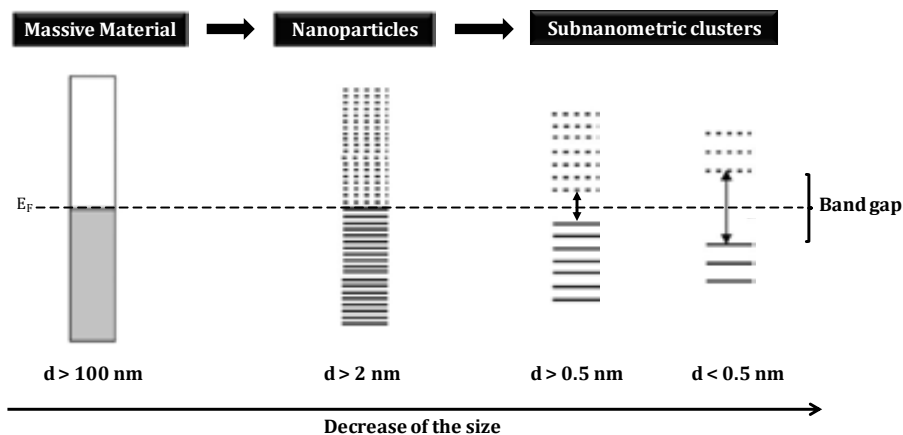


Figure 2. Evolution of the band gap and the DOS with the number of atoms of a particle from the massive material to clusters^[12, 14]. E_F : Fermi level.

The exceptional catalytic activity of small Au nanoparticles ($d < 5 \text{ nm}$) is also related to its structure. Bulk gold is known to have a face centered cubic (fcc) structure. Several studies about how the synthesis method and the support nature influence the structure of the gold nanoparticles have been made, mainly using TiO_2 as support, but also with some weak interacting surfaces. For example, by X-ray diffraction, both fcc cubo-octahedra and icosahedra structures were observed for the $\text{Au}/\text{Mg}(\text{OH})_2$ catalyst^[15, 16]. Nevertheless, due to the weak interaction between Au and the support, the icosahedra sinters quickly and originates a truncated dodecahedra structure.

Many theoretical calculations to predict the structure of these nanoparticles have been made^[17-20]. However, a clear agreement between calculations and the experimental data has not been fully accomplished. Depending on the number of atoms, different structures are attributed to each cluster (Figure 3). For example, perfect icosahedral structure is attributed to clusters with a certain special numbers of atoms (“magic numbers”) such as 13, 55, 147, 309, 561 and 923^[17]. Other stable configurations, as Marks decahedra, are assigned to clusters with 75, 77, 101 and 146 atoms^[21]. Also, clusters with a number of atoms between 35 and 500 are more stable in a truncated octahedral than in icosahedra or cuboctahedra configurations^[17].

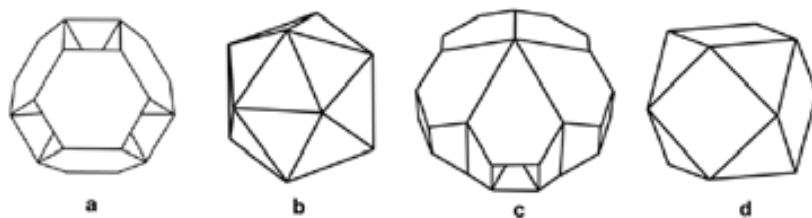


Figure 3. Schematic representation of a truncated octahedron (a), icosahedrons (b), Marks decahedron (c) and cuboctahedron (d) configurations^[17].

Importantly, different configurations of clusters imply different coordination numbers for Au. For example, the average coordination number of the Au₁₃ cluster (smallest cluster of the icosahedral theoretical sequence) with an ideal cuboctahedral morphology would be 5.5^[17]. Nevertheless, if the atoms are in an ideal icosahedron configuration this number is 6.5^[17].

It is essential to clarify the relation existent between the structure and coordination number of the Au nanoparticles since the activity of the catalyst is directly dependent of the Au coordination number (CN)^[22]. It has been found that low-coordinated Au atoms lead to a higher catalytic activity^[22]. Smaller nanoparticles have a larger number of low-coordinated Au atoms which among other properties consequently contributes to a higher activity. These are located in the edges and essentially in the corners of the nanoparticle (Figure 4) and, therefore, configurations that allow a high concentration of these active sites are preferable^[22]. Indeed, it has been proposed that the existence of a higher number of low-coordinated Au atoms, will lead to the easier formation of Au-CO bonds which will consequently increase the catalyst activity and allow the CO oxidation at room temperature^[22, 23].

Figure 4 shows that the number of surface atoms is very slightly varied for nanoparticles between 2 nm and 10 nm. Nevertheless, for nanoparticles with a diameter below 4 nm, a significant increase of the atoms in the corners is observed. Combining this result with the fact that experimentally a higher activity for the CO oxidation has been observed when smaller gold nanoparticles are used, it is possible to conclude that the existence of

low-coordinated Au atoms located in the corners of the nanoparticles is of major importance.

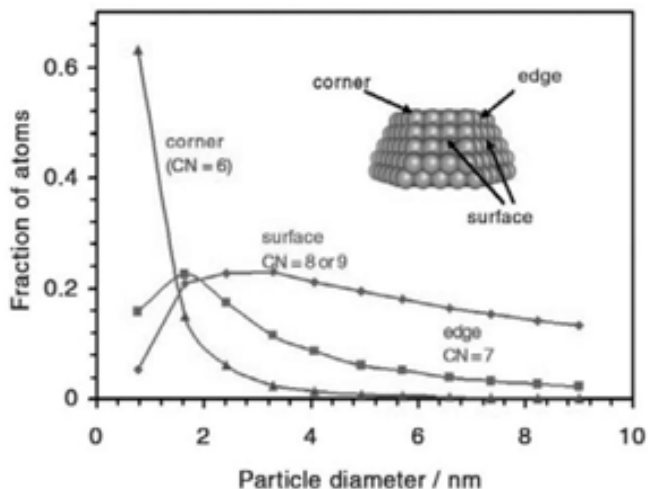


Figure 4. Representation of the calculated fractions of Au atoms in the corners, edges and crystal faces in uniform nanoparticles with a top half truncated octahedron structure^[22].

Additionally, the demonstration that the chemisorption strength increases with the decrease of the coordination number was experimentally presented^[22]. Hvolbæk *et al.* showed, that the CO desorption temperature increases with the decrease of the coordination number indicating therefore a stronger chemisorption of the CO molecules, by Temperature Programme Desorption (TPD)^[22].

1.2.2 METAL-SUPPORT INTERACTIONS

The activity of Au nanoparticles does not result from a single parameter but it is a result of a combination of different effects. It is very difficult to distinguish between the physical effects that are strictly dependent on particle size from metal-support interaction. Indeed, the smaller the particle, the higher the

number of atoms in direct contact with the support will be and, simultaneously, the fraction of low-coordinated surface atoms also increases.

The interaction between the metal and the support can also be responsible for a higher catalytic activity in the way that the stability and structure of the metal nanoparticles are totally dependent on the support surface and determined by the number of metal atoms that are in direct contact with the support. The contribution of this interaction will be greater as the particle size decreases for particles with similar shape. The nanoparticle shape can be determined with the contact angle defined by Equation (1). γ_{ms} , γ_{mg} , γ_{gs} are the interfacial energies of the interfaces, metal-support, metal-gas and gas-support respectively^[23].

$$\cos \theta = \frac{\gamma_{gs} - \gamma_{ms}}{\gamma_{mg}} \quad (1)$$

For high γ_{ms} energy, the metal wets the oxide surface and particles will have a hemispherical or truncated cubo-octahedral structure. In the same way, a lower value of this variable implies a lower contact area between the metal and the support, which will present a sphere structure (Figure 5).

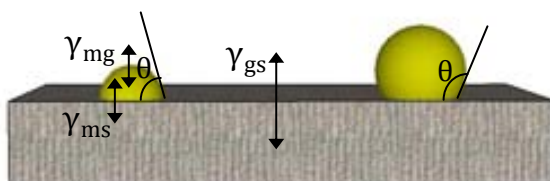


Figure 5. Schematic representation of different gold-support interactions^[24].

The importance of the Au small size in order to have a better contact between the Au particle and the support surface has been investigated by HRTEM characterisation. For example, the shape of Au on TiO₂ anatase supported catalysts obtained by deposition-precipitation has been characterised. In one hand, for smaller gold clusters ($d < 2$ nm) a contact angle lower than 90° has been observed. On the other hand, for Au nanoparticles with a diameter higher

than 5 nm a contact angle higher than 90° has been noticed. Thus an undesired decrease of the fraction of the gold atoms in direct contact with the support surface is obtained for Au nanoparticles larger than 5 nm^[29].

Furthermore, the importance of the metal-support interaction has been experimentally investigated using Au-Cu/TiO₂ catalysts^[25]. Different interactions between the metal nanoparticle and the support have been clearly observed. The authors showed how the calcination temperature affects the structure of the Au-Cu alloy nanoparticles. They noticed a strong metal-support interaction when the catalyst was calcined at 400 °C (Figure 6). Since the Au particle size was approximately maintained, this larger contact (higher number of active sites at the perimeter of the contact area between the alloy nanoparticles and TiO₂) led to an increase of the catalytic activity. Further increase of the calcination temperature led to an undesirable increase of the metal alloy particle size and to the decoration of the alloy nanoparticles with oxidised Cu species resulting in a decrease of the catalytic activity despite the strong particle-support interaction (Figure 7).

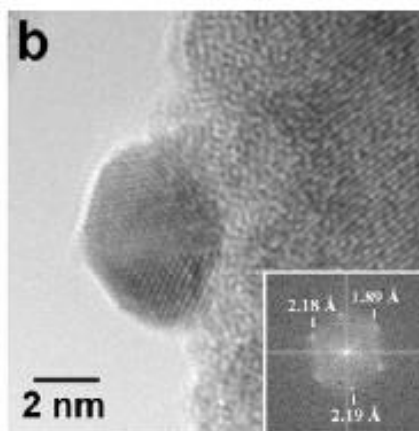


Figure 6. HRTEM and Fourier Transform (FT) image of a Au₁Cu₃/TiO₂ calcined at 400 °C^[25].

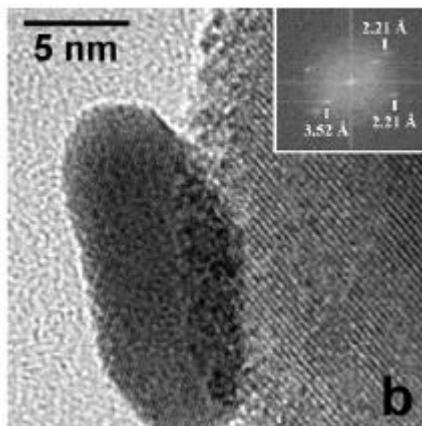


Figure 7. HRTEM and FT image of a $\text{Au}_1\text{Cu}_3/\text{TiO}_2$ catalyst calcined at 600 °C^[25].

1.3 SYNTHESIS OF SUPPORTED Au NANOPARTICLES/NANOCLUSTERS

Supported Au nanoparticles (NPs) catalysts can be obtained essentially by two approaches: *ex-situ* and *in-situ*^[26]. In the first one, the nanoparticles are pre-synthesised and then attached to the chemical modified support (*ex-situ*). The linkage between the pre-synthesised gold nanoparticles and the support can be done through covalent bonds or noncovalent interactions. Covalent bonding consists of attaching the gold nanoparticles to organic linkers or biomolecules connected to the support surface. In this way, the amount of nanoparticles that can be deposited on the support depends on the number of functionalities available on the surface^[26]. The noncovalent interaction consists in attaching the pre-synthesised nanoparticles to the support surface covered by polyelectrolytes (polymer wrapping), i.e. positive or negative charged support surfaces. The support is then decorated with NPs of the opposite charge by electrostatic interactions. In the second approach, gold nanoparticles are directly synthesised onto the support surface (*in-situ*). In this approach the support acts as template and stabiliser for the formation of the NPs. The main

advantage of this approach is avoiding the use of protective shells on the NPs that are very often used in the ex-situ approach for the stabilisation of the nanoparticles and their linkage to the support. Indeed, this shell might be responsible for an undesirable decrease of the catalyst activity by covering the metal active sites^[26].

The deposition of Au nanoparticles on different supports has been widely reported^[27-29]. Studies showed that, when the selected surface is functionalised with polymers with amine groups, the deposition of Au nanoparticles is observed^[8, 30-32]. Indeed, in 2010 our group patented a synthetic protocol to obtain subnanometric Au nanoparticles ($d < 3$ nm) on surfaces covered by amine groups^[33]. Later, in 2011, Lollmahomed *et al.* also observed the successful deposition of Au nanoparticles on the surface of polymer-functionalised SWCNTs^[31]. In this work the effective deposition of Au nanoparticles on the SWCNTs surface covered with different quantities of amine groups was discussed. Amine groups act as nucleation sites for well dispersed deposition of Au nanoparticles. Amine groups are able to stabilise Au nanoparticles by the formation of N-Au bonds (6 kcal/mol)^[34]. Therefore, a minimal amount of amine groups was required to obtain a uniform dispersion of Au nanoparticles. When amine groups quantity was lower than the critical a lower uniformity of the Au nanoparticles deposition was observed. The authors then concluded that amine groups allow a uniform deposition of Au nanoparticles and to stabilise them on the support.

Throughout the years gold catalysts have been prepared by several methods, which can be distinguished by the type of gold precursor used (chloride or chloride free gold precursors). Since, in this work, chloroauric acid (HAuCl_4) is used as gold precursor, in the description, presented in Section 1.3.1 to 1.3.6, chloride free gold precursors' synthesis' methodologies are excluded.

1.3.1 IMPREGNATION

This method was the first used to prepare supported gold catalysts. It is the simplest and it can be used with any type of support. The solution of the metal precursor is put in contact with the support and then it is aged, dried and calcined (Figure 8). This method can be named as “incipient wetness” impregnation or “wet” impregnation when the precursor solution volume does not exceed the pore volume of the support or is in excess, respectively.

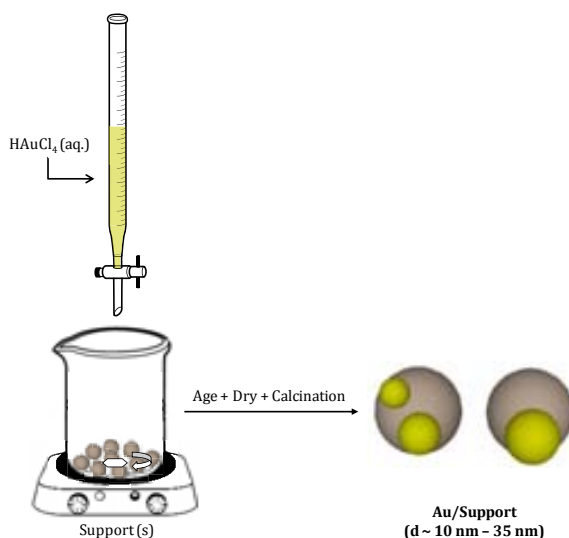


Figure 8. Schematic representation of the impregnation synthetic protocol. Au clusters/NPs: ●.

The precursors that have been used were essentially chloroauric acid (HAuCl_4) and gold chloride (AuCl_3). The first catalysts prepared were supported on silica (SiO_2), alumina (Al_2O_3) and magnesia (MgO), but, later, other oxides supports, as titania (TiO_2) and iron oxide (Fe_2O_3), were also applied^[35-37]. It has been observed that impregnation with HAuCl_4 led to low activity catalysts due to the formation of large gold nanoparticles (10-35 nm), even for low gold contents as 1 wt% or 2 wt%^[38]. The formation of large gold nanoparticles resulted from the presence of the chloride ion promoting agglomeration during the thermal treatment^[38]. This problem can be overcome by removing the chloride ion, by

reduction with H_2 , in the form of HCl ^[39]. Moreover, it has been observed that the pH also affects the activity of these catalysts. $Au/\gamma-Al_2O_3$ catalysts were prepared by aging the $HAuCl_4$ solution in the pH range of 5 to 11^[40]. It has been observed that, during this step, several species resulted from the $AuCl_4^-$ hydrolysis which influenced the Au particle size. This method has been then improved by using a new procedure using Au/Al_2O_3 catalysts^[41].

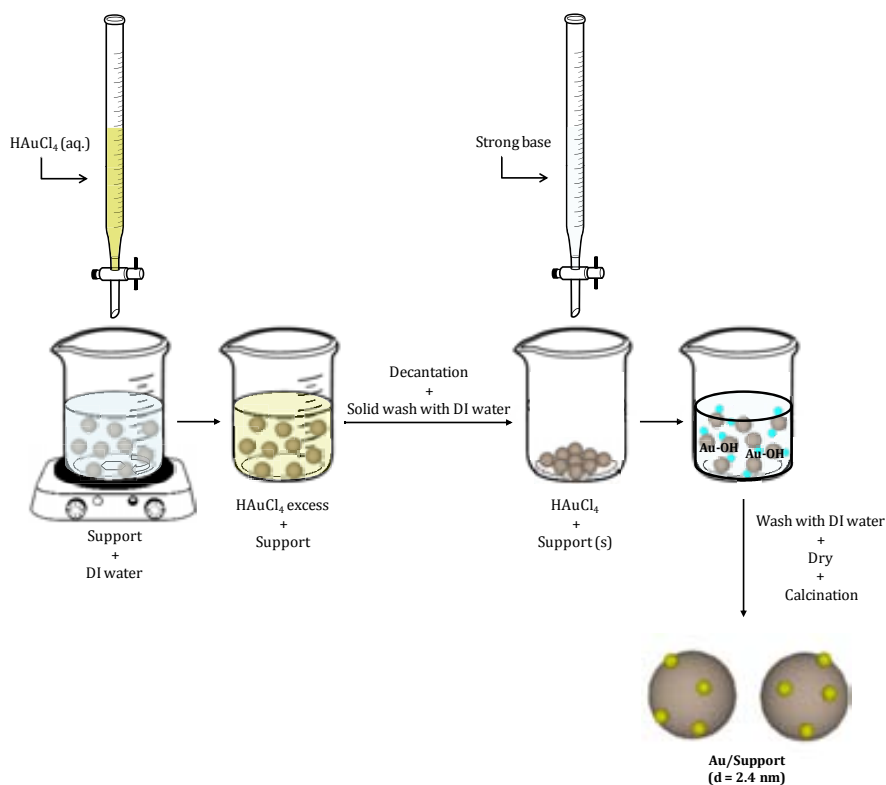


Figure 9. Schematic representation of the improved impregnation synthetic protocol.
Au clusters: ●; Cl^- : ●.

In a first step, the gold precursor is put in contact with the support which is in distilled water (Figure 9). Then, after removing the excess of gold precursor by washing with water, the solid is treated with a strong base (e.g. $NH_3.H_2O$). This treatment leads to the $AuCl_4^-$ hydrolysis, being thus the remaining chloride anions released and the Au is converted into the hydroxide form (Figure 9). The

released Cl^- is removed then by washing yielding an adsorbed Au complex that is easily decomposed at low temperature. With this improvement, it has been observed that after drying and calcination at $400\text{ }^\circ\text{C}$ a catalyst with gold nanoparticles with a mean diameter of 2.4 nm was obtained^[41].

1.3.2 CO-PRECIPITATION

The first small Au nanoparticles supported on several oxides, as $\alpha\text{-Fe}_2\text{O}_3$, NiO and Co_3O_4 , were obtained, in 1987, using this method^[1, 42].

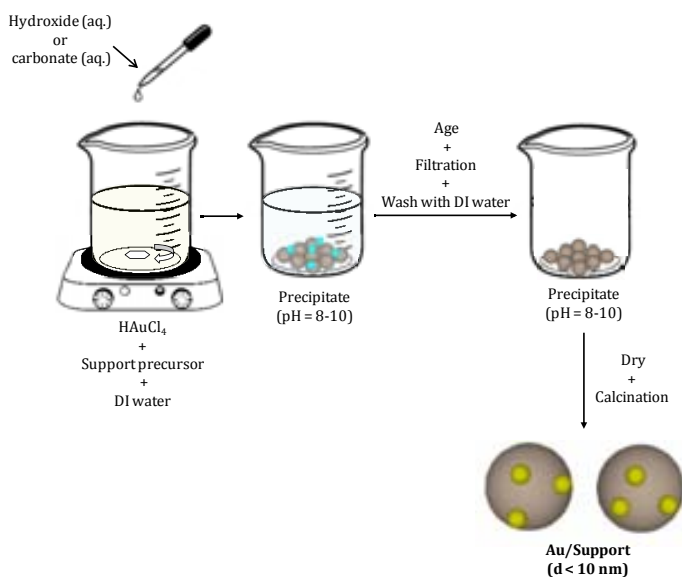


Figure 10. Schematic representation of the co-precipitation synthetic protocol. Au clusters/NPs: ●; Cl^- : ●.

This is a simple method that consists in first dissolving the support and the gold precursors in distilled water (Figure 10). Then, by adding an hydroxide (e.g.: NaOH) or a carbonate (e.g.: $(\text{NH}_4)_2\text{CO}_3$), a precipitate is produced after some time. Usually, the pH is adjusted in the range of $8-10$. This precipitate is left to age for a couple of hours and is then filtered and washed, usually with distilled water, to remove chloride ions. The filtered precipitate is then dried and

calcined, if desired^[43]. This method leads to a high gold dispersion with Au particles usually smaller than 10 nm (Table 1).

The main drawback of this method lies in the fact that it can only be applied for certain metal oxides, due to the rates of precipitation of the two hydroxides (Au and the metal of the support) and to the fact that the gold particle size is determined by their affinity. Table 1 shows the diameter of Au particles obtained by this method on different oxide supports.

Table 1. Au/oxide catalysts synthesised by co-precipitation^[44].

Oxide Support	[Au] (wt%)	T _{calcination} (°C)	d (nm)
MgO	2	200	< 2
TiO ₂	5	600	5
Fe ₂ O ₃	5	400	4
CO ₃ O ₄	5	400	6
NiO	10	400	8
ZnO	5	400	5
Al ₂ O ₃	5	400	5
In ₂ O ₃	5	400	5
SnO ₂	5	400	3
SiO ₂	5	300	20
Cr ₂ O ₃	5	400	>30
CdO	5	22	21

1.3.3 DEPOSITION-PRECIPITATION

This method has been used to synthesise oxide supported gold catalysts with a small particle size (< 5 nm). By this method, the metal hydroxide precipitates on the oxide support^[45]. Briefly, the support is dissolved in distilled water (DI) and the pH is adjusted to 9-10 by adding sodium hydroxide (e.g.: NaOH) or carbonate (e.g.: Na₂CO₃) (Figure 11). Then, an aqueous solution of HAuCl₄ is

added to the support suspension. Next, the precipitate is further aged with stirring for one hour at around 80 °C. Finally, after filtration a wash with water is performed, in order to remove the sodium and the chlorine. The resulting product is dried under vacuum at 100 °C and, usually, calcined in air at a higher temperature (Figure 11)^[46].

This method is versatile once that it can be performed in a huge range of pH solutions and temperatures, during the several steps, as well as it can be carried out using other bases such as ammonia (NH₃) and urea^[24, 47].

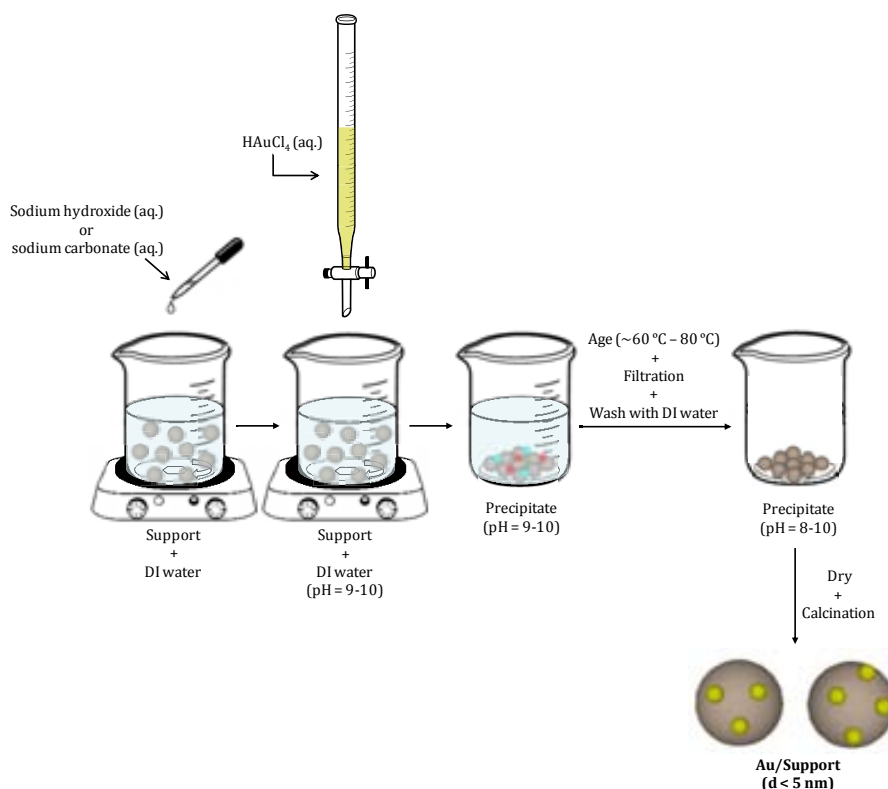


Figure 11. Schematic representation of the deposition-precipitation synthetic protocol. Au clusters/NPs: ●; Cl⁻: ●; Na⁺: ●.

1.3.4 ANION ADSORPTION

Anion adsorption is possible, once the gold precursor, HAuCl_4 , in aqueous solution, dissociates into anionic complexes providing that the pH of the solution is lower than the point of zero charge (PZC) of the support. This method was studied for the synthesis of Au/TiO_2 at a fixed pH ($\text{pH} = 2$) using several conditions of temperature and time^[48]. At 20 °C and 80 °C, the main species in solution are $\text{AuCl}_3(\text{OH})^-$ and AuCl_4^- which can interact electrostatically with the TiO_2 surface (PZC ~ 6) (Figure 12). Gold nanoparticles with a diameter between 4 nm and 6 nm have been obtained. Nevertheless, by this method, a complete gold deposition has not been observed. A maximum of 1.5 wt% of reduced Au has been obtained on the TiO_2 surface, which corresponds to about 20% of the gold in solution^[24].

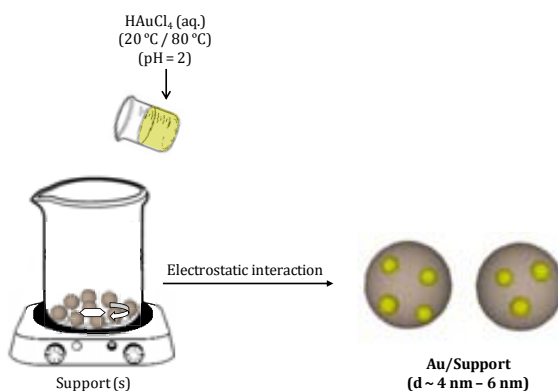


Figure 12. Schematic representation of the anion adsorption synthetic protocol.

Au NPs: •.

1.3.5 COLLOIDAL GOLD

Since the first works in the 1950s the colloidal route for preparing gold catalyst has been intensively investigated^[49-51]. The biggest advantage of this synthetic method is that tuning the size distribution can be achieved by simply varying the conditions of preparation. Generally, this method consists in the reduction of the gold precursor by a reducing agent (usually sodium citrate) at around

100 °C (Figure 13). When the gold precursor aqueous solution starts to boil sodium citrate is added and after approximately 15 minutes the liquid is cooled to room temperature. The whole procedure is carried out under stirring (Figure 13).

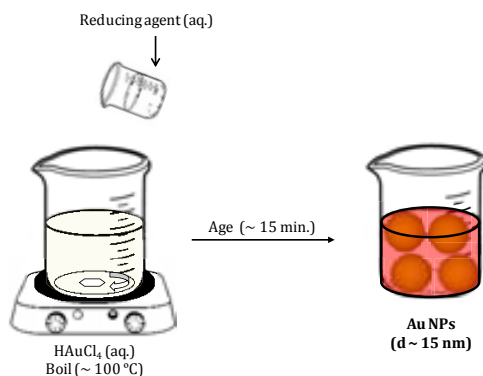


Figure 13. Schematic representation of the colloidal gold synthetic protocol.

The chemical citrate route to synthesise Au nanoparticles reduction protocol was first presented by Turkevich *et al.* in 1951^[50]. In the first works, particles around 20 nm were obtained using sodium citrate to reduce the $AuCl_4^-$ ion. An advantage of this method resides in the fact that it is an inexpensive and non-toxic method which uses water as solvent. In this first work, Turkevich concluded that the gold particle size varies with the amount of gold and the synthesis temperature. The gold nanoparticle size was augmented with the increase of both variables. Moreover, the effect of sodium citrate concentration on the gold nanoparticle size has also been investigated^[50]. Turkevich concluded that a decrease of the sodium citrate quantity led to an increase of the gold mean particle size. This results from the fact that this agent also acts as stabiliser of the gold nanoparticles. In this way, an excess of this agent will lead to a stronger stabilisation. Nevertheless, an adapted quantity of this reducing agent must be used in order to stabilise the metal particles (a higher quantity is preferable) but to avoid the complete cover of the Au nanoparticles catalytic active sites (a lower quantity is preferable).

The citrates reduction method generally leads to the formation of large gold nanoparticles with a diameter between 10 nm and 20 nm. In this way, this is not the most adequate method to produce active gold catalysts, for example, for CO oxidation, that requires sizes lower than approximately 5 nm^[52]. Nevertheless, recently, according to Li *et al.*, the colloidal gold particle size can be lowered to around 2 nm - 8 nm after the addition of the appropriate amount of NaOH, i.e. with the increase of the pH solution^[53]. Additionally, several other reducing agents, as sodium thiocyanate, poly(ethylene-imine), tetrakis[hydroxymethyl] phosphonium chloride ([HOCH₂)₄P]⁺Cl⁻) and sodium borohydride (NaBH₄) were also used decreasing the particle size to around 1 nm – 3 nm^[24]. In some cases, stabilising agents were often used although they are not indispensable. The most commonly used are polyvinylalcohol (PVA), polyvinylpyrrolidone (PVP), polydiallyldimethylammonium chloride (PDDA) and cetyltrimethylammonium bromide (CTAB).

1.3.6 SONOCHEMICAL SYNTHESIS

Another approach developed to synthesise metal nanoparticles or nanoclusters is the environmental friendly sonochemical procedure. The sonochemical synthesis of noble metal nanoparticles have been intensively studied in recent years^[54-56]. This method consists in an unusual route of which main advantages are that it does not require high temperatures, high pressures or long reaction times. The chemical and physical effects of ultrasound do not result from a direct interaction between the chemical species and the sound waves. It is a product of acoustic cavitation which is a physical phenomenon that consists in the formation, growth, and implosive collapse of bubbles^[57-59]. From this phenomenon results the production of high temperature and high pressure in the collapsing cavities which leads to the decomposition of water molecules into hydrogen (H[•]) and hydroxyl (OH[•]) radicals. This clean ultrasound methodology has been therefore seen as an interesting possibility to prepare nanoparticles or nanoclusters of noble metals, usually silver and gold.

The sonochemical preparation of gold nanoparticles ($d > 2$ nm) has been widely studied^[60-64]. In 2003, gold nanocrystals with a mean diameter of approximately 3 nm were obtained by ultrasonication using ascorbic acid as reducer of the gold precursor ($\text{KAu}(\text{CN})_2$)^[65]. In addition, gold nanoparticles with a mean diameter of 5.2 nm were ultrasonically synthesised using mesoporous silica as support to increase the nanoparticles stability^[61].

The synthesis of metal nanoclusters, usually silver and gold nanoclusters, has been carried out by different template-based methods^[66-68]. The majority of these methods used polymers as stabilisers of the nanoclusters.

For example, gold nanoclusters have been successfully synthesised using a hydroxylterminated ethylenediamine core – poly(amidoamine) (PAMAM) dendrimer (G4OH) – as template. By this procedure stable dendrimer-encapsulated gold nanoclusters are formed. The gold ions are sequestered into the dendrimer and then reduced. Gold sequestration results from the coordination between the gold ions and the tertiary amines of the dendrimer molecules^[69].

Moreover, gold nanoclusters with a diameter below 2 nm were prepared using a high molecular weight polymer – pentaerythritol tetrakis (3-mercaptopropionate)-terminated polymethacrylic acid (PTMP-pMAA) – as capping agent to control the growth of the gold nanoparticles. The method consisted firstly in mixing the gold precursor (HAuCl_4) with the polymer and, then the reduction of gold was achieved by adding to this mixture a NaBH_4 aqueous solution. Finally, the unreacted polymer was removed by preparative-scale size exclusion chromatography^[70].

Very little has been studied in relation to what concerns the sonochemical synthesis of gold nanoclusters ($d < 2$ nm). The first one-step sonochemical synthesis of Au nanoclusters was claimed by Liu *et al.* in 2011^[71]. In this method bovine serum albumin (BSA) was used to reduce the gold precursor (HAuCl_4) and Au nanoclusters with a diameter around 1.8 nm were obtained. Moreover, in 2012, the synthesis of gold nanoclusters prepared under

ultrasound irradiation using toluene as the solvent where the powder gold precursor (AuCl_3) was dissolved was presented^[66]. The method simply consisted of mixing under vigorous stirring the powder and the solvent which was then subjected to ultrasound irradiation. By AFM it has been observed that the larger Au nanoclusters formed (180 minutes) had a maximum height of 1.6 nm. Figure 14 shows a schematic diagram of the Au clusters sonochemical synthesis procedure.

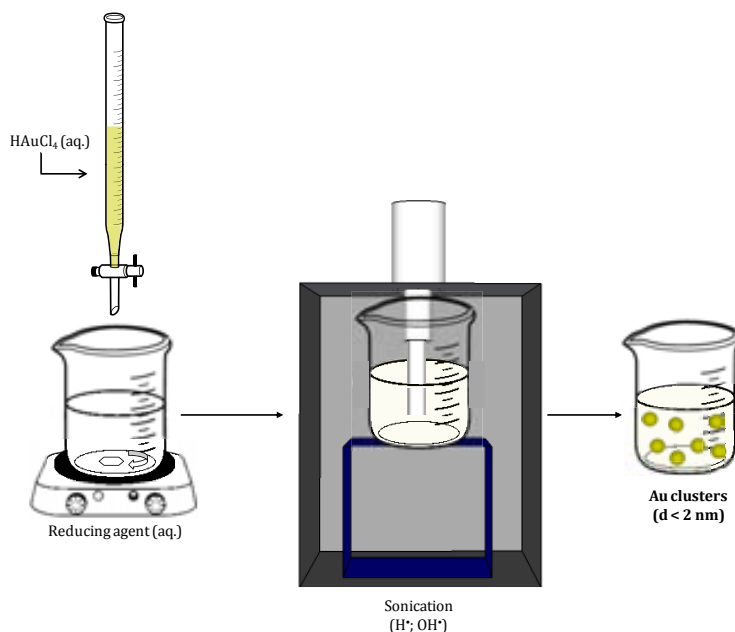
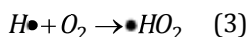
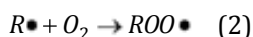


Figure 14. Schematic representation of the sonochemical synthesis synthetic protocol.

Moreover, by using gold nanoclusters synthesised using PTMP-pMAA it has been observed that the nanocluster particle size is affected by the polymer/metal ratio^[70]. On the one hand, when using a very low concentration of polymer, by ultraviolet-visible (UV-Vis) a weak plasmon band at 520 nm, which usually corresponds to nanoparticles ($d > 2$ nm), was observed. On the other hand, when using a higher polymer concentration, this plasmon band was no longer observed, what indicates the existence of only nanoclusters in solution.

Another factor that affects the metal particle size is the type of atmosphere in which the sonication is carried out. It is preferable to perform sonication under an argon (Ar) atmosphere instead of air due to the formation rate of gold nanoparticles. In air the formation rate of the metal nanoparticles will be significantly lower when compared with that under argon atmosphere^[61]. A decrease of this rate is undesirable once that would lead to the formation of larger nanoparticles. This difference can be explained by the smaller cavitation effect in air due to the fact that ratio (C_p/C_v) of air (1.40) is smaller than the one of argon (1.67). C_p and C_v are the constant pressure-specific heat and constant volume-specific heat of a medium respectively. It has been proposed that the oxygen from air inhibits the reduction of gold ions by scavenging reducing radicals ($R\bullet$) (Equation 2) and hydrogen ($H\bullet$) atoms (Equations 3)^[61].



1.3.7 OTHER METHODS

In addition to these synthetic protocols, physical routes have been also proposed to achieve the synthesis of metal clusters. These include, for example, the implantation of ions of Au on substrates or the evaporation of Au atoms on surfaces^[72, 73]. Nevertheless, these methods are expensive and complicated and therefore very difficult to scale-up. Thus the development of an alternative simpler economical process that allows obtaining a uniform dispersion of Au clusters represents an advantage over both physical methods and those that lead to the formation of inactive large Au NPs.

1.4 HETEROGENEOUS CATALYSIS WITH GOLD ATOMS (SYNTHESIS OF ISOLATED GOLD ATOMS)

Gold catalytic activity is extremely dependent on the gold particle size. Smaller particle catalysts are active but their efficiency on a per metal atom basis is very low since only the surface low coordinated active site atoms are used. Thus, downsizing the clusters to single atoms is highly desirable to increase the atom efficiency in catalytic reactions. However, obtaining stable isolated metal atoms on a surface is a challenge essentially because of their high mobility which might cause sinter under reaction conditions.

In 2011 the first Pt single-atom catalyst was synthesised by Qiao *et al.* and consists of only isolated single Pt atoms on FeOx^[74]. This catalyst was synthesised by a co-precipitation method. The authors also observed that this single Pt atoms catalyst had a very high activity for CO oxidation^[74]. The activity of this new catalyst was found to be almost the triple that of a catalyst containing isolated Pt atoms, two-dimensional Pt rafts with less than 10 atoms and three-dimensional Pt clusters ($d < 1\text{nm}$) for CO oxidation reaction. The activity obtained has been related by density functional theory calculations to the partially unoccupied $5d$ orbitals of the positively charged, high-valent Pt atoms. These will reduce the CO adsorption energy and the activation barriers for the CO oxidation^[74].

Since these first observations, the interest in the atomic catalysis field has grown significantly. The synthesis of catalysts with only single metal atoms has been achieved by other methods. Sun *et al.* using the Atomic Layer Deposition technique obtained a single atoms Pt/graphene catalyst^[75]. A 10 times higher catalytic activity for the methanol oxidation reaction has been observed for the single atom Pt/graphene catalyst when compared to the commercial Pt/C catalyst. Experimental X-ray Absorption Fine Structure (XAFS) data revealed that the partially unoccupied $5d$ orbitals of the Pt atoms are responsible for the increased activity observed as it was previously stated by Qiao *et al.*^[74]. The

synthesis of other metal isolated atoms catalysts was also achieved for example using Pd^[76, 77].

Regarding gold, using subnanometric Au clusters several studies were carried out and revealed its exceptional activity when compared to gold nanoparticles^[78-81]. Nevertheless, since it is difficult to synthesise a uniform catalyst with a unique population of single gold atoms, the study of the activity of these species has not been well investigated yet and the activity of single Au atoms is still unclear. It is claimed that the chemical reactivity of positively charged single Pt atoms is different from that of isolated Au atoms or cations^[74]. Generally, the results obtained until now indicate that single Au atoms are not active for CO oxidation. Lee *et al.* observed that isolate gold atoms (Au_n, n=1) were inactive for the CO oxidation and that gold clusters with a very low number of atoms (Au_n, n<3) are less active than clusters with a higher number of Au atoms (Au_n, n=6-7)^[82]. In addition, the same group observed that the catalysts prepared by Au₁^{δ+} or Au₂^{δ+} on TiO₂ are much less active than TiO₂. They claim that these gold species poison vacancy sites^[83]. In the same way, Herzing *et al.* observed that it was the 0.5 nm bilayer Au cluster rather than the 0.2-0.3 nm monolayer Au clusters or isolated Au atoms that was active for CO oxidation using FeOx as support^[84].

The synthesis of single Au atoms is therefore a challenge and a field of interest. Thus, the activity of these species in reactions with different mechanisms can be investigated. Recently, for the first time, the synthesis of isolated gold atoms on a support in the absence of clusters or nanoparticles was reported^[85, 86]. In 2009, Uzun *et al.* achieved for the first time the synthesis of a unique population of single gold atoms on a high area support (MgO)^[85]. Later in 2012, Lu *et al.* presented a catalyst composed only by isolated gold atoms supported on a crystalline zeolite support (NaY)^[86].

The discovery of single-atoms metal catalysts is very promising; not only due to the higher reactivities observed but also because it allows the reduction of the high cost of commercial noble-metal catalysts in industry.

1.5 CATALYSTS SUPPORTS

The interest of using supported catalysts resides in the fact that; in this way a higher dispersion of the active phase will be achieved. Importantly, the catalyst support can increase the catalytic activity due to their specific properties and the metal-support interaction (Section 1.2.2).

Different materials have been used as support where the metal clusters can be anchored. Usually, inorganic oxides such as for example CeO_2 , TiO_2 , ZrO_2 , Fe_2O_3 and SiO_2 are preferable for high temperature reactions due to their high thermal stability. This characteristic is essential, for example, for catalysts used in high temperature environments such in vehicle exhausts. These inorganic oxides materials are also preferable for oxidation reactions such as CO oxidation due to their intrinsic characteristics. Indeed, CeO_2 is a commonly used support of Au clusters catalysts for CO oxidation. The enhanced catalytic properties of this material are related to its high oxygen store capacity. This results from the high mobility of the oxygen vacancies in the solid, thereby giving it the ability to release stored oxygen under reaction conditions' tests (the shift between the Ce(III) and Ce(IV) oxidation states leads to a high oxygen mobility in the ceria lattice) [87, 88]. The high oxygen mobility in the ceria lattice results from the size, dispersion and quantity of oxygen vacancy defects in the lattice[89]. For this reason, the structure of the synthesised ceria is very important.

The most common method to prepare active Au/ CeO_2 catalysts is deposition-precipitation (DP).

Furthermore, TiO_2 , besides being active for CO oxidation reaction, due to its oxygen storage capacity it is also widely used in photocatalysis. Indeed, TiO_2 is known as the most adequate semiconductor for the photocatalytic production of H_2 [90]. Generally, the photocatalytic reaction consists in producing electron-hole pairs (e^- — h^+) that can either recombine or react with adsorbed species. Thus, by exciting TiO_2 with photons of equal or higher energy than the band gap energy, these pairs are obtained.

The methods used to synthesise Au/TiO₂ catalysts involve deposition-precipitation, wet impregnation and anion and cation adsorption^[91]. The most widely used method to prepare Au/TiO₂ catalysts is deposition-precipitation^[92, 93]. Using this method, active catalysts with a mean particle diameter of 3.2±0.7 nm have been synthesised^[92]. These were found to be active for CO oxidation at low temperature (80 °C). Also, Haruta developed a method that allows very small Au nanoparticles (2 < d (nm) < 5) on TiO₂ to be obtained^[94, 95]. This was the deposition-precipitation method with NaOH. Nevertheless, low gold contents such as 3 wt% must be used in order to decrease the Au particle size. Other possible synthesis methods, such as anion adsorption or cation adsorption, were also investigated. On the one hand anion adsorption led to a larger mean particle size (~ 4 nm) with a gold content of 1.5 wt%^[27]. On the other hand cation adsorption led to a lower particle size (~ 2 nm) for a determined solution/support contact time (1 hour) and for gold loadings not higher than 2 wt%.

Overall, the deposition-precipitation with urea has been considered the most efficient method to prepare high loadings Au clusters supported on TiO₂ catalysts. The advantage of this protocol over the DP with NaOH is that all gold in solution is deposited on TiO₂ leading to the same lower mean particle diameter (~2 nm) but using a higher gold content. For example, when using a TiO₂ with a surface area of 45 m²/g the amount of gold deposited corresponded to the maximum gold loading (8 wt%) on TiO₂. In this case 2.7 nm Au nanoparticles were formed. Decreasing the gold content to 3 wt% 2.3 nm Au NPs were formed and with 2 wt% 2 nm particles were obtained^[27].

Finally, carbon supports such as multiwalled carbon nanotubes (MWCNTs) are also suitable to obtain stable Au clusters active catalysts. Since their discovery, in 1991, by Iijima, carbon nanotubes (CNTs) interest in several fields has been growing significantly^[96]. They can be found as multiwalled (MWCNTs) or singlewalled (SWCNTs). It is the carbon nanotubes exceptional chemical, thermal, optical, magnetic, mechanical and electronic properties that give them a wide range of applications. Indeed, these can be found, for example, in

electronic devices, including field-effect transistors, single electron transistors and rectifying diodes, as well as in energy storage such as hydrogen storage^[97]. Furthermore, nowadays, catalysis is also known as a potential field for carbon nanotubes' applications. Indeed, since the last decade, a significant increase in the number of publications and patents was noticed. CNTs are considered as an attractive alternative to the common supports, due to their unique properties, namely: high purity (self-poisoning elimination); exceptional mechanical properties; high electrical conductivity and thermal stability; easy accessibility of the active phase; inexistence of any microporosity (elimination of diffusion and interparticle mass transfer); specific metal-support interaction. Besides, CNTs, when compared to common supports, show a high ability of dispersion of the active phase due to their high surface area.

Until now, CNTs catalysts' activity has been tested essentially in important liquid hydrogenation, hydroformylation or gas phase (Fischer-Tropsch process, ammonia decomposition) reactions and for electrocatalysis (fuel-cell electrodes)^[98].

Over the years several approaches have been developed in order to obtain active Au/CNTs catalysts with diameters lower than 5 nm. Some of the protocols used to synthesise Au/CNTs catalysts are presented in Table 2.

Table 2. Au/CNTs catalysts synthetic protocols.

Author	Year	Catalyst	Method	Particle diameter (nm)
Choi <i>et al.</i> ^[99]	2002	Au/SWCNTs	Redox reaction between Au ³⁺ ions (from HAuCl ₄) and SWCNTs in ethanol/water mixture (1:1).	< 7 nm (~ 30 s) ~ 7 nm (3 minutes) ~ 16 nm (> 3 minutes)
Tzitzios <i>et al.</i> ^[100]	2006	Au/SWCNTs	Au nanoparticles coated with olylamine obtained by reduction of HAuCl ₄ using polyethylene glycol-200 as reducing agent in singlewalled carbon nanotubes-dimethylformamide (SWCNTs-DMF) solution.	~ 5 nm
Zanella <i>et al.</i> ^[101]	2005	Au/MWCNTs	Gold nanoparticles synthesised using citric acid deposited on the surface of functionalised with aliphatic bifunctional thiols MWCNTS. Au nanoparticles were attached to the terminal thiol groups through Au-S bond.	~1.7 nm (1,6-hexanedithiol) ~ 5.5 nm (aminothiols)
Hu <i>et al.</i> ^[102]	2006	Au/MWCNTs	Deposition of Au NPs on MWCNTs functionalised with polyethyleneimine (PEI). The polymer was also used as reducer of the Au nanoparticles.	~ 15 nm (400:1 molar ratio PEI:HauCl ₄) 28 ~ 158 nm (2:1 molar ratio PEI:HauCl ₄)
Ismaili <i>et al.</i> ^[103]	2011	Au/MWCNTs	Deposition of functionalised Au nanoparticles on MWCNTs by a photoinitiated carbene addition reaction	3.9±0.9 nm 1.8±0.3 nm

1.6 GOLD CATALYSTS' PRACTICAL APPLICATIONS

In recent years, gold has been regarded with much more interest due to its catalytic properties. As it was mentioned in the beginning of this chapter, Haruta and other authors discovered that supported gold nanoparticles with a determined particle size ($d < 5$ nm) showed an exceptional catalytic activity in several oxidation reactions, such as the CO oxidation, selective oxidation of propene to propene oxide, water gas shift, NO reduction, selective hydrogenation of acetylene or butadiene among others^[1, 2].

In this section, the interest of the reactions used in this work to evaluate the catalysts activity is described.

1.6.1 CO OXIDATION

Catalysts able to promote the oxidation of carbon monoxide to carbon dioxide are required and are of great importance. Direct applications related to air purification give it an extreme importance not only at the academic level but also for human safety. In these applications the catalytic activity at room temperature is required.

In environmental applications, such as automotive catalytic converters, the CO oxidation is carried out by impregnating the catalyst in a monolith. These are honeycomb structures with many small, parallel square channels (Figure 15). The flow gas introduced into the monolith channels contacts with the catalyst that is deposited on the channel walls. The major advantages of monoliths are their high surface area per unit of volume (compactness), the large open frontal area (low pressure drop) and the very good attrition resistance^[104]. Indeed, when compared to other catalyst structures such as pellets or foams a significantly lower pressure drop is observed for the same geometric surface area. This fact in environmental applications is very important once that large volumetric flow rates are usually used^[105].



Figure 15. Monolithic catalyst substrates^[104].

The first observations during the 1980s of the high catalytic activity of gold for CO oxidation at room temperature led to innumerable studies^[1, 106]. An effective catalyst must be active at room temperature, be thermally stable and have a long term stability under reaction conditions or storage. The most commonly used supports for the CO oxidation reaction are TiO₂ and CeO₂. These are usually selected due to their great ability to create oxygen vacancies close to the Au particles. These sites were proposed to be active centers for oxygen activation during the CO oxidation reaction^[88, 107].

In respect to the CO oxidation reaction mechanism different authors suggest different pathways. Innumerable studies report the use of Au/TiO₂ catalysts and several are in accordance with the Langmuir-Hinshelwood mechanism^[108-111]. According to this mechanism, oxygen molecules adsorb at the Au particles edge being the O-O bond stretched by the gold electron transfer initialised by the presence of Ti cations and oxygen vacancies at the interface.

Based in theoretical calculations and experimental observations, Haruta proposed a mechanism for the CO oxidation reaction (Equations 4 to 7)^[5]. Haruta suggested that CO adsorbs preferentially on the edges and corners of the Au nanoparticles and O₂ adsorbs preferentially on the metal-support perimeter interface (Figure 16). The adsorbed O₂ reacts with CO adsorbed in the Au surface at the perimeter interfaces^[42]. The rate determining step should be the reaction between the two adsorbed species (Equation 6)^[112]. From this mechanism it is concluded that both support and Au nanoparticles nature have a crucial effect on the catalyst activity.

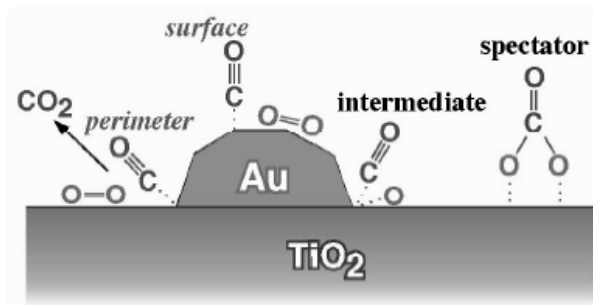
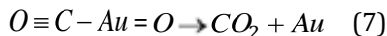
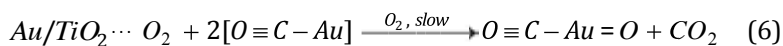
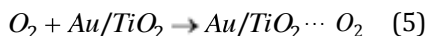
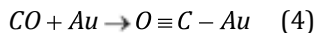


Figure 16. Schematic representation for the CO oxidation mechanism over a Au/TiO₂ catalyst^[5].

Nevertheless, the activity of the catalysts origin is still under investigation. It is believed that various parameters influence the catalytic activity. The Au particle size (higher number of low-coordinated Au atoms), the nature of the active Au species (metallic Au or positively charged Au), the influence of the support characteristic and its role in the reaction process, particularly in the activation of oxygen or the metal-support interaction, might influence significantly the catalysts' activity.

Au/CeO₂ is a kind of preferential catalyst for CO oxidation first reported by Gardner *et al.* in 1991^[113]. Indeed, Au/CeO₂ catalysts have been reported to be highly active for the CO oxidation reaction^[114-117]. The activity of these catalysts is highly dependent on the Au-CeO₂ interaction which depends on the Au particle size and the size/shape of the CeO₂^[114]. Nevertheless, the complete understanding of the origin of the activity of the Au/CeO₂ catalysts in the CO oxidation reaction is still under investigation. The role of metallic and cationic gold species in the catalyst's activity is still not clear. On the one hand it has been observed that Au^{δ+} species were directly related with the observed

activity in Au/CeO₂ catalysts^[118]. It has been shown that the interaction between cationic Au and CeO₂ is responsible for the high catalytic activity observed due to the consequent enhance of the ceria surface oxygen reducibility^[119]. On the other hand, the activity of these catalysts has been attributed to the interaction between the metallic Au with the defects on the ceria surface which leads to the formation of Au⁺-OH⁻ active species^[120]. According to Qian *et al.* Au^{δ+} species alone are not active for the CO oxidation^[121]. The authors claim that the metallic Au nanoparticles are more important for the efficient CO oxidation's reaction.

Some more important observations concerning the Au/CeO₂ catalysts activity in the CO oxidation reaction have been made. Carrettin *et al.* concluded that the structure of the CeO₂ highly influences the Au/CeO₂ catalytic activity^[115]. The authors showed that when Au was deposited on nanocrystalline particles of CeO₂ double the catalytic activity was observed when compared to Au/CeO₂ catalysts prepared by co-precipitation or to Au deposited on a regular CeO₂ support. In the same context the synthesis of Au/CeO₂ catalysts by different methods for the CO oxidation at room temperature has been carried out^[116]. CeO₂ with a large surface area (120 m²/g) was synthesised (crystallite size: 9-20 nm) by a hydrothermal method. Then, the Au was supported on this material in very low loads (0.44 wt% - 0.52 wt%) by different methods such as hydrothermal deposition-precipitation, hydrothermal precipitation, hydrothermal co-precipitation and by co-precipitation and deposition-precipitation. It has been observed that the Au/CeO₂ catalyst prepared by hydrothermal deposition-precipitation is the one that shows the higher catalytic activity (a complete conversion of CO was achieved around 20 °C). By ultraviolet-visible (UV-Vis) spectroscopy the authors observed that both Au clusters and nanoparticles coexist in this catalyst^[116]. The observed high catalytic activity was attributed to the catalyst larger surface area and the presence of both cationic (Au⁺ and Au³⁺) and metallic gold species, being the Au⁺ the dominant active species.

Furthermore, the influence of the Au particle size was also investigated by Tana *et al.*^[114]. The activity of Au/CeO₂ catalyts synthesised with a CeO₂ particle size of 12 nm and a Au particle size varied from 3.9 nm to 7.5 nm has been investigated. It has been observed that at 0 °C CO conversions of 63%, 30% and 12% were obtained when using Au/CeO₂ catalysts with a nanoparticle mean diameter of 3.9 nm, 5.4 nm and 7.5 nm respectively. These observations are in accordance with the fact that more low-coordinated Au sites exist in smaller particles (Section 1.2.1). The existence of more active sites on the Au-CeO₂ interface where the reaction occurs will lead to an efficient adsorption of CO and a faster surface reaction of CO with the oxygen species from CeO₂. In the same work the effect of metallic Au in the CO oxidation has also been investigated using the extremes in Au sizes (3.9 nm and 7.5 nm)^[114]. Metallic Au particles were removed by sodium cyanide leaching. A significant decrease of the catalytic activity was observed (CO conversion was only observed around 205 °C for both catalysts) which indicates that metallic Au is essential for the observed high catalytic activity in the Au/CeO₂ catalysts.

Finally, the effect of the pre-treatment atmosphere on the Au/CeO₂ catalytic activity has also been reported^[117]. It has been observed that none of the pre-treatments used (H₂, air, O₂, N₂, O₂ followed by 14 v/v% H₂ (balanced with N₂) and 14 v/v% H₂ (balanced with N₂) followed by O₂) affect the morphology and structure of the catalysts. The higher catalytic activity was obtained when the Au/CeO₂ catalyst was pre-treated with a oxidative atmosphere followed by a reductive atmosphere – O₂ followed by 14 v/v% H₂ (balanced with N₂). The different pre-treatments will lead to different ratios of cationic and metallic Au species on the CeO₂ surface (different Au^{δ+}/Au⁰ relations responsible for the activities observed are achieved). It has been claimed that an appropriate relation between cationic and metallic gold should exist in order to enhance the catalytic activity^[117]. The authors claimed that both species have a specific role in the reaction. While Au⁰ activates the O₂ molecule, the hydroxyl containing Au^{δ+} will facilitate the conversion of CO to CO₂. The untreated sample of this work only presents cationic gold. In this way, a Au^{δ+}/Au⁰ ratio approximately

closed to the ideal will be achieved by pre-treating the catalyst with O_2 followed by H_2 atmospheres leading thus to the higher catalytic activity observed.

Deposition-precipitation and co-precipitation synthesis methods are the most commonly used synthetic protocols to prepare highly active Au/CeO₂ catalysts for CO oxidation. When comparing some of these Au/CeO₂ deposition-precipitation and co-precipitation synthesised catalysts activities (Figure 17), it was firstly noticed that the catalysts prepared by the deposition-precipitation method (DP1^[122], DP2^[46], DP3^[46], DP4^[114]) are more active than the one prepared by co-precipitation (Co-P^[29]). The activity is represented in terms of reaction rate, i.e. mol of CO converted per second and square meter of Au.

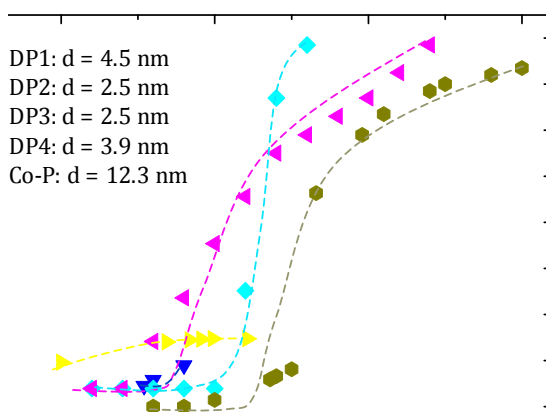


Figure 17. Comparison of the catalytic activity of the DP1 (---▼---), DP2 (---◆---), DP3 (---▲---), DP4 (---▶---) and Co-P (---●---) catalysts for the CO oxidation. The in-set indicates the Au nanoparticle diameter of each catalyst.

Furthermore, comparing the catalysts DP1, DP3 and DP4 which are composed by Au with a mean diameter of 4.5 nm, 2.5 nm and 3.9 nm respectively the effect of the Au particle size in the catalytic activity was noticed. Table 3 shows the reaction rate values obtained at the temperature of 40 °C using these catalysts. Larger particles led to a decrease of activity as it has been widely reported^[45, 114, 123].

Table 3. Activity of different sized DP synthesised Au/CeO₂ catalysts^[46, 114, 122].

Catalyst nomenclature	d (nm)	Reaction rate (mol.s ⁻¹ .m _{Au} ⁻²) T=40 °C
DP3	2.5	4.7x10 ⁻⁶
DP4	3.9	2.9x10 ⁻⁶ (a)
DP1	4.5	1.8x10 ⁻⁶

(a) T ~ 41.86 °C

So far, it could be concluded that small particle size Au clusters catalysts which have a high quantity of low coordinated Au atoms and a strong interaction with the support are those who lead to higher catalytic activities. Some synthetic protocols such as co-precipitation and deposition-precipitation are commonly used to prepare active CO oxidation Au/CeO₂ catalysts. Nevertheless, the methods that allow to obtain an uniform population of Au clusters ($d < 2$ nm) are still very few. For this reason, there is an ongoing search for new and alternative methods easily scaled-up that allow to obtain an uniform distribution of supported Au clusters active catalysts. Moreover, the development of a synthesis method that allows a unique population of single Au atoms to be obtained is also of great interest. The activity of these species is still unclear since very few authors have been able to synthesise single Au atoms.

1.6.2 CATALYTIC OXIDATION OF CARBONACEOUS MATERIALS

• SOOT OXIDATION

Diesel engines, among other pollutants, emit particulate matter such as soot that is harmful for the environment. In order to decrease these emissions catalytic filters are used in the exhaust pipe. Nonetheless, soot combustion occurs at a very high temperature (around 550 °C – 600 °C). This temperature is much higher than the typical operating temperature of an exhaust (approximately 200 °C – 400 °C)^[124]. For this reason, the development of catalysts able to decrease the soot combustion temperature down to the

temperature of gases in the exhaust pipe is required. A soot particle consists of a carbon core contaminated with metal compounds with different hydrocarbons and sulfates adsorbed on their surface. These particles usually have pore sizes higher than 20 nm, (Figure 18).

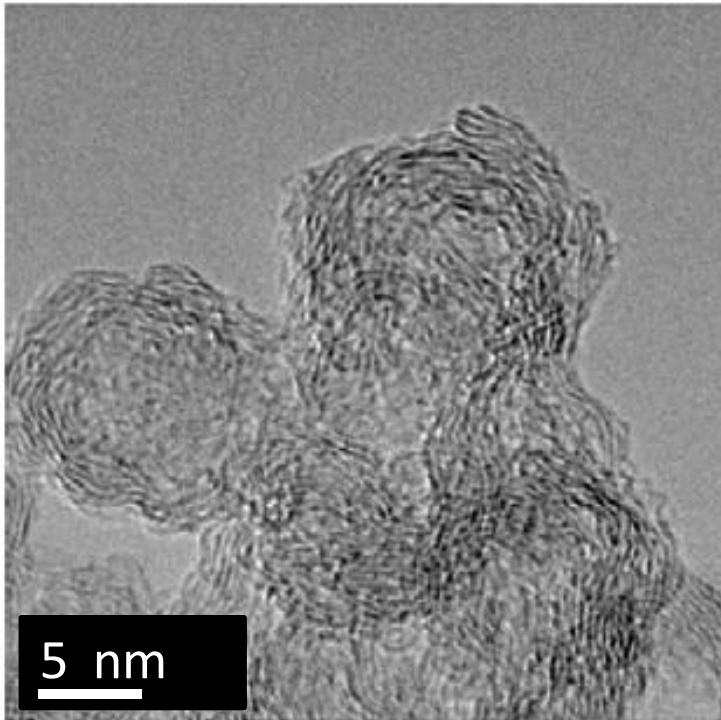


Figure 18. HRTEM image of soot particles from an engine collected using a Cummins ISB diesel engine^[125].

Numerous studies referring the catalytic oxidation of soot have been reported^[126, 127]. In order to determine the reaction rates these materials were oxidised under controlled conditions. The reaction rate of this oxidation reaction depends on several parameters, as the soot material used, the catalyst, the catalyst/soot ratio, the oxygen partial pressure and the contact between the soot and the catalyst. A sample pre-treatment also influences the reaction rate once that the desorption of adsorbed hydrocarbons on soot will take place. A first treatment in inert gases could also change the contact between the soot

and the catalyst or lead to the catalyst reduction by reaction between the soot and the metal oxide^[128].

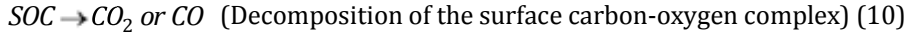
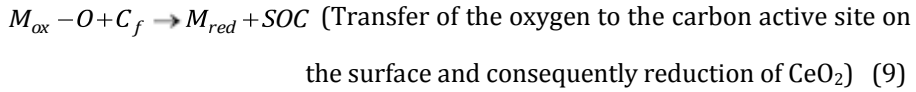
Usually, for this reaction the activity is measured in terms of the temperature at which 50% of the carbon material is converted (T_{50}). Nevertheless, in some cases, this is also presented as the temperature of the maximum combustion rate (T_m).

The contact between the soot and the catalyst is extremely important in order to observe a good catalytic activity. There are two types of contact named "loose" and "tight". Loose contact consists simply in mixing the catalyst and soot with a spatula for about 10 minutes in a reproducible way. The tight contact is achieved by grinding the catalyst with soot with a magnetically driven mortar for around 5 minutes^[129].

Evidences about the differences between both contact modes have been reported^[130]. For example, it was observed that Co_3O_4 or PbO catalysts are able to decrease the soot combustion temperature to around 430 °C when in the tight mode. The same Co_3O_4 catalyst using the loose contact was almost inactive ($T_m \sim 580$ °C), reaffirming the importance of the contact mode^[128].

Several catalysts have been presented as catalytic active for the soot oxidation reaction. Catalysts with a high oxygen store capacity, and with redox functions, are preferable due to the reaction mechanism. For this reason CeO_2 based catalysts are widely used for this reaction^[129, 131]

In what concerns to the mechanism reaction, several hypothesis were proposed^[131]. Many authors agree in a redox route pathway, over these catalysts (Equations 8 to 10). According to this mechanism the oxygen from the CeO_2 will react with soot. As a result of this reaction, carbonates will be formed and adsorbed on the support surface. Nevertheless, gas phase oxygen is able to decompose this carbonate species as well as provide the re-oxidation of the support:



where,

M_{red} - reduced state of CeO₂.

$M_{ox} - O$ - oxidised state of CeO₂.

$gas - O$ - oxidant gas (for example, O₂, NO, NO₂).

C_f - carbon active site on the carbon surface.

SOC - surface carbon-oxygen complex.

Finding a catalyst able to work efficiently for this purpose it is not easy. An effective catalyst must be able to operate efficiently at low temperatures and at the same time it must be thermally stable, i.e. it must not deactivate after being at the maximum temperatures of exhaust gases (from 200 °C to 850 °C approximately, depending on the engine).

The two main factors limiting soot oxidation are: the contact between soot and the catalyst and the intrinsic activity of the catalyst. Indeed, the commonly used catalysts have smaller pore sizes (< 10 nm) than soot particles (> 20 nm) which makes it difficult for soot particles to enter the inner pores of these catalysts^[132]. Due to the poor soot/catalyst contact the reaction rate is usually very low^[133].

Over the years, several catalysts have been proposed to decrease the soot oxidation temperature. For example, fuel borne catalysts (FBCs) (metal-based fuel soluble catalysts that are included in the fuel to catalyse the oxidation of soot) or molten salt catalysts have been developed and are able to increase the contact between the soot and the catalyst by wetting the soot surface, which is one of the main drawbacks of the soot catalytic conversion and thus decrease

the oxidation temperature^[134-137]. Using FBCs catalyts the reaction temperature can be decreased from approximately 600 °C to 350 °C^[138]. A good activity was also obtained for perovskites ($\text{La}_{1-x}\text{Cs}_x\text{CoO}_3$, LaMnO_3 and $\text{La}_{0.9}\text{K}_{0.1}\text{Cr}_{0.9}\text{O}_{3-\gamma}$) because of their good stability and intrinsic catalytic activity^[139, 140]. The activity of these catalysts is attributed to their capability to deliver α -type weakly chemisorbed oxygen species to the combustion reaction^[140, 141]. α -type oxygen desorption results from the oxygen accommodated in oxygen vacancies^[142]. Thus, an increase of oxygen vacancies leads to an increase of α -type oxygen species. This dissociatively adsorbed oxygen is believed to be responsible for the complete oxidation of hydrocarbons^[142]. In this way, a higher quantity of these species is favourable to achieve a complete oxidation^[142]. It has also been found that the addition of NO_2 helps to decrease the soot oxidation temperature since it is a strong oxidant^[143-145]. Furthermore, it has been observed that the most promising catalysts for soot oxidation are composed by potassium on oxides of transition metals such as Cu, V, Mo, Co or Fe^[135, 136, 146, 147] or in combined systems of Co, K/MgO or Ba, K/CeO₂ due to their strong oxidative properties^[143, 148, 149]. Several supports such as ZrO₂, TiO₂, Al₂O₃ and CeO₂ have been reported for the use in soot oxidation^[133, 150]. Van Doorn *et al.* concluded that for soot oxidation under an O₂ atmosphere Al₂O₃ and SiO₂ are not active. These authors observed a moderate activity for TiO₂ and ZrO₂ and a very high activity for CeO₂, La₂O₂CO₃ and V₂O₅ (Figure 19)^[150].

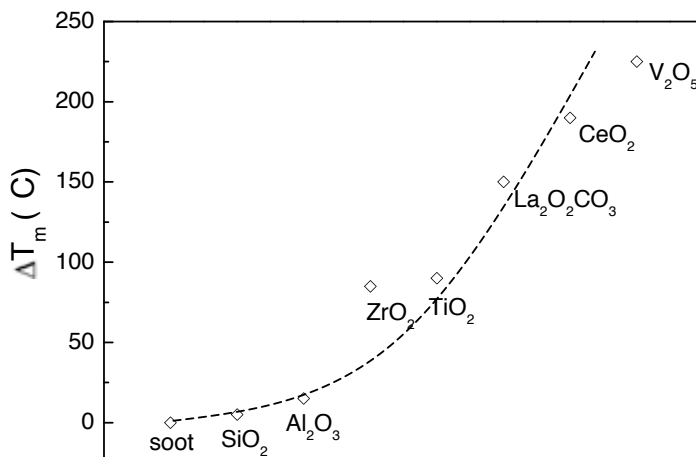


Figure 19. Effect of the type of support in the combustion temperature of soot under tight contact conditions in air^[150]. ΔT_m : Difference of temperatures of the maximum combustion rate between the bare soot and the catalyst-soot.

Several authors observed the activity of CeO₂ alone for soot oxidation^[133, 150-153]. The reactivity of CeO₂ is related with its high oxygen store capacity and redox properties. CeO₂ ability to change oxidation state during the reaction (CeO₂ to CeO_{2-x}) without structure modification will make easy oxygen uptake and release giving this catalyst a high oxygen storage capacity. This is an important property since the oxygen released from the lattice intervenes directly in the reaction^[153]. In this way, several authors justify the good activity of CeO₂ catalysts with the high availability of surface oxygen and high surface reducibility^[151-154]. The main drawback of using CeO₂ is its deactivation due the particle sinter after being at high temperatures in reaction conditions. In this way CeO₂-based binary and ternary mixed oxides have been studied as possible catalysts to overcome this handicap^[155]. It has been observed that the modification of CeO₂ with transition or rare earth metals (Zr⁴⁺, La³⁺, Y³⁺ or Sm³⁺) stabilises the surface area, improves the redox properties of CeO₂ and decreases the thermal deactivation^[155, 156]. Thus, these catalysts are known for their optimal redox properties, oxygen storage and releasing and thermal stability^[157].

The increase of the CeO₂ activity can also be achieved by simply doping CeO₂ with metals. This enhancement of activity results from the metal-support interaction that is responsible for the increase of the redox properties of the pure CeO₂^[143, 152, 158-160]. Different metals such as Ag, K, Co, Ba deposited on the CeO₂ surface were used as efficient catalysts to reduce the soot combustion temperature^[133, 144, 161].

Table 4 shows a compilation of the different types of catalysts described for this reaction in literature (the soot oxidation temperature was measured either with temperature programmed combustion or with thermogravimetric methods).

Table 4. Activity of different catalysts for soot oxidation under tight contact conditions in air.

	Catalyst	%O ₂	Soot/catalyst ratio	T ₅₀ ^(b) (°C)	ΔT ₅₀ ^(c) (°C)
Supported metal nanoparticles	Co/MgO ^[148]	6	1:20	>500 ^(a)	n.a.
	Ba/CeO ₂ ^[143]	6	1:20	480 ^(a)	n.a.
	KOH/MgO ^[149]	21	1:4	440 ^(a)	~210
	Co, K/MgO ^[148]	6	1:20	~ 400 ^(a)	n.a.
	Co, K/CeO ₂ ^[145]	6	1:20	350 ^(a)	~ 250
	Ag/ZrO ₂ ^[133]	20	1:20	341	n.a.
	Co/CeO ₂ ^[159]	6	1:20	300-340 ^(a)	300-260
Inorganic oxides	ZrO ₂ ^[133]	20	1:20	527	n.a.
	TiO ₂ ^[150]	15	4:1	502-517 ^(a)	~ 90
	La ₂ O ₂ CO ₃ ^[150]	15	4:1	442-457 ^(a)	~ 150
	CeO ₂ ^[133]	20	1:20	411	n.a.
	V ₂ O ₅ ^[150]	15	4:1	372-382 ^(a)	~ 220
Perovskites	LaMnBO, LaFeO ₃ , LaMnO ₃ , La _{1-x} K _x MnO ₃ ^[139]	20	1:9	500-550 ^(a)	~ 160-110
	LaCrO ₃ , LaCr _{0.9} O ₃ , LaCr _{0.8} O ₃ , LaVCr _{0.9} O ₃ ^[139]	20	1:9	450-500 ^(a)	~ 210-160

^(a) Temperature of the maximum combustion rate.

^(b) Temperature at which 50% of the soot is converted.

^(c) Difference of temperatures at which 50% of soot is converted between the bare soot and the catalyst-soot.

n.a. – not available data.

The catalytic activity of Au for soot oxidation has not been widely studied yet. In 2011, Ruiz *et al.* concluded that Au/support (SiO_2 , ZrO_2 or $\text{ZrO}_2 \cdot n\text{H}_2\text{O}$) catalysts present a very poor activity for soot oxidation in a O_2/He atmosphere ($\Delta T_m = 3 \text{ }^\circ\text{C}$)^[162]. Nonetheless, when performing soot oxidation in an atmosphere with NO, higher activities were obtained ($\Delta T_m = 54 \text{ }^\circ\text{C}$). The slight increase of activity observed for Au catalysts in the presence of NO is a result of the gold capacity to adsorb the NO and generate superficial NO_2 which is more oxidant than oxygen or nitrate ions^[162]. In the same way, these Au catalysts promoted with CsNO_3 showed a significant increase of activity in O_2 ($\Delta T_m = 230 \text{ }^\circ\text{C}$), since the high nitrate ion concentration favours the soot oxidation. For this reason, with these catalysts, the atmosphere effect was not so noticed ($\Delta T_m = 230 \text{ }^\circ\text{C}$ in O_2/He ; $\Delta T_m = 220 \text{ }^\circ\text{C}$ in $\text{NO}/\text{O}_2/\text{He}$). Finally, despite the high activity of bare CsNO_3 catalysts, the authors found that they were not selective to CO_2 . They concluded that the addition of Au was required to achieve a CO_2 selectivity of 100% indicating that all the CO formed in the combustion was transformed in CO_2 ^[162].

Later, in 2012, the same group, using lithium nitrate (LiNO_3) and Au catalysts, in accordance to what was previously observed, concluded that catalysts with lithium nitrate and gold were more active than catalysts containing only gold which was attributed to the presence of nitrate ions that will be part of the reaction in the redox cycle^[163]. As before, it was confirmed that the NO addition in the feed accelerates the combustion rate in all catalysts and that gold presence led to a total selectivity of CO_2 .

Furthermore, with the goal of achieving high activities, Craenenbroeck *et al.* combined the oxidation properties of Au NPs with the redox properties of vanadia (V) – Au-V/ TiO_2 or Au-V/ ZrO_2 – catalysts. These authors observed a much higher activity for the Au-V/ TiO_2 ($\Delta T_m = 113 \text{ }^\circ\text{C}$) or Au-V/ ZrO_2 catalytic systems ($\Delta T_m = 54 \text{ }^\circ\text{C}$) than to Au/ ZrO_2 ($\Delta T_m = 21 \text{ }^\circ\text{C}$) or Au/ TiO_2 ($\Delta T_m = 42 \text{ }^\circ\text{C}$) vanadia-free samples in air^[164]. Au-V catalysts were able to decrease the initial temperature at which oxidation of the carbon nucleus starts down to approximately the desired temperature range of $300 \text{ }^\circ\text{C} - 400 \text{ }^\circ\text{C}$ ^[164]. In these

catalysts the addition of gold produces two effects: Au particles promote the oxygen transfer which increases the activity in the combustion of soot particles; Au particles will provide active sites and therefore the soot combustion temperature will decrease^[164].

The activity of Au NPs supported on three-dimensionally ordered macroporous (3DOM) $Ce_{1-x}Zr_xO_2$ for soot combustion was studied by Wei *et al.* under loose contact conditions (atmosphere: 5 v/v% O_2 and 0.2 v/v% NO balanced with Ar)^[132]. The 3DOM $Ce_{1-x}Zr_xO_2$ catalysts showed a better catalytic activity for soot oxidation than the disordered macroporous and nanoparticles samples due to the bigger pore size (> 100 nm) (Table 5)^[165, 166]. In this way, soot particles (> 20 nm) can easily enter the catalysts inner pores and be easily transported and diffused leading to a higher number of contact points between soot and the catalyst^[132].

Table 5. Activity of Au nanoparticles supported on 3DOM $Ce_{1-x}Zr_xO_2$ catalysts for soot combustion under loose contact condition^[132]. Atmosphere: 5 v/v% O_2 and 0.2 v/v% NO balanced with Ar.

Catalysts	d (nm)	$T_{50}^{(a)}$ (°C)	$\Delta T_{50}^{(b)}$ (°C)	Soot/catalyst mass ratio	S_{CO_2} (%)
soot	-	585	0	-	55
3DOM ZrO_2	-	485	100		76.9
CeO_2	-	445	140		98.0
Au/(3DOM ZrO_2)	3.2	430	155		97.8
3DOM $Ce_{0.3}Zr_{0.7}O_2$	-	422	163		78.7
3DOM $Ce_{0.6}Zr_{0.4}O_2$	-	415	170		82.6
Au/(3DOM $Ce_{0.3}Zr_{0.7}O_2$)	3.2	407	178	1:10	98.5
3DOM CeO_2	-	390	195		97.3
3DOM $Ce_{0.9}Zr_{0.1}O_2$	-	378	207		85.7
Au/(3DOM $Ce_{0.6}Zr_{0.4}O_2$)	3.2	377	208		99.7
Au/(3DOM $Ce_{0.9}Zr_{0.1}O_2$)	3.3	361	224		99.7
Au/(3DOM CeO_2)	3.4	349	236		99.8

^(a)Temperature at which 50% of the soot is converted.

^(b)Difference of temperatures at which 50% of soot is converted between the bare soot and the catalyst-soot.

These authors also concluded about the positive effect of gold nanoparticles, in the soot combustion temperature and CO₂ selectivity (Table 5). The higher catalytic activity observed was attributed to metal-support interaction. This synergistic effect leads to the transference of lattice oxygen in the support and increases the quantity of oxygen vacancies and active oxygen species. Also, the direct activation of molecular oxygen on the gold nanoparticles surface was responsible for the higher activity observed^[167]. Small Au clusters are able to dissociate molecular O₂, adsorb it on their surface and release it to reaction increasing, thus the combustion rate of carbon. Moreover, the positive effect of doping Au/(3DOM CeO₂) with Zr was not noticed. An increase of T₅₀ was obtained with the increase of the content of Zr (Table 5). This decrease of activity was explained by the lower thermal stability of the supported Au nanoparticles in Au/(3DOM Ce_xZr_{1-x}O₂) catalysts^[132].

In the same way, Wei *et al.* obtained a very good result using Au NPs supported on 3DOM LaFeO₃ for soot oxidation under loose contact conditions (atmosphere: 5 v/v% O₂ and 0.2 v/v% NO balanced with Ar)^[167]. Using Au NPs with a mean diameter of approximately 3 nm, these authors observed a similar activity for the different gold content catalysts once that the contact area between soot and the catalyst is not affected by this variable. Nonetheless, it has been noticed that the Au particle size affects the catalytic activity since smaller gold nanoparticles will adsorb and activate the molecular O₂ on Au surface more effectively (Table 6). Additionally, the effect on the catalytic activity of the reaction atmosphere (existence or absence of NO) was also investigated by these authors. They concluded that for 3 nm Au catalysts due to the formation of active oxygen species on the Au surface, the catalytic activity is maintained even in the absence of NO. Then, using the same catalyst calcined at 550 °C, the Au mean particle size increased to 8.2 nm and its catalytic activity decreased significantly in air (initial temperature of combustion of the carbon material, T_i = 287 °C vs 231 °C), due to the existence of less small Au able to dissociate O₂ from the gas phase. Indeed, it has been shown that the intensity of

oxygen desorption peaks decreases significantly with the increase of the Au particle size, which confirms that the adsorption and activation of O₂ depends on this variable^[167]. Remarkably these 3 nm Au/(3DOM LaFeO₃) catalysts were able to decrease the initial soot combustion temperature (T_i) down to 228 °C with a CO₂ selectivity of 99.7% (Table 6). This temperature is the lowest reported among all the catalysts studied, including Pt-based catalysts (Pt/SiO₂ catalysts - T_i = 247 °C)^[167].

Table 6. Activity of Au NPs supported on 3DOM LaFeO₃ for soot oxidation under loose contact conditions^[167]. Atmosphere: 5 v/v% O₂ and 0.2 v/v% NO balanced with Ar.

Catalyst	d (nm)	T _m ^(a) (°C)	ΔT _m ^(b) (°C)	Soot/catalyst mass ratio	S _{CO2} (%)
Pure soot	-	585	0		55
LaFeO ₃	-	486	99		80
3DOM LaFeO ₃	-	415	170		82.2
Au/(3DOM LaFeO ₃)	7.8	384	201	1:10	99.6
	5.3	380	205		99.7
	4.0	371	214		99.5
	3.0	368	217		99.7

^(a)Temperature of the maximum combustion rate.

^(b)Difference of temperatures of the maximum combustion rate between the bare soot and the catalyst-soot.

• EFFECT OF NOBLE METALS IN THE COMBUSTION TEMPERATURE OF CARBONACEOUS MATERIALS

MWCNTs are known for their unique chemical, mechanical and electrical properties which make them useful in important applications. They are often used as support of metallic nanoparticles and have found application in catalysis and sensing^[168-171]. In this context, to know how the metal nanoparticles can affect the thermal stability of these carbon materials is extremely important for the development of potential applications and understand the limitations in other applications^[172].

Studies about how the decoration of carbon materials with metal nanoparticles affect their thermal stability have not been much reported. Nevertheless, some studies have shown that indeed the presence of metal nanoparticles in the carbon composition affects significantly the thermal stability of CNTs or other forms of carbon^[173-175]. Mckee *et al.* synthesised MWCNTs using different catalyst precursors and observed a significant reduced thermal stability for those contaminated with iron oxide and cobalt oxide^[173]. Other authors observed the same result, i.e. metallic particles used in the CNTs synthesis led to a decrease of the CNTs combustion temperature^[176, 177]. Moreover, the oxidation temperature of SWCNTs decreases with the enhancement of metal impurities of the sample^[178, 179]. Finally, it has been observed that SWCNTs can be purified (elimination of carbonaceous impurities and amorphous carbon) using gold nanoparticles deposited on soot followed by a controlled oxidation with O₂^[180]. The purification of SWCNTs has also been noticed using alkali metal salts (NaCl, KCl, CsCl)^[181]. Basically, it has been concluded that the thermal stability of CNTs depends on the metal nanoparticles properties, namely the nature of the metal, the size, the crystallinity and the interaction with the CNTs surface^[172].

In what concerns the combustion temperature of carbon materials by the impregnation of metal nanoclusters Qadeer *et al.* when impregnating nickel and cobalt on charcoal observed a decrease of the initial decomposition temperature ($\Delta T_i \sim 130$ °C) indicating a modification of the chemical properties of the activated charcoal^[174]. This decrease of combustion temperature has been attributed to the migration of mobile oxygen atoms formed on the metal surface to the metal-carbon interface leading then to gasification of the carbon in the vicinity of the metal particles^[174]. Furthermore, in 2013, Leino *et al.* decorated MWCNTs with Pt, Pd, Ni and CO clusters ($d < 2$ nm)^[182]. They used metal, metal oxide and metal acetylacetonate clusters on the surface of MWCNTs and observed that these metals led to a faster combustion of the MWCNTs at temperatures below 527 °C (temperature usually associated to the oxidation of pure nanotubes). This study was carried out under oxidative and

reductive atmospheres (here only oxidative is discussed once that the measurements in this thesis were carried out in O₂). The authors performed measurements by TGA in air (Table 7). In this case, the activity is presented in terms of T_s which corresponds to the temperature of the inflection point of the corresponding TG curves. These authors observed that oxides showed in general a lower temperature than the metal acetylacetonate (Table 7). The decrease of combustion temperatures could be explained by the fact that the oxygen in contact with carbon atoms from the oxide can react directly with the support. Oxidation might also take place at the catalysts support boundary due to the oxygen atoms that are adsorbed and diffuse on the surface. Since the oxidation of carbon is exothermic, the heating close to the catalyst nanoparticles will enhance the oxidation process. These results indicated that by simply applying low cost Co and Ni metal oxide nanoparticles on surfaces such as exhaust pipes, catalytic converters and sensors the low temperature oxidation of carbon can be achieved, which is useful, for example, in the decoking process^[182].

Table 7. Thermal decomposition temperatures of Pt, Ni, Co and Pd decorated MWCNTs in air^[182].

Catalyst	Nomenclature	d (nm)	T _s ^(a) (°C)	ΔT _s ^(b) (°C)	T _i (°C)	ΔT _i (°C)
Pre-treated MWCNTs	MWC	-	554	0	407	0
Pt(acac) ₂ /MWCNT	Pt(a)-MWC	1.3±0.3	559	0	n.a.	-
NiO _x /MWCNT	NiO-MWC	1.9±0.8	541	13	n.a.	-
Pd(acac) ₂ /MWCNT	Pd(a)-MWC	1.4±0.3	533	21	377	30
PtO _x /MWCNT	PtO-MWC	1.9±1.3	522	32	377	30
PdO _x /MWCNT	PdO-MWC	1.6±0.5	508	46	n.a.	-
Ni(acac) ₂ /MWCNT	Ni(a)-MWC	1.3±0.3	465	89	327	80
CoO _x /MWCNT	CoO-MWC	1.4±0.4	381	173	n.a.	-
Co(acac) ₃ /MWCNT	Co(a)-MWC	1.5±0.4	261	293	227	180

^(a) Temperature of the inflection point of the TG curve.

^(b) Difference of temperatures of the inflection point of the TG curves between the bare MWCNTs and the metal/MWCNTs catalyst.

Lorençon *et al.* also studied the effect of gold nanoparticles in the thermal stability of three different carbon materials, namely MWCNTs, SWCNTs and soot (Table 8)^[172]. These forms of carbon were decorated with gold nanoparticles with different sizes (2 nm – 25 nm) in order to understand how carbon combustion temperature is affected by the Au particle size. Measurements were made by TGA using synthetic air (25 °C – 800 °C). These authors observed a decrease of the carbon oxidation temperature by O₂ when decorated with Au nanoparticles on their surface. They concluded that the effect of Au in the carbon combustion temperature is directly dependent on the particle size in the range of 3 nm – 25 nm. Indeed, the effect of the larger Au nanoparticles (d ~ 25 nm) in the carbon oxidation was negligible, unlike the smaller particles (Table 8). This is because this effect is attributed to the spillover of oxygen existent on the Au cluster surface. Small Au particles activate the molecular oxygen from the gas phase by dissociation and then this oxygen is transferred to the carbon support which will oxidise it and produce CO (Figure 20b).

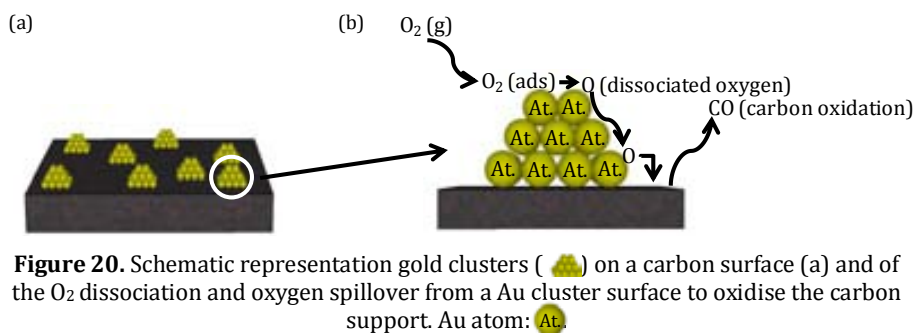




Figure 20. Schematic representation gold clusters () on a carbon surface (a) and of the O₂ dissociation and oxygen spillover from a Au cluster surface to oxidise the carbon support. Au atom: .

Nevertheless, in order to be able to dissociate molecular oxygen, the Au particles must be small as it was experimentally demonstrated by our group^[8]. Theoretical studies also indicate that the energy required for O₂ dissociation on gold surfaces is highly influenced by the particle diameter. There is a critical size for Au nanoparticles to dissociate O₂^[8, 183-185]. Indeed, in our published work, the ability of Au nanoparticles with 1.1 nm to dissociate ¹⁶O₂ and ¹⁸O₂

unlike 4 nm Au nanoparticles was demonstrated. The 1.1 nm Au clusters were able to dissociate both molecular oxygen isotopes at room temperature. The release of $^{16}\text{O}^{18}\text{O}$ occurred at higher temperature (80 °C), which might be probably related to a higher energetic barrier for desorption. Au NPs with 4 nm did not show molecular oxygen dissociation or release demonstrating the importance of the Au particle size for the O_2 molecular dissociation^[8].

Table 8. Thermal decomposition temperatures of pure and gold decorated carbon in synthetic air^[172].

Catalyst	Nomenclature	wt% Au	d (nm)	T _s ^(b) (°C)	ΔT _s ^(c) (°C)	T _i ^(d) (°C)	ΔT _i ^(e) (°C)
MWCNTs	-		-	607	0	390	0
Au/MWCNTs	Au-MWC-30 ^(a)	n.a.	30	619	0	n.a.	-
	Au-MWC-25 ^(a)		25	595	12	n.a.	-
	Au-MWC-5.8 ^(a)		5.8±2.3	481	126	300	90
Soot	-		-	581	0	460	0
Au/soot	Au-soot-22 ^(a)		22	580	1	n.a.	-
	Au-soot-11 ^(a)	n.a.	11	448	133	n.a.	-
	Au-soot-6.3 ^(a)		6.3	415	166	n.a.	-
	Au-soot-3.7 ^(a)		3.7	397	184	290	170

^(a)Au-MWC-x or Au-soot-x where x corresponds to the Au particle diameter.

^(b)Temperature of the inflection point of the TG curve.

^(c)Difference of temperatures of the inflection point of the TG curves between the bare carbon and the Au/carbon catalysts.

^(d)Initial temperature of combustion of the carbonaceous material.

^(e)Difference of temperatures of the initial temperature of combustion between the bare carbon and the Au/carbon catalysts.

n.a. – not available data.

The ability of several different types of catalysts to decrease the oxidation temperature of soot has been widely investigated and promising results have been obtained. Nevertheless, the investigation of the Au catalysts' activity for this reaction has not yet been reported on much. Despite this, the first results indicate the potential of Au for this reaction, which opens a new field of investigation to this metal. Also, although very little investigated, the effect of

metals, including Au, in the thermal stability of carbonaceous materials (MWCNTs and soot), using metal decorated carbon catalysts, has been observed leading to the opening of a field which requires a deeper investigation.

1.8 OBJECTIVES

The goal of this Doctoral Thesis is the synthesis of stable gold clusters by wet chemical routes, its characterisation and the study of their catalytic performance. A synthetic route that prevents the agglomeration and aggregation of the subnanometric gold particles is essential to allow the industrial scale-up of active Au catalysts.

The aim is to prepare uniform Au catalysts with a mean particle diameter lower than 2 nm supported on amine surfaces. Synthesis methods that are versatile enough to be reproduced using several supports with different characteristics such as MWCNTs, CeO₂ and TiO₂ are desired. Simple, clean, not expensive and easily scaled-up synthetic protocols are intended to be developed to achieve this goal.

In order to understand how the Au particle size can be affected by different variables, different techniques such as HRTEM, aberration-corrected HRTEM, Scanning Electron Microscopy (SEM) and Atomic Force Microscopy (AFM) will be used to characterise the synthesised Au particles and surface area measurements will be carried out to obtain the supports' surface area. It is also intended to investigate the chemical nature of gold by X-Ray Photoelectron Spectroscopy (XPS) and X-ray Absorption spectroscopy (XAS).

Once the synthesis of new reproducible synthetic protocols is achieved, the goal is to test these new catalysts' activity in reactions such as the CO oxidation and compare their activity with the co-precipitation and deposition-precipitation methods commonly used to synthesise active Au/CeO₂ catalysts for this reaction. It is also a goal to investigate the catalysts activity for the oxidation of

carbonaceous materials and compare their activity with gold and other metal catalysts commonly used for this reaction.

1.9 REFERENCES

- [1] M. Haruta, T. Koybayasi, H. Sano, M. Yamada, *Chemistry Letters* **1987**, 16, 405-408.
- [2] R. Meyer, C. Lemire, Sh. K. Shaikhutdinov, H.-J. Freund, *Gold Bulletin* **2004**, 37/1-2, 72-124.
- [3] D. T. Thompson, *Nanotoday* **2007**, 2/4, 40-43.
- [4] <http://apps.webofknowledge.com>, consulted 21/02/2014.
- [5] M. Haruta, *The Chemical Record* **2003**, Vol. 3, 75-87.
- [6] C. W. Corti, R. J. Holliday, D. T. Thompson, *Applied Catalysis A* **2005**, General 291, 253-261.
- [7] T. G. Schaaff, M. N. Shafigullin, J. T. Khoury, I. Vezmar, R. L. Whetten, W. G. Cullen, P. N. First, *Journal of Physical Chemistry B* **1997**, 101, 7885-7891.
- [8] L. Alves, B. Ballesteros, M. Boronat, J. R. Cabrero-Antonino, P. Concepción, A. Corma, M. A. Correa-Duarte, E. Mendoza *Journal of the American Chemical Society* **2011**, 133 (26), 10251-10261.
- [9] G. C. Bond, D. T. Thompson, *Catalysis Reviews-Science and Engineering* **1999**, 41, 319-388.
- [10] G. C. Bond, *Surface Science* **1985**, 156, 966-981.
- [11] R. Van Hardeveld, F. Hartog, *Surface Science* **1969**, 15, 189-230.
- [12] E. Roduner, *Chemical Society Reviews* **2006**, 35, 583-592.
- [13] J. Li, X. Li, H.-J. Zhai, L.-S. Wang, *Science* **2003**, 299, 864-867.
- [14] D. B. Fernández, PhD Thesis, *Caracterización y propiedades catalíticas de clústeres cuánticos subnanométricos*, Universidad de Santiago de Compostela, Departamento de Química Física **2011**.
- [15] W. Vogel, J. Bradley, O. Vollmer, I. Abraham, *Journal of Physical Chemistry B* **1998**, 102, 10853-10859.
- [16] W. Vogel, D.A.H. Cunningham, K. Tanaka, M. Haruta, *Catalysis Letters* **1996**, 40, 175-181.
- [17] M. B. Cortie, E. van der Lingen, *Materials Forum* **2002**, 26, 1-14.

- [18] T. X. Li, S. Y. Yin, Y. L. Ji, B. L. Wang, G. H. Wang, J. J. Zhao, *Physics Letters A* **2000**, 267, 403-407.
- [19] J. M. Soler, I. L. Garzón, J. D. Joannopoulos, *Solid State Communications* **2001**, 117, 621-625.
- [20] I. L. Garzón, K. Michaelian, M. R. Beltrán, A. Posada-Amarillas, P. Ordejón, E. Artacho, D. Sánchez-Portal, J. M. Soler, *Physical Review Letters* **1998**, 81 (8), 1600-1603.
- [21] H. B. Liu, J. A. Ascencio, M. Perez-Alvarez, M. J. Yacaman, *Surface Science* **2001**, 491, 88-98.
- [22] B. Hvolbæk, T. V. W. Janssens, B. S. Clausen, H. Falsig, C. H. Christensen, J. K. Nørskov, *Nanotoday* **2007**, 2 (4), 14-18.
- [23] T. V. W. Janssens, A. Carlsson, A. Puig-Molina, B. S. Clausen, *Journal of Catalysis* **2006**, 240, 108-113.
- [24] G. C. Bond, C. Louis, D. T. Thompson, *Catalysis by Gold – Catalytic Science Series – Vol. 6*, Imperial College Press.
- [25] J. Llorca, M. Domínguez, C. Ledesma, R. J. Chimentão, F. Medina, J. Sueira, I. Angurell, M. Seco, O. Rossell, *Journal of Catalysis* **2008**, 258, 187-198.
- [26] G. Tobias, E. Mendoza, B. Ballesteros, *Encyclopedia of Nanotechnology*, SpringerLink **2012**, 911-919.
- [27] R. Zanella, S. Giorgio, C. R. Henry, C. Louis, *Journal of Physical Chemistry B* **2002**, 106, 7634-7642.
- [28] R. Zhang, M. hummelgard, H. Olin, *Materials Science and Engineering B* **2009**, 158, 48-52.
- [29] X.-Y. Wang, S.-P. Wang, S.-R. Wang, Y.-Q. Zhao, J. Huang, S.-M. Zhang, W.-P. Huang, S.-H. Wu, *Catalysis Letters* **2006**, 112, 115-119.
- [30] J. D. S Newman, G. J. Blanchard, *Langmuir* **2006**, 22, 5882-5887.
- [31] F. B. Lollmahomed, R. Narain, *Langmuir* **2011**, 27, 12642-12649.
- [32] M. Ahmed, Z. Deng, S. liu, R. Lafrenie, A. Kumar, R. Narain, *Bioconjugate Chemistry* **2009**, 20, 2169-2176.

- [33] L. Lechuga Gómez, E. Mendoza Gómez, M. A. Correa Duarte, M. Sanles Sobrido, *Patent WO2010031890 A1*, available on-line <http://patentscope.wipo.int/search/en/WO2010031890>.
- [34] R. Di Felice, A. Selloni, *Journal of Chemical Physics* **2004**, 120, 4906-4914.
- [35] S. D. Lin, M. Bollinger and M. A. Vannice, *Catalysis Letters* **1993**, 17, 245-262.
- [36] P. A. Sermon, G. C. Bond and P. B. Wells, *Journal of the Chemical Society, Faraday Transactions I* **1979**, 75, 385-394.
- [37] N. W. Cant and W. K. Hall, *Journal of Physical Chemistry* **1971**, 75, 2914-2921.
- [38] C. Corti, R. Holliday, *Gold Science and Applications*, CRC Press **2010**.
- [39] L. Prati, A. Villa, *Catalysts* **2012**, 2, 24-37.
- [40] S. J. Lee, A. Gavriilidis, *Journal of Catalysis* **2002**, 206, 305-313.
- [41] Q. Xu, K. C. C.Kharas, A. K. Datye, *Catalysis Letters* **2003**, 229-235.
- [42] M. Haruta, *Journal of New Materials for Electrochemical Systems* **2004**, 7, 163-172.
- [43] X.-Y. Wang, S.-P. Wang, S.-R. Wang, Y.-Q. Zhao, J. Huang, S.-M. Zhang, W.-P. Huang, S.-H. Wu, *Catalysis Letters* **2006**, 112, 115-119.
- [44] M. Haruta, H. Kageyama, N. Kamijo, T. Kobayashi and F. Delannay, *Studies in Surface Science and Catalysis* **1989**, 44, 33-42.
- [45] M. Haruta, *Catalysis Today* **1997**, 36, 153-156.
- [46] R.-R. Zhang, L.-H. Ren, A.-H. Lu, W.-C. Li, *Catalysis Communications* **2011**, 13, 18-21.
- [47] A. Sandoval, C. Louis, R. Zanella, *Applied Catalysis B: Environmental* **2013**, 140-141, 363-377.
- [48] R. Zanella, S. Giorgio, C.R. Henry, C. Louis, *Journal of Physical Chemistry B* **2002**, 106, 7634-7642.
- [49] J. Turkevich, *Gold Bulletin* **1985**, 18, 86-91.
- [50] J. Turkevich, J. Hillier and P.C. Stevenson, *Discussions of the Faraday Society* **1951**, 11, 55-75.

- [51] J. Turkevich, G. Garton and P.C. Stevenson, *Journal of Colloid Science, Supplement 1* **1954**, 26-35.
- [52] D. T. Thompson, *Nanotoday* **2007**, 2/4, 40-43.
- [53] C. Li, D. Li, G. Wan, J. Xu, W. Hou, *Nanoscale Research Letters* **2011**, 6, 440.
- [54] Y. Nagata, Y. Watanabe, S. Fujita, T. Dohmaru, S. Taniguchi, *Chemical Communications* **1992**, 1620-1622.
- [55] S. A. Yeung, R. Hobson, S. Biggs, F. Grieser, *Chemical Communications* **1993**, 378-379.
- [56] K. Okitsu, H. Bandow, Y. Maeda, Y. Nagata, *Chemistry of Materials* **1996**, 8, 315-317.
- [57] K. S. Suslick, *Scientific American*, **1989**, 260, 80-86.
- [58] C. E. Brenner, *Cavitation and Bubble Dynamics*, Oxford university Press, Oxford, **1995**, available on-line: <http://authors.library.caltech.edu/25017/1/cavbubdynam.pdf>.
- [59] H. Xu, B. W. Zeiger, K. S. Suslick, *Chemical Society Reviews* **2013**, 42, 2555-2567.
- [60] K. Okitsu, M. Ashokkumar, F. Grieser, *Journal of Physical Chemistry B* **2005**, 109, 20673-20675.
- [61] W. Chen, W. Cai, L. Zhang, G. Wang, L. Zhang, *Journal of Colloid and Interface Science* **2001**, 238, 291-295.
- [62] K. Leonard, M. Kawashima, H. Okamura, J. Kurawaki, *Materials Letters* **2010**, 64, 2240-2243.
- [63] K. Okitsu, Y. Mizukoshi, T. A. Yamamoto, Y. Maeda, Y. Nagata, *Materials Letters* **2007**, 61, 3429-3431.
- [64] M.-Y. Wei, L. Famouri, L. Carroll, Y. Lee, P. Famouri, *Ultrasonics Sonochemistry* **2013**, 20, 610-617.
- [65] X.-F. Qiu, J.-J. Zhu, H.-Y. Chen, *Journal of Crystal Growth* **2003**, 257, 378-383.
- [66] J. K.-J. Li, C.-J. Ke, C.-A. J. Lin, Z.-H. Cai, C.-Y. Chen, W. H. Chang, *Journal of Medical and Biological Engineering* **2012**, 33, 23-28.

- [67] H. Xu, K. S. Suslick, *American Chemical Society Nano* **2010**, 4, 3209-3214.
- [68] J. Zheng, C. Zhang, R. M. Dickson, *Physical Review Letters* **2004**, 93, 077402-077408.
- [69] Y. Bao, C. Zhong, D. M. Vu, J. P. Temirov, R. B. Dyer, J. S. Martinez, *Journal of Physical Chemistry C* **2007**, 111, 12194-12198.
- [70] N. Schaeffer, B. Tan, C. Dickinson, M. J. Rosseinsky, A. Laromaine, D. W. McComb, M. M. Steven, Y. Wang, I. Petit, C. Barentin, D. G. Spiller, A. I. Cooper, R. Levy, *Chemical Communications* **2008**, 3986-3988.
- [71] H. Liu, X. Zhang, X. Wu, L. Jiang, C. Burda, J.-J. Zhu, *Chemical Communications* **2011**, 47, 4237-4239.
- [72] K. Takahiro, S. Oizumi, A. Terai, K. Kawatsura, B. Tsuchiya, S. Nagata, S. Yamamoto, H. Naramoto, K. Narumi, M. Sasase, *Journal of Applied Physics* **2006**, 100, 84325-84325-6.
- [73] E. Gross, M. Asscher, *Journal of Physical Chemistry C* **2007**, 111, 16197-16201.
- [74] B. Qiao, A. Wang, X. Yang, L. F. Allard, Z. Jiang, Y. Cui, J. Liu, J. Li, T. Zhang, *Nature Chemistry* **2011**, 3, 634-641.
- [75] S. Sun, G. Zhang, N. Gauquelin, N. Chen, J. Zhou, S. Yang, W. Chen, X. Meng, D. Geng, M. N. Banis, R. Li, S. Ye, S. Knights, G. A. Botton, T.-K. Sham, X. Sun, *Scientific Reports* **2013**, 3, article number: 1775.
- [76] C. I. Contescu, K. van Benthem, S. Li, C. S. Bonifacio, S. J. Pennycook, P. Jena, N. C. Gallego, *Carbon* **49** **2011**, 4050-4058.
- [77] G. Kyriakou, M. B. Boucher, A. D. Jewell, E. D. Lewis, T. J. Lawton, A. E. Baber, H. L. Tierney, M. Flytzani-Stephanopoulos, E. C. H. Sykes, *Science* **2012**, 335, 1209-1212.
- [78] J. Oivier-Meseguer, J. R. Cabrero-Antonino, I. Domínguez, A. Leyva-Pérez, A. Corma, *Science* **2012**, 338, 1452-1455.
- [79] S. Lee, C. Fan, T. Wu, S. L. Anderson, *Journal of Chemical Physics* **2005**, 123, 124710-124722.
- [80] S. Lee, C. Fan, T. Wu, S. L. Anderson, *Surface Science* **2005**, 578, 5-19.

- [81] C. Harding, V. Habibpour, S. Kunz, A. N. Fambacher, U. Heiz, B. Yoon, U. Landman, *Journal of the American Chemical Society* **2009**, 131, 538-548.
- [82] S. Lee, C. Fan, T. Wu, S. L. Anderson, *Journal of Chemical Physics* **2005**, 123, 124710.
- [83] S. Lee, C. Fan, T. Wu, S. L. Anderson, *Surface Science* **2005**, 578, 5-19.
- [84] A. A. Herzing, C. J. Kiely, A. F. Carley, P. Landon, G. J. Hutchings, *Science* **321** **2008**, 1331-1334.
- [85] A. Uzun, V. Ortalan, Y. Hao, N. D. Browning, B. C. Gates, *Journal of Physical Chemistry C* **2009**, 113, 16847-16849.
- [86] J. Lu, C. Aydin, N. D. Browning, B. C. Gates, *Angewandte Chemie International Edition* **2012**, 51, 5842-5846.
- [87] N. J. Lawrence, PhD thesis, *Synthesis and Catalytic Activity of Nanostructured Cerium Oxide*, University of Nebraska - Lincoln, Department of Chemistry **2010**.
- [88] N. Kruse, A. Frennet, J.-M. Bastin, *Catalysis and Automotive Pollution IV*, Elsevier **1998**.
- [89] K. Jiang, *Fabrication and Catalytic Property of Cerium Oxide Nanomaterials*, PhD thesis, University of Nebraska-Lincoln - Chemistry Department **2001**.
- [90] M. Murdoch, G. I. N. Waterhouse, M. A. Nadeem, J. B. Metson, M. A. Keane, R. F. Howe, J. Llorca, H. Idriss, *Nature Chemistry* **2011**, 3, 489-492.
- [91] D. Widmann, Y. Liu, F. Schuth, R. J. Behm, *Journal of Catalysis* **2010**, 276, 292-305.
- [92] Y. Denkwitz, B. Schumacher, G. Kucerová, R. J. Behm. *Journal of Catalysis* **2009**, 267, 78-88.
- [93] W.-Y. Yu, C.-P. Yang, J.-N. Lin, C.-N. Kuo, B.-Z. Wan, *Chemical Communications* **2005**, 354-356.
- [94] S. Tsubota, M. Haruta, T. Kobayashi, A. Ueda, Y. Nakahara, *Studies in Surface Science and Catalysis* **1991**, 72, 695-704.

- [95] S. Tsubota, D. A. H. Cunningham, Y. Bando, M. Haruta, *Studies in Surface Science and Catalysis* **1995**, 91, 227-235.
- [96] S. Iijima, *Nature* **1991**, 354, 56-58.
- [97] M. Meyyappan, *Carbon Nanotubes – Science and Applications*, CRC Press.
- [98] P. Serp, E. Castillejos, *ChemCatChem* **2010**, 2, 41-47.
- [99] H. C. Choi, M. Shim, S. Bangsaruntip, H. Dai, *Journal of the American Chemical Society* **2002**, 124, 9058-9059.
- [100] V. Tzitis, V. Georgakilas, E. Oikonomou, M. Karakassides, D. Petridis, *Carbon* **2006**, 44, 848-853.
- [101] R. Zanella, E. V. Basiuk, P. Santiago, V. A. Basiuk, E. Mireles, L. Puente-Lee, J. M. Saniger, *Journal of Physical Chemistry B* **2005**, 109, 16290-16295.
- [102] X. Hu, T. Wang, X. Qu, S. Dong, *Journal of Physical Chemistry B* **2006**, 110, 853-857.
- [103] H. Ismaili, F. Lagugné-Labarthe, M. S. Workentin, *Chemistry of Materials* **2011**, 23, 1519-1525.
- [104] http://www.dieselnet.com/tech/cat_substrate.php, consulted 24/02/2014.
- [105] T. Boger, A. K. Heibel, C. M. Sorensen, *Industrial & Engineering Chemistry Research* **2004**, 43, 4602-4611.
- [106] M. Haruta, N. Yamada, T. Kobayashi, S. Iijima, *Journal of Catalysis* **1989**, 115, 301-309.
- [107] H.-F. Li, N. Zhang, P. Chen, M.-F. Luo, J.-Q. Lu, *Applied Catalysis B: Environmental* **2011**, 110, 279-285.
- [108] Z.-P. Liu, P. Hu, A. Alavi, *Journal of the American Chemical Society* **2002**, 124, 14770-14779.
- [109] Z.-P. Liu, X.-Q. Gong, J. Kohanoff, C. Sanchez and P. Hu, *Physical Review Letters* **2003**, 91, 266102-266105.
- [110] L.M. Molina, B. Hammer, *Applied Catalysis A: Gen.* **2005**, 291, 21-31.

- [111] L.M. Molina, M.D. Rasmussen, B. Hammer, *Journal of Chemical Physics* **2004**, 120, 7673-7680.
- [112] D. Astruc, *Nanoparticles and Catalysis – Vol. 1*, Wiley-VCH **2007**.
- [113] S. D. Gardner, G. B. Hoflund, D. R. Schrywer, J. Shryer, B. Upchurch, E. J. Kielin, *Langmuir* **1991**, 7, 2135.
- [114] Tana, F. Wang, H. Li, W. Shen, *Catalysis Today* **2011**, 175, 541-545.
- [115] S. Carretin, P. Concepción, A. Corma, J. M. López Nieto, V. F. Puntes, *Angewandte Chemie International Edition* **2004**, 43, 2538-2540.
- [116] M. Han, X. Wang, Y. Shen, C. Tang, G. Li, R. L. Smith, Jr., *Journal of Physical Chemistry C* **2010**, 114, 793-798.
- [117] R.-R. Zhang, L.-H. Ren, A.-H. Lu, W.-C. Li, *Catalysis Communications* **2011**, 13, 18-21.
- [118] J. Guzman, S. Carretin, A. Corma, *Journal of the American Chemical Society* **2005**, 127, 3286.
- [119] A. M. Venezia, G. Pantaleo, A. Longo, G. D. Carlo, M. P. Casaletto, F. L. Liotta, G. Deganello, *Journal of Physical Chemistry B* **2005**, 109, 2821-2827.
- [120] U. R. Pillai, S. Deevi, *Applied Catalysis A* **2006**, 299, 266-273.
- [121] K. Qian, S. Lv, X. Xiao, H. Sun, J. Lu, M. Luo, W. Huang, *Journal of Molecular Catalysis A* **2009**, 306, 40-47.
- [122] S. Y. Lai, Y. F. Qiu, S. J. Wang, *Journal of Catalysis* **2006**, 237, 303-313.
- [123] M. Comotti, W.-C. Li, B. Spliethoff, F. Schuth, *Journal of the American Chemical Society* **2006**, 128, 917-924.
- [124] J. Liu, Z. Zhao, C. Xu, A. Duan, L. Zhu, X. Wang, *Catalysis Today* **2006**, 118, 315-322.
- [125] R. L. V. Wal, A. Yezerets, N. W. Currier, D. H. Kim, C. M. Wang, *Carbon* **2007**, 45, 70-77.
- [126] M. L. Ruiz, I. D. Lick, M. I. Ponzi, E. Rodriguez-Castellon, A. Jimenez-Lopez, E. N. Ponzi, *Applied Catalysis A* **2011**, General 392, 45-46.
- [127] J. V. Craenenbroeck, D. Andreeva, T. Tabakova, K. VanWerde, J. Mullens, F. Verpoort, *Journal of Catalysis* **2002**, 209, 515-527.

- [128] A. Frennet, J.-M. Bastin, *Catalysis and Automotive Pollution Control III*, Elsevier **1995**.
- [129] K. Yamazaki, T. Kayama, F. Dong, H. Shinjoh, *Journal of Catalysis* **2011**, 282, 289-298.
- [130] S. Lorentzou, E. Papaioannou, M. Kostoglou, A. G. Konstandopoulos, K. Ohno, K. Ogyu, T. Oya, *Third European Combustion Meeting ECM 2007*.
- [131] E. Aneggi, C. de Leitenburg, J. Llorca, A. Trovarelli, *Catalysis Today* **2012**, 197, 119-126.
- [132] Y. Wei, J. Liu, Z. Zhao, A. Duan, G. Jiang, *Journal of Catalysis* **2012**, 287, 13-29.
- [133] E. Aneggi, J. Llorca, C. de Leitenburg, G. Dolcetti, A. Trovarelli, *Applied Catalysis B* **2009**, 489-498.
- [134] P. Richards, *Fuel Borne Catalysts for DPF Regeneration*, available online:
ftp://ftp.aqmd.gov/pub/kdurkee/UltraFineCourse/November%2012%202008/Session%204%20Regeneration%20of%20Filters/3%20P%20Richards_Fuel%20Borne%20Catalysts.pdf.
- [135] P. Ciambelli, V. Palma, P. Russo, S. Vaccaro, *Journal of Molecular Catalysis A: Chemical* **2003**, 204, 673-681.
- [136] G. Saracco, C. Badini, N. Russo, V. Specchia, *Applied Catalysis B: Environmental* **1999**, 21, 233-242.
- [137] Y. Ma, M. Zhu, D. Zhang, *Applied Energy* **2014**, 113, 751-757.
- [138] <http://www.infineum.com/Pages/FuelBorneCatalysts.aspx>, consulted 18/02/2014.
- [139] D. Fino, P. Fino, G. Saracco, V. Specchia, *Korean Journal of Chemical Engineering* **2003**, 20, 445-450.
- [140] D. Fino, N. Russo, G. Saracco, V. Specchia, *Journal of Catalysis* **2003**, 217, 367-375.
- [141] F. E. López-Suárez, A. Bueno-López, M. J. Illán-Gómez, A. Adamski, B. Ura, J. Trawczynski, *Environmental Science & Technology* **2008**, 42, 7670-7675.

- [142] H. X. Dai, C. F. Ng, C. T. Au, *Journal of Catalysis* **2000**, 189, 52-62.
- [143] M. L. Pisarello, V. Milt, M. A. Peralta, C. A. Querini, E. E. Miró, *Catalysis Today* **2002**, 75, 465-470.
- [144] V. G. Milt, C. A. Querini, E. E. Miró, M. A. Ulla, *Journal of Catalysis* **2003**, 220, 424-432.
- [145] E. E. Miró, F. Ravelli, M. A. Ulla, L. M. Cornaglia, C. A. Querini, *Catalysis Today* **1999**, 53, 631-638.
- [146] H. An, C. Kilroy, P. J. McGinn, *Catalysis Today* **2004**, 98, 423-429.
- [147] G. Neri, G. Rizzo, S. Galvagno, M. G. Musolino, A. Donato, R. Pietropaolo, *Thermochimica Acta* **2002**, 381, 165-172.
- [148] C. A. Querini, M. A. Ulla, F. Requejob, J. Soria, U. A. Sedrán, E. E. Miró, *Applied Catalysis B: Environmental* **1998**, 15, 5-19.
- [149] R. Jiménez, X. García, C. Cellier, P. Ruiz, A. L. Gordón, *Applied Catalysis A: General* **2006**, 297, 125-134.
- [150] J. Van Doorn, J. Varloud, P. Meriaudeau, V. Perrichon, M. Chevrier, C. Gauthier, *Applied Catalysis B* **1992**, 1, 117-127.
- [151] E. Aneggi, C. De Leitenburg, G. Dolcetti, A. Trovarelli, *Catalysis Today* **2006**, 114, 40-47.
- [152] E. Aneggi, C. De Leitenburg, G. Dolcetti, A. Trovarelli, *Catalysis Today* **2008**, 136, 3-10.
- [153] X. Wu, D. Liu, K. Li, J. Li, D. Weng, *Catalysis Communications* **2007**, 8, 1274-1278.
- [154] H. Muroyama, S. Hano, T. Matsui, K. Eguchi, *Catalysis Today* **2010**, 153, 133-135.
- [155] I. Atribak, A. Bueno-López, A. García-García, *Journal of Molecular Catalysis A: Chemical* **2009**, 300, 103-110.
- [156] K. Krishna, A. Bueno-López, M. Makkee, J. A. Moulijn, *Applied Catalysis B: Environmental*, **2007**, 75, 189-200.
- [157] Y. Zhang, L. Zhang, J. Deng, H. Dai, H. He, *Inorganic Chemistry* **2009**, 48, 2181-2192.

- [158] E. E. Miró, F. Ravelli, M. A. Ulla, L. M. Cornaglia, C. A. Querini, *Catalysis Today* **1999**, 53, 631-638.
- [159] P. G. Harrison, I. K. Ball, W. Daniell, P. Lukinskas, M. Céspedes, E. E. Miró, M. A. Ulla, *Chemical Engineering Journal* **2003**, 95, 47-55.
- [160] H. Laversin, D. Courcot, E. A. Zhilinskaya, R. Cousin, A. Aboukais, *Journal of Catalysis* **2006**, 241, 456-464.
- [161] K. Yamazaki, T. Kayama, F. Dong, H. Shinjoh, *Journal of Catalysis* **2011**, 282, 289-298.
- [162] M. L. Ruiz, I. D. Lick, M. I. Ponzi, E. Rodriguez-Castellón, A. Jiménez-Lopez, E. N. Ponzi, *Applied Catalysis A: General* **2011**, 392, 45-56.
- [163] M. L. Ruiz I. D. Lick, M. S. L. Aparicio, M. I. Ponzi, E. Rodriguez-Castellón, E. N. Ponzi, *Industrial & Engineering Chemistry Research* **2012**, 51, 1150-1157.
- [164] J. V. Craenenbroeck, D. Andreeva, T. Tabakova, K. V. Werde, J. Mullens, F. Verpoort, *Journal of Catalysis* **2002**, 209, 515-527.
- [165] M. Sadakane, T. Horiuchi, N. Kato, C. Takahashi, W. Ueda, *Chemistry of Materials* **2007**, 19, 5779-5785.
- [166] G. Zhang, Z. Zhao, J. Liu, G. Jiang, A. Duan, J. Zheng, S. Chen, R. Zhou, *Chemical Communications* **2010**, 46, 457-459.
- [167] Y. Wei, J. Liu, Z. Zhao, Y. Chen, C. Xu, A. Duan, G. Jiang, H. He, *Angewandte Chemie International Edition* **2011**, 50, 2326-2329.
- [168] V. Georgakilas, D. Gournis, V. Tzitzios, L. Pasquato, D. M. Guldi, M. Prato, *Journal of Materials Chemistry* **2007**, 17, 2679-2694.
- [169] P. Serp, M. Corrias, P. Kalck, *Applied Catalysis A: General* **2003**, 253, 337-358.
- [170] S. X. Yang, W. P. Zhu, X. Li, H. B. Wang, Y. R. Zhou, *Catalysis Communications* **2007**, 8, 2059-2063.
- [171] G. G. Wildgoose, C. E. Banks, R. G. Compton, *Small* **2006**, 2, 182-193.
- [172] E. Lorençon, R. G. Lacerda, L. O. Ladeira, R. R. Resende, A. S. Ferlauto, U. Schuchardt, R. M. Lago, *Journal of Thermal Analysis and Calorimetry* **2011**, 105, 953-959.

- [173] G. S. B. Mckee, K. S. Vecchio, *Journal of Physical Chemistry B* **2006**, 110, 1179-1186.
- [174] R. Qadeer, R. Hussain, *Journal of Chemical Society of Pakistan* **1998**, 20, 8-11.
- [175] A. W. Musumeci, G. G. Silva, W. N. Martens, E. R. Waclawik, R. L. Frost, *Journal of Thermal Analysis and Calorimetry* **2007**, 88, 885-891.
- [176] B. J. Landi, C. D. Cress, C. M. Evan, R. P. Raffaele, *Chemistry of Materials* **2005**, 17, 6819-6834.
- [177] S. Arepalli, P. nikolaev, O. Gorelik, V. G. Hadjiev, W. Holmes, B. Files, L. Yowell, *Carbon* **2004**, 42, 1783-1791.
- [178] R. Brukh, O. Sae-Khow, S. Mitra, *Chemical Physics Letters* **2008**, 459, 149-152.
- [179] C. X. Wu, J. X. Xu, J. X. Li, G. F. Dong, L. H. Guan, *Physica E* **2009**, 41, 1591-1595.
- [180] E. Mizoguti, F. Nihey, M. Yudasaka, S. Iijima, T. Ichihashi, K. Nakamura, *Chemical Physics Letters* **2000**, 321, 297-301.
- [181] Y. Kobayashi, M. Sano, *ChemCatChem*. **2010**, 2, 397-401.
- [182] A.-R. Leino, M. Mohl, J. Kikkola, P. Maki-Arvela, T. Kokkonen, A. Schukarev, K. Kordas, *Carbon* **2013**, 57, 99-107.
- [183] A. Roldan, S. Gonzalez, J. M. Ricart, F. Illas, *ChemPhysChem* **2009**, 10, 348-351.
- [184] M. Boronat, A. Corma, *Dalton Transactions* **2010**, 39, 8538-8546.
- [185] A. Roldan, J. M. Ricart, F. Illas, *Theoretical Chemistry Accounts* **2009**, 123, 119-126.

CHAPTER 2:
CHARACTERISATION
TECHNIQUES AND METHODS

2.1 TRANSMISSION ELECTRON MICROSCOPY (TEM)

TEM is a technique that allows obtaining images of the sample at very small scales (\AA) using accelerated electrons. The basic principle of Transmission Electron Microscopy consists in an electron source which emits electrons that cross through a vacuum in the microscope column. For a typical operating voltage of 200 kV the electrons wavelength is 2.51×10^{-3} nm. This much lower wavelength than the wavelength of visible light (~ 400 nm) pushes the resolution down to the order of angstrom (10^{-10} m).

The electron microscope can use three different electron sources, namely a plain tungsten filament, a tungsten filament with a LaB_6 crystal tip or a field emission gun. Depending on the source used, different levels of brightness will be obtained. While the tungsten filament gives the lowest brightness, the field emission leads to the higher brightness. The filament is held in an uncharged wehnelt cap (0 kV) and is heated in vacuum to excite electrons. The excited free electrons will then be directed through the anode, that is located below the wehnelt cap, due to the positive voltage (usually 200 kV).

Figure 21 shows a schematic representation of the column of a transmission electron microscope. The electron beam passes through a series of lenses and apertures as it moves down the column. The beam is focused onto the sample by the first lens that it encounters (condenser lens). The sample contrast can be varied by modifying the sizes of the condenser apertures which are located under the lens. Then, after passing through the sample (specimen), the beam is refocused by the objective lens which allows the diffraction plane to be viewed. By changing the objective aperture, the sample contrast can be increased and dark field imaging can be viewed. Finally, the beam passes through the projector lens, which leads to the resulting image on the viewing screen^[1]. The image depends mainly on the density of the materials of the sample.

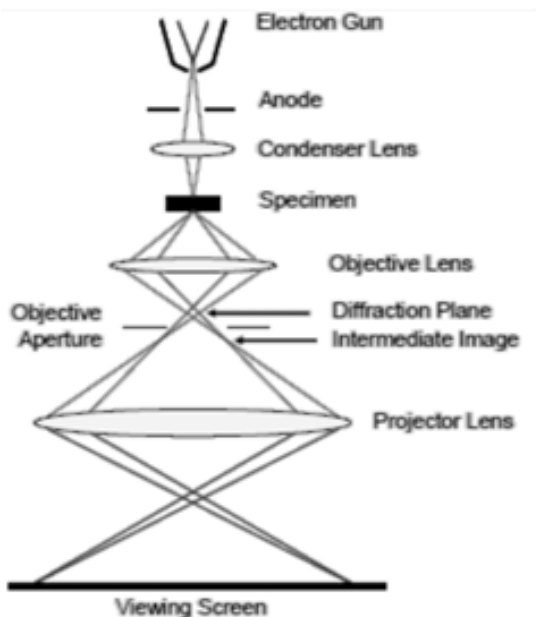


Figure 21. Schematic outline of a Transmission Electron Microscope^[1].

In order to have a high quality image resolution, it is essential that the electron beam is well aligned. Nevertheless, since it is almost impossible to make a 100% perfectly curved lens, there are always defects (aberrations). In TEM lens, aberrations play both a beneficial and detrimental role in the high resolution imaging. On the one hand, they give place to undesired blurring in any image plane, thus obscuring the finest object details. On the other hand, they are required once that they produce the desired phase contrast of the very thin objects. Among all aberrations of the electron microscope, the stronger is the spherical aberration of the objective lens^[2].

Scherzer in 1949 claimed that the resolution of an image is only dependent on the electron wavelength and the constant of spherical aberration^[3]. In this way, resolution can only be improved by using a smaller wavelength at higher acceleration voltages or by reducing the spherical aberration. Because the spherical aberration coefficient of a round lens is always positive and on the order of its focal length the reduction of this parameter can only be achieved within certain limits. To overcome this limitation, over decades, instrumental

improvements have been made. In 1990, Rose, invented the spherical aberration correctors^[4]. Then, since its implementation into commercial TEMs in 1998 the coefficient of spherical aberration started to be used as an additional parameter^[5]. This can now be varied over a wide range and can even be tuned to negative values giving place to new imaging modes, namely high resolution amplitude contrast and extension of the point resolution to the information limit and enhanced image intensity modulation for negative phase contrast^[2]. The electron microscopes equipped with these correctors then have a resolution imaging on the atomic scale. These microscopes can operate between 80 kV and 300 kV.

TEM analysis were performed using an High Resolution Transmission Electron Microscope (HRTEM) at the *Universitat Autònoma de Barcelona*. A JEOL JEM-2011 microscope equipped with LaB₆ tungsten filament as the electron source operating at an accelerating voltage of 200 kV was used. With this technique the size distributions of Au clusters were obtained by measuring the diameter of at least 40 metal clusters. To this end the programme *Gatan Digital Micrograph* was used. The mean particle diameter was determined by calculating the arithmetic mean of the particles diameter measured.

The aberration-corrected HRTEM analyses were carried out by Dr. Alvaro Mayoral at the *Advanced Microscopy Laboratory* at the *Instituto de Nanociencia de Aragón*. A TITAN3 microscope with an accelerating voltage of 80 kV was used. This microscope was used to observe the existence of isolate Au atoms, atomic clusters (Au_n, n ~ 2-3), clusters or the three populations on the supports' surface.

Samples were prepared by depositing a drop of the catalyst suspension on a Lacey Carbon 400 Mesh Cu grade which was left to dry.

2.2 SCANNING ELECTRON MICROSCOPY (SEM)

The principle employed by the SEM is similar to that of the TEM. Figure 22 shows a schematic representation of the column of a scanning electron microscope. An electron gun emits electrons through the column and the electron beam is focused by a series of lenses. After passing through the final lens, the electrons come in contact with the sample and secondary electrons, backscattered electrons and characteristic X-rays will be generated from the sample surface and received by the different detectors^[6]. Depending on the type of emitted electrons that are desired to be detected, different types of detectors are used.

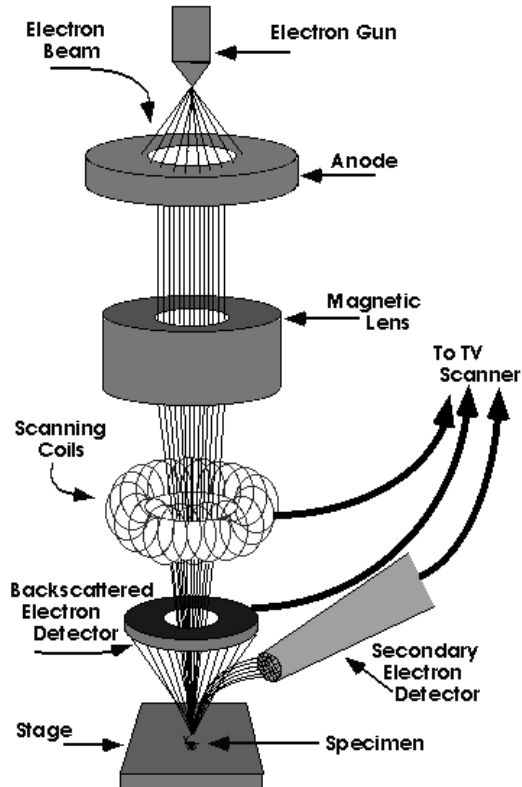


Figure 22. Schematic outline of a Scanning Electron Microscope^[7].

Moreover, if the sample is non-conducting, there can be a charge effect. If the amount of electrons that reaches the sample is higher than the amount of electrons that leave the sample by diffusion to ground the sample becomes negatively charged. This charge creates an electric field which can affect the incidence beam consequently leading to distortions in the image. When the sample is conducting, this charge effect will not be noticed at high voltage. In order to avoid this effect at high voltage usually non-conducting samples are coated with carbon or gold and thus a good conducting surface is obtained. This effect can also be overcome by using low voltage, which has the advantage of maintaining the original specimen surface.

SEM measures were carried out at the *Centre de Recerca en Nanoenginyeria* of the *Universitat Politècnica de Catalunya* using a Zeiss Neon 40 microscope equipped with a field emission gun.

SEM was used to analyse the catalysts with bigger Au nanoparticles ($d > 10$ nm) and to observe the increase of the Au particle size of catalysts used in reactions. Samples were prepared by dropping 10 μL of the catalyst suspension in a 3 mm x 3 mm silicon wafer. This was then washed with mili-Q water and dried with compressed air.

SEM images were obtained using an accelerating voltage of 2.0 kV (MWCNTs) or 5.0 kV (CeO_2) and the *InLens* secondary electron detector with a working distance (WD) of about 4.0 mm and an aperture size of 10 μm .

2.3 ATOMIC FORCE MICROSCOPY (AFM)

Atomic force microscopy is a technique that allows the analysis and characterisation of samples from the microscopic level (100 μm - 1 μm) to the nanometer scale. It is also a very versatile technique since it allows the analysis of insulators, semiconductors or electrical conductors. This technique is complementary to the SEM and HRTEM characterisation. Indeed, despite not

providing a real image of the sample, it is very useful to characterise its surface since the electron beam, which could modify the surface, is not used.

The AFM works using a fine sharp tip that is placed at the end of a cantilever (Figure 23). This technique is based in the measure of interaction forces between the tip and the sample. Different forces between the tip and the sample surface will deflect or bend the cantilever. The position of the cantilever is usually measured using a laser beam that impacts the back of the cantilever and is reflected to a position-sensitive photodetector (PSPD) (Figure 23). As the cantilever deflects the position of the laser beam on the detector shifts. The measured deflections are processed by imaging software and a map of the sample surface topography is obtained. Topography images can be obtained using different scanning modes, namely non-contact, contact mode or tapping can be applied. The tapping mode, employed in this work, basically consists of vibrating the cantilever tip. In this mode, the tip oscillates in a way it barely hits the sample and the surface topography image is obtained by measuring the differences of amplitude resulting from the tip to sample spacing^[8].

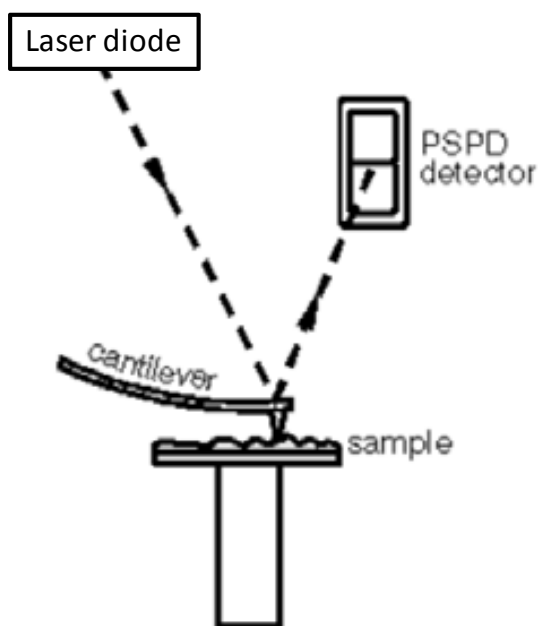


Figure 23. Schematic representation of an AFM^[8].

AFM measures were carried out at the *Centre de Recerca en Nanoenginyeria* of the *Universitat Politècnica de Catalunya*. This technique was used to investigate the size of the ex-situ synthesised Au nanoclusters. Size distributions were obtained by measuring at least 100 clusters using the *WSxM 5.0 Develop 6.0* program. The mean particle diameter obtained corresponds to the arithmetic mean of all the measured values.

A VEECO Dimension 3100 atomic force microscope and a Nanosensors PPP-NCHR-50 silicon tip were used. Topography images were collected using the tapping mode and a scan rate between 1.0 Hz and 2.0 Hz. Parameters, such as amplitude and proportional and integral gains were adjusted during the image formation.

The samples were simply prepared by depositing a drop of the ex-situ synthesised Au clusters suspension in a square of approximately 1 cm x 1 cm of freshly cleaved mica surface.

2.4 X-RAY PHOTOELECTRON SPECTROSCOPY (XPS)

XPS is a surface analysis technique that allows us to know the oxidation state of surface species and their concentrations^[9]. The XPS spectrum is obtained by irradiating the sample surface with a beam of X-rays (Figure 24). The X-rays penetrate the sample to a depth of about 2 nm - 5 nm. Consequently, some photoelectrons are more easily released presenting kinetic energies characteristic of their elements. The number of electrons that escape from the surface and their kinetic energy are measured. Other electrons will have a lower energy and contribute to the spectrum noise signal, because they come from the inner layers and collide with electrons of the upper layers.

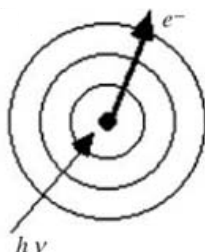


Figure 24. Schematic outline of a XPS.

XPS measures were carried out by Montserrat Domínguez at the *Centre de Recerca en Nanoenginyeria* of the *Universitat Politècnica de Catalunya*.

XPS characterisation was used to identify the oxidation state of the Au clusters synthesised. The measures were carried out using a SPECS Phoibos 150 MCD-9 detector, an X-ray source XR-50 (Mg/Al twin anode) at 100 W. Spectra were acquired at room temperature.

The data obtained was treated using the program *CasaXPS*. Binding energy (BE) values were referenced to C1s (284.5 eV when using MWCNTs as support or 284.8 eV for TiO₂ and CeO₂ catalysts^[10]).

Samples were prepared by simply depositing approximately 3 mL of the catalyst suspension on a Mo sample holder. This was dried at 50 °C in a heating plate.

2.5 X-RAY ABSORPTION SPECTROSCOPY (XAS)

XAS spectroscopy gives information about the structure of the sample. Depending on the spectral region this is defined as X-ray Absorption Near Edge Structure (XANES) or Extended X-ray Absorption Fine Structure (EXAFS). This technique allows to know the chemical environment of a single element in terms of the number and type of neighbours, the interatomic distances and structural disorders. Experimentally, a synchrotron light is used as a source. The scattering process consists in focus a photon with equal or greater energy

than the edge energy. In these conditions a core electron will be extracted. When the absorbing atom is isolated, the ejected electron (photoelectron) propagates as an unperturbed isotropic wave (Figure 25A). If other atoms surround the absorber, as usually happens, these will be scattering centers of the photoelectron wave (Figure 25B). The final state of the photoelectron is the sum of the original and scattered waves. Due to the created interference, the interaction probability between core electrons and incident photons will be modified. The absorption coefficient atom (μ_X) is decreased or increased by destructive or constructive interferences respectively. This interference phenomenon for a given energy of the photoelectron depends on the distance between emitting and scattering atoms and their atomic numbers^[11].

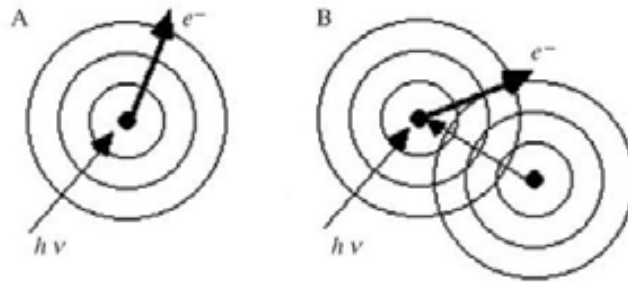


Figure 25. Schematic representation of scattering processes^[11].

The EXAFS signal $\chi(k)$ is defined as a function of the wave vector k and given by the Equation 11. The signal is normalised by dividing it by μ_{1X} . The peaks obtained in an EXAFS spectrum are assigned to different bonds that the atom can exhibit in the sample.

$$\chi(k) = \frac{\mu_X - \mu_{1X}}{\mu_{1X}} = \frac{\mu_X}{\mu_{1X}} - 1 \quad (11)$$

where,

μx - experimental absorption coefficient (directly proportional to the probability of absorption of one photon and decreases with the increase of energy).

μ_{1x} - intrinsic atomic absorption coefficient.

Measures of Au/MWCNTs catalysts were carried out by Dr. Gemma Guilera at the *Trieste Elettra-Synchrotron Light Facility* at Italy.

XAS measures were performed in order to characterise the type of neighbours of the Au atoms of the in-situ Au/MWCNTs catalysts. These measures give the information about the existence of only metallic Au or the existence of isolated Au atoms simply bonded to low molecular weight atoms.

XAS data at the Au L₃-edge (11919 eV) was collected on the XAFS beamline. The storage ring operated at 2 GeV electron energy with a current of 300 mA. A Si (111) crystal was used in the double crystal monochromator. To eliminate higher harmonics this crystal was detuned to 30% of the intensity. The X-ray absorption measures were carried out at room temperature using the fluorescence mode. The fluorescence signal was obtained using a Ketek silicon drift's detector. The incident x-rays were recorded using an ion chamber with the optimal gas. Solid samples were used as pressed pellets. Spectra of these samples were also recorded in transmission mode. Fluorescence measurements of the Au/MWCNTs catalyst were very long (9 hours). Nevertheless, the data quality was not enough for the EXAFS' data quantification. As such a qualitative approach was carried out and the EXAFS' signal was inspected within a wave number range of 3.6-9.6 Å⁻¹. The *VIPER* program was used to data treatment.

2.7 THERMOGRAVIMETRIC MEASUREMENTS (TGA)

Thermogravimetric Analyses (TGA) consists in determining the samples' weight variations in a certain range of temperatures and atmosphere. This

technique consists in a continuously following of the sample weight on a sensitive balance as the temperature is increased in air or in an inert atmosphere. Results are represented in a weight (%) vs temperature graphic. At lower temperatures the weight loss might result from the evaporation of residual moisture or solvent.

TGA measures were carried out at the *Departament de Física i Enginyeria Nuclear* of the *Universitat Politècnica de Catalunya*.

TGA was used to identify the temperature of decomposition of bare MWCNTs. Measures were carried out using a thermobalance TA Instruments Q50 TGA. Approximately 9 mg of the solid sample was deposited in the crucible of Pt. The parameters used in the measures are presented in the Table 9.

Table 9. Parameters used for the TGA measures

Flow rate (mL/min)	50
Ramp	5 °C/min
Temperature range (°C)	25-900
Atmosphere	Air

2.8 SURFACE AREA MEASUREMENTS

The specific surface area of a powder can be calculated by the Brunauer-Emmett-Teller (BET) equation (Equation 12). This technique is based on the physical adsorption of a gas on the solid surface. Surface area is determined by calculating the amount of the physical adsorbed gas on a monolayer on the surface of the solid by a continuous flow procedure. This analysis is usually carried out at liquid nitrogen temperature. In order to obtain the surface specific area of the solid, the experimental data is treated according to the BET adsorption isotherm equation (Equation 12)^[12].

$$\frac{1}{\left[V_a \left(\frac{P_0}{P} - 1 \right) \right]} = \frac{C-1}{V.C} \times \frac{P}{P_0} + \frac{1}{V.C} \quad (12)$$

where,

P - partial vapour pressure of the adsorbate gas in equilibrium with the surface at -195.75 °C, in Pa.

P_0 - saturated pressure of the adsorbate gas, in Pa.

V_a - volume of gas adsorbed ($T = 0$ °C $P = 1$ atm), in mL.

V - volume of gas adsorbed ($T = 0$ °C; $P = 1$ atm), in mL.

C - dimensionless constant related with the enthalpy of adsorption of the adsorbate gas on the powder sample.

Representing $\frac{1}{\left[V_a \left(\frac{P_0}{P} - 1 \right) \right]}$ in function of $\frac{P}{P_0}$ a linear straight line is obtained

(at least 3 points are required and the correlation coefficient, r^2 , must be higher than 0.995). From this linear correlation the values of V_m and C are determined. The specific surface area S can then be calculated according to the Equation 13^[12].

$$S = \frac{V.N.a}{V_m \cdot m} \quad (13)$$

where,

S - specific surface area of the solid, in m²/g.

N - Avogadro number (6.022×10^{23} mol⁻¹).

a - effective cross-sectional area of one adsorbate molecule (0.162×10^{-18} m² for N₂).

m - mass of the analysed powder, in g.

V_m - molar volume of an ideal gas at 1 atmosphere of pressure and 0 °C ($V_m = 22400 \text{ mL/mol}$).

The measures were carried out by Meritxell Molmeneu at the *Laboratori de Nanotecnologia de Biomaterials* of the *Universitat Politècnica de Catalunya*.

Using this technique the surface area of the different supports, namely MWCNTs, TiO₂ and CeO₂, was obtained. Around 150 mg of powder was used. The measures of the solid supports were carried out under N₂ at -196.3 °C (equilibration interval: 10 s). A surface area and porosity Micromeritics ASAP 2020 analyser was used.

2.9 INDUCTIVELY COUPLED PLASMA-OPTICAL EMISSION SPECTROSCOPY (ICP-OES)

ICP-OES is the measurement of light emitted by elements in a sample introduced into an ICP source. It is a very precise chemical elemental analysis allowing the detection of metals and non-metals at very low concentrations (ppm). Another advantage of this technique is its ability to measure several elements simultaneously unlike atomic absorption spectroscopy. This complex technique combines a high temperature ICP source with an optical emission spectrometer.

Briefly, firstly if the sample is solid a particular preparation is required. In this phase, the solid sample is dissolved by wet digestion. The wet digestion is used to oxidise the organic matter of the samples or to extract the present metals from inorganic matrices^[13]. This is carried out by mixing the solid sample with a specific concentrated acid mixture. Depending on the solid composition different acid mixtures are used^[13]. Generally, HNO₃, HCl, H₂SO₄, H₃PO₄ are used as acids. Notice that the wet digestion is simply one of the methods of preparing the sample. Other procedures of sample preparation, depending on the sample

nature, are also carried out^[13]. Once the metals are separated from the sample matrices, using the ICP source (argon plasma, 8000 °C – 10 000 °C), the complete atomization of the sample is achieved producing characteristic optical emissions at different wavelengths. The real elemental concentration of the sample is obtained by comparing the measured emission intensities to intensities of standards of known concentration^[14].

Measures were carried out by Susanna Mas at the *Centres Científics i Tecnològics* of the *Universitat de Barcelona*.

This analysis was performed in order to know the real content of gold in Au/MWCNTs in-situ synthesised catalysts. In this way, a relation between the nominal gold content and the real one was obtained.

Experimentally, 25 mg of the Au/MWCNTs solid catalysts were dissolved in 8 mL of aqua regia in a millstone reactor. This mixture was heated up to 200 °C (ramp: 20 °C/min) and left at this temperature for 15 minutes. After cold, the mixture was filtered. The resultant solid filtered was washed and re-dispersed in a 100 mL of thiourea – SC(NH₂)₂ (200 ppm in 1 v/v% HCl). After this pre-treatment to extract the metal of interest of the solid catalysts, the real quantity of Au was obtained using a simultaneous ICP-OES optical emission spectrometer Perkin Elmer Optima 3200 RL.

2.10 REACTION SYSTEMS

2.10.1 SONOCHEMICAL SYNTHESIS OF Au NANOCCLUSERS

The last step of ex-situ synthesised Au nanoclusters synthetic protocol presented in Chapter 4 consists in the Au-PMAA solution sonication in order to form the Au nanoclusters. The solution was sonicated during 20 minutes under a N₂ atmosphere in a refrigerated cell using 100 W of power. This process was carried out at the *Centre de Recerca en Nanoenginyeria* of the *Universitat*

Politécnica de Catalunya. Figure 26 shows the equipment used to achieve this goal. Firstly, the cell where the solution is placed is cooled down to approximately 0 °C. For this, a reflux of the refrigerated fluid (ethylene glycol) is passed continuously by the external walls of the cell. The temperature set point of the fluid temperature (-10° °C) is selected using the refrigeration bath controller. Then, in order to have a deaerated atmosphere, a low flow of N₂ from the network is inserted in the compartment where the solution will be placed. Finally, the Au-PMAA solution is put in the refrigerated cell and the cell is attached to the sonicator tip (Branson 2500) (the tip is not visible in Figure 26 because it is inside the cell). The power (100 W), maximum security temperature of the tip (60 °C) and the sonication time (20 minutes) are manually selected using the sonicator controller.

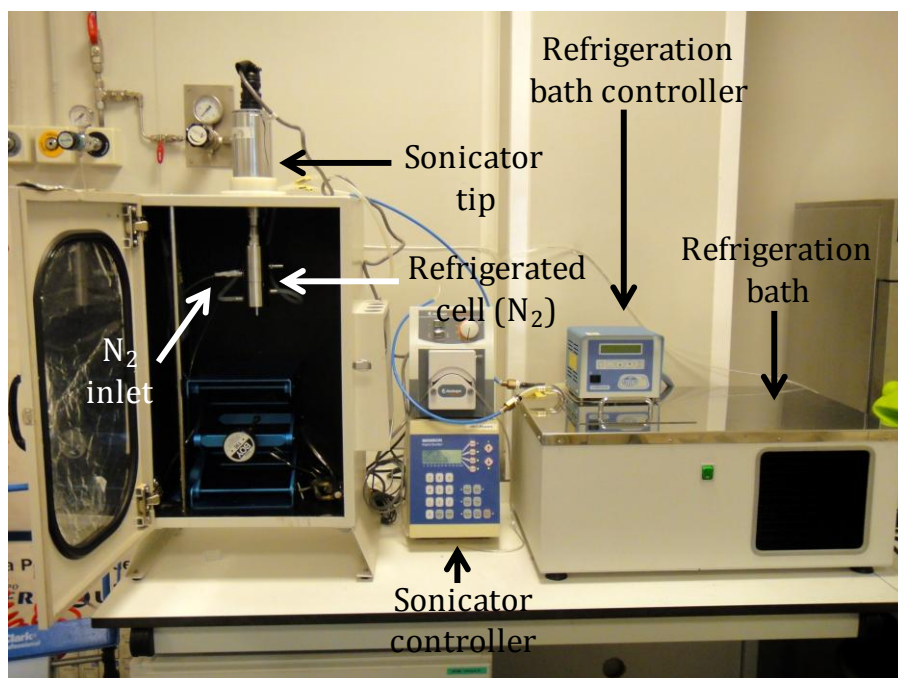


Figure 26. Sonochemical synthesis in a refrigerated cell.

2.10.2 CO OXIDATION

Figure 27 shows a simplified chemical engineering draw of the reaction system used to test the catalytic activity for CO oxidation (Chapter 3 and Chapter 4). These catalytic activity tests were carried out at the *Goldemar Solutions* company located at the *Parc Científic de Barcelona*.

The reaction is carried out in a commercial *Microactivity-Reference* reactor from PID Eng&Tech^[15]. Firstly, the solid catalyst is placed in a quartz reactor with a diameter of 0.92 cm and 32 cm of length. The catalyst is placed between two layers of quartz wool (Figure 27) in order not to contaminate the reactor porous plate and to avoid the formation of preferential pathways when the gases arrive to the catalyst. Then, the height of the catalytic bed is measured and the thermopar is introduced into the reactor to better control the temperature at the catalyst position. After these steps, the reactor is introduced in the oven, which is placed in a hot box like the rest of the system. Then, the sequences of temperatures and gases' flows desired are programmed by computer using the program *Process@*. Once it is ensured that all the system valves are opened and that there is pressure in the line, the gases controlled by mass flow controllers (Bronkhorst, $\pm 1\%$ of full scale accuracy) are introduced in the system and pass through a series of valves. Once the gases' flow is stabilised, the gases pass through the catalyst entering from the top of the reactor. The exit of the reactor is connected to a 7820A Agilent gas chromatograph (GC-MS), where the reactor outlet gases' flows are analysed, using the software *Enhanced Data Analysis*. In order to better control the quantity of the contaminant that is pretended to eliminate (CO), the reaction is alternated with by-pass, i.e. analysis of the gases quantity before entering the reactor. By-pass analyses can be carried out due to the 6 way valve existent in the system. The pressure of the system is usually in the range of 0.1 bar - 0.2 bar.

The reactions were performed using high purity N₂ 5.0 ($\geq 99.999\%$) and O₂ 5.0 ($\geq 99.999\%$) from Linde and CO (99.99%) from *Praxair*.

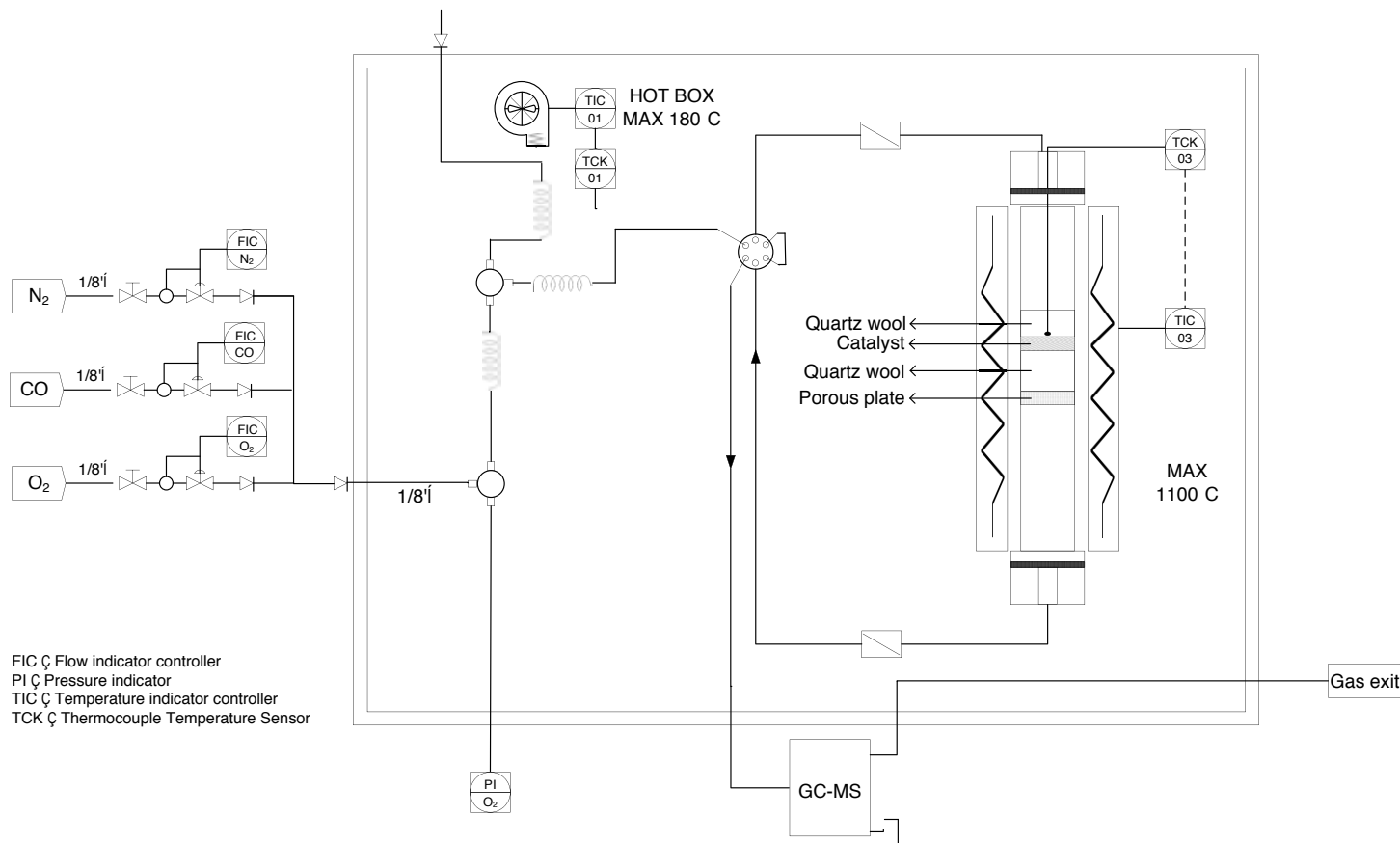


Figure 27. PID diagram of the CO oxidation reaction system.

2.10.3 CARBONACEOUS MATERIALS OXIDATION

Figure 28 shows a simplified chemical engineering drawing of the reaction system used to investigate both the effect of Au clusters in decreasing the combustion temperature of carbonaceous materials and the catalysts' activity for soot oxidation (Chapter 5). Measurements were carried out at the *Institut de Tècniques Energètiques* of the *Universitat Politècnica de Catalunya*.

The combustion was followed by temperature programmed oxidation (TPO) coupled with a mass spectrometer (mks cirrus). Temperature programmed oxidation was carried out in a commercial Catalyst Analyser BELCAT-M (BEL Japan, Inc.) equipped with a water trap and a thermal conductivity detector (TCD). The software used to collect data measurement was *Belcat* and *Process Eye Professional* for the TCD and mass signals respectively.

Firstly, the catalyst is placed in a U-tube quartz reactor with a diameter of 1.0 cm and 19.5 cm in length. Then the reactor is inserted into the furnace and a thermopar is put into the reactor in order to better control the temperature at the catalyst position. After, the flow gases (35 mL/min, 14 v/v% O₂ balanced with Ar) controlled by mass flow controllers (mks, 1% of full scale accuracy) are inserted in the top of the reactor. The flow is left to stabilise at room temperature and the desired ramping temperature sequence is programmed by computer using the program *Belcat*. Once the flow of gases is stable, the reactor is heated from 30 °C to 900 °C (ramp temperature: 5 °C/min). When reaching the maximum temperature of the ramp, i.e. at the end of the reaction the reactor starts to cool down to room temperature.

Reactions were performed using high purity Ar 5.0 (≥ 99.999 %) and O₂ 5.0 (≥ 99.999 %) from Linde.

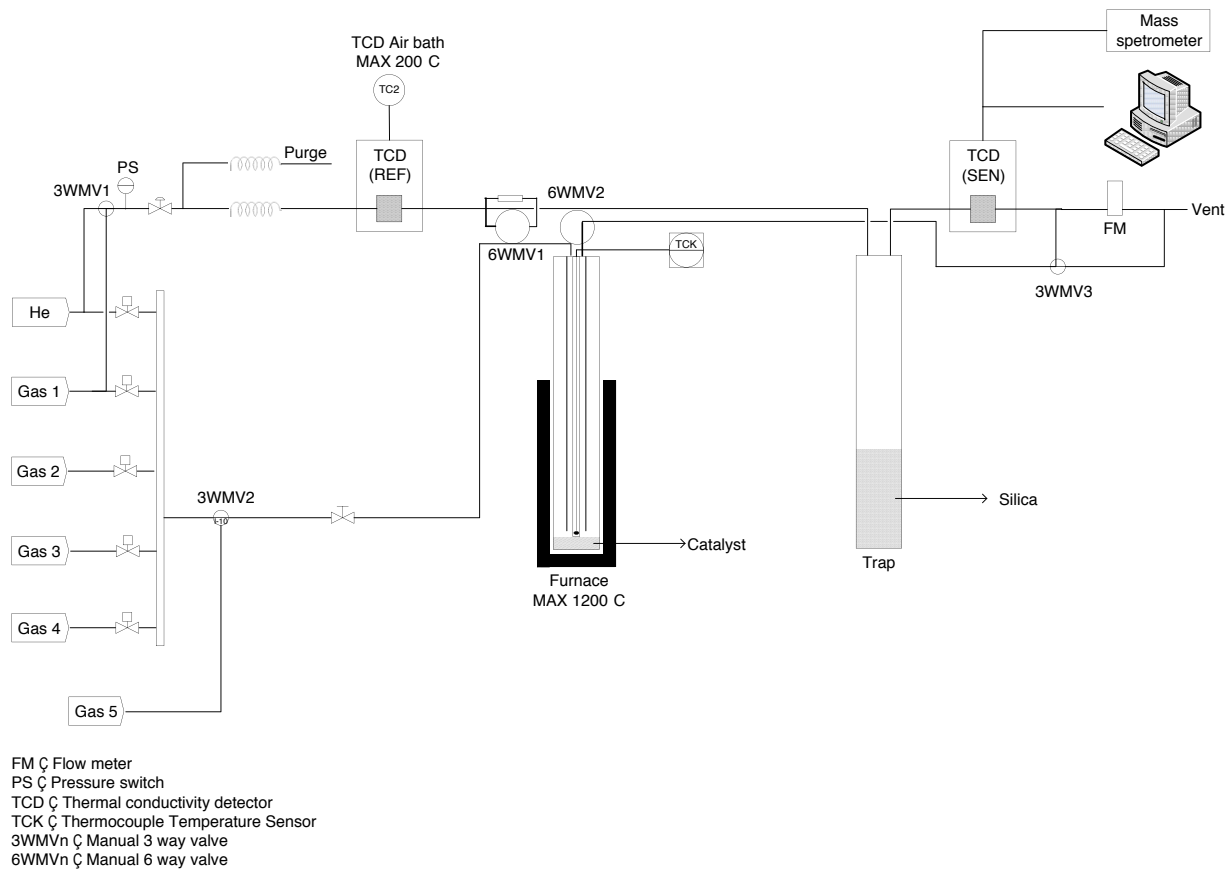


Figure 28. PID diagram of the TPO measures reaction system.

2.11 REFERENCES

- [1] C. Dickinson, PhD Thesis, *Metal Oxide Porous Single Crystals and other nanomaterials: An HRTEM study*, University of St. Andrews **2007**, available on-line: <http://hdl.handle.net/10023/217>.
- [2] M. Lentzen, *Microscopy and Microanalysis* **2006**, 12, 191-205.
- [3] O. Scherzer, *Journal of Applied Physics* **1949**, 20, 20-29.
- [4] H. Rose, *Optik* **1990**, 85, 19-24.
- [5] M. Haider, H. Rose, S. Uhlemann, E. Schwan, B. Kabius, K. Urban, *Ultramicroscopy* **1998**, 75, 53-60.
- [6] <http://wings.buffalo.edu/faculty/research/scic/sem-eds.html>, consulted 24/02/2014.
- [7] <http://www.purdue.edu/rem/rs/sem.htm>, consulted 24/02/2014.
- [8] R. Howland, L. Benatar, *A practical guide to scanning probe microscopy*, ThermoMicroscopes **2000**.
- [9] J. L. Figueiredo, F. R. Ribeiro, *Catálise Heterogénea*, 2nd edition, Fundação Calouste Gulbenkian **2007**.
- [10] T. I. T. Okpalugo, P. Papakonstantinou, H. Murphy, J. McLaughlin, N. M. D. Brown, *Carbon* **43** **2005**, 153-161.
- [11] G. Vlaic, L. Olivi, *Croatica Chemica Acta* **2004**, 77 (3), 427-433.
- [12] <http://particle.dk/methods-analytical-laboratory/surface-area-bet/surface-area-bet-theory/>, consulted 24/02/2014.
- [13] M. Welna, A. Szymczycha-Madeja, P. Pohl, *Quality of the Trace Element Analysis: Sample Preparation Steps*.
- [14] <http://www.elementalanalysis.com/services/inductively-coupled-plasma-icp/>, consulted 13/02/2014.
- [15] <http://www.pidengtech.com/thereference.html>, consulted 12/02/2014.

CHAPTER 3:

**IN-SITU SYNTHESIS OF GOLD
CLUSTERS AND CATALYTIC
ACTIVITY STUDY**

3.1 SYNTHETIC PROTOCOL

A synthetic protocol where gold clusters ($d < 2$ nm) are directly synthesised and stabilised onto different surfaces is presented (in-situ). The materials used as support were: commercial multiwalled carbon nanotubes (MWCNTs) (3100 – Thin Multiwalled Carbon nanotubes from Nanocyl), titanium oxide (TiO_2) and cerium oxide (CeO_2).

The titanium oxide powder was prepared using as precursor titanium (IV) isopropylate (MW = 284.2 g/mol; $\text{C}_{12}\text{H}_{28}\text{O}_4\text{Ti}$; Alfa Aesar) which was firstly dried at 80 °C and then at 120 °C and finally was calcined at 400 °C during 2 hours (ramp temperature: 2 °C/min).

The CeO_2 was synthesised using 0.1 M cerium (III) nitrate hexahydrate (MW= 434.2 g/mol; $\text{Ce}(\text{NO}_3)_3 \cdot 6\text{H}_2\text{O}$; Sigma-Aldrich) and 1 M ammonia (MW= 17.0 g/mol; NH_3 ; Chem-Lab NV) aqueous solutions. The procedure consisted of adding the 0.1 M $\text{Ce}(\text{NO}_3)_3 \cdot 6\text{H}_2\text{O}$ dropwise to the 1 M NH_3 stirring solution until it reached pH=9 at room temperature. Then, this solution was left stirring aging for 1 hour at room temperature. After wash and filtration with mili-Q water, the resultant filtered was dried at 80 °C overnight. Finally, a calcination at 600 °C during 2 hours (ramp temperature: 2 °C/min) was carried out.

The synthesis method presented here was patented in 2009^[1]. It claims the synthesis of subnanometric Au particles ($d < 3$ nm) on a surface covered by amine groups. This method is very simple, allows a high level of control of the Au particle size and is easily scaled-up.

Experimentally, the method consists of firstly, the coating of the support by a polymer with amine groups. In this work, polyallylamine hydrochloride (PAH) (MW ~ 15000 g/mol; $(\text{C}_3\text{H}_8\text{ClN})_n$; Aldrich) (Figure 29) was used as the wrapping agent driving the gold clusters' stabilisation on the support surface.

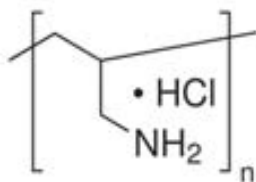


Figure 29. Polyallylamine hydrochloride basic structure.

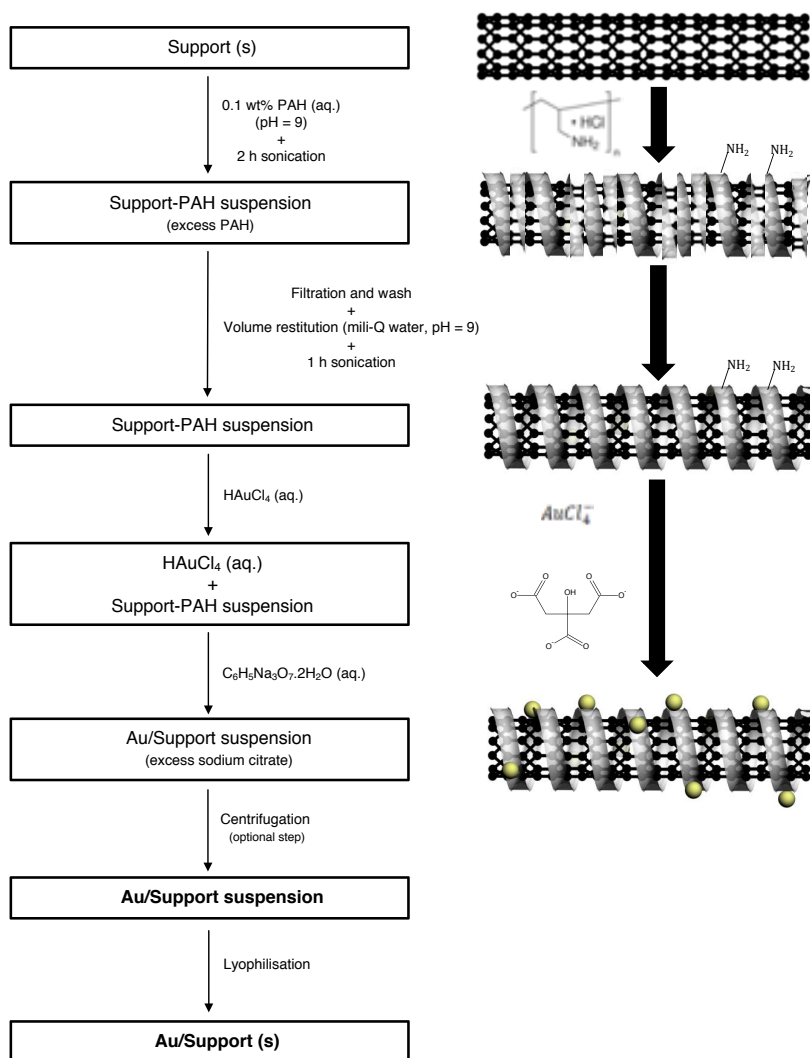


Figure 30. In-situ synthesis procedure (left) and respective schematic representation using MWCNTs as support (right).

Then, by reducing the gold precursor (chloroauric acid, MW = 339.79 g/mol; HAuCl_4 ; Sigma Aldrich) with sodium citrate (trisodium citrate dihydrate, MW = 394.1 g/mol; $\text{C}_6\text{H}_5\text{Na}_3\text{O}_7 \cdot 2\text{H}_2\text{O}$; Sigma-Aldrich), uniformly sized gold clusters were formed on the support-PAH hybrid surface as schematically represented in Figure 30 using MWCNTs as support. The different steps of the synthesis procedure are presented in Figure 30.

Firstly, the preparation of the support-PAH solution consisted of dispersing the support in a 0.1 wt% aqueous solution of PAH with pH=9 – 1 mg of support / 1 mL of 0.1 wt% PAH (aq.) (Figure 30). The polyelectrolyte solution pH was obtained by adding to it an aqueous solution of 1.25 M sodium hydroxide (MW = 40 g/mol; NaOH, Sigma-Aldrich). In order to obtain a homogeneous dispersion and to ensure the individual suspension of the support material, the support-PAH solution was then ultrasonicated during two hours in an ice bath at 100 W (the sonication was carried out using a Branson 2500 sonicator tip). The amine groups of the polymer that cover the support surface act as nucleation centers where the gold clusters' will reduce, stabilise and anchor (Figure 30).

Because an excess of polymer would inhibit the catalytic activity either by decreasing the metal-support interaction or by covering the Au active sites, this was removed by filtration after the two hour sonication of the support with the PAH aqueous solution (Figure 30). Using MWCNTs, when this polymer was in excess a large layer of PAH (~ 9 nm) was observed on their surface (Figure 31a). This would surely impede the contact between the Au cluster and the support's surface and/or cover the catalyst active sites and consequently decrease the catalytic activity. Indeed, the inhibition of the catalytic activity due to the lack of the Au-support interaction was demonstrated in propene epoxidation^[2]. According to these authors the activity of a Au-Cu/TiO₂ catalysts was significantly enhanced after a 400 °C calcination (up to 1.4 higher conversion of propene was obtained). This enhancement of activity resulted from the large alloy (Au-Cu)-support interaction that was formed at this temperature. Using this calcination temperature a small particle size (5-6 nm)

was maintained as well as the nature of the alloy surface. As the particle size remained small, the better contact with the support results in a higher number of active sites at the perimeter of the contact area between the alloy nanoparticles and TiO_2 (Section 1.2.2, Figure 6)^[2].

After the filtration and wash with mili-Q water the support-PAH was re-suspended in mili-Q water at pH=9 (Figure 30). This aqueous solution was finally ultrasonicated for one hour in an ice bath at 100 W. The PAH layer on the MWCNTs surface decreased to around 1 nm after this process (Figure 31b).

When using TiO_2 or CeO_2 as support, the removal of the excess of PAH was carried out by centrifugation (twice: 6000 rpm; 10 °C; 30 minutes). Due to their fine particle size these cannot be filtered.

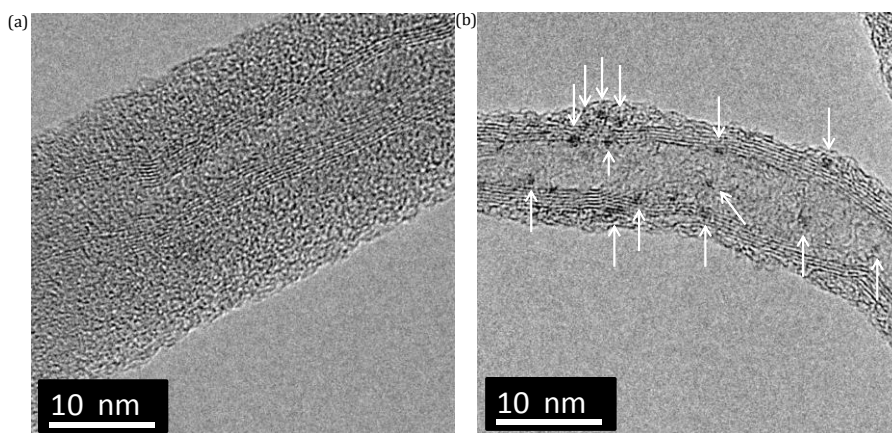


Figure 31. HTREM images of unfiltered (a) and filtered (b) MWCNTs. In image (b) the dark dots are Au clusters.

Once the support-PAH solution was prepared, the synthesis of the Au on the support surface was carried out. This consisted of adding the desired volume of the gold precursor (HAuCl_4) to the support-PAH suspension (Figure 30). An aqueous solution of the reducing agent sodium citrate was then added to this solution (Figure 30). The formation of Au nanoparticles is only possible in the presence of sodium citrate which is usually applied as a stabiliser and soft reducing agent. Sodium citrate can be added in a molar relation in respect to Au

or in excess. If this is in excess, catalytic activity will be affected, since more active centers will be covered by this agent. However, once Au clusters are anchored and stabilised on the support-PAH surface, the reducing agent can be easily removed by centrifugation without Au loss (Figure 30). Finally, the powder catalyst can be obtained by lyophilisation ($P \sim 2 \times 10^{-2}$ mbar; $T \sim -74$ °C) of the suspension. The catalysts synthesised in this work are presented in Table 10.

Table 10. List of the in-situ synthesised catalysts.

Catalyst	Nomenclature	Au loading (wt%)
Au/MWCNTs	Au(0.1wt%)/MWCNTs	0.1
	Au(0.3wt%)/MWCNTs	0.3
	Au(0.5wt%)/MWCNTs	0.5
	Au(1wt%)/MWCNTs	1
	Au(3wt%)/MWCNTs	3
	Au(6wt%)/MWCNTs	6
	Au(13wt%)/MWCNTs	13
	Au(50wt%)/MWCNTs	50
Au/CeO ₂ (CeO ₂ - 74.0 m ² /g)	Au(0.1wt%)/CeO ₂	0.1
	Au(0.5wt%)/CeO ₂	0.5
	Au(1wt%)/CeO ₂	1
	Au(3wt%)/CeO ₂	3
Au/CeO ₂ (CeO ₂ - 12.0 m ² /g)	Au(0.05wt%)/CeO ₂ _12.0	0.05
	Au(1wt%)/CeO ₂ _12.0	1
Au/TiO ₂	Au(0.3wt%)/TiO ₂	0.3
	Au(1wt%)/TiO ₂	1
	Au(3wt%)/TiO ₂	3

The successful achievement of synthesise Au catalysts using different supports, namely MWCNTs, CeO₂ and TiO₂, was observed by HRTEM characterisation.

Figure 32 shows a HRTEM image of a MWCNT-PAH hybrid decorated with gold nanoclusters. The carbon atomic layers of the MWCNT and a large number of homogeneous gold clusters attached to their walls can be clearly identified. The high density and homogeneous distribution of clusters observed onto the carbon-based structures with a very reduced size was attributed to the heterogeneous nucleation at the surface of the MWCNT-PAH composite. This heterogeneous nucleation results from the presence of amine groups at the surface of the PAH coating the MWCNTs as it had been observed^[3]. Also, wrapping agents like poly(4-sulphonate) styrene (PSS) do not favour the formation of gold nanoclusters corroborating the importance of the presence of amine groups on the surface of the support^[4].

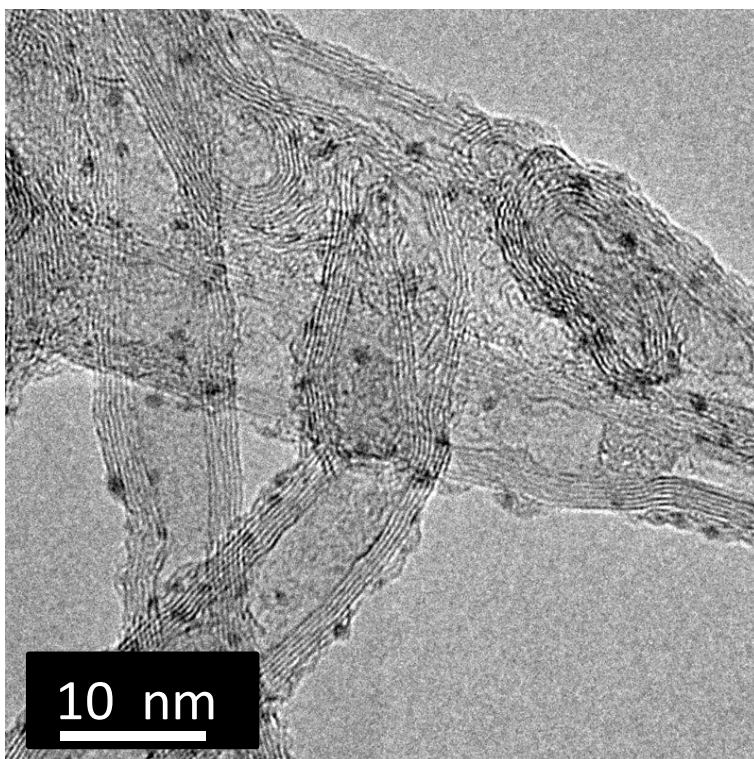


Figure 32. HRTEM image of a MWCNT decorated with gold nanoclusters using a 6 wt% nominal Au content – Au(6wt%)/MWCNTs.

A mean particle diameter of 1.1 ± 0.3 nm was obtained for a Au/MWCNTs catalyst with a nominal gold content of 6 wt% (Figure 37).

Following the same approach, Au clusters were synthesised on CeO_2 -PAH surfaces. HRTEM images showed a narrow size distribution of Au clusters and the inexistence of large nanoparticles (Figure 33). A mean particle diameter of 1.2 ± 0.6 nm was obtained using a nominal gold content of 3 wt% (Figure 42).

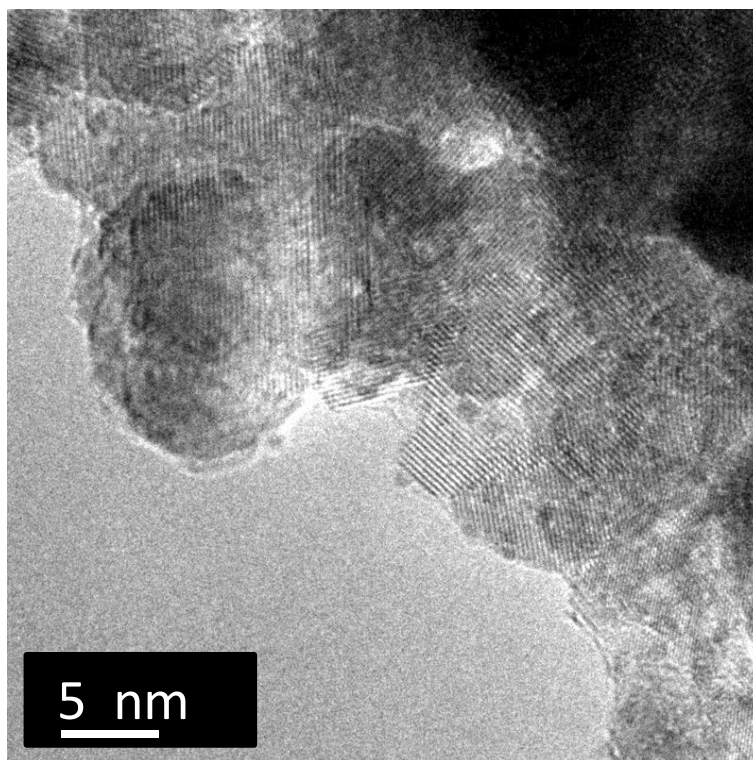


Figure 33. HRTEM image of CeO_2 decorated with gold nanoclusters using a 3 wt% nominal Au content – Au(3wt%)/ CeO_2 .

Using TiO_2 -PAH surfaces, the same result was obtained. HRTEM characterisation of Au/ TiO_2 catalysts revealed a very narrow size distribution of gold clusters anchored and well dispersed on the TiO_2 surface (Figure 34). A mean particle diameter of 1.1 ± 0.5 nm was obtained for a catalyst with a

nominal gold content of 1 wt% (Figure 44). Besides, HRTEM images did not show large gold nanoparticles.

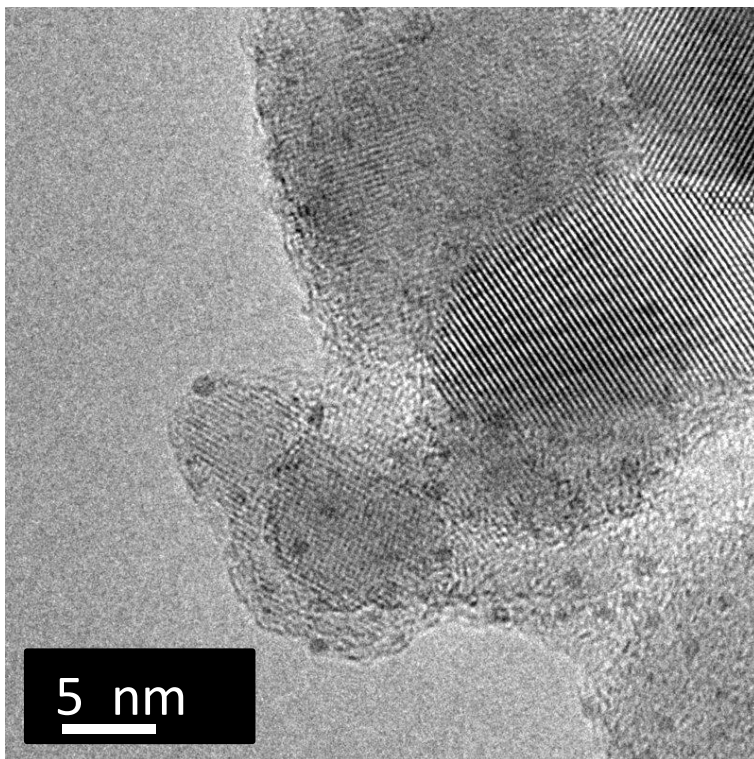


Figure 34. HRTEM image of TiO₂ decorated with gold nanoclusters using a 1 wt% nominal Au content – Au(1wt%)/TiO₂.

The successful synthesis of gold clusters on these three different surfaces demonstrated the ability of this in-situ synthesis method to be easily expanded to several other PAH coated surfaces. This result is extremely useful. In this way, the catalytic activity of these gold clusters catalysts can be properly investigated by using the most adequate support for the chemical reaction of interest.

Additionally, these results are extremely innovative since Au clusters are obtained by a clean environmental friendly and extremely simple synthetic protocol. Comparing this method with the ones developed over time to

synthesise Au/CNTs catalysts (Chapter 1, Section 1.5, Table 2) it is concluded that, definitely, this via citrate reduction method is much more clean and easy. Also, this method allows gold clusters with less than 2 nm to be obtained on different surfaces using the citrate reduction protocol. Then, innovating the first developed Turkevich method where ~ 15 nm Au nanoparticles were obtained. Furthermore, this in-situ method represents an alternative to the common used deposition-precipitation (DP) method to synthesise small metal particle size Au/CeO₂ and Au/TiO₂ catalysts. Thus, the activity of catalysts prepared by distinct synthetic protocols can be easily compared.

3.2 ICP-OES CHEMICAL ANALYSES

All the gold contents referred in this work are nominal gold contents. Considering the nominal desired Au content, the respective volume of gold precursor (HAuCl₄) aqueous solution necessary to add to the liquid support-PAH solution was calculated. In this way, and in order to access the real gold content existent in the catalysts, ICP-OES chemical analyses were carried out using MWCNTs catalysts. The catalysts were prepared using a sodium citrate/Au 1:1 molar relation.

ICP-OES measures of the Au/MWCNTs catalysts revealed that the nominal Au content is very similar to the real reduced Au loading existent in the catalysts, which indicates that all the gold precursor was reduced. The Au(0.1wt%)/MWCNTs and Au(3wt%)/MWCNTs catalysts showed a real gold content of 0.13 wt% and 3.18 wt% respectively.

3.3 Au CLUSTERS SIZE DISTRIBUTION DEPENDENCE PARAMETERS

3.3.1 NOMINAL GOLD CONTENT

Until now the most widely used method to synthesise Au/TiO₂ or Au/CeO₂ catalysts was deposition-precipitation (DP). The most active catalysts for CO oxidation have been prepared using DP^[5-8]. Indeed, several groups were able to obtain very small Au nanoparticle ($2 < d \text{ (nm)} < 5$) using this method^[9-12]. Nevertheless, the main disadvantage of the DP method is that the Au nanoparticles size significantly varies with the precursor concentration. To obtain Au clusters with 2 nm low Au loadings such as 2 wt% are required^[9]. In this context, an investigation about how the Au particle size varies with the gold content was carried out using this here developed in-situ synthesis method.

For this study, series of MWCNT-PAH hybrids were decorated with nanoclusters with different gold contents. This detailed study was centered in MWCNTs because of their high electron transparency which makes them an ideal support for HRTEM characterisation.

Figure 35 shows HRTEM images of MWCNT-PAH hybrids coated with gold nanoclusters for various nominal gold contents, namely 3 wt%, 6 wt%, 13 wt% and 50 wt%. The amount of gold clusters clearly rises when increasing the gold loading. However, this trend was not followed by the sample containing 50 wt% of gold where fewer clusters than the sample containing 13 wt% of gold were visible. In this sense, Figure 36 shows a lower magnification TEM image of the 50 wt% sample showing that, for high gold contents, small gold clusters coexist with larger nanoparticles with diameters higher than 10 nm and with gold agglomerates with approximately 50 nm - 150 nm. In this sample the increase of the amount of clusters on the support results in smaller interparticle distance which will lead to coalescence.

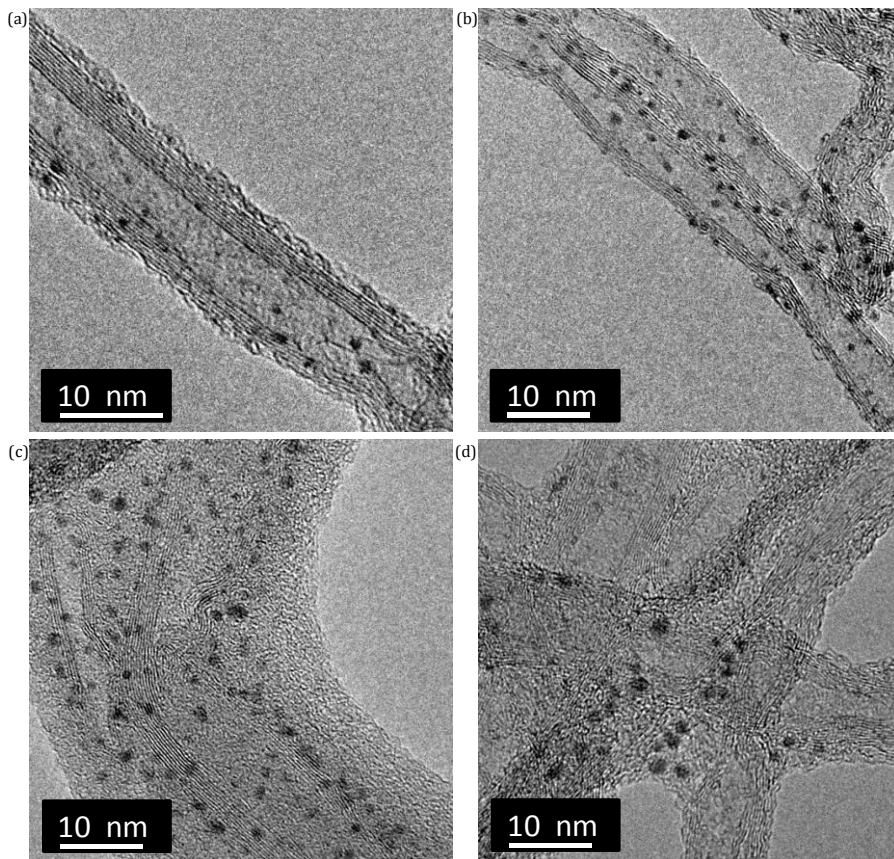


Figure 35. HRTEM images of gold clusters decorated MWCNTs with different nominal gold contents: 3 wt% (a), 6 wt% (b), 13 wt% (c) and 50 wt% (d).

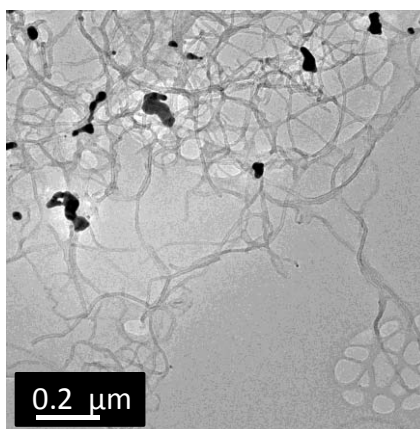


Figure 36. Low magnification TEM image of a Au(50wt%)/MWCNTs catalyst.

The particle size distribution derived from HRTEM observations is presented in Figure 37. The size distribution and mean Au particle diameter of the Au(50wt%)/MWCNTs catalyst is not shown. Due to the very different sized Au nanoparticles that coexist in this catalyst, a very high error was obtained for the mean Au particle diameter which does not represent the real value.

Firstly, notice that, as observed in the HRTEM images, the population of gold clusters has a very narrow size distribution with extremely low dispersions of the order of 0.3 nm to 0.4 nm. Secondly, a clear trend to obtain larger particles can be observed by increasing the gold content. Increasing the gold content does not only raise the amount of particles at the surface of the MWCNT but also the average size of the particles, which varies from 1.1 nm to 1.6 nm (Figure 38, Table 11).

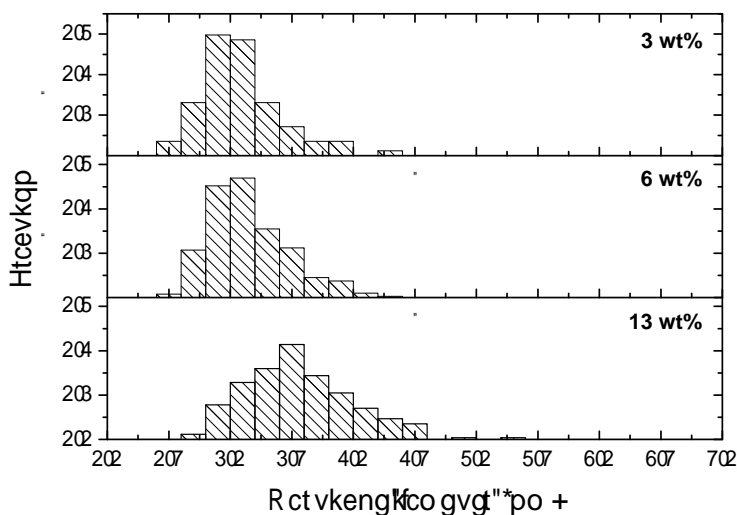


Figure 37. Particle size distribution histograms for gold clusters obtained at different nominal gold loadings on MWCNTs.

Remarkably, this method allows by simply varying the final reduced gold content from 3 wt% to 13 wt%, tailoring the gold nanoparticles size between 1.1 nm and 1.6 nm when MWCNTs are used as the support. It can then be concluded that the main advantage of this method over DP is that, even when synthesised with high gold loadings such as 13 wt%, an almost uniform

distribution of Au clusters ($d < 2$ nm) is still obtained. Nevertheless, a lower quantity of Au nanoparticles with diameters between 2 nm and 3.5 nm also coexist with the clusters population (Figure 37) which makes it preferable to use gold contents up to 6 wt%.

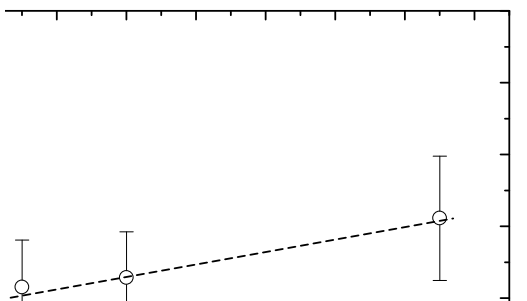


Figure 38. Dependence of the mean Au particle diameter with the Au loading for Au/MWCNTs catalysts.

Table 11. Mean particle diameter of the different gold content Au/MWCNTs catalysts.

Catalyst	Particle diameter (nm)
Au(3wt%)/MWCNTs	1.1±0.3
Au(6wt%)/MWCNTs	1.1±0.3
Au(13wt%)/MWCNTs	1.6±0.4

3.3.2 SUPPORT SURFACE AREA

Based on the previous observations and discussion, different sized gold clusters are obtained by this in-situ synthetic protocol, depending on the gold content. Nevertheless, the metal nanoparticle size is also highly dependent of the surface area of the material used as the catalyst support^[13]. A lower surface

area will lead to an easy aggregation of the Au clusters. Indeed, when using Au/TiO₂ catalysts for the CO oxidation, Moreau *et al.* concluded that the more active catalysts were those which were supported in higher TiO₂ surfaces areas^[14]. The authors explained the lower activity when using a lower support surface area by the easier agglomeration of the Au particles due to their stronger proximity favoured by the heat of the reaction. Besides if the support selected has a low surface area all the gold might not be deposited on its surface. The observed lower deactivation of the catalyst prepared with a higher support surface area was explained by the fact that the inhibiting carbonate ions formed during reaction would readily migrate from the Au neighbour to more distant places where they do not affect the activity^[14].

Li *et al.* using Au/CeO₂ catalysts for the formaldehyde oxidation also observed a significantly enhancement of the catalytic activity for higher surface area values^[13]. As it is widely known, the oxygen vacancies play a very significant role in oxidation reactions such as the CO oxidation. In this way, a higher surface area is preferable once that the relative concentration of oxygen vacancies increase with this parameter. Indeed, the higher quantity of defect sites in the high surface area CeO₂ will provide more oxygen vacancies that are able to adsorb and activate O₂. Therefore, these authors, attributed the higher catalytic activity observed when using a high CeO₂ surface area to two facts: the increase of oxygen vacancies that will lead to the formation of Au_xCe_{1-x}O_{2-γ} solid solution, on which oxygen molecules could be transformed into active species for the reaction, and the fact that the Au nanoparticles may have a strong interaction with the support and a consequently higher adsorption of the reagent on the Au particles will take place^[13].

In this context, the influence of the support surface area on the Au nanoparticle size was investigated. HRTEM characterisation allowed to conclude about the size of the Au clusters or nanoparticles formed on the different support surfaces. Firstly, the gold clusters size using gold contents of 0.3 wt% or 0.5

wt%, 1 wt% and 3 wt% was compared for each support. The surface area calculated by BET of the different supports is shown in Table 12.

Table 12. Surface area calculated by BET of MWCNTs, TiO₂ and CeO₂ supports.

Support	Surface area (m²/g)
MWCNTs	375.3
CeO ₂	74.0
TiO ₂	26.8

Using catalysts up to a 3 wt% gold content, gold clusters ($d = 1.1 \pm 0.3$ nm) were formed with a Au content of 3 wt%, when using MWCNTs as support (Figure 39). When the gold loading was decreased to 1 wt%, clusters were still present but in a smaller quantity. For this catalyst, the Au mean particle size distribution is not presented, due to the very low number of clusters observed by HRTEM. For gold contents lower than 0.5 wt%, gold clusters were not observed (Figure 39).

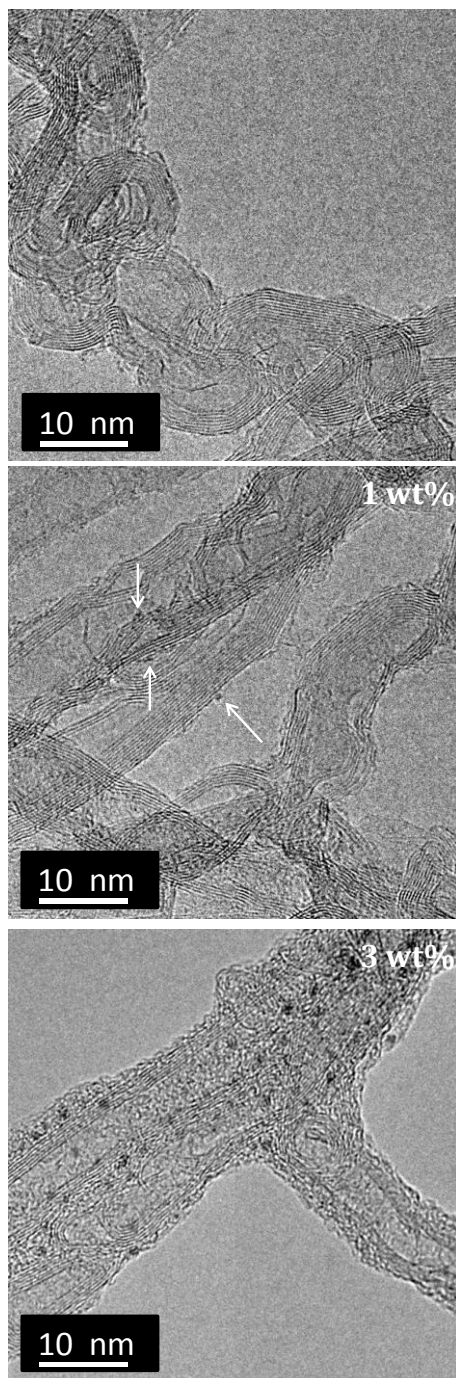


Figure 39. HRTEM images of MWCNTs decorated with gold clusters using different nominal gold loadings.

Furthermore, when comparing the number of Au clusters observed on the MWCNTs surface by HRTEM and the nominal number of Au clusters that should be observed considering that these have a mean particle diameter of 1.1 nm (~ 40 atoms), differences were observed^[15]. The nominal number of Au clusters per MWCNT was determined considering a nanotube with 100 nm of length and 10 nm of diameter with a density of 2 g/cm³^[16]. The equations used to determine this value are presented in Section A1 of Annexes (Equations 18 to 24). The nominal number of Au clusters per nanotube resultant for each Au loading is schematically represented in Figure 40.

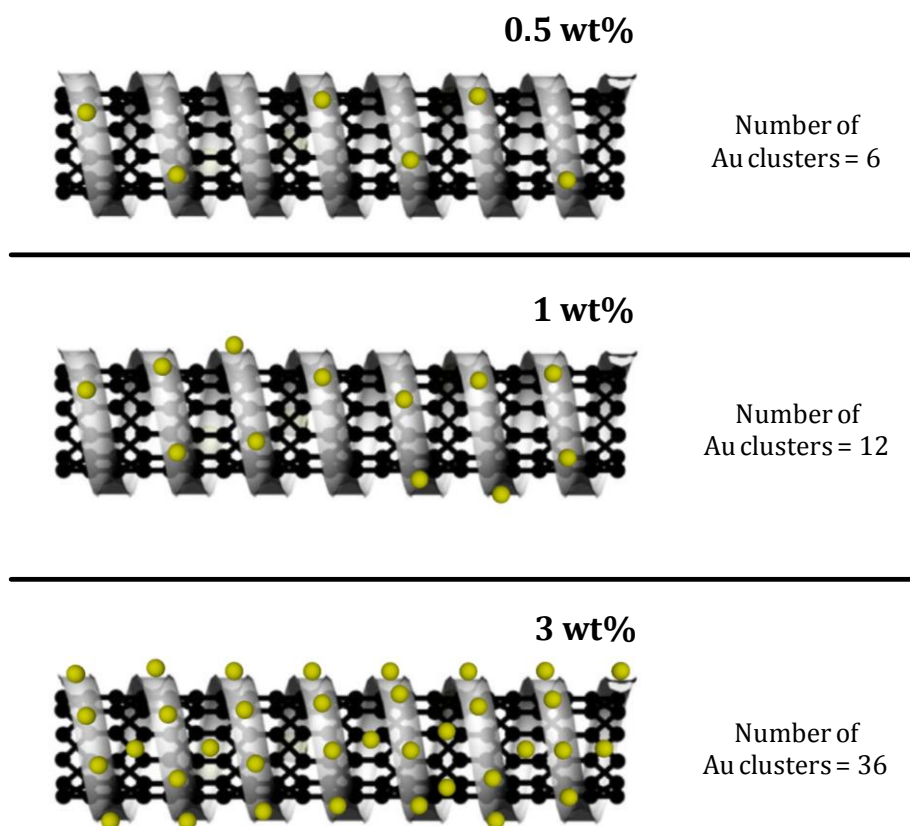


Figure 40. Nominal number of Au clusters (•; d 1.1 nm) per MWCNT for different gold contents.

It was then concluded that in the Au(3wt%)/MWCNTs catalyst, the number of Au clusters observed approximately coincides with the respective nominal number (Figure 39 vs Figure 40). Nevertheless, the same does not occur for the 0.5 wt% and 1 wt% catalysts. In these catalysts a much lower number of Au clusters exist on the MWCNTs surface when comparing to the nominal number (Figure 39 vs Figure 40). This result has left then the question about what happened to the gold in these catalysts. Thus, firstly, it was verified that, in the synthesis suspension recipient, residues were not left. Moreover, large Au agglomerates were not observed in the suspensions. Finally, ICP-OES analysis revealed that Au was not lost during the synthesis and that all the gold precursor is reduced. Thus, the inexistence of gold in the lowest Au content catalysts was discarded. In this way further characterisation of these catalysts by aberration-corrected HRTEM was carried out (Section 3.4.1). This microscope, due to its properties (Chapter 2, Section 2.1), allows the constituent elements of the catalysts to be seen in more detail.

The successful synthesis of Au clusters on MWCNTs has only been demonstrated by a few authors. Zanella *et al*, by reduction of HAuCl_4 with citric acid in propanol and consequent deposition of Au on 1,6 hexanedithiol functionalised MWCNTs achieved the formation of Au clusters with a mean diameter of approximately 1.7 nm^[17]. In the same way, Au/MWCNTs with a mean Au diameter of 1.8 ± 0.3 nm and 3.9 ± 0.9 nm were also obtained by a photoinitiated carbene addition reaction^[18]. Other reported synthesis methods lead to the formation of larger nanoparticles as it was outlined in Chapter 1 (Section 1.5, Table 2). Hence, the two major advantages of the in-situ synthesis method developed here are: the uniform and narrow size distribution of Au nanoclusters; the fact that only uses water as solvent makes it much cleaner than the others as it uses less organic reagents which might inhibit the catalytic activity.

In respect to the Au/CeO₂ catalysts, these showed a similar result to the MWCNTs (Figure 33, Figure 41). For gold loadings of 1 wt% or 3 wt%, gold clusters with a mean particle size of 1.3 ± 0.6 nm and 1.2 ± 0.6 nm were formed on the CeO₂ surface respectively (Figure 42, Table 13).

Again, gold clusters were not observed for a gold content of 0.5 wt% (Figure 41).

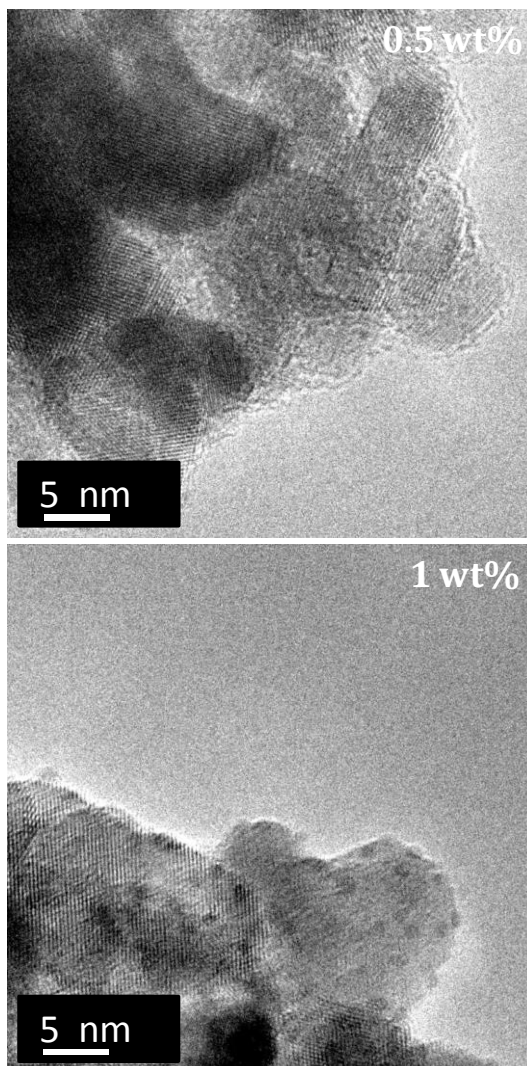


Figure 41. HRTEM images of CeO₂ decorated with gold clusters using different nominal gold loadings.

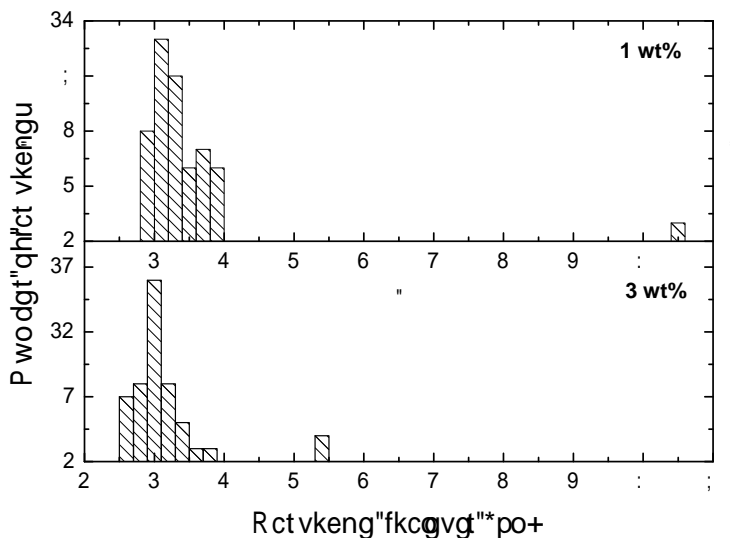


Figure 42. Particle size distribution histograms for gold clusters obtained at different gold loadings on CeO₂.

Notice that the mean particle diameter of the Au(1wt%)/CeO₂ catalyst was determined exceptionally excluding the unique Au nanoparticle of approximately 8.4 nm of diameter once that it would introduce a high error and lead to a false mean Au particle diameter value (Table 13).

Table 13. Mean particle diameter of the different gold content Au/CeO₂ catalysts.

Catalyst	Particle diameter (nm)
Au(1wt%)/CeO ₂	1.3±0.6
Au(3wt%)/CeO ₂	1.2±0.6

Based on these results, it was concluded that this in-situ synthetic protocol allows smaller Au nanoparticles on Au/CeO₂ catalysts to be obtained than either the deposition-precipitation (DP) or co-precipitation (co-P) methods commonly reported, and this represents an advantage over these common methods. Generally, by DP, Au particles around 2.5 nm were obtained using a Au loading of 0.34 wt% by Zhang *et al.*^[5]. In addition, Tana *et al.* revealed that gold loadings of approximately 3 wt% led to the formation of Au nanoparticles

with a diameter around 3.9 nm^[8]. With this in-situ method gold clusters ($d < 2$ nm) were obtained using a gold content of 3 wt%.

Finally, Au/TiO₂ catalysts (Figure 43) showed, for a nominal gold loading of 3 wt%, the coexistence of large Au nanoparticles and Au clusters. When decreasing the loading to 0.3 wt% or 1 wt%, only gold nanoclusters were observed. The particle size distributions and the respective mean particle diameter obtained for each catalyst are presented in Figure 44 and Table 14 respectively.

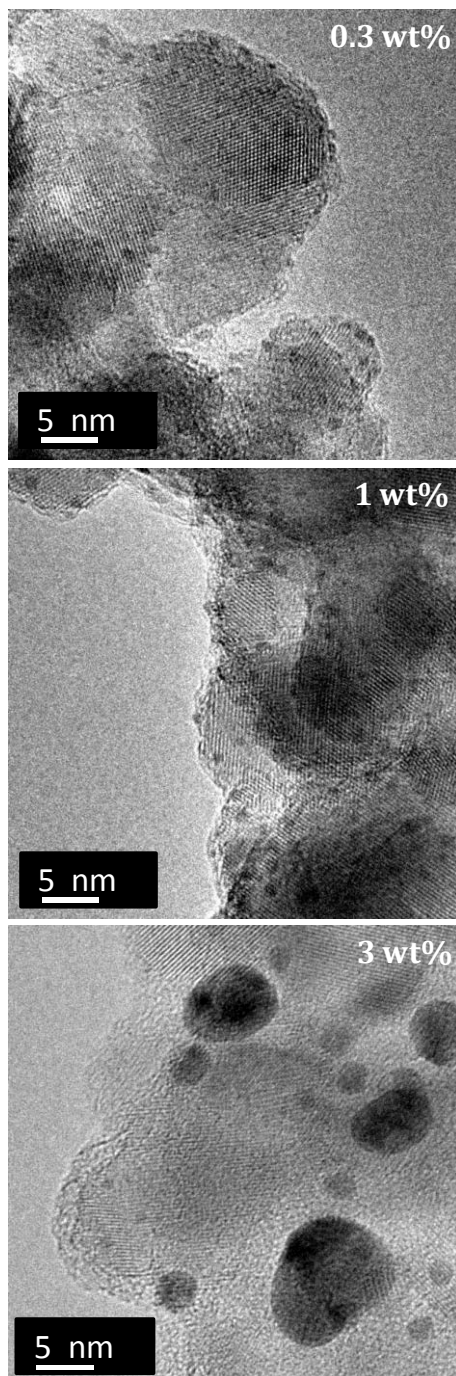


Figure 43. HRTEM images of TiO₂ decorated with gold clusters/nanoparticles using different nominal gold loadings.

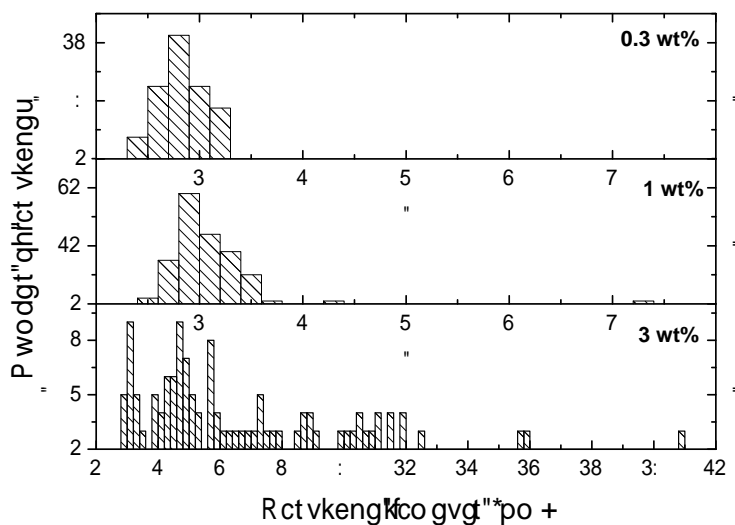


Figure 44. Particle size distribution histograms for gold clusters obtained at different gold loadings on TiO₂.

Table 14. Mean particle diameter of the different gold content Au/TiO₂ catalysts.

Catalyst	Particle diameter (nm)
Au(0.3wt%)/TiO ₂	0.8±0.2
Au(1wt%)/TiO ₂	1.1±0.5
Au(3wt%)/TiO ₂	4.6±3.4

The Au/TiO₂ catalysts showed the ability of obtaining an uniform size distribution of gold clusters up to a gold loading of 1 wt%. Nevertheless, when using higher gold contents, such as 3 wt%, a significantly increase of the mean Au particle size ($d = 4.6 \pm 3.4$ nm) was obtained, unlike the deposition-precipitation with urea (DPU) method reported by Zanella *et al.* which, at this Au loading showed a mean Au particle diameter of 2.3 nm^[9]. This poor result is a consequence of the low quality TiO₂ support used in this work. Its very low surface area (26.8 m²/g) led to the easy agglomeration of gold for Au loadings as 3 wt%, which is not that high.

The different sizes of Au observed using the same gold contents on the three supports allowed conclusions about its intrinsic dependence on this variable with the support surface area. Using the same nominal gold contents, different sized gold nanoparticles were observed, depending on the support used. For example, comparing the Au/MWCNTs and the Au/TiO₂ catalysts prepared using the same Au loading (3 wt%), different sized clusters were found (Figure 39 vs Figure 43). The Au(3wt%)/MWCNTs catalysts showed a uniform size distribution with a mean particle diameter of Au of 1.1 ± 0.3 nm and the Au(3wt%)/TiO₂ catalyst showed a larger mean particle diameter (4.6 ± 3.4 nm) due to the existence of some large Au nanoparticles with diameters between 5 nm and 10 nm. This result is in accordance with the significantly different surface areas of both supports (MWCNTs surface area is 14 times higher than TiO₂ surface area, Table 12).

Furthermore, the evidence of this dependence (surface area/Au agglomeration) was also noticed using CeO₂. Besides the synthesised CeO₂ previously referred, which presents a surface area of 74.0 m²/g, an offered CeO₂ was also used. This last has a much lower surface area (12.0 m²/g). The size of the Au nanoparticles formed on both supports, using the same nominal gold content (1 wt%), was compared (Table 15). HRTEM characterisation revealed that, on the lower CeO₂ surface area (Figure 45), large Au nanoparticles of approximately 15 nm coexist with gold clusters with a mean particle diameter of 1.4 ± 0.2 nm (Figure 46). Nevertheless, when the higher CeO₂ surface area was used only gold clusters were present on the support surface ($d = 1.3\pm 0.6$ nm) (Figure 41).

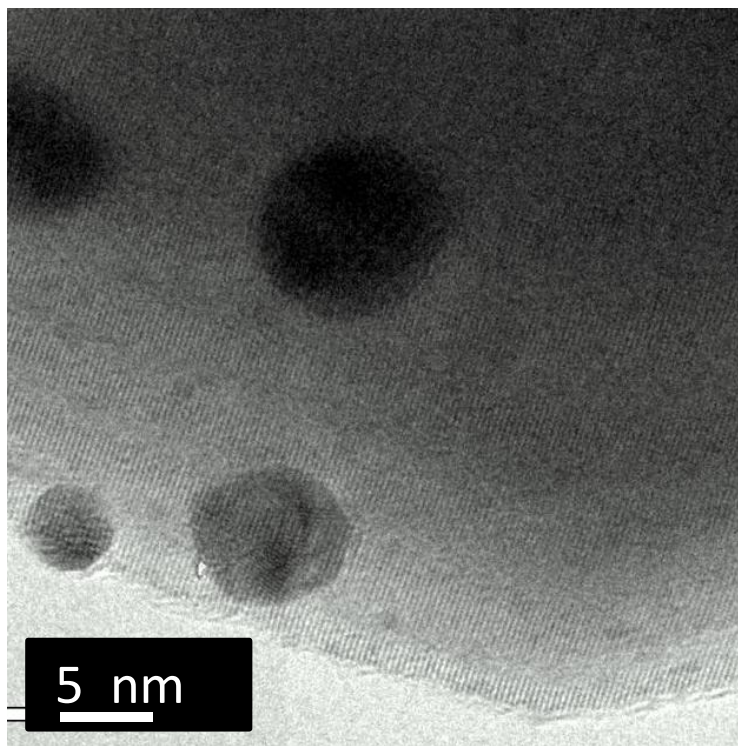


Figure 45. HRTEM images of Au(1wt%)/CeO₂_12.0 catalyst. CeO₂ surface area: 12.0 m²/g.

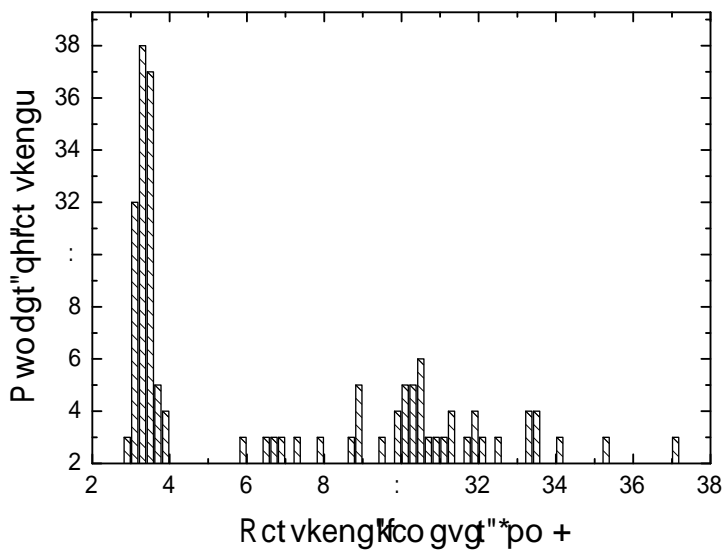
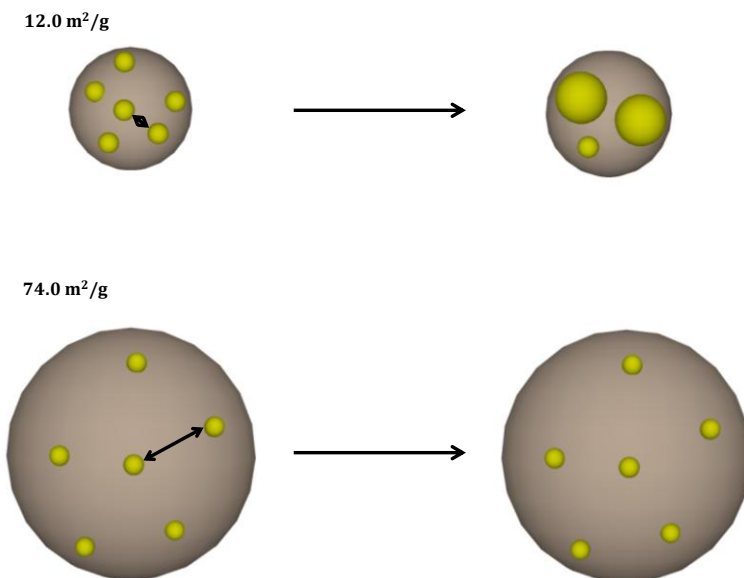


Figure 46. Particle size distribution histogram of a Au(1wt%)/CeO₂_12.0 catalyst. CeO₂ surface area: 12.0 m²/g.

Table 15. Mean particle diameter of the different Au/CeO₂ catalysts synthesised using different support surface areas.

Catalyst	Particle diameter (nm)
Au(1wt%)/CeO ₂ _12.0 (12.0 m ² /g)	4.7±4.0
Au(1wt%)/CeO ₂ (74.0 m ² /g)	1.3±0.6

The sinter of the Au clusters in the supports with a low surface area results from the lower Au interparticle distance (Figure 47). In the lower surface area CeO₂ Au clusters will be much closer than in the 74.0 m²/g CeO₂ leading to the Au aggregation into large nanoparticles. In the highest surface area CeO₂ Au clusters are further apart and will therefore maintain their size.

**Figure 47.** Schematic representation of the Au clusters (•) interparticle distance in different surface area CeO₂ supports.

Indeed, using the CeO₂ with a lower surface area, in order to observe almost only Au clusters on the surface of the support, a very low nominal reduced Au content (0.05 wt%) was required (Figure 48). When using such low nominal reduced Au content large Au agglomerates were not observed at low magnification.

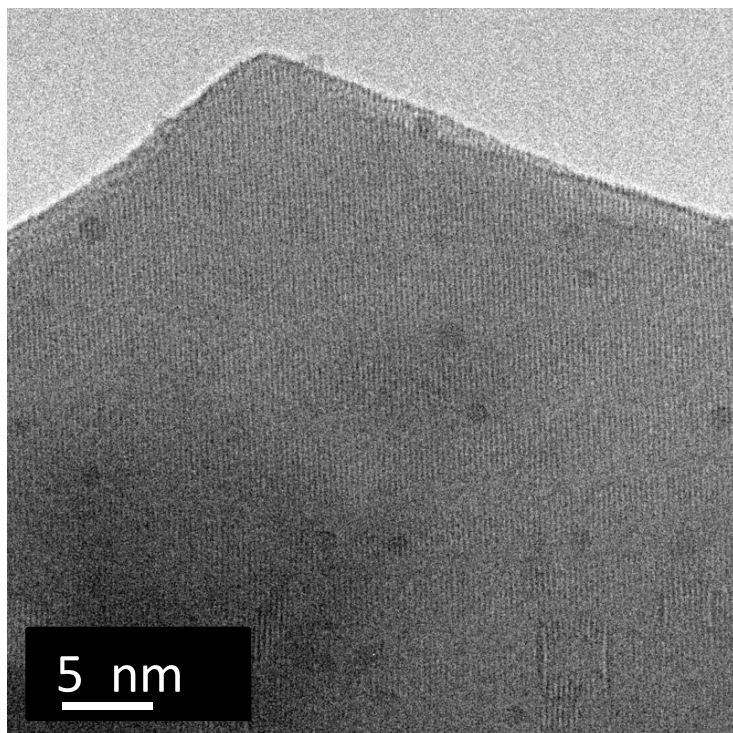


Figure 48. HRTEM image of a Au(0.05wt%)/CeO₂_12.0 catalyst (CeO₂ surface area: 12.0 m²/g).

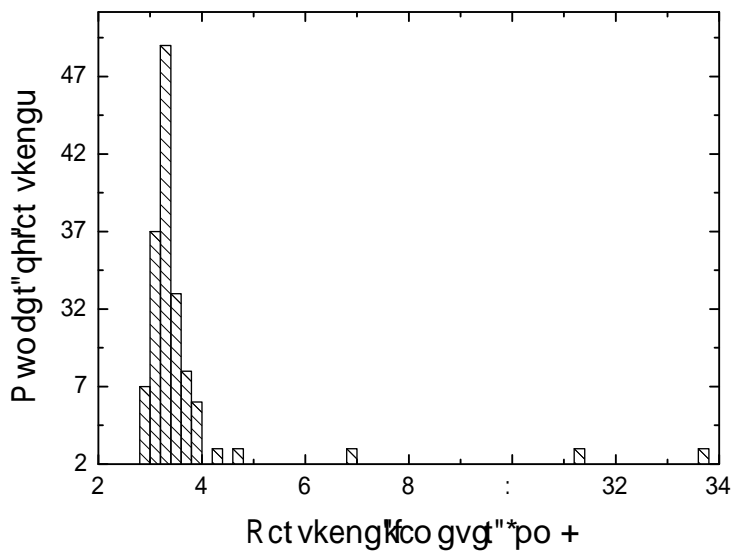


Figure 49. Particle size distribution histogram for the Au(0.05wt%)/CeO₂_12.0 catalyst. CeO₂ surface area: 12.0 m²/g.

A size distribution of 1.4 ± 0.3 nm was obtained for the Au(0.05wt%)/CeO₂_12.0 catalyst (Figure 49). Notice that, exceptionally, the three particles with diameter higher than 2 nm were not used to obtain this mean value.

In conclusion, it was experimentally verified that the Au particle size increases with the decrease of the support surface area which is in accordance with literature^[13, 14].

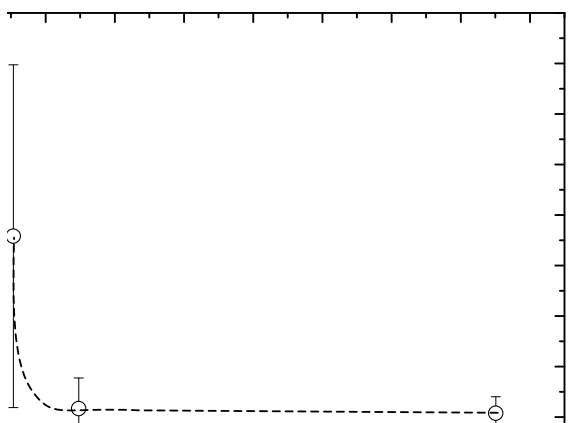


Figure 50. Dependence of the mean Au particle diameter with the support surface area using a nominal Au loading of 3 wt%.

Figure 50 shows how the particle size varies with the selected support using a nominal Au loading of 3 wt%. The Au(3wt%)/CeO₂ and Au(3wt%)/MWCNTs catalysts present a very similar Au mean particle size. This indicates that, even though the surface area of CeO₂ is approximately five times lower than the one of MWCNTs, up to 3 wt% of nominal loading although with a lower interparticle distance only Au clusters can still be obtained.

This study leads us to conclude that; lower gold loading in a high support surface area catalysts are preferable to avoid sinter of the Au and a faster deactivation.

These observations demonstrate that besides the importance of the use of stabiliser agents like sodium citrate or the presence of amine groups on the support surface it is also essential to select a high quality support. Depending on the synthesis methodology, the same material can have different surface areas. When a homogenous distribution of gold clusters is pretended, this factor is very important, requiring high surface areas to achieve this goal.

Additionally, the absence of gold clusters concluded by HRTEM characterisation on both MWCNTs and CeO₂ surfaces when using very low gold contents (< 0.5 wt%) led to a deep characterisation of these catalysts. Au/MWCNTs catalysts with a low gold content (0.1 wt%, 0.3 wt% and 0.5 wt%) were characterised by aberration-corrected HRTEM and XAS (Section 3.4).

3.3.3 STABILITY

The variation of the particle size with time was also investigated, in order to assess its stability. Gold clusters with 6 wt% nominal reduced gold content were characterised after being 30 minutes, 2 days and 13 days in the Au/MWCNTs suspension (Figure 51). Figure 52 shows the mean Au size diameter based on HRTEM observations. The mean size after 30 minutes, was around 1.2 nm and remained constant with time (Table 16). This result suggests that, after 30 minutes of reaction, the gold precursor is already depleted and the clusters cannot continue growing. Importantly, the resulting gold clusters are stable and do not coalesce and sinter. The stability of the clusters attached to the MWCNTs-PAH hybrids is a fundamental condition for the use of these materials for applications such as catalysis.

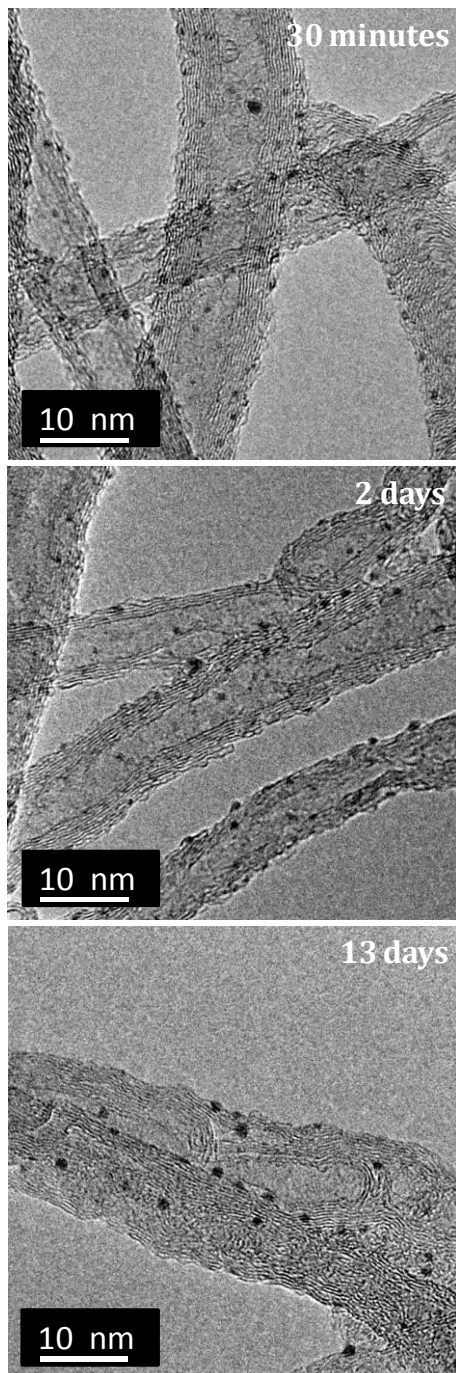


Figure 51. HRTEM images of Au(6wt%)/MWCNTs catalyst with different times in suspension.

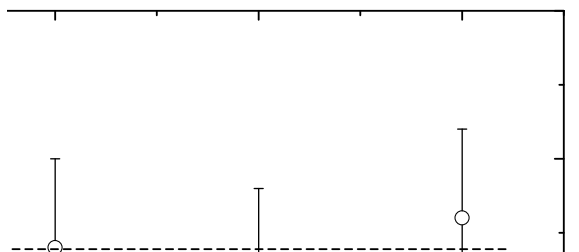


Figure 52. Dependence of the mean Au particle diameter of a Au(6wt%)/MWCNTs catalyst with time.

Table 16. Mean Au particle diameter of a Au(6wt%)/CeO₂ catalyst for different times in suspension.

Time	Particle diameter (nm)
30 minutes	1.2±0.3
2 days	1.1±0.3
13 days	1.3±0.3

Even though it is not shown here, months after the date of preparation several catalysts were sent to several different places to be tested in reactions. It was observed that the activity of these catalysts was similar to fresh prepared catalysts. This corroborates that the catalysts synthesised by this in-situ protocol are stable. Indeed, if they grow this would happen during the next 13 days. After this time, they would not sinter, indicating then its stability.

3.3.4 SYNTHESIS TEMPERATURE

Finally, the synthetic temperature was changed to investigate the effect of this variable on the mean gold nanocluster size distribution. The synthesis of a Au(6wt%)/MWCNTs catalyst was carried out at room temperature, 50 °C, 70 °C and 90 °C. There were no significant differences between the reactions performed at room temperature, 50 °C or 70 °C. Nevertheless, the synthesis performed at 90 °C showed few gold nanoclusters at the surface of the MWCNTs and a significant amount of nanoparticles larger than 10 nm appeared (Figure 53 and Figure 54) leading to a mean particle diameter of 10 ± 9 nm (Table 17). This indicates that, at this temperature, the nucleation does not occur preferentially at the amine groups of the MWCNT-PAH hybrids. This result is in accordance to literature. By the Turkevich method, Au nanoparticles around 15 nm are obtained at high temperatures (~ 90 °C – ~ 100 °C)^[19-21].

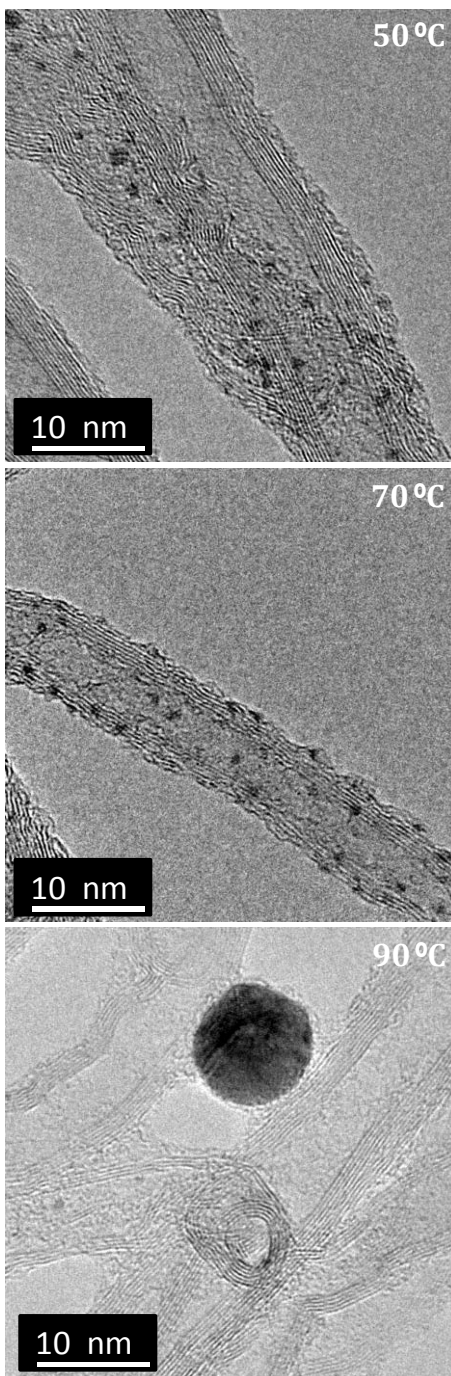


Figure 53. HRTEM images of Au(6wt%)/MWCNTs catalysts synthesised at different temperatures.

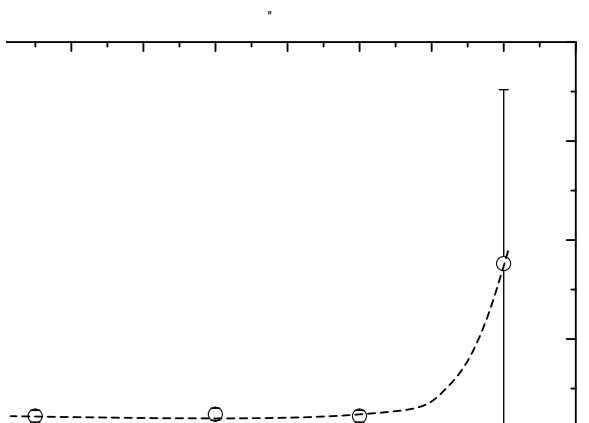


Figure 54. Dependence of the Au mean particle size with the synthesis temperature for a Au(6 wt%)/MWCNTs catalyst.

Table 17. Au mean particle diameter obtained for the different synthesis temperature.

T (°C)	Particle diameter (nm)
Room temperature	1.1±0.3
50	1.2±0.3
70	1.1±0.3
90	10±9

3.4 ATOMIC RESOLUTION OF Au/MWCNTs CATALYSTS

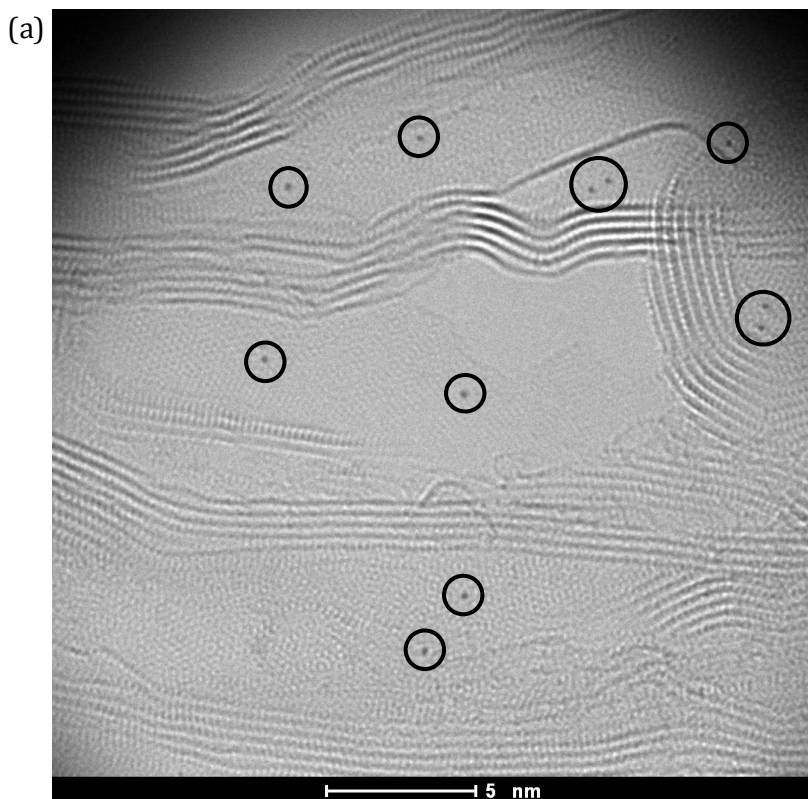
3.4.1 ABERRATION-CORRECTED HRTEM

In this chapter, a very simple and versatile synthetic protocol to obtain very small Au clusters ($d < 2$ nm) on surfaces covered with amine groups has been presented. An intensive characterisation, using a traditional 200 kV high resolution transmission electron microscope, was carried out. Using MWCNTs as support, for a gold content of 1 wt% and 0.5 wt%, gold clusters were barely

or completely not seen by this technique (Section 3.3.2, Figure 39). This observation combined with the discarded hypotheses that Au was lost during the synthesis or agglomerate led then to this deeply characterisation.

In this context, different gold content catalysts, namely 0.3 wt%, 3 wt% and 6 wt%, were characterised by a aberration-corrected high resolution transmission electron microscope. These images are unique and allow to deeply characterise the Au formed on the support surface. Using this microscope, the atoms of carbon (C) of the MWCNTs were easily distinguished between the walls of the MWCNTs (Figure 55b).

An initial general comparison of the three different gold contents catalyst revealed that, the very low gold content catalyst (0.3 wt%) only present isolated Au atoms (dark dots) on the MWCNTs' surface (Figure 55a).



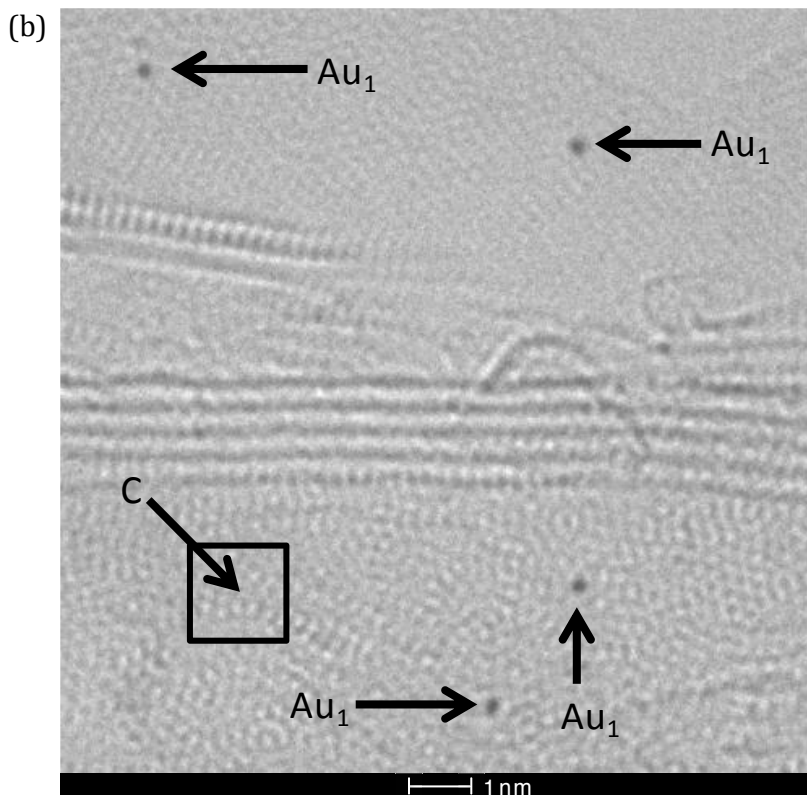


Figure 55. Aberration-corrected HRTEM image of a Au(0.3wt%)/MWCNTs catalyst (a) and zoom of a zone (b). Single Au atoms are marked with a circle line in image (a).

The Au(3wt%)/MWCNTs catalyst showed the existence of isolated gold atoms, atomic clusters (Au_n , $n \sim 2-3$) and gold clusters ($d \sim 1.3$ nm) on the MWCNTs surface (Figure 56). In the same way, when higher Au contents, such as 6 wt%, were used, isolated Au atoms were observed in a much lower quantity. In this catalyst, Au atoms were almost all grouped forming clusters with a mean particle diameter around 1.3 nm. Some very small Au clusters (atomic clusters) composed of approximately 2-3 atoms of Au were also found (Figure 57). Observing the structure of the 1.3 nm gold clusters, it could be seen that the Au atoms that form the clusters are grouped with no crystallographic facets. It could then be concluded that, by HRTEM, a lower number of gold clusters were observed on the MWCNTs surface, when using 0.5 wt% and 1 wt%, than

the nominal Au clusters that should be observed (Section 3.3.2), due to the fact that in these catalysts the Au is all (0.5 wt%) in the form of single Au atoms or part (1 wt%) in the form of single Au atoms or very small Au clusters not observable by HRTEM.

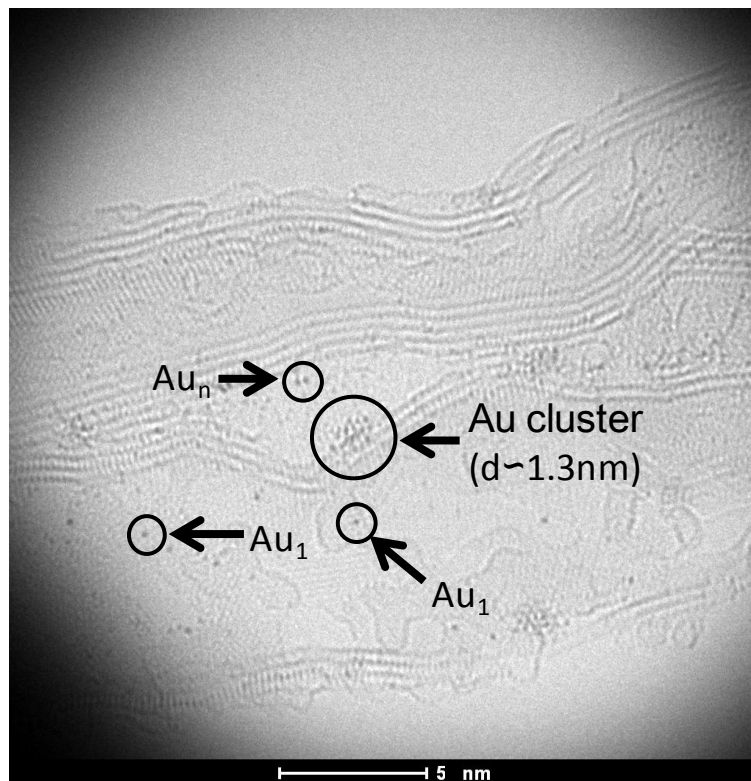


Figure 56. Aberration-corrected HRTEM image of a Au(3wt%)/MWCNTs catalyst. Single Au atoms and clusters are marked with a circle line.

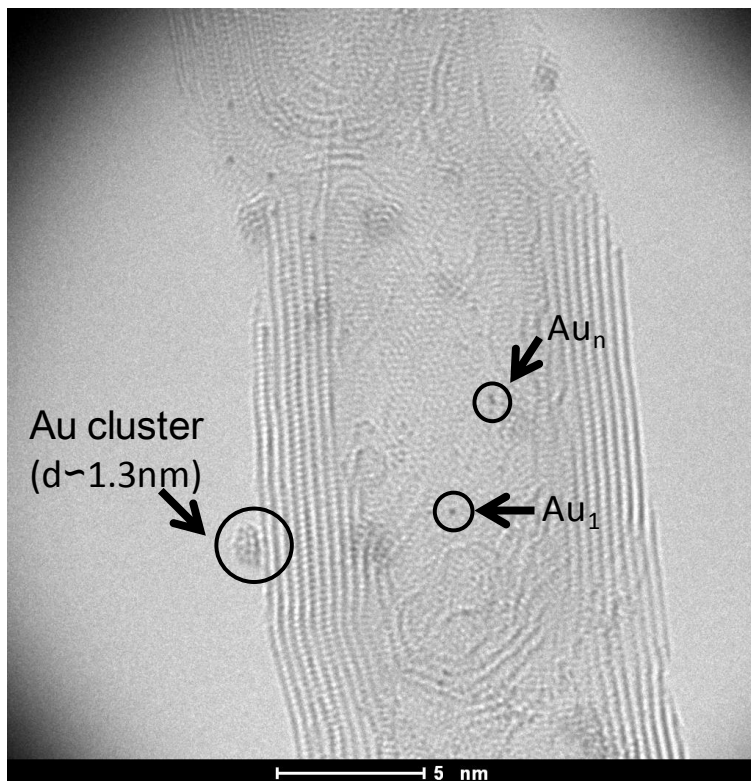


Figure 57. Aberration-corrected HRTEM image of a Au(6wt%)/MWCNTs catalyst. Single Au atoms and clusters are marked with a circle line.

From the beginning, due to the different contrasts observed in the images, it was assumed that the observed dark dots are Au atoms. This assumption could be easily justified with several reasons and helping techniques at the *Instituto de Nanociencia de Aragón*.

Firstly it was concluded that the observed dark dots are individual atoms since the resolution of the microscope using the experimental conditions applied in the measures is typically of 1.5 Å. If the dark dots were groups with a few atoms they would form structures with a larger size that would be observable in the images. Moreover, the number of constituent atoms (2, 3, n) would be easily differentiated. In the case that they were clusters or nanoparticles the casi or totally crystalline structure would be also observable.

Besides, the integrated high angle annular dark field (HADDF) intensity of a same element is directly related to the thickness^[22]. The integrated HADDF intensity increases with the number of atoms of the cluster^[22]. In the institute they can compare profiles of intensity of individual atoms and clusters with a maximum high of about 3 atoms and observe how the signal is related (Figure 58).

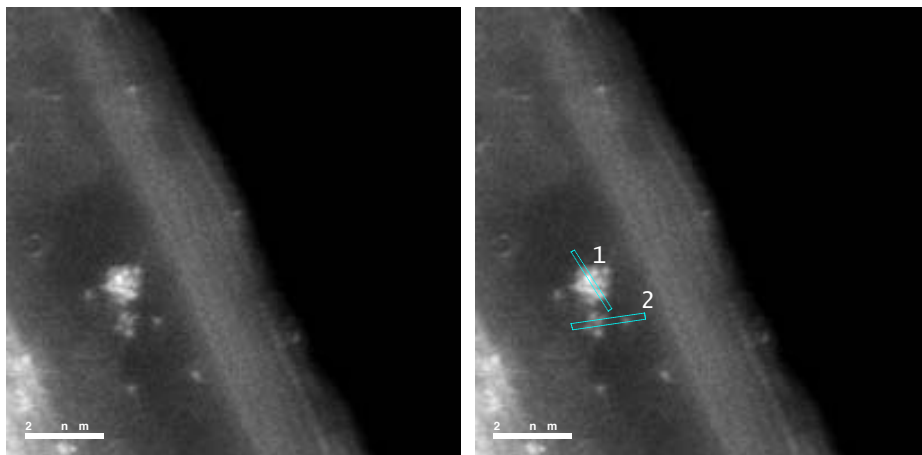


Figure 58. HADDF-STEM images of a Au(3wt%)/MWCNTs catalyst where Au clusters (1) and single Au atoms (2) coexist.

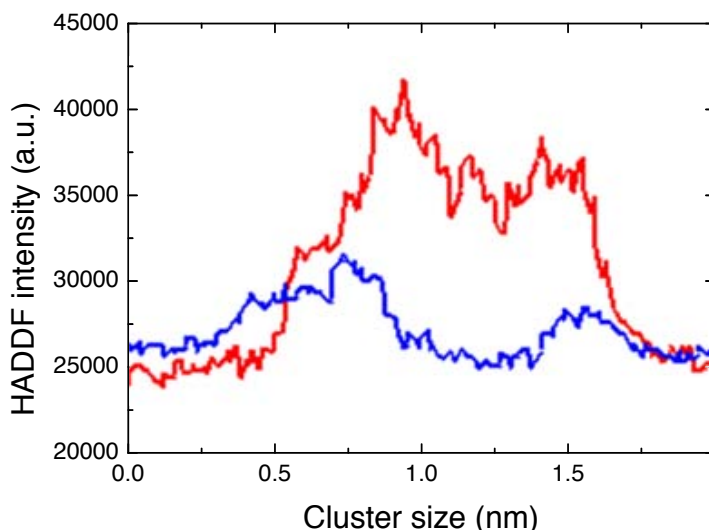


Figure 59. Comparison of the intensities profiles of a Au cluster (—) and a Au atom (—).

Taking into account the effect that the “background”, i.e. the effect that the support (MWCNTs) can have in the total intensity, they observed similar intensity profiles of an Au cluster and an individual atom (Figure 59). The individual Au atom profile showed a lower HADDF intensity area. Thus, they concluded that the bright spots were an individual atom of the same material as the cluster.

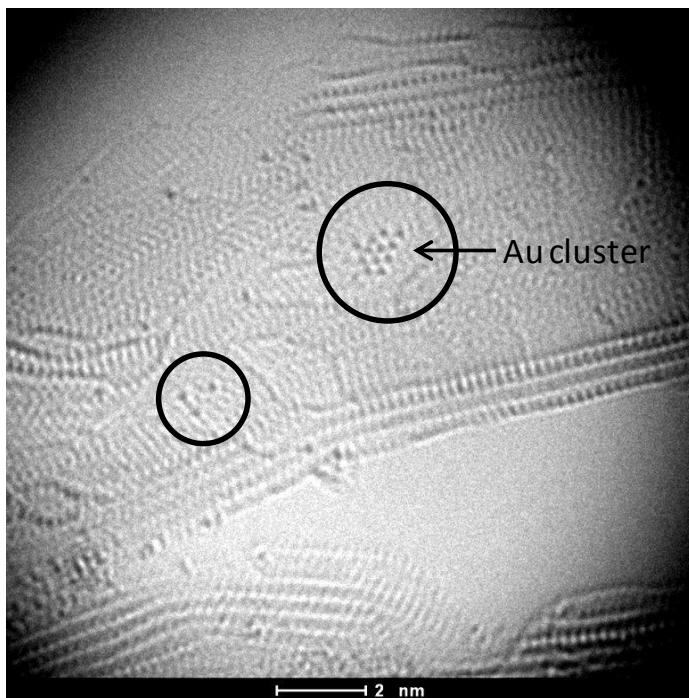
Additionally, it was concluded that these individual atoms are heavier than carbon. This conclusion was clearly observed by HRTEM but it was much more obvious in Scanning Transmission Electron Microscopy (STEM) which gives the Z contrast. The intensity is proportional to the atomic number raised to a exponent that can vary typically between 1.4 and 1.6. This implies that the atomic number of the individual atoms is much higher than the one from carbon since the intensity in the image that the nanotube produces (a system of carbon with a finite thickness, i.e. with a thickness of several atoms dispersing and contributing to the intensity in the image in each point of the sample) is much lower than the intensity produced for each one of the individual atoms that are observed^[23].

Besides, it is not reasonable to think that these individual atoms are not gold since during the synthesis process the unique heavy material used was gold and the rest of components were organic composed by light atoms that would give a negligible contrast if they adopted the form of individual atoms or small molecules.

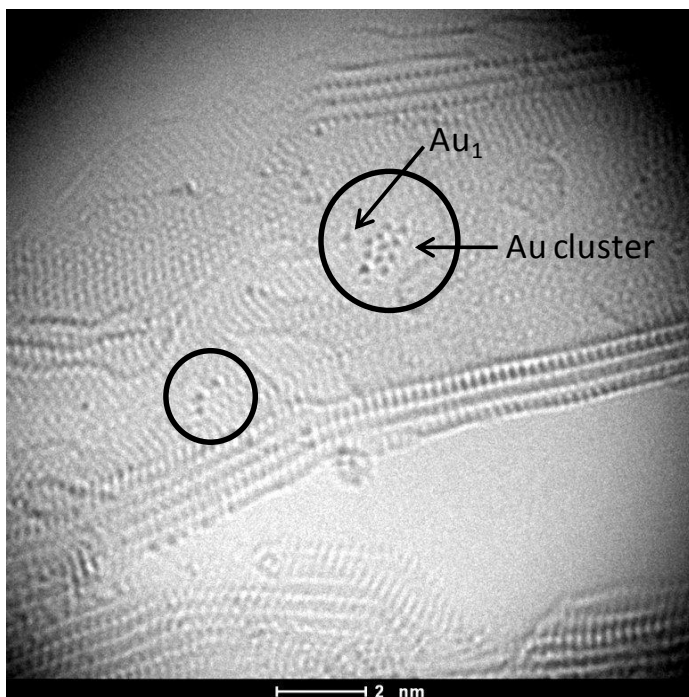
Finally, it could be affirmed that no sputtering phenomenon was produced that could lead to the presence of these gold atoms in the MWCNTs surface (for example, for sputtering of the clusters and nanoparticles). The working voltage (60 kV - 80 kV) was much lower than the one of knock on damage or of sputtering for gold^[24]. If those atoms were on the MWCNTs' surface from a sputtering phenomena inside the microscope between electrons of the beam and the material (the carbon of the nanotube or the gold), a dynamic process in each would be seen the atoms appearing when depositing in the place observed after being “sputtered” in other part would be observed. This did not happened

once the atoms were on the MWCNTs surface since the first moment of the observation completely discarding the hypothesis of sputtering.

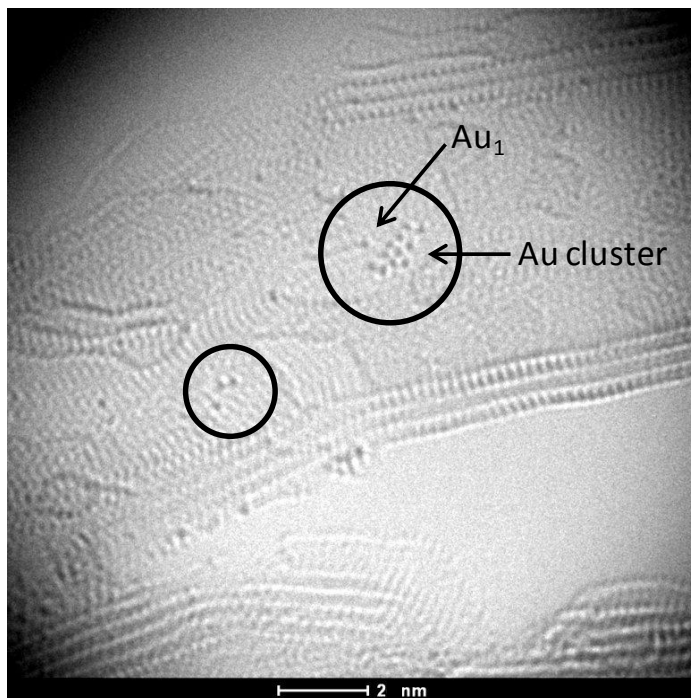
Lastly, the mobility of the Au atoms was observed. Figure 60 shows a sequence of a video obtained by this microscope where the mobility of both single gold atoms and the atoms that form the clusters was clearly seen. It could be concluded that the mobility observed in the conditions of temperature and pressure of the aberration-corrected microscope and under a voltage electron beam of 80 kV was not significant. The sinter of single Au atoms into clusters did not occur. The mobility was more at the level of a same gold cluster that regrouped in a different way. Thus, this result reaffirmed that these in-situ catalysts are stable at room temperature.



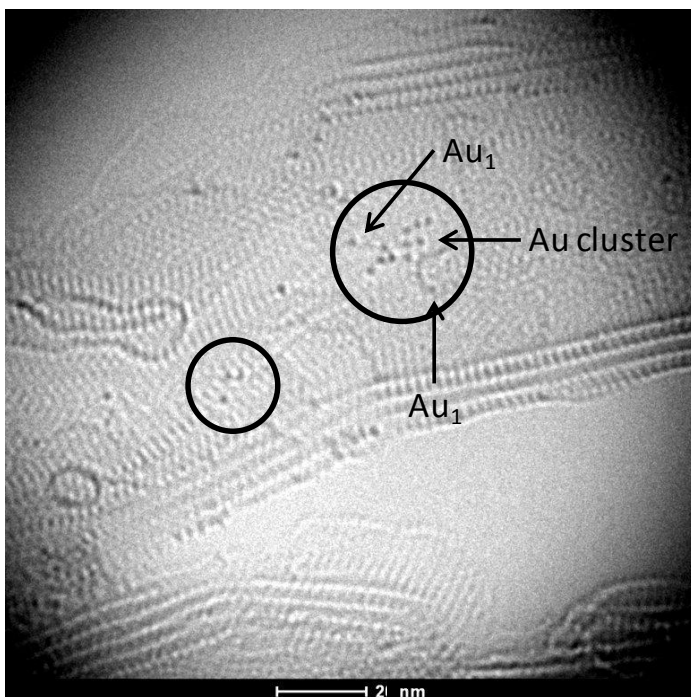
t = 0 s



t = 0.3 s



t = 0.6 s



t = 0.9 s

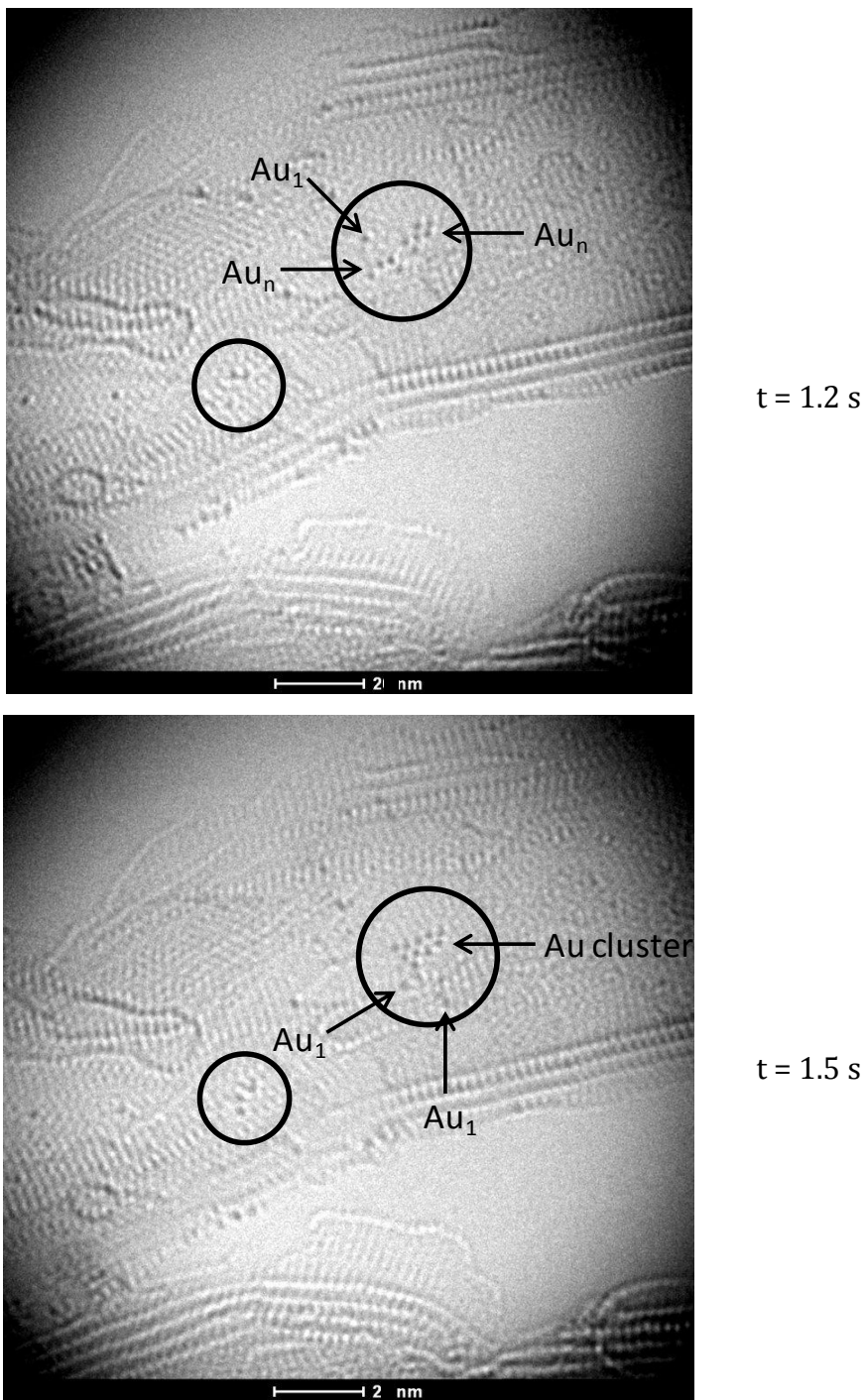


Figure 60. Sequence of snapshots obtained for a Au(3wt%)/MWCNTs catalysts by aberration-corrected HRTEM.

Combining HRTEM and aberration-corrected HRTEM observations, it seems that, when using nominal reduced gold contents, lower or equal to 0.5 wt%, a unique population of isolated gold atoms is obtained on the MWCNTs' surface. This result is extremely important and innovative because the synthesis of only single Au atoms is to date very little reported (Chapter 1, Section 1.4). Moreover, aberration-corrected HRTEM images revealed the coexistence of both populations of single gold atoms and gold clusters in the Au(3wt%)/MWCNTs and Au(6wt%)/MWCNTs catalysts.

3.4.2 XAS

The chemical nature of the Au of the very low gold content Au/MWCNTs catalysts was investigated by X-ray Absorption spectroscopy (XAS). Au/MWCNTs' catalysts with a gold content of 0.1 wt% and 0.5 wt% were analysed by this technique. The FT of the Extended X-ray Absorption Fine Structure (EXAFS) spectrum or the basic X-ray Absorption Near Edge Structure (XANES) spectrum from these catalysts and the Au foil are shown in Figure 61a and Figure 61b respectively. It was observed that both Au(0.1wt%)/MWCNTs and Au(0.5wt%)/MWCNTs catalysts present a peak at 1.7 Å (Figure 61a) that is attributed to Au atoms directly attached to citrate ligands or oxygen atoms (neighbour atoms with a low molecular weight). Moreover, the characteristic peaks of the Au-Au bonds of the Au foil located between 2 Å and 3 Å were not observed in these catalysts, which indicates the existence of only single Au atoms on the MWCNTs' surface (Figure 61a). This result is in accordance with the aberration-corrected HRTEM observations.

Although the data quality of EXAFS analysis is not enough for a quantitative analysis and, in this way, it is not possible to distinguish between the coexistence of Au atoms and very small clusters, it is believed, for the all the evidences presented, that, at least up to a nominal Au content of 0.5 wt%, Au/MWCNTs catalysts only present single Au atoms on the MWCNTs' surface.

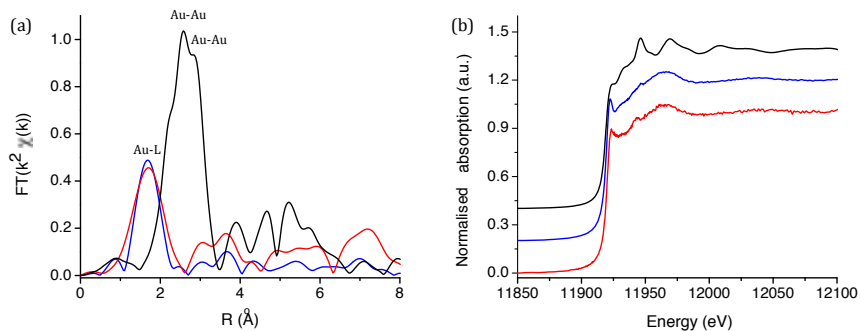


Figure 61. EXAFS FT (a) and XANES absorption spectrum (b) of Au foil (—), Au(0.1wt%)/MWCNTs (—) and Au(0.5wt%)/MWCNTs (—) catalysts. L: ligand.

Furthermore, the XANES absorption spectrum of the both low gold content catalysts is different from the one of Au foil (Figure 61b) and similar to the one of Au^I reference, [(PPh₃)AuCH₃], (Figure 62). This result corroborates once again the existence of only single Au atoms (Au^{δ+}) on the MWCNTs' surface when gold contents lower than 0.5 wt% are used.

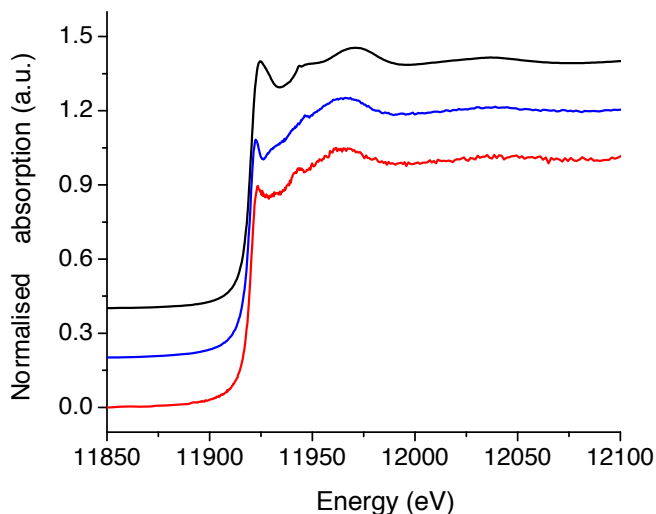


Figure 62. XANES absorption spectrum of (PPh₃)AuCH₃ (—), Au(0.1wt%)/MWCNTs (—) and Au(0.5wt%)/MWCNTs (—) catalysts.

In this Chapter, the possibility of obtaining single Au atoms on the MWCNTs' surface by the in-situ synthesis method was demonstrated. Even though this result was not investigated using other materials as support, such as TiO₂ and CeO₂, it is believed that isolated Au atoms can also be obtained on these supports. For a successful achievement of this result it is necessary to take into account the quality of the support, i.e. the support surface area, as it was discussed in this chapter (Section 3.3.2). In this context, since the surface area of both CeO₂ and TiO₂ is much lower than the MWCNTs, a gold content mandatorily lower than 0.5 wt% must be used in order to obtain only isolated Au atoms on their surfaces.

3.5 X-RAY PHOTOELECTRON SPECTROSCOPY

The chemical nature of the synthesised Au clusters was investigated by XPS. This revealed that the state of oxidation of Au when supported on MWCNTs varies with the particle size. Indeed, for the Au 4f_{7/2} a binding energy (BE) increase of ~ 2 eV relative to the bulk value of 84.0 eV was observed by our group when the gold particle size decreases to 1.1 nm^[4]. This result indicates that the Au clusters are positively charged. This positive charge is related to the fact that oxygen species are bonded to the Au surface. In the work published by our group in 2011, it was also demonstrated that these oxygen species are able to oxidise CO and be regenerated by molecular oxygen on the Au clusters surface^[4].

Additionally, a correlation between the BE and the oxidation state of gold was defined. BEs values of 84.0, 84.6-85.1 and 85.9-86.3 eV have been associated to Au⁰, Au⁺ and Au³⁺ species respectively^[4].

Nevertheless, in literature there is a strong discussion about whether the observed BE shifts result from the size effect by small Au clusters or from the oxidation state of the Au clusters. It is affirmed that the shift to higher binding energies observed with adsorbed small metal particles on a metal oxide

support can result from final state effects, i.e. reduced screening of the core hole leading to the decrease of the kinetic energy of the ejected electrons^[25]. In this context, and in order to eliminate these possible contributions, the Au auger parameter (α) was determined according to the Equation 14^[25].

$$\alpha = BE(\text{Au } 4f_{7/2}) + KE(\text{Au } M_5N_{67}N_{67}) \quad (14)$$

where,

$BE(\text{Au } 4f_{7/2})$ – binding energy of the Au $4f_{7/2}$ electrons.

$KE(\text{Au } M_5N_{67}N_{67})$ – kinetic energy of the Au $M_5N_{67}N_{67}$ auger electrons.

The Auger parameter value is independent of substrate charging and is a sensitive probe of the physical and chemical environment of the analysed atoms. How this value varies with the particle size is complex and takes into account both initial and final state influences^[26].

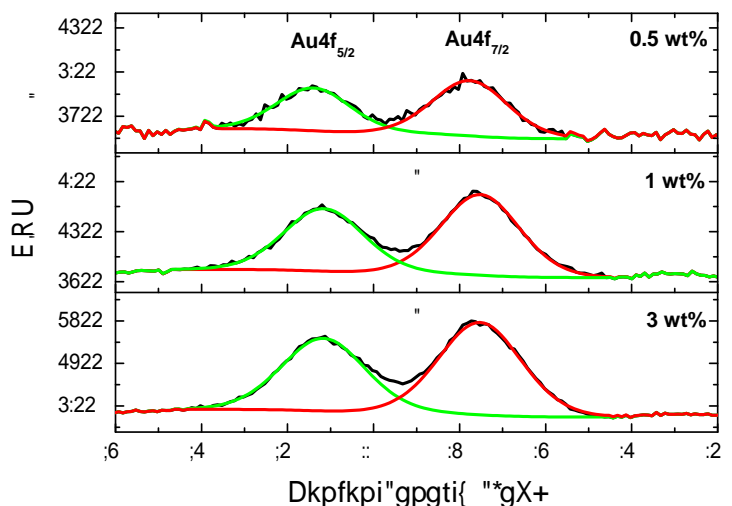
By the Au auger parameters values obtained, it was demonstrated that the Au in the MWCNTs catalysts with a particle size between 0.9 nm and 1.5 nm is positively charged (Au^{6+})^[4]. When the particle diameter was larger than 4 nm “bulklike” gold species were observed^[4].

Further XPS’ analysis of the Au/MWCNTs, Au/TiO₂ and Au/CeO₂ catalysts were carried out (Table 18). For these, the Au auger parameter was not determined, since it had already been demonstrated that the BE shifts observed are due to the oxidation state of the Au clusters^[4]. The particle diameter presented in Table 18 was determined by HRTEM (Section 3.3). For all the evidences discussed it is believed that the Au(0.5wt%)/MWCNTs catalyst is composed by only single Au atoms (At.).

Table 18. XPS data for different Au content Au/MWCNTs, Au/CeO₂ and Au/TiO₂ catalysts.

Au content (wt%)		0.5	1	3
Au/MWCNTs	d (nm)	At.	n.a.	1.1±0.3
	Au 4f _{7/2} BE (eV)	85.8	85.5	85.5
Au/CeO ₂	d (nm)	-	1.3±0.6	1.2±0.6
	Au 4f _{7/2} BE (eV)	-	84.2/85.7 (Au ⁰ /Au ^{δ+} =2)	84.1/85.6 (Au ⁰ /Au ^{δ+} =2)
Au/TiO ₂	d (nm)	-	1.1±0.5	4.6±3.4
	Au 4f _{7/2} BE (eV)	-	84.2/85.7 (Au ⁰ /Au ^{δ+} =2)	84.2/85.8 (Au ⁰ /Au ^{δ+} =4)

n.a. – not available data.

**Figure 63.** XPS spectra of the Au4f peak and respective fit components for gold clusters obtained at different nominal gold loadings on MWCNTs.

In what concerns Au/MWCNTs catalysts, for both Au(3wt%)/MWCNTs and Au(1wt%)/MWCNTs catalysts, a BE value of 85.5 eV was obtained which reveals that Au is positively charged (Figure 63). Lowering the nominal Au content to 0.5 wt%, the presence of only cationic Au species was also observed (BE = 85.8 eV, Figure 63). These results revealed that, in the range of 0.5 wt%

to 3 wt%, gold is either in the form of clusters, where the Au of the surface is bonded to oxygen species, or simply in the form of single Au atoms ($\text{Au}^{\delta+}$).

Moreover, comparing these results with the XAS obtained data (Section 3.4.2), coherence was found. Both characterisation techniques showed that in the Au(0.5wt%)/MWCNTs catalyst Au is positively charged ($\text{Au}^{\delta+}$).

Furthermore, when using CeO_2 as support, it was observed that the Au(1wt%)/ CeO_2 catalyst presents two types of gold. Both metallic (Au^0 , 84.2 eV) and positively charged gold ($\text{Au}^{\delta+}$, 85.7 eV) coexist in this catalyst (Figure 64). The same result was obtained for the Au(1wt%)/ TiO_2 catalyst; two components (metallic and positively charged) were also observed. For this catalyst, the Au $4f_{7/2}$ BEs were also located at 84.2 eV and 85.7 eV (Figure 65). The $\text{Au}^0/\text{Au}^{\delta+}$ concentration ratio of both catalysts is approximately 2.

In the same way, the higher gold content catalysts – Au(3wt%)/ CeO_2 and Au(3wt%)/ TiO_2 – are also composed by both metallic and cationic gold. In the Au(3wt%)/ CeO_2 catalyst, Au $4f_{7/2}$ BEs are located at 84.1 eV and 85.6 eV (Figure 64). Similar to the Au(1wt%)/ CeO_2 catalyst, the Au(3wt%)/ CeO_2 catalyst presents a $\text{Au}^0/\text{Au}^{\delta+}$ concentration ratio of approximately 2. The Au(3wt%)/ TiO_2 catalyst presents the Au $4f_{7/2}$ BEs at 84.2 eV and 85.8 eV (Figure 65). An increase of the $\text{Au}^0/\text{Au}^{\delta+}$ concentration ratio from around 2 to 4 was observed when comparing Au(1wt%)/ TiO_2 and Au(3wt%)/ TiO_2 catalysts. These results are in accordance with HRTEM observations (Section 3.1 and 3.3.2). In the case of the CeO_2 catalysts, for both gold contents (1 wt% and 3 wt%), only clusters were observed on the support surface (Figure 33 and Figure 41). Thus, the quantity of metallic and cationic gold was not altered. Nevertheless, in the case of TiO_2 catalysts, a significant increase of the mean Au particle size was verified for the Au(3wt%)/ TiO_2 catalyst due to the coexistence of Au nanoparticles with Au clusters in this catalyst (Figure 43). The existence of large Au nanoparticles in this catalyst, unlike in the Au(1wt%)/ TiO_2 where only gold clusters were formed (Figure 43), led then to an increase of double of the $\text{Au}^0/\text{Au}^{\delta+}$ concentration ratio.

By these measures, it was also concluded that, even though the clusters formed on the CeO_2 surface using gold contents of 1 wt% and 3 wt% have diameters similar to those formed on the MWCNTs surface, not all were oxidised.

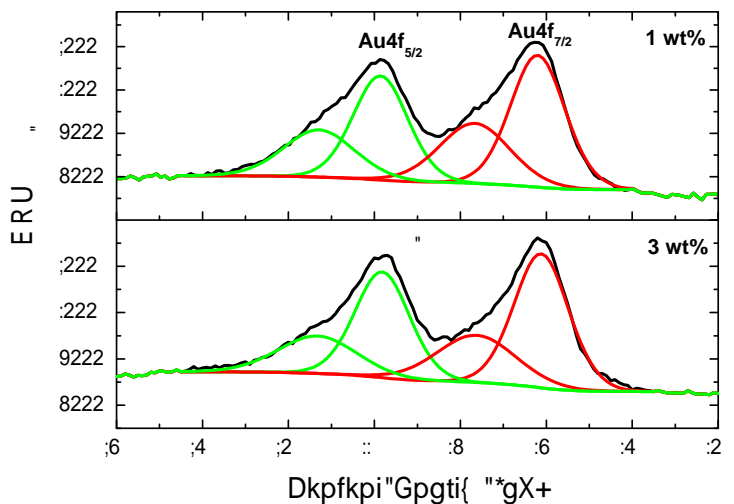


Figure 64. XPS spectra of the Au4f peak and respective fit components for gold clusters obtained at different nominal gold loadings on CeO_2 .

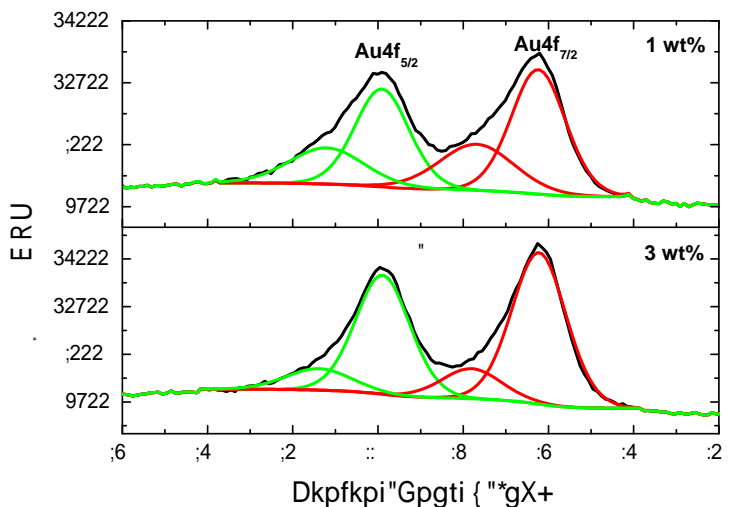


Figure 65. XPS spectra of the Au4f peak and respective fit components for gold clusters obtained at different nominal gold loadings on TiO_2 .

3.6 CATALYTIC ACTIVITY

As it has been well reported, to show a good catalytic activity it is essential that the catalyst gold nanoparticles do not exceed the 5 nm of diameter^[27]. In this context, having a synthesis method that allows a narrow size distribution of very small gold nanoparticles represents an advantage in this field. Thus, the activity of the in-situ synthesised Au clusters catalysts was investigated for CO oxidation.

3.6.1 Au/MWCNTs CATALYSTS

MWCNTs were discarded to be used as support in this reaction, although they present a much higher surface area than CeO₂ (375.3 m²/g vs 74.0 m²/g respectively). This was due to the loss of approximately 89% of the catalyst weight verified in a Au(2wt%)/MWCNTs catalyst after being oxidised under a flow of 100 mL/min (10 v/v% O₂ in N₂) at 400 °C. Indeed, it was clearly observed that the majority of the MWCNTs was decomposed at this temperature (Figure 66). In this case, exceptionally, the reaction was carried out by washcoating of the catalyst suspension on a cordierite (2MgO-2Al₂O₃-5SiO₂) monolith (Chapter 1, Section 1.6.1).



Figure 66. Cordierite monolith after impregnation with a Au(2wt%)/MWCNTs catalyst (left) and after being oxidised at 400 °C in a continuous flow of 100 mL/min (right).

Unlike it was observed, carbon nanotubes are known for its high thermal stability. A TGA analysis of pure MWCNTs revealed that these are not decomposed up to a temperature of 490 °C (Figure 67). By TGA a unique weight loss of approximately 90% between 490 °C and 600 °C was observed. In this way, the fact of having observed a weight loss of 89% at 400 °C on the Au(2wt%)/MWCNTs catalyst led us to think that the presence of Au might be responsible for accelerating the decomposition of the MWCNTs. In this context, a study about the effect of Au in the MWCNTs and other carbonaceous materials oxidation temperature was carried out. These results are presented in Chapter 5.

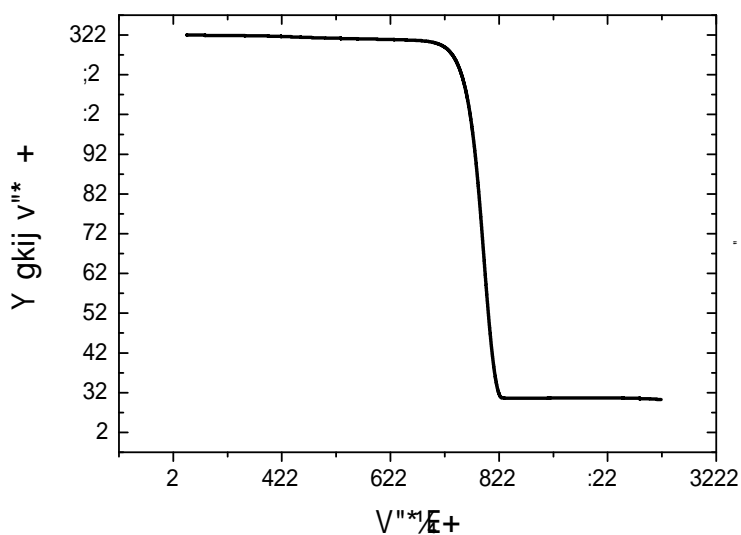


Figure 67. TGA curve of bare MWCNTs. Atmosphere: air.

3.6.2 Au/CeO₂ CATALYSTS

The catalytic activity of the in-situ synthesised Au catalysts was investigated using CeO₂ as support. CeO₂ is preferable for this reaction due to its capacity for releasing oxygen under reaction conditions' which result from the high mobility of the oxygen vacancies in the solid (Chapter 1, Section 1.5).

In order to compare the catalytic activity of the different sized Au/CeO₂ clusters, catalysts with a gold content of 0.1 wt%, 0.5 wt% and 3 wt% were prepared in the powder form. The conditions used to carry out this reaction, the experimental protocol followed and the equations used to determine the catalytic activity in terms of reaction rate are detailed described in Annexes (Section A.2).

When comparing the conversion of the Au(0.1wt%)/CeO₂ catalyst and the support used to synthesise it, CeO₂, it was observed that these are similar and both are able to convert the same quantity of CO at 400 °C (Figure 68). This Au inactivity can be explained by the fact that its active sites might be covered by PAH and by intermediate products formed during the citrate ions and AuCl₄⁻ reaction. A mechanism of reaction to obtain Au nanoparticles by citrate reduction was proposed by Romero *et al.*^[21]. According to this mechanism, dicarboxyacetone – (COO⁻)(CH₂)CO(CH₂)(COO⁻) – will be formed from the oxidation of the citrate ion^[20, 28]. Thus these species may probably cover both Au and CeO₂ active sites inhibiting the catalytic activity. In this way, when increasing the Au loading, since a higher quantity of sodium citrate is used, the surface of the higher Au loading catalysts will be more covered and therefore a lower conversion than bare CeO₂ was observed (Figure 68).

It was then concluded that the activity of these Au catalysts could not be measured because even after calcination, the catalysts surface was covered by species formed during the synthesis reaction.

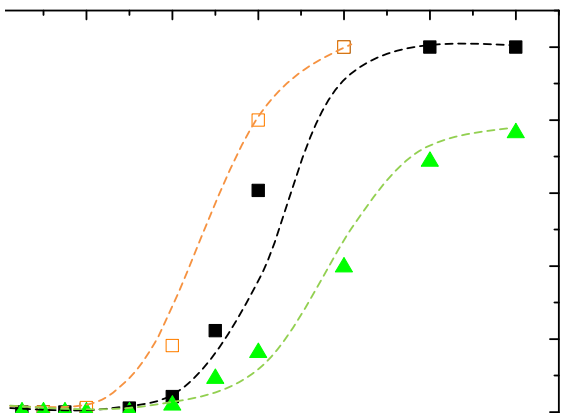


Figure 68. Comparison of the CO conversion of the CeO_2 (---□---), $\text{Au}(0.1\text{wt}\%)/\text{CeO}_2$ (---■---) and $\text{Au}(3\text{wt}\%)/\text{CeO}_2$ (---▲---) catalysts. Flow rate: 50 mL/min (96 v/v% N_2 ; 2 v/v% O_2 ; 2 v/v% CO).

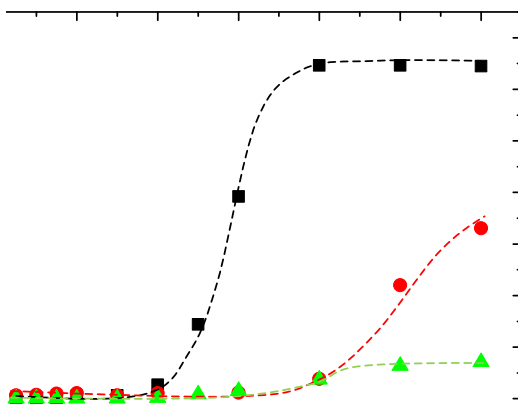


Figure 69. Catalytic activity of the $\text{Au}(0.1\text{wt}\%)/\text{CeO}_2$ (---■---), $\text{Au}(0.5\text{wt}\%)/\text{CeO}_2$ (---●---) and $\text{Au}(3\text{wt}\%)/\text{CeO}_2$ (---▲---) catalysts for CO oxidation (1st cycle). Flow rate: 50 mL/min (96 v/v% N_2 ; 2 v/v% O_2 ; 2 v/v% CO).

Figure 69 shows the catalytic activity obtained for the three catalysts. The same result was observed, i.e. a significant decrease of the catalytic activity was observed when increasing the Au loading. This results from the fact that the

quantity of sodium citrate used increases with the Au loading. Thus, in the higher Au loading catalysts more intermediate species resultant from the $AuCl_4^-$ and citrate ion reaction will be formed covering a higher quantity of catalytic active sites.

Furthermore, there was a decrease of activity for both catalysts in the second cycle (Figure 70).

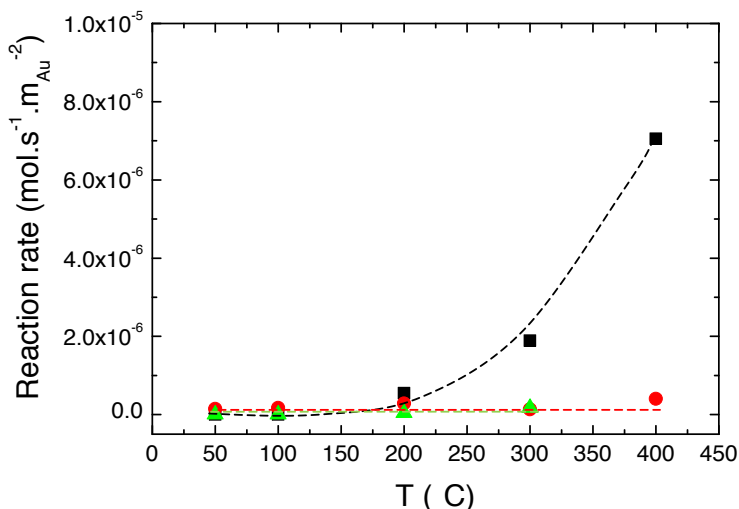


Figure 70. Catalytic activity of the Au(0.1wt%)/CeO₂ (-■-), Au(0.5wt%)/CeO₂ (-●-) and Au(3wt%)/CeO₂ (-▲-) catalysts for CO oxidation (2nd cycle). Flow rate: 50 mL/min (96 v/v% N₂; 2 v/v% O₂; 2 v/v% CO).

SEM characterisation, after both reaction cycles, revealed that the lowest gold content catalyst (0.1 wt%) did not show Au agglomeration (Figure 71). Nevertheless, the lower activity in the second cycle can be explained by the fact that the CeO₂ surface area after being at such high temperatures will decrease due to the CeO₂ nanoparticles sinter. Indeed, Lai *et al.* observed that the increase of the calcination temperature leads to a significantly decrease of the CeO₂ surface area^[6]. Using the same CeO₂ they obtained a surface area of 65.5 m²/g, 60.7 m²/g and 29.1 m²/g after calcinations at 300 °C, 500 °C and 700 °C respectively^[6]. The decrease of the CeO₂ surface area leads then to a decrease of

the activity due to the lower number of oxygen vacancies available for reaction^[7, 13].

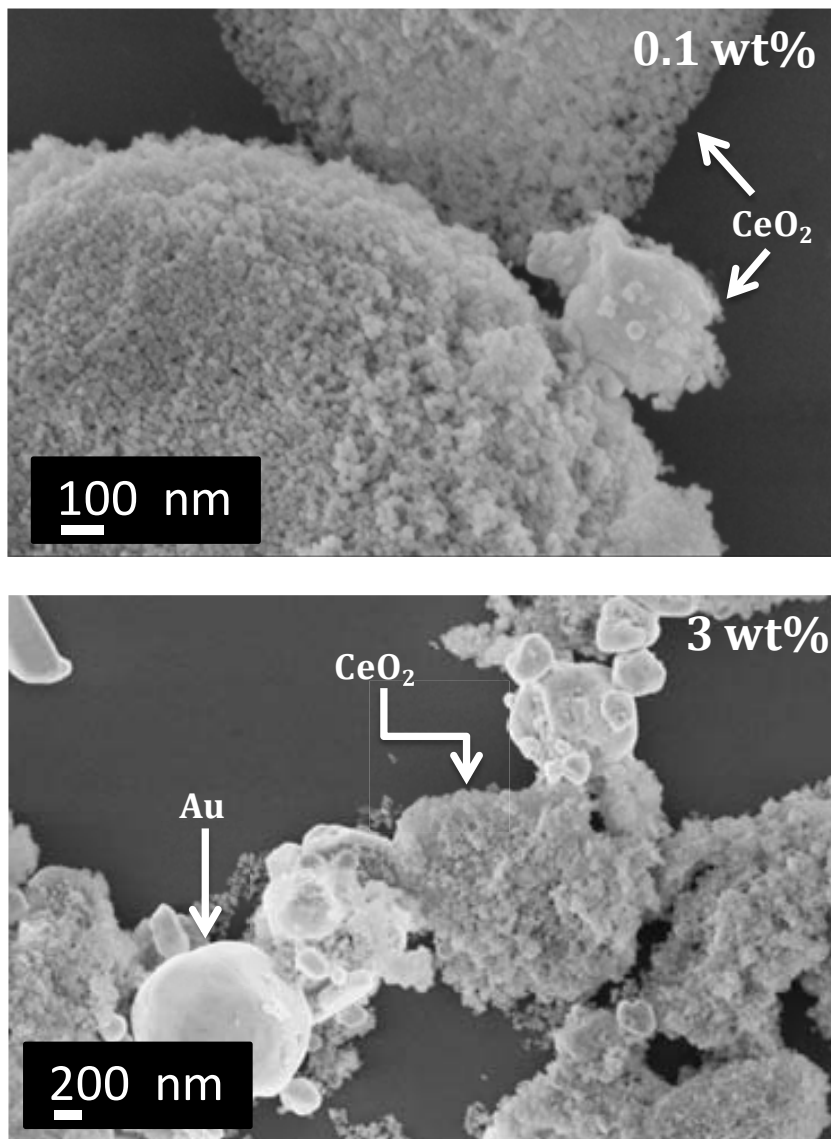


Figure 71. SEM images of the Au(0.1wt%)/CeO₂ and the Au(3wt%)/CeO₂ catalysts after CO oxidation.

In addition, for the highest gold content catalyst (3 wt%), the sintering of the Au clusters was observed after both cycles of CO oxidation, contributing also to the decrease of activity obtained in the second cycle (Figure 71). SEM characterisation also showed that, although some CeO₂ was covered by large Au nanoparticles in the Au(3wt%)/MWCNTs catalyst, the major part of the support was still free to react. The observation then corroborates the hypothesis that the lower conversion of this catalyst observed in the first cycle when compared to bare CeO₂ results from the cover of both CeO₂ and Au active catalytic sites.

Even though, in the Au(0.1wt%)/CeO₂ catalyst, large Au agglomeration was not observed the fact that the catalysts were strongly covered by agents impeding the CO access to the active centers the study of these in-situ catalysts real activity for CO oxidation was not possible. Thus, lamentably, the role of Au^{δ+} in CO oxidation could not be concluded. Nevertheless, it could be concluded that low gold content catalysts are preferable in order to avoid the gold sinter. In the same way, unfortunately, the activity of the single Au atoms that can be easily obtained by this synthesis method using very low gold contents (< 0.5 wt%) could not be investigated for this reaction. The activity of these single Au atoms has to date been subject to very little investigation due to the difficulty in obtaining these species, stable without sinter. This is so, even though the activity of single Au atoms in-situ synthesised catalysts can be investigated for other reactions of interest using different mechanisms. Indeed, the ability to produce H₂ at room temperature by a photocatalytic process using in-situ Au/TiO₂ catalysts has been recently reported by our group^[29]. In this work, the high activity of the single Au atoms catalysts in comparison to Au clusters catalysts is discussed.

Finally, the comparison of the experimentally obtained results and the ones reported in literature revealed that the in-situ synthesised catalysts are

significantly less active than the DP or co-P synthesised catalysts (Figure 72). In-situ catalysts were not able to convert CO at low temperatures and much higher temperatures were required to reach similar values of activity (Table 19). These significantly lower results can be explained by the cover of the active sites as explained.

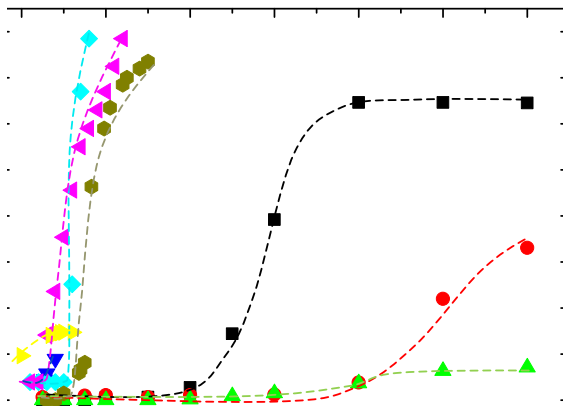


Figure 72. Comparison of the catalytic activity of the Au(0.1wt%)/CeO₂ (—■—), Au(0.5wt%)/CeO₂ (—●—), Au(3wt%)/CeO₂ (—▲—) catalysts with the literature catalysts: DP1^[6] (—▼—), DP2^[5] (—◆—), DP3^[5] (—▲—), DP4^[8] (—▲—), Co-P^[30] (—◆—) for the CO oxidation.

Table 19. Comparison of the catalytic activity obtained for in-situ, DP and Co-P Au/CeO₂ synthesised catalysts.

Nomenclature	Reaction rate (mol.s ⁻¹ .m _{Au} ⁻²) T=100 °C	Reaction rate (mol.s ⁻¹ .m _{Au} ⁻²) T=600 °C
	Au(0.1wt%)/CeO ₂	1.0x10 ⁻⁷
Au(0.5wt%)/CeO ₂	2.1x10 ⁻⁷	6.6x10 ⁻⁶
Au(3wt%)/CeO ₂	0	1.4x10 ⁻⁶
DP3 ^[5]	1.3x10 ⁻⁵	-
Co-P ^[30]	1.3x10 ^{-5(a)}	-

^(a)T=105 °C

The catalytic activity results revealed that the in-situ synthesis method was not adequate to prepare active catalysts for the CO oxidation. Nevertheless, it could be concluded that Au clusters deposited in very low gold contents (< 0.5 wt%) are preferable in order to prevent sintering of Au (increase of the Au interparticle distance). In this context a new cleaner synthesis method that allows a uniform distribution of stable gold nanoclusters ($d < 2$ nm) to be obtained was developed (Chapter 4).

3.7 CONCLUSIONS

In this chapter the development of a very simple, versatile and reproducible in-situ synthesis method that allow to obtain from stable single Au atoms to Au clusters ($d < 2$ nm) supported on MWCNTs, TiO₂ and CeO₂ covered by amine groups at room temperature was presented.

Importantly, ICP-OES' measures revealed that, when using MWCNTs, the nominal and the real Au content present on the catalyst is very similar. A deep characterisation of the parameters that might influence the Au particle size was carried out by HRTEM. From this study it was concluded that different sized Au clusters can be obtained by simply altering the quantity of the gold precursor (HAuCl₄) on surfaces covered by amine groups. Additionally, another parameter that strongly influences the Au particle size is the support surface area. A lower support surface area leads to an easier sintering of Au demanding then lower Au loadings in order to prevent agglomeration of gold. Finally, concerning the synthesis temperature no significant differences on the Au cluster size were observed up to 70 °C.

Moreover, by XPS characterisation it was concluded that up to 3 wt% of Au content catalysts, when supported on MWCNTs, show only cationic Au species (isolated Au atoms or oxidised Au clusters). When supported on TiO₂ and CeO₂, metallic Au coexists with positively charged gold for Au contents between 1 wt% and 3 wt%.

Importantly, the synthesis of stable single Au atoms on MWCNTs-PAH surfaces was successfully demonstrated using Au loadings of 0.5 wt% or lower. Hence, further study about the activity of these single Au atoms for different reactions can be carried out, as to date it has been little investigated.

Despite the simplicity of this method and its advantages the activity of different sized in-situ Au/CeO₂ catalysts for the CO oxidation could not be investigated due to the cover of the catalysts active sites. In-situ Au/CeO₂ catalysts showed a much lower activity than the ones prepared by DP or co-P methods. Despite, it was concluded that catalysts with Au contents lower than 3 wt% are preferable in order to avoid the Au sinter at high reaction temperatures. It was then concluded that this in-situ synthesis method is not the most adequate to produce active catalysts for CO oxidation. Thus, this study led then to the development of a new cleaner synthesis method that allows Au catalysts with a uniform population of gold nanoclusters ($d < 2$ nm) to be prepared, which is presented in Chapter 4.

Additionally, it has been observed that Au clusters strongly affect the thermal stability of MWCNTs. This observation led to the study about the Au effect on the decomposition temperature of carbonaceous materials presented in Chapter 5.

3.8 REFERENCES

- [1] L. Lechuga Gómez, E. Mendoza Gómez, M. A. Correa Duarte, M. Sanles Sobrido, *Patent WO2010031890 A1: Síntesis de Partículas Subnanométricas de Au catalíticas soportadas en superficies con grupos amino* **2010**, available on-line <http://patentscope.wipo.int/search/en/WO2010031890>.
- [2] J. Llorca, M. Dominguez, C. Ledesma, R. J. Chimentão, F. Medina, J. Sueiras, I. Angurell, M. Seco, O. Rossell, *Journal of Catalysis* **2008**, 258, 187–198.
- [3] F. B. Lollmahomed, R. Narain, *Langmuir* **2011**, 27, 12642-12649.
- [4] L. Alves, B. Ballesteros, M. Boronat, J. R. Cabrero-Antonino, P. Concepción, A. Corma, M. A. Correa-Duarte, E. Mendoza *Journal of the American Chemical Society* **2011**, 133 (26), 10251-10261.
- [5] R.-R. Zhang, L.-H. Ren, A.-H. Lu, W.-C. Li, *Catalysis Communications* **2011**, 13, 18-21.
- [6] S. Y. Lai, Y. F. Qiu, S. J. Wang, *Journal of Catalysis* **2006**, 237, 303-313.
- [7] S. Carretin, P. Concepción, A. Corma, J. M. López Nieto, V. F. Puentes, *Angewandte Chemie International Edition* **2004**, 43, 2538-2540.
- [8] Tana, F. Wang, H. Li, W. Shen, *Catalysis Today* **2011**, 175, 541-545.
- [9] R. Zanella, S. Giorgio, C. R. Henry, C. Louis, *Journal of Physical Chemistry B* **2002**, 106, 7634-7642.
- [10] S. Tsubota, M. Haruta, T. Kobayashi, A. Ueda, Y. Nakahara, *Studies in Surface Science and Catalysis* **1991**, 72, 695-704.
- [11] S. Tsubota, D. A. H. Cunningham, Y. Bando, M. Haruta, *Studies in Surface Science and Catalysis* **1995**, 91, 227-235.
- [12] R.-R. Zhang, L.-H. Ren, A.-H. Lu, W.-C. Li, *Catalysis Communications* **2011**, 13, 18-21.
- [13] H.-F. Li, N. Zhang, P. Chen, M.-F. Luo, J.-Q. Lu, *Applied Catalysis B: Environmental* **2011**, 110, 279-285.
- [14] F. Moreau, G. C. Bond, *Catalysis Today* **2007**, 122, 215-221.

- [15] T. G. Schaaff, M. N. Shafigullin, J. T. Khoury, I. Vezmar, R. L. Whetten, W. G. Cullen, P. N. First, *Journal of Physical Chemistry B* **1997**, 101, 7885-7891.
- [16] <http://www.nanocyl.com/en/CNT-Expertise-Centre/Carbon-Nanotubes>, consulted 07/01/2014.
- [17] R. Zanella, E. V. Basiuk, P. Santiago, V. A. Basiuk, E. Mireles, L. Puente-Lee, J. M. Saniger, *Journal of Physical Chemistry B* **2005**, 109, 16290-16295.
- [18] H. Ismaili, F. Lagugné-Labarthe, M. S. Workentin, *Chemistry of Materials* **2011**, 23, 1519-1525.
- [19] J. Kimling, M. Maier, B. Okenve, V. Kotaidis, H. Ballot, A. Plech, *Journal of Physical Chemistry B* **2006**, 110 (32), 15700-15707.
- [20] J. Turkevich, P. C. Stevenson, J. Hillier, *Discussions of the Faraday Society* **1951**, 11, 55-75.
- [21] I. O.-J. F. M. Romero, N. G. Bastús, V. Puntes, *Journal of Physical Chemistry C* **2010**, 114, 1800-1804.
- [22] Z. Y. Li, N. P. Young, M. Di Vece, S. Palomba, R. E. Palmer, A. L. Bleloch, B. C. Curlwy, R. L. Johnston, J. Jiang, J. Yuan, *Nature* **2008**, 451, 46-48.
- [23] A. Mayoral, D. A. Blom, M. M. Mariscal, C. Guitierrez-Wing, J. Aspiazú, M. Jose-Yacamán, *Chemical Communications* **2010**, 46, 8758-8760.
- [24] R. F. Egerton, P. Li, M. Malac, *Micron* **2004**, 35, 399-409.
- [25] J. D. S Newman, G. J. Blanchard, *Langmuir* **2006**, 22, 5882-5887.
- [26] S. Zafeiratos, S. Kennou, *Surface Science* **1999**, 443, 238-244.
- [27] D. T. Thompson, *Nanotoday* **2007**, 2/4, 40-43.
- [28] B. Rodríguez-González, P. Mulvaney, L. M. Liz-Marzán, *Zeitschrift für Physikalische Chemie* **2007**, 221, 415-426.
- [29] J. Llorca, L. Alves, M. Torrens, A. Mayoral, E. Mendoza, *article in preparation*.
- [30] X.-Y. Wang, S.-P. Wang, S.-R. Wang, Y.-Q. Zhao, J. Huang, S.-M. Zhang, W.-P. Huang, S.-H. Wu, *Catalysis Letters* **2006**, 112, 115-119.

CHAPTER 4:

EX-SITU SYNTHESIS OF GOLD NANOCCLUSERS AND CATALYTIC ACTIVITY STUDY

4.1 SYNTHETIC PROTOCOL – Au NANOCCLUSERS

Gold nanoclusters were synthesised following the experimental method described by Xu *et al.* to obtain Ag nanoclusters^[1]. This refers to a simple sonochemical synthesis of Ag clusters using a polymer – poly(methacrylic acid) sodium salt (PMAA) (Figure 73) – (MW ~ 9500 g/mol; density = 1.251 g/mL; $[C_4H_5O_2Na]_n$, 30 wt% in H₂O, Aldrich) as reducing and capping agent to stabilise and protect the Ag nanoclusters in the solution.

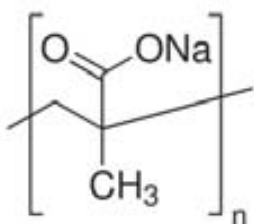


Figure 73. PMAA chemical structure.

Studies showed that PMAA whose carboxylic acid groups have a strong affinity for silver ions and silver surfaces is suitable to prepare Ag nanoclusters under UV irradiation^[1, 2]. The charged carboxylate groups (RCO_2^-) will stabilise the Ag nanoclusters and avoid its sinter or ripening. Moreover, PMAA will be oxidised by OH• leading to radicals that are unable to oxidise the metal ions^[3]. Thus, this polymer also acts as OH• radical scavengers preventing, in this way, the formation of metal oxide^[1, 4]. At the same time, the secondary radicals that result from the reaction of PMAA with OH• have a strong reducing power associated, therefore producing Ag atoms connected with the polymer chains^[1].

In this context, the possibility of using this method to synthesise Au nanoclusters was investigated. Experimentally, Au nanoclusters were prepared using HAuCl₄ as gold precursor. The synthesis was carried out at room temperature and consisted in adding the desired volume of HAuCl₄ to the PMAA aqueous solution (Figure 74). Then, the pH of the resulting solution was

adjusted to 4.5 using a 2.5 M HNO_3 aqueous solution (Figure 74). The resultant solution was then deaerated with N_2 for one hour (Figure 74) to avoid the aggregation of the nanoclusters (Chapter 1, Section 1.3.6), and finally ultrasonicated for 20 minutes using 100 W of power under a N_2 atmosphere in a refrigerated cell (Chapter 2, Section 2.10.1, Figure 26). This time period of sonication was chosen since, for Ag, it was observed that clusters were formed after 10 minutes of sonication^[1]. Moreover, the increase of the sonication time leads to an undesirable increase of the nanoclusters' mean diameter^[1].

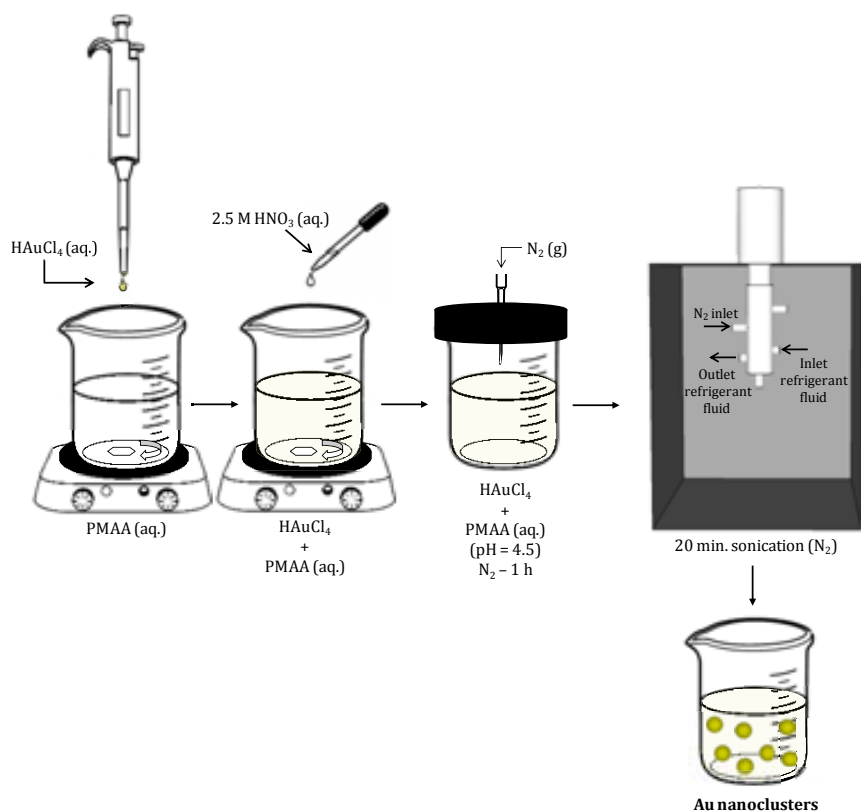


Figure 74. Schematic representation of the ex-situ Au nanoclusters sonochemical synthesis procedure.

The solution pH was maintained at 4.5 since it has been reported that both levels of ionisation of the carboxylic acid groups and PMAA structure are

affected significantly by the pH^[2]. The sonochemical reaction consists in the dissociation of the PMAA into ionised carboxylic acid groups (RCO_2^-) that will sequester the metallic Au. Thus, on the one hand, the degree of ionisation of the carboxylic acid groups will be different, depending on the pH solution, and therefore, the ability of these groups to bind to gold is varied. For example, if the pH is too low (pH \sim 2.3), all the carboxylic acid groups will be protonated and there will not exist available RCO_2^- groups to bind to Au, and consequently nanoclusters will not be formed^[2]. On the other hand, the conformation of this polymer is also highly dependent on the pH solution and it influences the size of the nanoclusters formed^[2]. It is known that, at pH=5, the PMAA in aqueous solution suffers a conformational change. At lower pH, the Au is captured by the ionised carboxylic acid groups and protected by a compact structure formed by the polymer molecule and it is, in this way, stabilised. At these pHs, the polymer isolates the formed nanoclusters by a hydrophobic core^[2]. If the pH is increased (pH > 5), this protection will be weaker due to the lower compactness of the structure.

Au nanoclusters were successfully obtained following this procedure. These nanoclusters were easily characterised by atomic force microscopy (AFM). Au nanoclusters appeared as bright dots easily distinguished in the topography images (Figure 75). Additionally, Au agglomerates were not found.

4.2 RCO_2^- /Au MOLAR RATIO INFLUENCE IN THE Au PARTICLE SIZE

It has been observed that the size of the metal nanoclusters is directly dependent on the quantity of polymer added (Chapter 1, Section 1.3.6)^[1, 5]. A higher stabilisation, i.e. an increase of the polymer quantity, leads to smaller metal nanoclusters^[1, 5]. With the goal of synthesising the smallest gold

nanoclusters, a study about how the RCO_2^- / Au ratio influences the mean Au cluster size was carried out. Thus, different values of this variable, namely 0.1, 0.5 and 2, were used in order to conclude about the optimal RCO_2^- / Au molar ratio. In this study, the concentration of Au was fixed in 0.02 mg/mL, once that higher concentrations lead to an easier agglomeration of gold, due to the lower Au interparticle distance. The Au nanoclusters synthesised with different RCO_2^- / Au molar ratios were characterised by AFM (Figure 75). AFM characterisation allowed the Au particle size distributions of the three different RCO_2^- / Au molar ratios samples to be obtained (Figure 76).

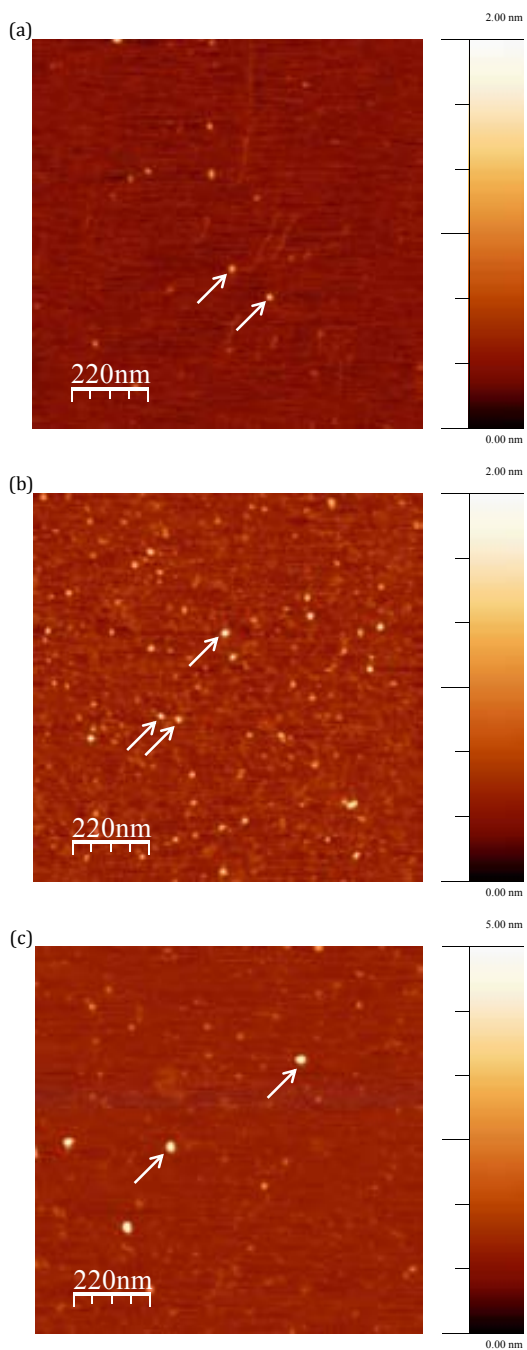


Figure 75. AFM topography images of Au nanoclusters prepared with a RCO_2^-/Au molar ratio of 0.1 (a), 0.5 (b) and 2 (c). Selected particles are indicated by arrows.

The size distributions obtained revealed an increase of Au nanoparticles ($d > 2$ nm) population for higher molar ratios (Figure 76). Although these nanoparticles have a diameter lower than 5.0 nm they appear for the molar ratios of 0.5 and 2. Nevertheless, no significant differences of the Au mean particle diameter were observed for the three different samples (Table 20). For the RCO_2^- / Au molar ratios of 0.1, 0.5 and 2, a mean particle diameter of 1.3 ± 0.3 nm, 1.2 ± 0.4 nm and 1.5 ± 0.8 nm was obtained respectively. A slight increase of the mean Au cluster size for the $RCO_2^- / Au = 2$ sample results from the slightly higher quantity of Au nanoparticles formed (the quantity of Au nanoparticles with a diameter higher than 2 nm represents 15% of the counted particles). It was then concluded that in the 0.5 and 2 samples Au nanoclusters are formed in major quantity while the population of Au nanoparticles ($d > 2$ nm) is not significant for the lower RCO_2^- / Au molar ratio, i.e. 0.5 (the quantity of Au NPs represents 3% of the counted particles).

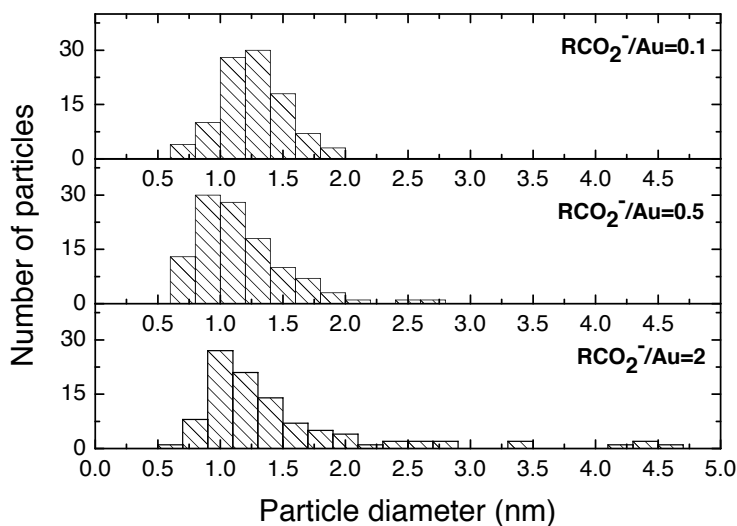


Figure 76. Particle size distribution histogram for gold nanoclusters synthesised with different RCO_2^- / Au molar ratios.

Table 20. Mean Au particle diameter obtained by AFM using different RCO_2^- / Au molar ratios.

RCO_2^- / Au	Particle diameter (nm)
0.1	1.3±0.3
0.5	1.2±0.4
2	1.5±0.8

This result is not in accordance with the ones previously stated by other authors who observed lower metal particle sizes due to the stronger polymer stabilisation that impeded the aggregation of the formed metal nanoclusters into nanoparticles^[1, 5]. Notice, however, that the referred studies concern different metals and polymers combinations (Ag with PMAA and Au with PTMP-pMAA)^[1, 5]. Thus, when reducing $H AuCl_4$ by PMAA different results, due to the different species that interfere in the synthesis reaction mechanism, can be obtained. Nevertheless, this result might be also explained due to the higher viscosity of the solution prepared with an excess of the very viscous PMAA (110 000 cps – 375 000 cps polymer viscosity). The mechanism proposed by Okitsu *et al.* indicates that Au^{3+} is reduced to metallic gold and that the particle size is lowered for a higher rate of reduction^[6]. In this context, the increase of the polymer in solution will lead to a higher viscosity leading then to a slower reduction of Au^{3+} to Au^0 once that more energy would be necessary to form the reactive species. Moreover, the influence of the PMAA molecular weight in the formation of Ag nanoclusters has been observed^[1]. Xu *et al.* noticed a decrease of the fluorescence intensity indicating an augment of the Ag nanoclusters size with the increase of the polymer viscosity. This observation was attributed to the slower diffusion of the reactive species produced by sonolysis into the interior of the longer chain length polymers^[1].

From this characterisation study, due to the coexistence of a higher quantity of Au NPs with the Au clusters the sample of $RCO_2^- / Au = 2$ was discarded. A most uniform size distribution with a lower mean diameter dispersion of Au nanoclusters is desired. Thus, based on these results both 0.1 and 0.5 RCO_2^- / Au

molar ratios could be used as optimal values. Nevertheless, in general AFM images showed a higher quantity of Au nanoclusters for the 0.5 sample. This indicates that maybe in the 0.1 sample not all Au precursor was reduced into Au nanoclusters. Thus, it was concluded that the RCO_2^- / Au optimal molar ratio was the medium value, i.e. 0.5.

As conclusion, the successful synthesis of Au nanoclusters by a green sonochemical synthesis was demonstrated by simply using a gold precursor, water and PMAA. The advantage of this method over other methods that use polymer microgels or dendrimers as reducing agents is the fact that this uses a common polymer, commercially available. Thus, this is an extremely simple method, economic and environmentally-friendly. The different RCO_2^- / Au ratios samples characterisation revealed that the Au NPs population is augmented with the increase of the polymer concentration which might be explained by the higher viscosity of the ncAu-PMAA solution that would require more energy to form the reactive active species and therefore a slower rate of diffusion will take place and consequently the Au nanoclusters size will be increased^[1, 6]. Other polymers such as poly(acrylic acid) (PAA, MW = 8000 g/mol) are also feasible to produce Au nanoclusters^[2]. However, this polymer is not as efficient as PMAA once that the interaction of the PAA with the metal is slower. The faster interaction observed, when using PMAA, results from the presence of a methyl group in its chain that attributes to it a higher hydrophobicity favouring thus the formation of Au nanoclusters^[2].

4.3 SYNTHESIS OF SUPPORTED Au NANOCUSTERS CATALYSTS

The synthesised Au nanoclusters ($RCO_2^- / Au = 0.5$; $[Au] = 0.02$ mg/mL) were effectively deposited on MWCNTs, CeO_2 and TiO_2 surfaces covered with amine groups. The preparation of the support-PAH hybrids was performed as it was described in Chapter 3 (Section 3.1). The deposition of the ex-situ synthesised Au nanoclusters was carried out by simply dropwising the nanoclusters' solution into the liquid support-PAH suspension under sonication (Figure 77). The ncAu/support liquid catalysts were left 15 minutes under sonication in an ice bath. After this time, the pre-synthesised Au nanoclusters were uniformly dispersed, anchored and stabilised on the supports' surface (Figure 77). The catalysts prepared in this work are presented in Table 21.

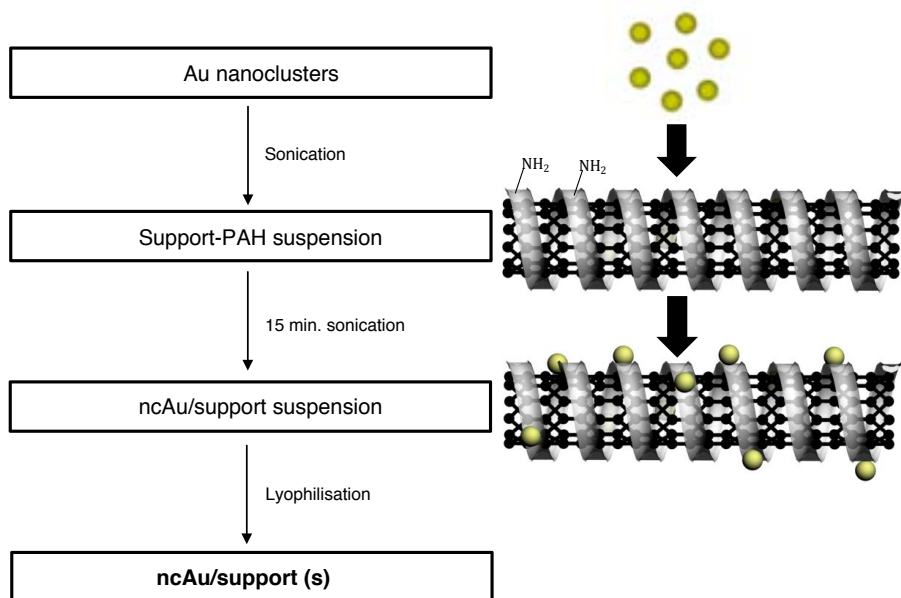


Figure 77. Ex -situ synthesis scheme procedure (left) and respective schematic representation using MWCNTs as support (right).

Table 21. List of the ex-situ synthesised catalysts.

Catalyst	Nomenclature	Au loading (wt%)
Au/CeO ₂ (74.0 m ² /g)	ncAu(0.1wt%)/CeO ₂	0.1
	ncAu(0.3wt%)/CeO ₂	0.3
	ncAu(0.5wt%)/CeO ₂	0.5
	ncAu(3wt%)/CeO ₂	3
Au/TiO ₂	ncAu(0.5wt%)/TiO ₂	0.5

4.3.1 HIGH RESOLUTION TRANSMISSION ELECTRON MICROSCOPY

By HRTEM characterisation it was observed the existence of Au nanoclusters on the supports' surface. Taking into account the different surface areas of these materials, as it was discussed in Chapter 3 (Section 3.3.2), different Au contents were chosen when using MWCNTs, CeO₂ or TiO₂ as support. The successful deposition of Au nanoclusters in these three distinct supports indicates that ex-situ Au nanoclusters can also be anchored to several different types of surfaces when these are covered by amine groups, which shows the versatility of this method. Figure 78 shows an HRTEM image of a ncAu(0.5wt%)/TiO₂ catalyst. A mean particle diameter of 1.4±0.4 nm was obtained for this catalyst (Figure 79).

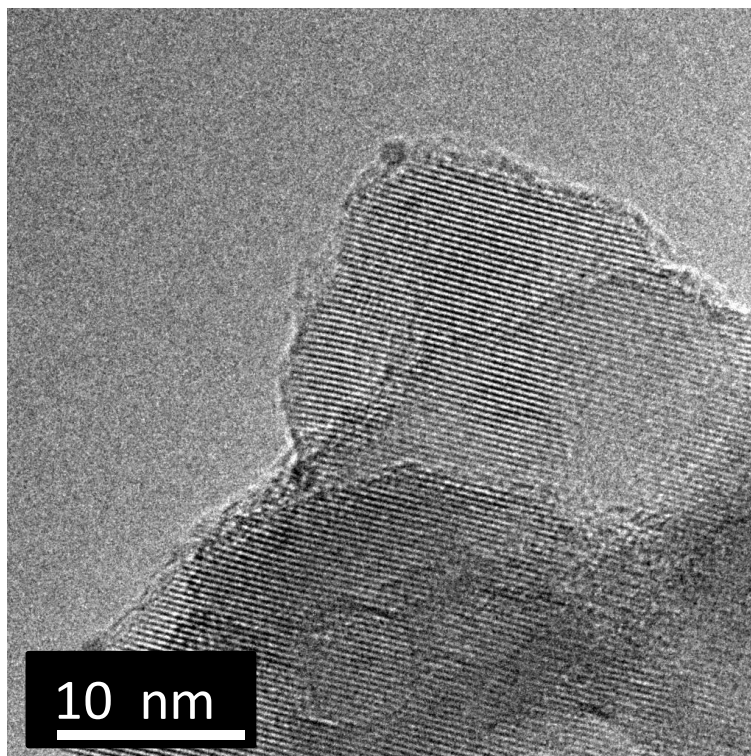


Figure 78. HRTEM images of a ncAu(0.5wt%)/TiO₂ catalyst.

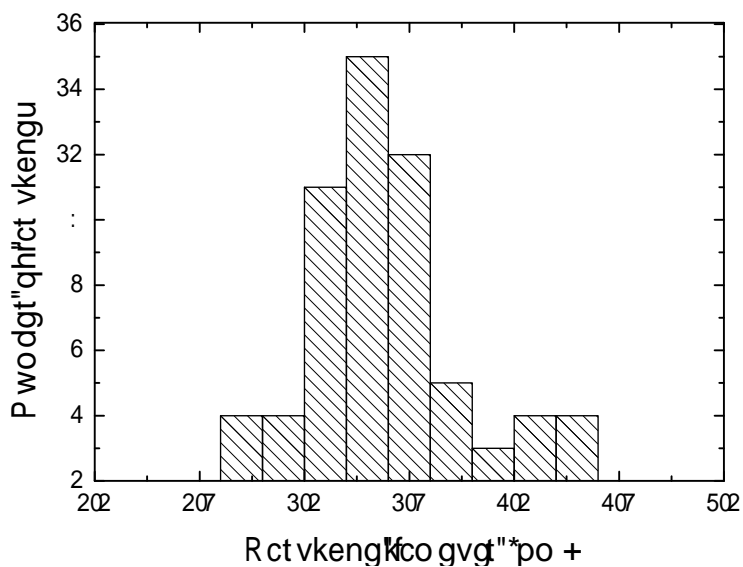


Figure 79. Particle size distribution histogram for a ncAu(0.5wt%)/TiO₂ catalyst.

Furthermore, comparing this mean value (1.4 ± 0.4 nm) with the one obtained by AFM (1.2 ± 0.4 nm), it was concluded that gold nanoclusters did not agglomerate while in solution and, were well dispersed on the supports maintaining their size without sinter, by a 15 minute ultrasonication. Using other supports a similar mean Au particle diameter (1.3 nm – 1.4 nm) was obtained.

Moreover, the activity of these catalysts was tested after more than one month of preparation and similar results to fresh catalysts were obtained indicating that these ex-situ catalysts are stable. This is a very good result once that the ability to obtain an uniform and stable size distribution of Au nanoclusters catalysts have been reported essentially using just the DP synthetic protocol^[7-9]. This simple sonochemical water soluble synthesis method represents then a new approach since it is the first time reported to obtain ncAu/support catalysts by an sonochemical environmental-friendly and economically viable method.

4.3.2 X-RAY PHOTOELECTRON SPECTROSCOPY

The chemical nature of the ncAu/CeO₂ catalysts was investigated by XPS (Figure 80). Catalysts with a gold loading of 0.1 wt%, 0.5 wt% and 3 wt% were prepared. The three catalysts showed a BE value close to the bulk Au4f_{7/2} BE (84.0 eV) indicating that gold nanoclusters are metallic (Table 22). Thus, it was concluded that the chemical nature of the Au clusters synthesised by the in-situ or ex-situ synthesis method is different. Unlike the in-situ synthesised catalysts, these do not present positively charged gold species. This can be explained by the different mechanisms of formation of Au clusters of the two synthetic protocols.

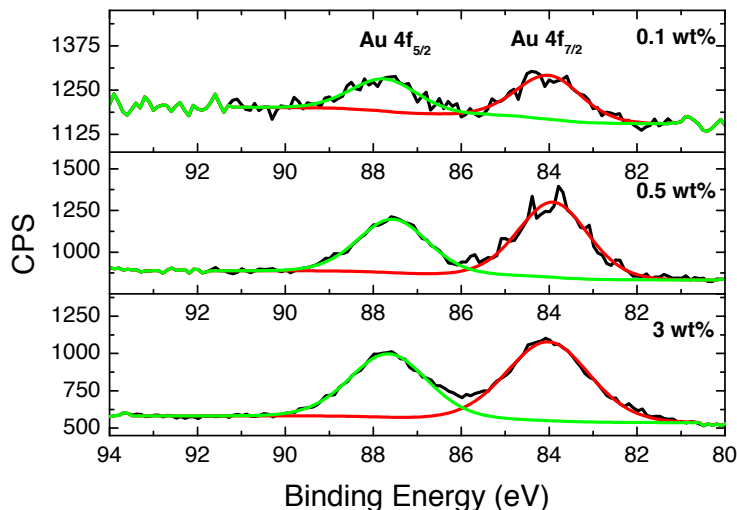


Figure 80. XPS spectra of the Au4f peak and respective fit components for gold nanoclusters obtained at different nominal gold loadings on CeO₂.

Table 22. XPS data for different Au content ncAu/CeO₂ catalysts.

Au content (wt%)	0.1	0.5	3
4f _{7/2} BE (eV)	84.0	83.9	84.0

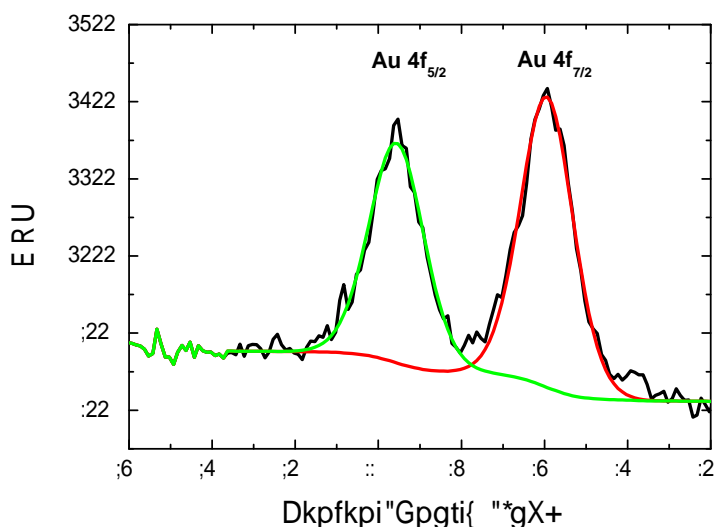
The chemical nature of the sonochemically prepared of gold clusters has not been much reported. Liu *et al.* observed that the 1.8 nm Au nanoclusters sonochemically prepared using BSA as reducing agent were composed by both metallic (Au⁰) and cationic gold (Au^{δ+}) (Table 23)^[10].

Moreover, the synthesis of gold nanodots using different reagents, such as HAuCl₄·3H₂O, tetrakis(hydroxymethyl)phosphonium chloride (THPC), trisodium tetraborate and 11-mercaptoundecanoic acid (11-MUA), by Huang *et al.*, showed that the BE values of the Au4f_{7/2} vary with the Au mean particle diameter (Table 23)^[11]. In accordance to what has been observed in Chapter 3 (in-situ), Huang *et al.* noticed that a decrease of the Au particle size leads to an increase of the Au4f_{7/2} BE shift. These authors obtained Au^{δ+} (~ 85.0 eV) for the smallest gold nanodots (1.2±0.2 nm). The larger nanodots (1.7±0.2 nm and 2.1±0.1 nm) showed a BE similar to the bulk metallic gold (Au⁰)^[11].

Table 23. Au 4f_{7/2} BE values of gold nanoclusters synthesised by different methods.

Synthesis method	d (nm)	Au4f _{7/2}
Sonochemical (using BSA as reducing agent of HAuCl ₄) ^[10]	~ 1.8	84.0/85.1
1 - Reduction of HAuCl ₄ .3H ₂ O with THPC by a vigorously vortexing;	[THPC]/[HAuCl ₄]	-
	1.0	1.2±0.2
2 - Reaction between DI water, trisodium tetraborate, 11-MUA and THPC-Au NPs ^[11] .	2.0	1.7±0.2
	3.5	2.1±0.1

Furthermore, in order to check if the surface of Au nanoclusters was modified, the ncAu(0.5wt%)/CeO₂ catalyst was analysed after a three hour calcination at 300 °C. XPS results revealed (Figure 81) that after calcination Au maintains its metallic state (BE = 83.9 eV). Therefore, the Au that will participate in the CO oxidation will be all metallic, when using this ex-situ synthesis method to prepare the catalysts. In this way, the role of Au⁰ in the CO oxidation can be easily concluded.

**Figure 81.** XPS spectrum of the Au4f peak and respective fit components for the ncAu(0.5wt%)/CeO₂ catalysts after a three hour calcination at 300 °C.

Briefly, the advantages of this simple method include nonhazardous, fast reaction rate, controllable reaction conditions and the ability to form nanoclusters with a narrow size distribution^[10]. Moreover, the ex-situ synthesised metallic Au nanoclusters deposition on different surfaces covered by amine groups was successfully achieved. Despite the successful synthesis of sonochemical prepared Au nanoclusters in 2011, this field was very poorly developed since then^[10]. Indeed, the deposition of sonochemical prepared Au nanoclusters on catalytic active surfaces in order to test the catalysts activity was not reported yet. Hence, this is the first time that such procedure was carried out. Activity results could be compared with the Au/CeO₂ catalysts synthesised by DP and co-P protocols reported by other authors (Chapter 1, Section 1.6.1, Figure 17).

Besides all the named advantages, this synthetic protocol can also be easily scaled-up to be used in industry. Indeed, in the end of 2012 this synthetic protocol was patented by the *Universitat Politècnica de Catalunya* in collaboration with a private company (*Goldemar Solutions*)^[12]. This ex-situ synthesis method was easily scaled-up and currently operates as a highly reproducible continuous method which makes it a more economical process. Nowadays, these ex-situ catalysts are being used for several practical applications of air purification by *Goldemar Solutions* (Section 4.4)^[13].

4.4 CATALYTIC ACTIVITY

The catalytic activity of the ncAu/CeO₂ ex-situ catalysts in CO oxidation was investigated. The catalysts were prepared by depositing ex-situ synthesised Au nanoclusters on the CeO₂ surface (Section 4.3, Figure 77). Powder catalysts with a very low gold content (0.1 wt%, 0.3 wt% and 0.5 wt%) were prepared in order to avoid the sinter of the nanoclusters during reaction. The conditions used and the experimental protocol followed to carry out the catalytic tests are presented in Annexes (Section A.3).

Unlike the in-situ catalysts, all the ncAu/CeO₂ catalysts showed a higher CO conversion than the support CeO₂ (Figure 82). This result revealed that metallic Au nanoclusters are active for the CO oxidation.

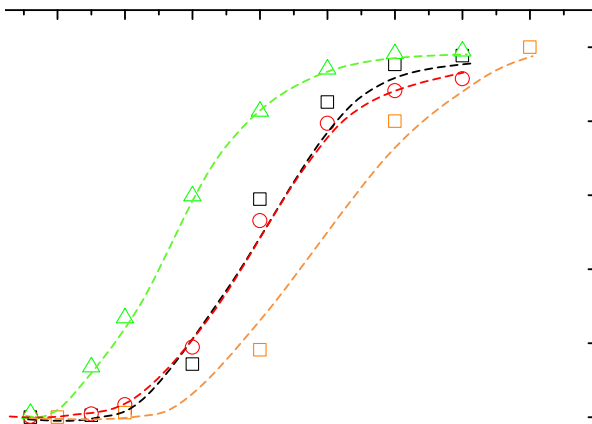


Figure 82. Comparison of the CO conversion of CeO₂ (---□---), ncAu(0.1wt%)/CeO₂ (---□---), ncAu(0.3wt%)/CeO₂ (---○---) and ncAu(0.5wt%)/CeO₂ (---△---) catalysts. Flow rate: 100 mL/min (96 v/v% N₂; 2 v/v% O₂; 2 v/v% CO).

Additionally, the higher CO conversion was obtained for the ncAu(0.5wt%)/CeO₂ catalyst. Nevertheless, when normalising these values to reaction rate (Figure 83) it can be seen that the most active catalyst is the ncAu(0.1wt%)/CeO₂. Thus, it was concluded that the higher conversion observed for the ncAu(0.5wt%)/CeO₂ catalyst is due to the higher quantity of Au in this catalyst.

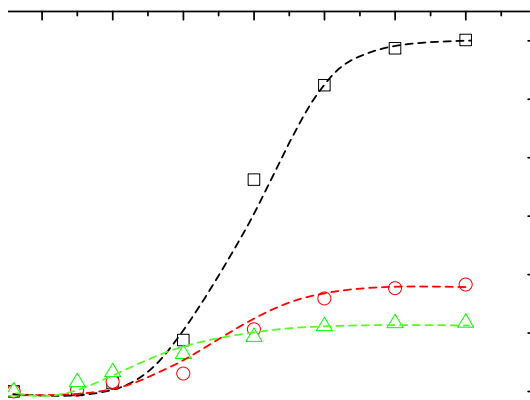


Figure 83. Catalytic activity of the ncAu(0.1wt%)/CeO₂ (---□---), ncAu(0.3wt%)/CeO₂ (---○---) and ncAu(0.5wt%)/CeO₂ (---△---) catalysts for CO oxidation (1st cycle). Flow rate: 100 mL/min (96 v/v% N₂; 2 v/v% O₂; 2 v/v% CO).

Results showed that independently of the Au content, catalysts are not active at room temperature (Figure 83). Its activity starts only around 150 °C. Also, the ncAu(0.1 wt%)/CeO₂ catalyst showed a significant increase of activity, when compared to the higher gold content catalysts, at high temperatures ($T > 150$ °C) (Figure 83). This result can be explained by the sinter of the Au nanoclusters in the 0.3 wt% and 0.5 wt% catalysts despite the low gold contents used. These last catalysts show a similar activity in the complete range of temperatures due to the Au loading similarity (Figure 83). The slightly lower activity verified for the ncAu(0.5wt%)/CeO₂ catalyst at high temperatures ($T > 150$ °C) might be explained by the more significant agglomeration of Au nanoclusters in this higher gold content catalyst (Figure 83).

The CO oxidation activity is extremely dependent on the Au particle size. Large Au NPs are not active for this reaction. Haruta observed a significant increase of the catalytic activity of Au/TiO₂ catalysts when the Au particle size is lower than 5 nm. Au nanoparticles with a diameter around 7 nm and 18 nm show a similar and very near to zero turnover frequency (TOF) number^[14]. When the

Au particle size is subsequently lower than 4 nm a consequent increase of the TOF for CO oxidation over Au/TiO₂ has been observed by this author^[14]. Thus, this study indicates that Au nanoparticles larger than around 20 nm are no longer active for CO oxidation. It seems, then, that the ncAu(0.3wt%)/CeO₂ and the ncAu(0.5wt%)/CeO₂ catalysts sinter led to the formation of nanoparticles larger than 5 nm.

Using the ncAu(0.5wt%)/CeO₂ catalyst, a second cycle of temperature increase was carried out. In this, it was observed that this catalyst maintains approximately its first cycle activity (Figure 84). It was then concluded that, after the sinter of the Au nanoclusters that occurred, Au did not grow more, maintaining therefore its catalytic activity.

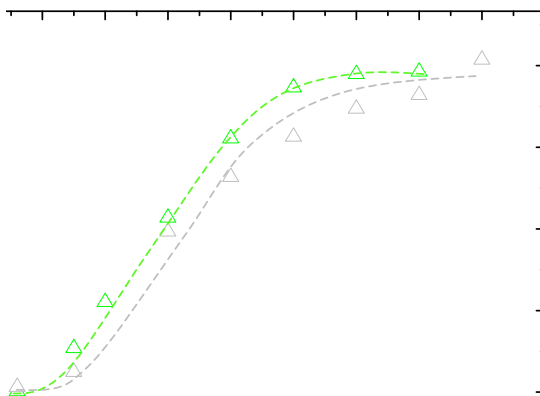


Figure 84. Catalytic activity comparisons of the 1st (---) and 2nd (---) cycle for the ncAu(0.5wt%)/CeO₂ catalyst. Flow rate: 100 mL/min (96 v/v% N₂; 2 v/v% O₂; 2 v/v% CO).

Furthermore, when comparing the activity of both most active in-situ and ex-situ synthesised 0.1 wt% gold loading catalysts – Au(0.1wt%)/CeO₂ and ncAu(0.1wt%)/CeO₂ respectively – a significant higher activity for the catalyst synthesised using the ex-situ Au nanoclusters (Figure 85) was observed.

Indeed, not even at 600 °C the in-situ catalyst was able to reach the activity of the ex-situ catalyst at 350 °C.

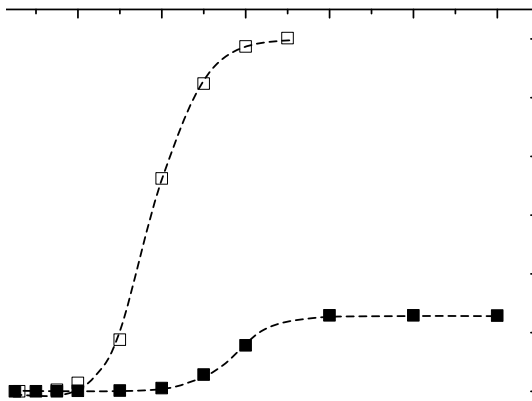


Figure 85. Comparison of the catalytic activity of both synthetic protocols: in-situ Au(0.1wt%)/CeO₂ (---■---) and ex-situ ncAu(0.1wt%)/CeO₂ (---□---).

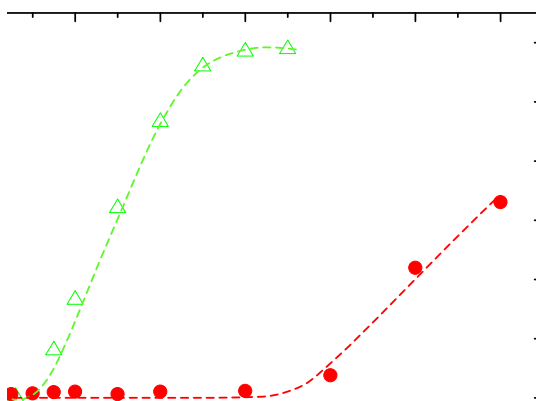


Figure 86. Comparison of the catalytic activity of both synthetic protocols: in-situ Au(0.5wt%)/CeO₂ (---●---) and ex-situ ncAu(0.5wt%)/CeO₂ (---△---).

The same result was observed for the 0.5 wt% gold content catalysts (Figure 86). As before, this gold content catalyst showed a much lower activity when prepared by the in-situ protocol at 600 °C, than the ex-situ synthesised at 350 °C (Figure 86). This difference results essentially from the fact that the ex-situ synthetic protocol is cleaner, i.e the Au nanoparticles and CeO₂ active sites are not covered by intermediate species formed during the synthesis reaction.

Although it was not observed by XPS, due to the very low signal for the Au4f and therefore reliable values could not be obtained, it is believed that the in-situ very low gold content synthesised Au/CeO₂ catalysts (0.1 wt% and 0.5 wt%) are composed only by Au^{δ+}. Indeed, by XAS, using the same gold content MWCNTs catalysts it was concluded that these catalysts were only composed by Au^{δ+}. Due to the inability of measuring the catalytic activity of the in-situ catalysts due to the cover of their active sites, the role of the positively charged Au species in CO oxidation could not be investigated as discussed in Chapter 3 (Section 3.6.2). Nevertheless, using the ex-situ catalysts which are composed only by metallic gold nanoclusters the role of these species in this reaction could be concluded. It was concluded that this specie is active for the CO oxidation. Despite the controversy that exists about which is the Au active specie for the CO oxidation, these results lead to conclude that metallic gold is essential to observe the CO oxidation in accordance to what has been observed by Pillai *et al.* and Qian *et al.*^[15, 16]. Nevertheless, some authors claimed that cationic gold species (Au^{δ+}) are more active than Au⁰ for CO oxidation^[17, 18]. Even so, Haruta *et al.* questioned the role of the cationic species since the majority of XPS analysis show the presence of metallic gold in the most active gold catalysts^[19-21]. Moreover, these authors also affirmed that oxidised gold should be reduced during the CO oxidation. Indeed, Han *et al.*, although claiming that the activity observed was due mostly to the Au^{δ+} species, noticed a significant increase of Au⁰ after CO oxidation^[22].

Besides, the results experimentally obtained for the sonochemical prepared ncAu/CeO₂ catalysts were compared with the activities observed using different synthesis methods, namely deposition-precipitation and co-precipitation (Figure 87).

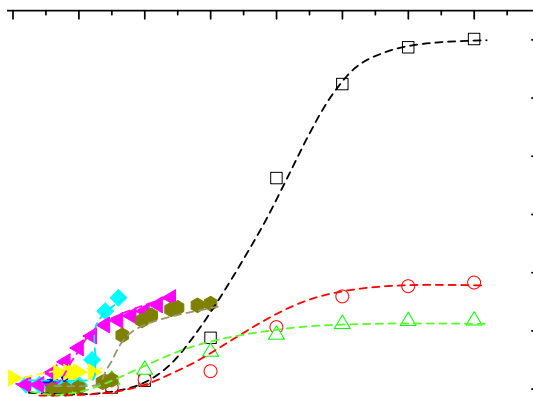


Figure 87. Comparison of the catalytic activity of the reaction rate of the ncAu(0.1wt%)/CeO₂ (---□---), ncAu(0.3wt%)/CeO₂ (---○---), ncAu(0.5wt%)/CeO₂ (---△---) catalysts with the literature catalysts: DP1^[23] (---▽---), DP2^[9] (---◇---), DP3^[9] (---▲---), DP4^[24] (---▾---), Co-P^[25] (---◆---) for the CO oxidation.

Figure 88 shows a zoom of the temperature range zone between 0 °C and 150 °C. Importantly, the ex-situ catalysts showed a similar activity to the co-precipitation catalyst. Indeed, the activity of the co-precipitation synthesised catalyst is approximately only twice higher than the ncAu(0.1wt%)/CeO₂ catalyst at 150 °C. In fact, the ncAu(0.1wt%)/CeO₂ catalyst reaches the co-precipitation catalyst maximum activity observed at 150 °C around a very similar temperature (160 °C) (Figure 87).

In general, the DP synthesis gives origin to more active catalysts than the sonochemical prepared in the range of temperatures of 30 °C to 150 °C (Figure 88). Indeed, temperature increases of approximately 60 °C and 50 °C were required to achieve the maximum activity of the DP1 and DP4 respectively, by the ncAu(0.1wt%)/CeO₂ catalyst. Moreover, an approximate 80 °C increase was

necessary to the ncAu(0.1wt%)/CeO₂ catalyst to achieve the maximum activity of the DP2 catalyst.

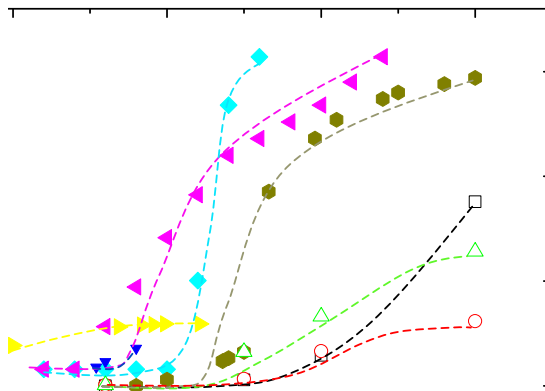


Figure 88. Comparison of the catalytic activity of the reaction rate of the ncAu(0.1wt%)/CeO₂ (—□—), ncAu(0.3wt%)/CeO₂ (—○—), ncAu(0.5wt%)/CeO₂ (—△—) catalysts with the literature catalysts: DP1^[23] (—▽—), DP2^[9] (—◇—), DP3^[9] (—▲—), DP4^[24] (—▶—), Co-P^[25] (—◆—) for the CO oxidation in the range of 0-150 °C.

In conclusion the ex-situ ncAu/CeO₂ catalysts present similar activities to the catalysts prepared by co-P and, even though, in general, they do not show a better catalytic activity than the ones prepared by DP method these results are very promising. This was the first time that active catalysts were prepared for CO oxidation by a pre-synthesis of Au nanoclusters clean sonochemical procedure.

Still, this method could be improved by changing some variables that certainly will lead to an increase of the catalytic activity of these ex-situ synthesised Au nanoclusters catalysts. For example, the effect of the support characteristics is extremely important and affects significantly the catalytic activity, as it has been reported by Carretin *et al.* where the increase of activity of Au for CO oxidation in two order of magnitudes was observed by simply using as support nanocrystalline particles of cerium oxide instead of a regular cerium oxide support^[26]. Thus, by simply changing this variable, an increase of activity will

be likely observed. Besides regular, the cerium here used has a low surface area (74.0 m²/g) which will also lead to the easier agglomeration of Au at high temperatures.

Additionally, Zhang *et al.*, despite the discussion between the role of Au⁰ and Au^{δ+} as active species for CO oxidation, claimed that a balanced quantity between both species is required to obtain higher activities^[9]. By XPS it was concluded that the Au in these ex-situ catalysts is all in the form of Au⁰ indicating that these species are active and necessary for the CO oxidation. Nevertheless, the co-existence of Au⁰ with Au^{δ+} species could possibly increase the catalytic activity.

This ex-situ synthesis method is very promising due to the ability of obtaining a uniform population of Au nanoclusters by a simple and environmental-friendly protocol. Although CO oxidation catalytic activity was not observed at room temperature, putting these catalysts below several other developed Au catalysts actives at this temperature they could be used in other higher temperature applications. For example, they could be an alternative to the Pt catalysts used in high temperature proton exchange membrane (HT-PEM) fuel cells which work at 150 °C – 200 °C^[27, 28].

Improvements of the synthetic protocol have been carried out since the start of the company *Goldemar Solutions* in Barcelona. Since the first synthesis in 2011 and all the characterisation study this protocol was patented in the end of 2012 by *Universitat Politècnica de Catalunya* in collaboration with *Goldemar Solutions*^[12]. During the same year the company started to apply this synthetic protocol to the development of highly active Au nanoclusters catalysts for air purification applications in an industrial scale^[13]. Further characterisation studies and catalytic activity tests that allowed improvements to the ex-situ protocol were the object of two final career projects at the *Universitat Politècnica de Catalunya* that were carried out in the company^[29, 30]. Besides the supports presented in this work, Au nanoclusters have been successfully anchored to other surfaces covered with amine groups, such as ZrO₂, Fe₂O₃ and

SiO₂. For example, promising results have been obtained using Au/CeO₂, Au/ZrO₂ and Au/Ce_xZr_{1-x}O₂ for the elimination of formaldehyde (a typical volatile organic compound (VOC) molecule and one of the most common and noxious indoor gaseous pollutants)^[30]. Thus, further improvements in the synthetic protocol were and are still being carried out by the *Goldemar Solutions* team. In this way, more active catalysts were obtained and its commercialisation is expected soon. Currently, these catalysts are being tested for environmental interest applications of air purification at low temperature such as:

- " Reduce of the vehicle emissions (CO oxidation at low temperature; low temperature combustion of soot) and cost of catalytic converters;
- " Removal of VOCs (formaldehyde or toluene) and pollutants from indoor air at room temperature;
- " Purification of air in closed environments;
- " Improvement of respirator protective equipment.

Indeed, another patent was submitted in 2013 by our group in collaboration with *Goldemar Solutions*^[31]. In this document it is demonstrated the oxidation of CO at room temperature by a 0.1 wt% gold content ncAu/CeO₂ catalyst. Additionally, it was showed that this catalyst was stable after three cycles of reaction in a temperature range of 30 °C – 850 °C. In addition, the ability of these Au nanoclusters to decrease the carbon black combustion temperature was also demonstrated (this study is presented in Chapter 5). Finally, the ability of these catalysts to reduce several different VOCs was also demonstrated. It was concluded that a 0.1 wt% ncAu/CeO₂ catalyst is more active to reduce aldehydes contents than the until now reported catalysts^[31].

4.5 CONCLUSIONS

In this chapter a simple and reproducible sonochemical ex-situ synthesis method of Au nanoclusters was successfully presented and developed. The sonochemical synthesis of Au nanoclusters was successfully achieved using PMAA as the reducing and capping agent of the Au nanoclusters. How the RCO_2^- / Au ratio influences the Au particle size, was investigated by AFM characterisation. This study revealed that an increase of the polymer quantity in solution leads to a slight increase of Au NPs in the Au nanoclusters solution. A RCO_2^- / Au molar ratio of 0.5 was concluded as the optimal value. Au nanoclusters with a mean diameter of approximately 1.2 nm were obtained using a Au concentration of 0.02 mg/mL and a RCO_2^- / Au molar ratio of 0.5.

The fresh sonochemical pre-synthesised Au nanoclusters were, for the first time, successfully anchored to surfaces with amine groups, namely MWCNTs, CeO_2 and TiO_2 . Stable ncAu/support catalysts were obtained. Agglomerates of gold were not observed. A Au mean particle diameter similar to the one obtained by AFM of the unsupported nanoclusters was achieved. XPS analysis revealed that gold nanoclusters were in the form of metallic gold (Au^0) independently of the gold loading (0.1wt%, 0.5wt% or 3 wt%) of the ncAu/ CeO_2 catalysts. The metallic state of gold is maintained after the catalyst calcination.

Furthermore, for the first time the catalytic activity of supported ex-situ sonochemical prepared Au clusters catalysts was presented. These ex-situ ncAu/ CeO_2 catalysts are active for the CO oxidation. It was, thus, demonstrated that Au^0 is an active specie for the CO oxidation. The ncAu(0.1wt%)/ CeO_2 catalyst is the most active for this reaction since Au aggregation that takes place at high temperatures is avoided in such lower Au loading. The ncAu(0.3wt%)/ CeO_2 and ncAu(0.5wt%)/ CeO_2 catalysts showed a low activity for CO oxidation probably due to the Au sinter. After a first CO oxidation reaction cycle, the activity of the ncAu(0.5wt%)/ CeO_2 catalyst was maintained indicating the end of the Au sinter. It was then concluded that ex-situ catalysts

are more active for CO oxidation than in-situ catalysts due to its cleaner surface (higher amount of active sites available). Furthermore, it was concluded, the ex-situ ncAu/CeO₂ catalysts are less active than the deposition-precipitation catalysts but have a comparable activity to the co-precipitation catalysts reported by other authors for CO oxidation.

The results obtained are very promising. Indeed, this synthetic protocol was patented by the *Universitat Politècnica de Catalunya* in collaboration with the *Goldemar Solutions* company. Also, since this first study, ex-situ catalysts improvements have been carried out by this company and, currently, these catalysts are being tested for different practical applications with an environmental interest.

4.6 REFERENCES

- [1] H. Xu, K. S. Suslick, *ACS Nano* **2010**, 4, 3209-3214.
- [2] L. Shang, S. Dong, *Chemical Communications* **2008**, 1088-1090.
- [3] J. Belloni, M. Mostafavi, H. Remita, J.-L. Marignier, M.-O. Delcourt, *New Journal of Chemistry* **1998**, 1239-1255.
- [4] E. Janata, A. Henglein, B. G. Ershov, *Journal of Physical Chemistry* **1994**, 98, 10888-10890.
- [5] N. Schaeffer, B. Tan, C. Dickinson, M. J. Rosseinsky, A. Laromaine, D. W. McComb, M. M. Steven, Y. Wang, I. Petit, C. Barentin, D. G. Spiller, A. I. Cooper, R. Levy, *Chemical Communications* **2008**, 3986-3988.
- [6] K. Okitsu, M. Ashokkumar, F. Grieser, *Journal of Physical Chemistry B* **2005**, 109, 20673-20675.
- [7] S. Tsubota, M. Haruta, T. Kobayashi, A. Ueda, Y. Nakahara, *Studies in Surface Science and Catalysis* **1991**, 72, 695-704.
- [8] S. Tsubota, D. A. H. Cunningham, Y. Bando, M. Haruta, *Studies in Surface Science and Catalysis* **1995**, 91, 227-235.
- [9] R.-R. Zhang, L.-H. Ren, A.-H. Lu, W.-C. Li, *Catalysis Communications* **2011**, 13, 18-21.
- [10] H. Liu, X. Zhang, X. Wu, L. Jiang, C. Burda, J.-J. Zhu, *Chemical Communications* **2011**, 47, 4237-4239.
- [11] C.-C. Huang, H.-Y. liao, Y.-C. Shiang, Z.-H. Lin, Z. Yang, H.-T. Chang, *Journal of Materials Chemistry* **2009**, 19, 755-759.
- [12] E. Mendoza, J. Llorca, *Patent WO2013057349 A1: Method for producing a substrate with Au nanoclusters affixed to the surface and substrate and catalyst obtained by means of said method* **2013**.
- [13] <http://www.goldemar.com>, consulted 03/03/14.
- [14] Haruta, *Journal of New Materials for Electrochemical Systems* **2004**, 7, 163-172.
- [15] U. R. Pillai, S. Deevi, *Applied Catalysis A* **2006**, 299, 266-273.
- [16] K. Qian, S. Lv, X. Xiao, H. Sun, J. Lu, M. Luo, W. Huang, *Journal of Molecular Catalysis A* **2009**, 306, 40-47.

- [17] J. Guzman, B. C. Gates, *Journal of the American Chemical Society* **2004**, 126, 2672-2673.
- [18] J. Guzman, B. C. Gates, *Journal of Physical Chemistry B* **2002**, 7659-7665.
- [19] M. Haruta, *The Chemical Record* **2003**, 3, 75-87.
- [20] J.-D. Grunwaldt, M. Maciejewski, O. S. Becker, p. Fabrizioli, A. Baiker, *Journal of Catalysis* **1999**, 186, 458-469.
- [21] L. Guzzi, D. Horváth, Z. Pászti, L. Tóth, Z. E. Horváth, A. Karacs, G. Peto, *Journal of Physical Chemistry B* **1999**, 186, 458.
- [22] M. Han, X. Wang, Y. Shen, C. Tang, G. Li, R. L. Jr. Smith, *Journal of Physical Chemistry C* **2010**, 114, 793-798.
- [23] S. Y. Lai, Y. F. Qiu, S. J. Wang, *Journal of Catalysis* **2006**, 237, 303-313.
- [24] Tana, F. Wang, H. Li, W. Shen, *Catalysis Today* **2011**, 175, 541-545.
- [25] X.-Y. Wang, S.-P. Wang, S.-R. Wang, Y.-Q. Zhao, J. Huang, S.-M. Zhang, W.-P. Huang, S.-H. Wu, *Catalysis Letters* **2006**, 112, 115-119.
- [26] S. Carretin. P. Concepción, A. Corma, J. M. López Nieto, V. F. Puntes, *Angewandte Chemie International Edition* **2004**, 43, 2538-2540.
- [27] G. Naveen, P. Bhat, O. Bhaskar, S. T. Dasari, *Fuel Cell System* **2012**, ME 436, 1-9.
- [28] O. Shamardina, A. A. Kulikovskiy, A. V. Chertovich, A. R. Khokhlov, *Fuel Cells* **2012**, 12, 577-582.
- [29] E. Galindo, Final Course Project: *Estudi del procés en continu de producció de nanoclústers d'or*, ETSEIB, Universitat Politècnica de Catalunya **2013**.
- [30] N. Zuasti, Final Course Project: *Synthesis of novel catalysts containing gold nanoclusters for VOCs removal*, ETSEIB, Universitat Politècnica de Catalunya **2013**.
- [31] E. Mendoza Gómez, J. Llorca Piqué, L. Rodrigues Alves, E. Galindo, M. Santiago Redondo, *Patent submitted* **2013**, European Patent Application No: 12382137.1.

CHAPTER 5:
OXIDATION OF
CARBONACEOUS MATERIALS

5.1 CATALYSTS SYNTHESIS

While testing the catalytic activity of Au/MWCNTs catalysts for CO oxidation, it was noticed, after a 400 °C oxidation, that Au seems to decrease the oxidation temperature of MWCNTs (Chapter 3, Section 3.6.1). Thus, following this observation a deeper study about the effect of Au in the thermal stability of carbonaceous materials was carried out.

Firstly, commercial multiwalled carbon nanotubes (MWCNTs) were decorated with different contents of Au synthesised in-situ using sodium citrate as reducing agent of the gold precursor (HAuCl_4), according to the method described in Chapter 3 (Section 3.1, Figure 30). This approach allows tuning the gold particle size easily (higher Au loads lead to larger particles - Chapter 3, Section 3.3.1). In this way, with the goal of determining the reactivity-selectivity-particle size relationships Au/MWCNTs catalysts with Au contents of 0.1 wt%, 0.5 wt%, 1 wt%, 3 wt%, 6 wt%, 13 wt% and 23 wt% were synthesised. These catalysts were prepared using a sodium citrate/Au molar excess of 1700. Thus, before lyophilisation, the sodium citrate excess of the catalysts was removed by centrifugation (twice: 6000 rpm; 10 °C; 30 minutes). The solid powder catalyst was then obtained by lyophilisation ($P \sim 2 \times 10^{-2}$ mbar; $T \sim -74$ °C).

Besides these catalysts, a 0.5 wt% of 15 nm Au nanoparticles catalyst - Au15nm(0.5wt%)/MWCNTs - was also prepared. This catalyst was prepared in order to do a complementary comparison of the effect of the size of the Au nanoparticle in the catalyst activity and selectivity to CO_2 . In this case, the Au nanoparticles with a concentration of Au of 0.04 mg/mL were firstly pre-synthesised following the Turkevich method^[1]. This method simply consists in adding a certain quantity of the gold precursor (HAuCl_4) to milli-Q water under stirring. This mixture was left to stir approximately at 100 °C until it starts to boil. Then, an aqueous solution of sodium citrate was added to the previous mixture and left to boil for 10 minutes. During this time the solution changed its

colour and, at the end, a red solution of 15 nm Au nanoparticles was obtained. These nanoparticles were then deposited on the MWCNTs-PAH surface under a 15 minutes sonication in an ice bath. The catalyst was finally lyophilised in order to obtain the solid powder ($P \sim 2 \times 10^{-2}$ mbar; $T \sim -74$ °C). HRTEM characterisation of a higher 15 nm Au content catalyst – Au15nm(3wt%)/MWCNTs – revealed a good dispersion on the MWCNTs-PAH hybrid surface of the 15 nm Au nanoparticles (Figure 89).

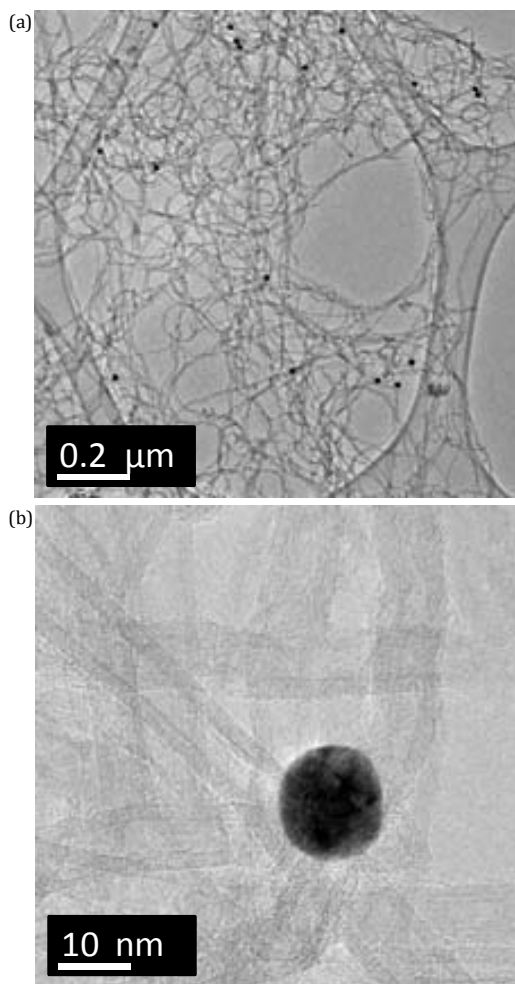


Figure 89. Low (a) and high (b) magnification HRTEM images of a Au15nm(3wt%)/MWCNTs catalyst. The dark dots are 15 nm Au nanoparticles.

Then, other carbon material, a type of soot (commercial carbon black, CB – Printex zeta A, Orion), was decorated with different loadings (0.1 wt%, 0.3 wt%, 0.5 wt% and 1.5 wt%) of ex-situ gold nanoclusters with a mean diameter of approximately 1.3 nm. These gold nanoclusters were pre-synthesised according to the method explained in Chapter 4 (Section 4.1). Au nanoclusters were deposited on the CB surface by direct impregnation. As CB is extremely hydrophobic, the solid material was first impregnated with a few drops of ethanol, then the nanoclusters suspension was added dropwise under sonication. The catalysts were left to dry in the oven at 65 °C during the night.

Finally, using the in-situ synthesis method, Au/CeO₂ catalysts were prepared (Chapter 3, Section 3.1), in order investigate its activity in decreasing the soot (Printex-U, Degussa) combustion temperature. Two catalysts with gold loadings of 0.5 wt% and 3 wt% were synthesised using a molar ratio of sodium citrate/Au of 1.

The catalysts prepared for this study are presented in Table 24 to Table 26. The mean Au particle diameter of the in-situ Au/MWNCTs and Au/CeO₂ catalysts presented (Table 24 and Table 26) was obtained by HRTEM characterisation (Chapter 3, Section 3.3). Moreover, the in-situ catalysts with a gold content lower than 0.5 wt% are composed by single Au atoms (At.) as it has been demonstrated and discussed in Chapter 3 (Section 3.4). Finally, the mean Au particle diameter of the ex-situ ncAu/CB catalysts was considered to be around 1.3 nm (Table 25) since the HRTEM size distributions of Au nanoclusters in the different supports has mean values between 1.3 and 1.4 nm (Chapter 4, Section 4.3.1) and by AFM characterisation the mean Au diameter of unsupported Au nanoclusters is 1.2 nm (Chapter 4, Section 4.2). The catalysts mass used in each measure is also presented.

Table 24. In-situ Au/MWCNTs catalysts used in TPO experiments.

Nomenclature	Au loading (wt%)	Mean Au particle diameter (nm)	Catalyst mass (mg)
MWCNTs	0	-	19
Au(0.1wt%)/MWCNTs	0.1	At.	13
Au(0.5wt%)/MWCNTs	0.5	At.	21
Au15nm(0.5wt%)/MWCNTs	0.5	15	19
Au(1wt%)/MWCNTs	1	n.a.	21
Au(3wt%)/MWCNTs	3	1.1	20
Au(6wt%)/MWCNTs	6	1.1	25
Au(13wt%)/MWCNTs	13	1.6	20
Au(23wt%)/MWCNTs	23	n.a.	22

n.a. – not available data.

Table 25. Ex-situ ncAu/CB catalysts used in TPO experiments.

Nomenclature	Au loading (wt%)	Mean Au particle diameter (nm)	Catalyst mass (mg)
CB	0		18
ncAu(0.1wt%)/CB	0.1		20
ncAu(0.3wt%)/CB	0.3	1.3	20
ncAu(0.5wt%)/CB	0.5		21
ncAu(1.5wt%)/CB	1.5		28

Table 26. In-situ Au/CeO₂ catalysts used in soot oxidation.

Nomenclature	Au loading (wt%)	Mean Au particle diameter (nm)	Catalyst mass (mg)
Soot	0	-	23
Au(0.5wt%)/CeO ₂	0.5	At.	20 (+ 5 mg soot)
Au(3wt%)/CeO ₂	3	1.2	20 (+ 5 mg soot)

5.2 CATALYTIC ACTIVITY

Experimentally, the combustion of the MWCNTs, CB or soot was followed by temperature programmed oxidation (TPO) coupled with a mass spectrometer. A simplified chemical engineering draw and description of the reaction system is presented in Chapter 2 (Section 2.10.3, Figure 28).

The oxidation reactions were performed using approximately 20 mg of the solid catalysts (Au/MWCNTs – Table 24 or ncAu/CB – Table 25 or Au/CeO₂-soot – Table 26). The investigation about soot oxidation was carried out using a soot/catalyst weight ratio of 1:4. The mixture of catalyst with soot was made with a spatula (loose contact). All the TCD values of the TPO profiles were normalised with the carbon mass used in each measure.

The catalytic activity was measured in terms of the temperature at which 50% of the carbon material was converted (T_{50}). Due to the lack of this temperature, some literature data is compared in terms of the initial temperature of combustion of the carbon material (T_i). Moreover, due to the different combustion temperatures of bare carbon materials, activity is always compared in terms of ΔT (Equation 15).

$$\Delta T = T(\text{bare carbon}) - T(\text{Au/carbon}) \quad (15)$$

where,

$T(\text{bare carbon})$ - temperature of oxidation of bare carbon, in °C.

$T(\text{Au/carbon})$ - temperature of oxidation of the catalyst-soot mixture, in °C.

The difficulty of decomposing each type of carbon used, i.e., the initial or the T_{50} temperature necessary to decompose the bare carbon is also taken into account when comparing literature data. Carbon materials with similar temperatures of combustion should be used in order to have a valid comparison of activities.

At the same time as the TPO measurements the evolution of the reaction products was followed by mass spectrometry. In this way, the CO₂ selectivity was obtained for the several catalysts according to Equation 16. The CO₂ (m/z = 44) and CO (m/z = 28) masses were quantified, by integrating the respective peaks obtained from the mass spectrometer (Figure 90).

$$S_{CO_2} = \frac{(CO_2)_{out}}{(CO + CO_2)_{out}} \times 100 \quad (16)$$

where,

S_{CO_2} - CO₂ selectivity, in %.

$(CO_2)_{out}$ - quantified mass of CO₂ that exists the reactor.

$(CO + CO_2)_{out}$ - sum of the quantified masses of CO and CO₂ that exit the reactor.

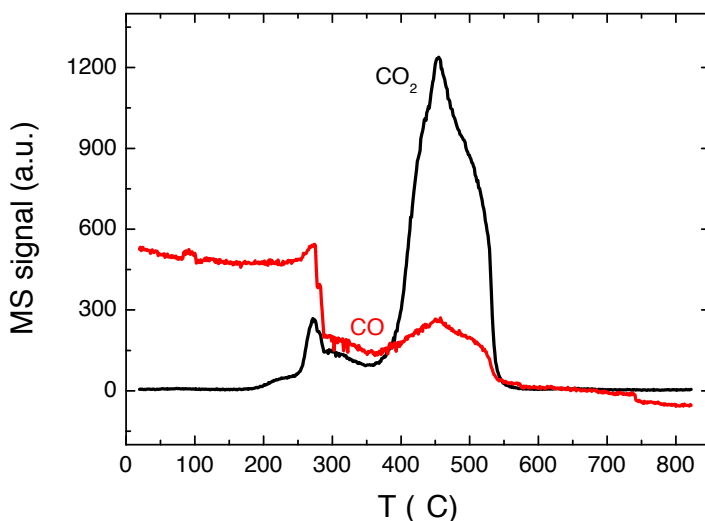


Figure 90. CO₂ (—) and CO (—) masses obtained from the mass spectrometer for an in-situ Au(0.5wt%)/MWCNTs catalyst.

5.2.1 COMBUSTION TEMPERATURE OF Au DECORATED MWCNTs (in-situ)

The effect of the Au loading in the thermal stability of MWCNTs was investigated using a large range of Au contents (Table 24). Using such a large range of Au loadings, the determination of reactivity-selectivity-particle size relationships was obtained. Figure 91 shows the TPO profiles obtained for the thermal decomposition of the MWCNTs decorated with different Au contents (in-situ synthesis method).

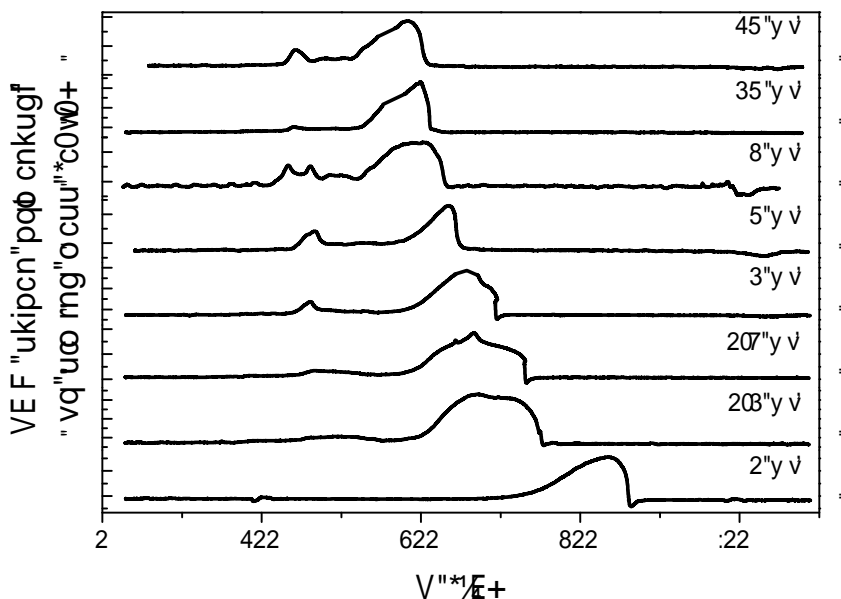


Figure 91. TPO measures of the different gold content in-situ Au/MWCNTs catalysts.

In literature, the activity results of this type of reaction is presented either using the temperature at which 50% of the carbon material is converted (T_{50}) or the temperature of maximum combustion rate (T_m). It is more correct to use the value of T_{50} since diffusion limitations usually occur during the reaction. The catalytic reaction is constituted by several consecutive steps that involves the mass transport of the reagents and products on the particle surface and in the interior of the pores and chemical steps of adsorption of the reagents,

reaction and desorption of the products^[2]. Thus, the global velocity of reaction depends on the velocity of each one of the referred steps. In this way, if there are internal or external diffusion limitations, the global reaction rate will be lower^[3].

In the case that there is only one type of active site and there are not any diffusion effects at the beginning (adsorption of the reagents) or at the end (release of products) of the reaction the TPO peak will be symmetric and T_m will coincide with T_{50} . Nonetheless, despite not being very significant, TPO profiles of the Au/MWCNTs catalysts revealed the existence of diffusion limitations during the catalytic process and therefore asymmetric peaks were obtained (Figure 91, Table 27). Thus, in this work, the measure of the catalytic activity is in terms of T_{50} (Figure 92).

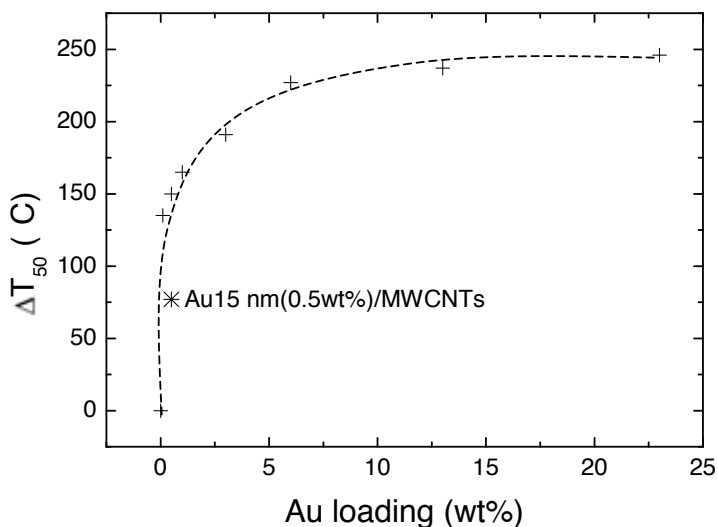


Figure 92. Dependence of the MWCNTs ΔT_{50} with the Au loading using in-situ Au/MWCNTs catalysts.

The results obtained clearly reveal that Au has a beneficial effect in decreasing the temperature of combustion of MWCNTs. A maximum decrease of this temperature when compared to the pure MWCNTs was obtained when using a Au(23wt%)/MWCNTs catalyst ($\Delta T_{50} = 246$ °C) (Figure 92). The conversion of

50% of MWCNTs was achieved at lower temperatures for higher Au content catalysts (Table 27) indicating therefore a higher combustion rate for these catalysts. Between the Au loadings of 6 wt% and 23 wt%, the ΔT_{50} increase noticed was not so significant (Figure 92).

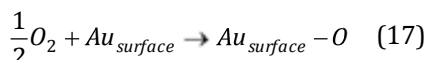
Table 27. Temperatures of maximum combustion rate (T_m) and where 50% of carbon (MWCNTs) is converted (T_{50}) obtained for different in-situ Au/MWCNTs catalysts.

Catalyst	T_m (°C)	T_{50} (°C)
MWCNTs	634	615
Au15nm(0.5wt%)/MWCNTs	538	538
Au(0.1wt%)/MWCNTs	471	480
Au(0.5wt%)/MWCNTs	466	465
Au(1wt%)/MWCNTs	455	450
Au(3wt%)/MWCNTs	435	424
Au(6wt%)/MWCNTs	403	388
Au(13wt%)/MWCNTs	399	378
Au(23wt%)/MWCNTs	380	369

Furthermore, when comparing the decrease of the temperature T_{50} of MWCNTs combustion of the Au(0.5wt%)/MWCNTs ($\Delta T_{50} = 150$ °C) with the catalyst with the same gold content of 15 nm Au nanoparticles – Au15nm(0.5wt%)/MWCNTs ($\Delta T_{50} = 77$ °C) (Figure 92), it was concluded that the Au atoms or clusters are responsible for the significant decrease of the MWCNTs combustion temperature. Thus, even though the catalysts with a gold content of 23 wt% present large gold nanoparticles resultant of sinter due the high Au content, there are still a significant quantity of Au clusters or atoms that remain on the MWCNTs surface which are responsible for the significant decrease of the oxidation temperature of the MWCNTs observed. The decrease of T_{50} with the enhancement of the Au loading results then from the faster combustion rate resultant from the existence of a higher quantity of Au active species. Between 6 wt% and 23 wt%, this increase is not so significant due to the fact that at high temperatures part of the Au sinter and is no more catalytic active.

Both size of Au and its chemical nature are related to the temperature differences observed. By XPS it was observed that, when synthesised by the in-situ method independently of the Au content, up to 3 wt%, Au in Au/MWCNTs catalysts is positively charged (Chapter 3, Section 3.5). These positively charged gold species observed for the catalysts with a small particle size (~1.1 nm to ~1.6 nm) were attributed to gold bonded to oxygen species^[4]. Moreover, by XAS it was also observed Au⁶⁺ on the 0.1 wt% and 0.5 wt% Au/MWCNTs catalysts (Chapter 3, Section 3.4.2). Therefore, the ability to deliver this surface oxygen to the reaction will surely be responsible for an increase of the combustion rate of the MWCNTs and therefore for the decrease of its thermal stability.

Additionally, combustion temperature variations can be explained taking into account the role of Au in the mechanism of the combustion of carbon materials. When gold is present, the mechanism of combustion of the carbon material is accelerated by the ability of Au to dissociate molecular oxygen (O₂) from the gas phase (Equation 17), adsorb it on its surface and by spillover release it and deliver it to the metal-carbon interface causing the oxidation of carbon in the vicinity of Au particles (Chapter 1, Section 1.6.2, Figure 20)^[5, 6].



In this context, our work has demonstrated that 1.1 nm Au clusters are able to dissociate molecular oxygen at room temperature and release it at 80 °C^[4]. In this way, considering that these active clusters are able to dissociate molecular oxygen at room temperature and release it at around 80 °C the fact that a higher quantity exist will lead to a major quantity of oxygen available to oxidise the MWCNTs^[4]. The process of oxygen spillover from the Au surface to the Au-MWCNTs interface is not faster in each cluster, but the fact that more active Au exists in the MWCNTs surface will increase the oxidation reaction rate. Indeed, our group by theoretical calculations demonstrated that more than one O₂ dissociation on partially oxygen covered Au clusters is possible and requires a

low activation barrier (6 kcal/mol). It was determined that for example, gold clusters with a cuboctahedral structure with a diameter of approximately 1 nm, and considering that each cluster has six active sites where at least two O₂ molecules can be dissociated, it is possible to obtain an oxygen monolayer on the Au cluster surface^[4]. As well, the oxygen recombination of two oxygen atoms adsorbed on the Au surface into O₂ is difficult since it requires a much higher energy barrier (30 kcal/mol) to occur.

Hence, the highest activity of the catalysts with higher gold content is related to the major quantity of active Au atoms on the Au clusters surface available to reaction. There will be more active sites available to dissociate and adsorb molecular oxygen from the gas phase that is then delivered by spillover to the Au/MWCNTs interface participating in the reaction, increasing for this reason the MWCNTs combustion rate. In this way, if sinter does not occur, the Au(23wt%)/MWCNTs should show a sharpest decrease of T₅₀, due to the larger quantity of active species, when comparing to the lowest Au content catalysts.

Furthermore, using a Au(3wt%)/MWCNTs catalyst and bare MWCNTs, SEM characterisation was carried out in order to clearly observe the effect of Au in the combustion of MWCNTs and to complement and corroborate the results obtained. SEM images of the same zone were acquired using the fresh samples and then heated in a muffle during 5 hours at different temperatures, namely 100 °C, 200 °C, 300 °C, 400 °C and 500 °C (ramp temperature: 5 °C/min). This characterisation revealed that up to 300 °C MWCNTs were not decomposed independently of being bare or doped with Au. The presence of MWCNTs was observed in the samples prepared at room temperature (Figure 93a, b) and after being at 100 °C, 200 °C or 300 °C (Figure 93c, d). Then, after being five hours at 400 °C, differences were observed for both samples (Figure 93e, f). While the MWCNTs of the catalyst containing 3 wt% of Au were all decomposed (Figure 93f), bare MWCNTs were still present (Figure 93e). SEM images clearly revealed that five hours was enough time to decompose all the MWCNTs doped with Au at 400 °C. Indeed, only the bright dots of Au nanoparticles of the

Au(3wt%)/MWCNTs catalyst could be identified in the respective SEM image (Figure 93f). This result is easily related to that obtained by TPO experiments. By the TPO profiles obtained (Figure 91), it was concluded that a Au(3wt%)/MWCNTs catalyst starts to oxidise at 351 °C, while pure MWCNTs only start combustion at 460 °C. Thus, in accordance with these results, by SEM characterisation, the complete decomposition of MWCNTs in a Au(3wt%)/MWCNTs catalyst was observed at 400 °C unlike bare MWCNTs. Then, increasing the temperature up to 500 °C, bare MWCNTs were completely decomposed (Figure 93g). After being five hours at 500 °C, it was observed, by SEM, a complete combustion of the pure MWCNTs which is also in accordance with the initial combustion temperature obtained by TPO for bare MWCNTs (460 °C). In this way, after being at 500 °C (Figure 93g, h), the presence of only gold nanoparticles (bright dots) can be easily distinguished in the Au(3wt%)/MWCNTs' sample (Figure 93h), while in the bare MWCNTs sample nothing but some impurity is left on the silicon wafer surface (Figure 93g). These results clearly corroborate those obtained by the TPO experiments showing once again the strong effect of gold on decreasing the thermal stability of MWCNTs.

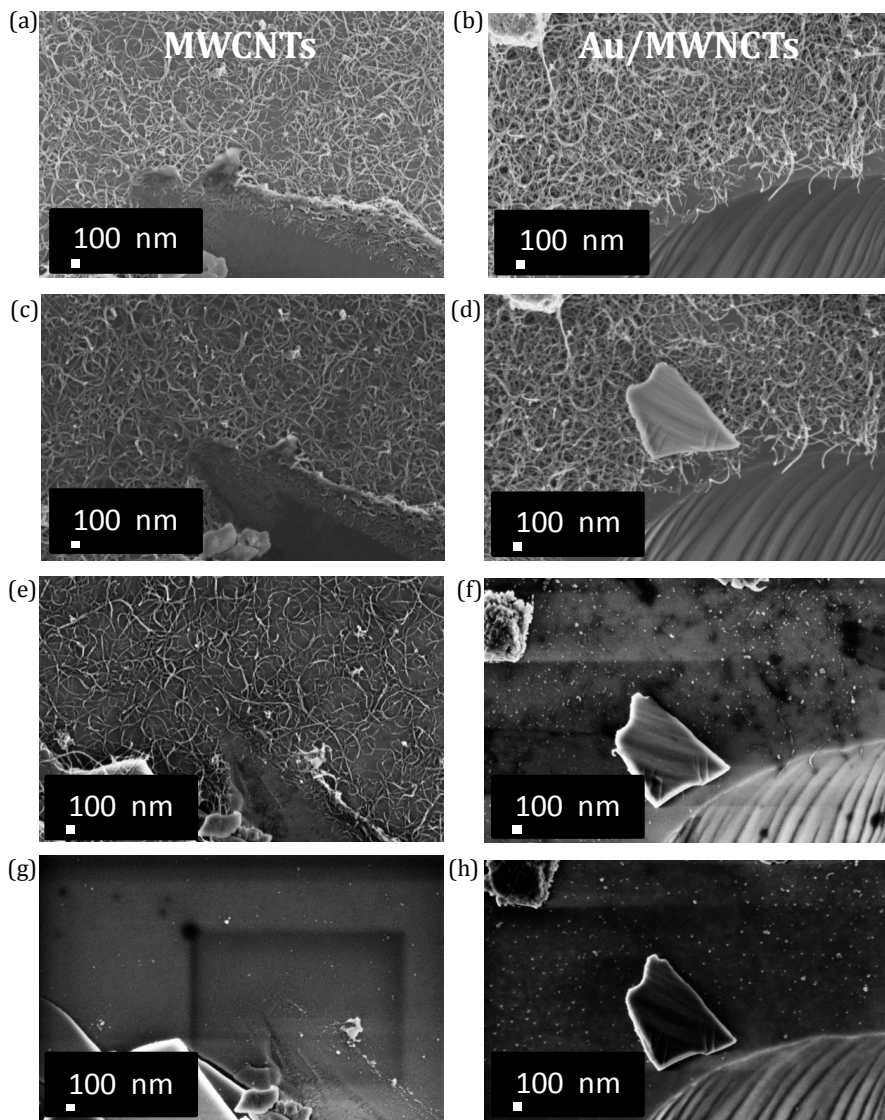


Figure 93. SEM images of MWCNTs (left) and a Au(3wt%)/MWCNTs catalyst (right) at room temperature (a)/(b), and 300 °C (c)/(d), at 400 °C (e)/(f) and 500 °C (g)/(h), respectively.

The effect of Au in the combustion temperature of MWCNTs has not been reported on much. Nevertheless, the in-situ synthesised catalysts show a higher activity than the different sized Au/MWCNTs reported by Lorençon *et al.* (Chapter 1, Section 1.6.2, Table 8)^[5]. The difference between the ΔT_i of

combustion of MWCNTs ($\Delta T_{i, \text{Au}(13\text{wt}\%)/\text{MWCNTs}} - \Delta T_{i, \text{Au-MWC-5.8}}$) is 63 °C lower for the Au-MWC-5.8 ($\Delta T_i = 90$ °C) when compared to the Au(13wt%)/MWCNTs catalyst ($\Delta T_i = 153$ °C). This difference is even more significant since the MWCNTs used in this work are more difficult to decompose ($T_i = 460$ °C) than the MWCNTs used by Lorençon *et al.* ($T_i = 390$ °C). This lower activity results from the larger Au nanoparticle size (~ 1.3 nm vs 5.8 ± 2.3 nm). Au large nanoparticles are less active due to their lower capacity of activate molecular oxygen. Therefore the process of combustion of the carbon material will be slower in these catalysts and higher temperatures to initiate the combustion are required.

Moreover, the thermal decomposition of MWCNTs decorated with metal or metal oxides nanoclusters ($d < 2$ nm) was recently reported by Leino *et al.*^[6]. Metals like Pt, Pd, Ni and Co were used to decorate this carbonaceous material (Chapter 1, Section 1.6.2, Table 7). The oxidation temperature of MWCNTs depends on several intrinsic properties of the MWCNTs, such as the degree of graphitisation of the materials, the concentration of surface defects and the diameter of the MWCNTs. As so, in this case, non-decorated MWCNTs (acid pre-treated nanotubes) started to decompose at 407 °C (53 °C lower than the initial temperature of combustion of MWCNTs used in this work, $T_i = 460$ °C)^[6].

When decorating the MWCNTs with PtO_x or $\text{Pd}(\text{acac})_2$ nanoclusters, a decrease of the carbon initial combustion temperature up to approximately 377 °C ($\Delta T_i = 30$ °C) was noticed (Figure 94). Furthermore, it was concluded that the highest decrease of the combustion temperature of the MWCNTs occurs when these are decorated with the metal precursor, cobalt acetylacetonate - $\text{Co}(\text{acac})_3$ -. An initial temperature of combustion of around 227 °C ($\Delta T_i = 180$ °C) was obtained with this metal (Figure 94). When using nickel acetylacetonate - $\text{Ni}(\text{acac})_2$ - a decrease up to around 327 °C ($\Delta T_i = 80$ °C) was obtained (Figure 94). Comparing these results with the Au/MWCNTs used in this work, a higher activity was obtained when compared to almost all the other metal catalysts except for the most active Co(a)/MWC catalyst (Figure 94). This Co catalyst was able to start oxidising MWCNTs at 79 °C and 27 °C lower temperature than the

Au(0.5wt%)/MWCNTs and Au(13wt%)/MWCNTs respectively (Table 28). Nonetheless, this activity can be considered very similar since the pure MWCNTs of the in-situ synthesised catalysts require a higher temperature to be decomposed (460 °C vs 407 °C).

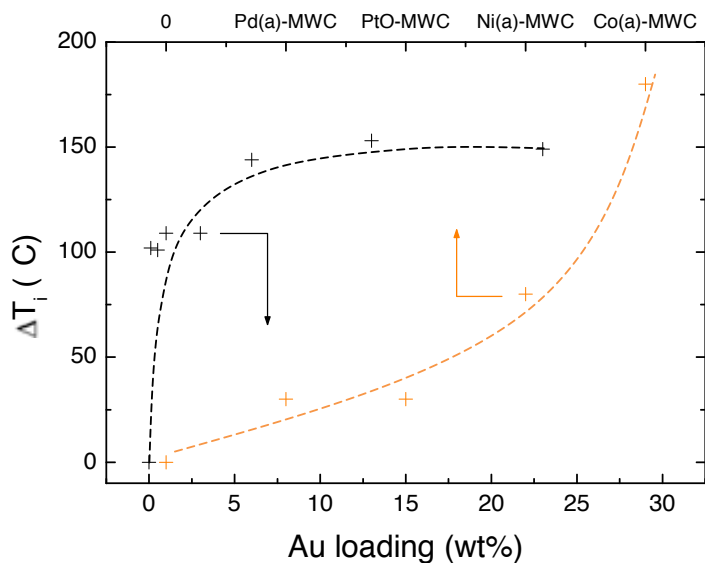


Figure 94. Comparison of the initial temperature difference of combustion of MWCNTs using in-situ Au (---) or other metals (-o-)[6].

Table 28. Comparison of the catalytic activity of the in-situ synthesised catalysts and MWCNTs decorated with different metals.

Catalysts	ΔT_i (°C)
Au(0.5wt%)/MWCNTs	101
Au(13wt%)/MWCNTs	153
Pd(a)-MWC / PtO-MWC ^[6]	30
Ni(a)-MWC ^[6]	80
Co(a)-MWC ^[6]	180

These results are then extremely satisfactory and clearly show the important role of Au in the thermal decomposition of MWCNTs. However it is also necessary to take into account the catalysts selectivity to CO₂. Active catalysts

with higher capacity to oxidise CO to CO₂ are required and preferable for the complete soot combustion^[7].

The temperature range at which CO conversion occurs corresponds to that where MWCNTs are decomposed. As MWCNTs combustion starts at high temperatures, the CO conversion to CO₂ starts immediately as schematically represented in Figure 95.

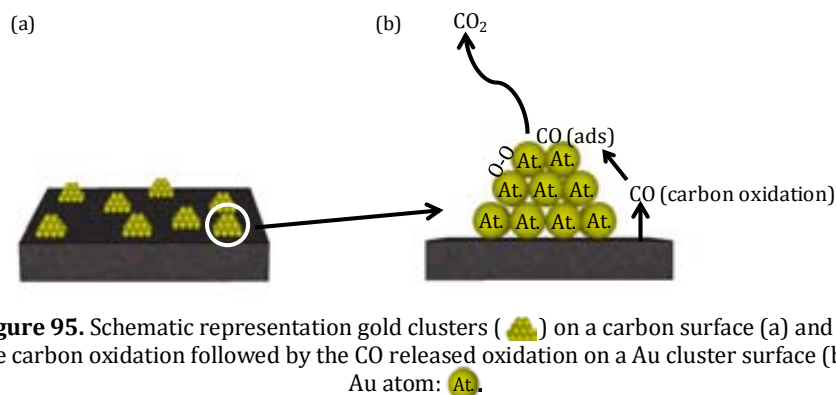

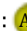


Figure 95. Schematic representation gold clusters () on a carbon surface (a) and of the carbon oxidation followed by the CO released oxidation on a Au cluster surface (b). Au atom: .

CO₂ selectivity was determined according to Equation 16. High selectivities of the order of 75% - 85% were obtained using in-situ Au/MWCNTs catalysts. Importantly, the ability of the smallest gold (lower gold content catalysts) to oxidise the CO was verified leading in this way to a higher CO₂ selectivity (Figure 96). As expected, the increase of the Au content/Au particle size led to a lower CO₂ selectivity (Figure 96). Nevertheless, the Au(0.1wt%)/MWCNTs catalyst showed the lowest S_{CO₂} of the different gold content in-situ catalysts. This can be explained by the almost inexistence of Au in this catalyst. The Au(23wt%)/MWCNTs catalyst, even though poorly, was also able to convert some of the CO formed during the oxidation reaction. This is in accordance to the previous results and confirms the coexistence of gold clusters on the MWCNTs surface among larger Au nanoparticles. These small Au clusters are then responsible for the selectivity to CO₂ observed for this catalyst. Finally, also corroborating the fact that large Au nanoparticles are not able to oxidise the CO to CO₂, it was observed that when using the Au15nm(0.5wt%)/MWCNTs

catalyst the CO₂ selectivity obtained is similar to pure MWCNTs (Figure 96). A decrease of this parameter of 78% was observed for the Au15nm(0.5wt%)/MWCNTs catalyst when compared to the Au(0.5wt%)/MWCNTs catalyst. Due to the lack of documented data, the values of CO₂ selectivity cannot be compared.

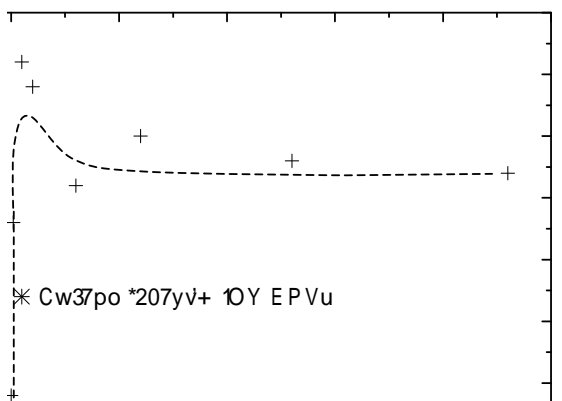


Figure 96. Effect of the Au loading in CO₂ selectivity using in-situ Au/MWCNTs catalysts.

This first study allowed conclusions about the optimal Au cluster size (~ 1.1 nm) with which an important decrease in the combustion temperature of the MWCNTs and also a good selectivity to CO₂ were achieved. These results lead us then to conclude that, in order to achieve a good catalytic activity and selectivity, gold clusters (not only single atoms or a mixture of single atoms, clusters and nanoparticles) should be used.

Taking into account these observations, different gold content uniform sized ex-situ synthesised Au nanoclusters (0.1 wt%, 0.3 wt%, 0.5 wt% and 1.5 wt%) were then supported on carbon black (CB) (a common used model compound for diesel soot for diesel oxidation experiments)^[8-10]. The catalysts activity and selectivity to CO₂ was investigated using the same procedure.

5.2.2 COMBUSTION TEMPERATURE OF Au DECORATED CARBON BLACK (ex-situ)

The role of gold in the decrease of the oxidation temperature of soot was investigated using gold nanoclusters supported on a model soot (CB) surface. Since a compromise between the lowest oxidation temperature and the highest CO conversion is pretended, only ~ 1.3 nm gold nanoclusters ex-situ synthesised were used in these experiments. Gold catalysts with different gold contents (0.1 wt%, 0.3 wt%, 0.5 wt% and 1.5 wt%) were prepared in order to determine the relation existent between the reactivity, selectivity and particle size (an increase of the gold content lead to the increase of the particle size due to sinter).

As for in-situ Au/MWCNTs catalysts ex-situ ncAu/CB catalysts also showed differences between the temperature of maximum combustion rate and the temperature at which 50% of the CB is converted (Table 29). This may result from the diffusion limitations that occur during the catalytic reaction.

Table 29. Temperatures of maximum combustion rate and where 50% of carbon (CB) is converted obtained for different ex-situ ncAu/CB catalysts.

Catalyst	T _m (°C)	T ₅₀ (°C)
CB	635	625
ncAu(0.1wt%)/CB	412	424
ncAu(0.3wt%)/CB	397	407
ncAu(0.5wt%)/CB	304	333
ncAu(1.5wt%)/CB	491	456

The results obtained show that indeed Au has a crucial role in decreasing the CB oxidation temperature (Figure 97). As before, higher gold contents led to a lower combustion temperature of the CB due to the existence of a higher quantity of active species. A maximum decrease of 292 °C was obtained when using a gold content of 0.5 wt% when comparing to temperature at which 50% of bare CB was converted (625 °C) (Figure 97). The role of Au in this oxidation

process is also related with its ability of dissociate molecular oxygen. Au nanoclusters will dissociate molecular oxygen, adsorb it in their surface and release it increasing thus the CB combustion rate. Nonetheless, when a ncAu(1.5wt%)/CB catalyst was used, the beneficial effect of Au was not so significant ($\Delta T_{50} = 169$ °C). This result indicates that Au is only effective to reduce the CB combustion temperature when present in very low loadings. The decrease of ΔT_{50} observed when using a gold content of 1.5 wt% results from the fact that Au will aggregate in bigger particles in this catalyst and consequently the catalytic activity will decrease. This easier aggregation of the Au nanoclusters when using CB that is not observed while using MWCNTs is explained due to the significantly different surface areas of CB and MWCNTs. MWCNTs and CB have surface areas of 375.3 m²/g and 63.2 m²/g respectively. In this way, Au will sinter much easier on the CB surface which justifies the re-increase of the oxidation temperature when 1.5 wt% of Au is used.

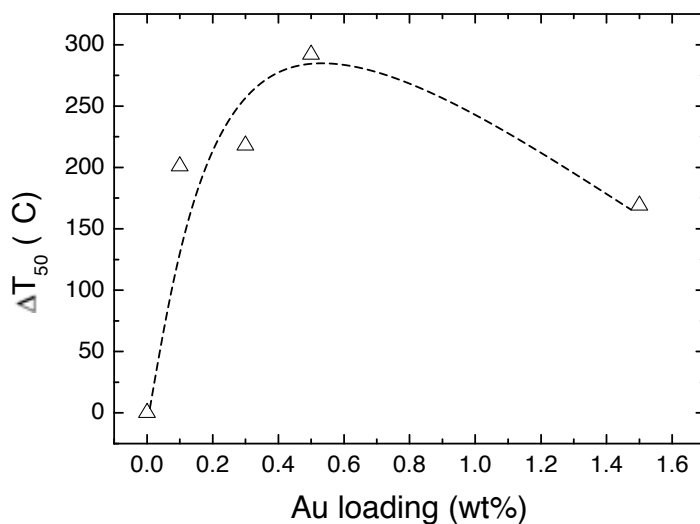


Figure 97. Dependence of the CB ΔT_{50} with the Au nanoclusters loading using ex-situ ncAu/CB catalysts.

The study of the combustion of Au decorated soot particles has been very little investigated. Comparing the reported results by Lorençon *et al.* (Chapter 1,

Section 1.6.2, Table 8) with the ones obtained using ncAu/CB catalysts, promising results were observed^[5]. The most active ex-situ ncAu/CB catalyst – ncAu(0.5wt%)/CB – is able to start to oxidise carbon at 55 °C lower temperature than the most active catalyst reported (Au-soot-3.7) (Table 30). Moreover, the bare CB used in this work and the soot used by Lorençon *et al.* start to oxidise at similar temperatures (470 °C and 460 °C, respectively). This highest activity surely results from the smallest Au particle size of the ex-situ synthesised Au nanoclusters (~ 1.3 nm vs 3.7 nm) demonstrating clearly the ability of these ex-situ nanoclusters to aid the combustion reaction by O₂ dissociation. Moreover, a lower activity of the ncAu(1.5wt%)/CB when compared to Au-soot-3.7 was observed (Table 30). This lower activity can be explained by the Au sinter indicating that probably Au particles larger than 3.7 nm exist in this catalyst.

Table 30. Comparison of the activity of Au catalysts on the combustion of CB.

Catalysts	ΔT_i (°C)
ncAu(0.5wt%)/CB	225
ncAu(1.5wt%)/CB	121
Au-soot-3.7 ^[5]	170

All the different gold content ncAu/CB catalysts are selective towards CO₂ (Figure 98). Similar selectivities between 67% and 75% were obtained for the different Au content catalysts. A maximum selectivity was achieved for both ncAu(0.3wt%)/CB or ncAu(0.5wt%)/CB catalysts. The slightly lower selectivity of the ncAu(0.1wt%)/CB catalyst might be explained by the very low gold content that exists in this catalyst. These results are in accordance with the tendency noticed in Chapter 4 (Section 4.4, Figure 82) where a higher CO conversion was obtained for the higher Au content catalyst (0.5 wt%). The 1.5 wt% ncAu catalyst showed a slight decrease of this parameter when compared to the 0.3 wt% and 0.5 wt% due to the less efficient conversion of CO by large Au nanoparticles. This observation is in accordance with the CB combustion

temperature previously discussed (Figure 97). It was then concluded that lower Au contents, such as 0.5 wt%, are the most indicate to combine the beneficial effect of the gold nanoclusters in decreasing the model soot (CB) combustion temperature with a high CO₂ selectivity.

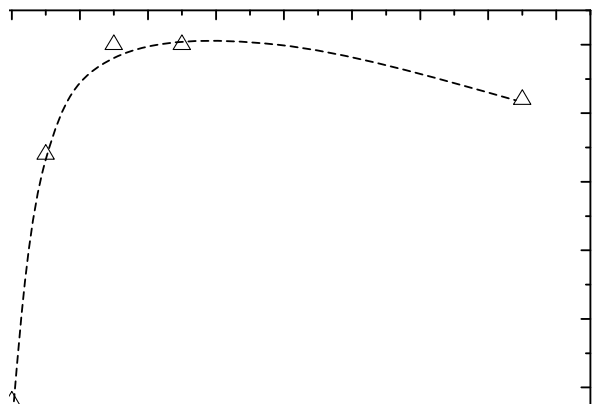


Figure 98. Effect of the Au loading in CO₂ selectivity using ex-situ ncAu/CB catalysts.

The ncAu/CB catalysts CO₂ selectivity cannot be compared to documented data due to the lack of this information by the authors. Nonetheless, when comparing the CO₂ selectivity of both Au/MWCNTs and ncAu/CB catalysts, it was concluded that the ex-situ ncAu/CB catalysts have a slightly lower CO₂ selectivity than in-situ Au/MWCNTs catalysts (Figure 99). This difference can be explained by the different surface areas of MWCNTs and CB (375.3 m²/g vs 63.2 m²/g). The significantly large surface area of MWCNTs will lead to a difficult sinter of Au clusters and thus these catalysts show a higher selectivity to CO₂ at the high temperatures at which the CO from the carbon materials combustion is oxidised. This result is in accordance to the one observed for the in-situ Au/MWCNTs and ex-situ ncAu/CB catalysts where a slightly decrease of selectivity was obtained for higher Au loadings due to the Au sinter (Section 5.2.1 - Figure 96 and Figure 98).

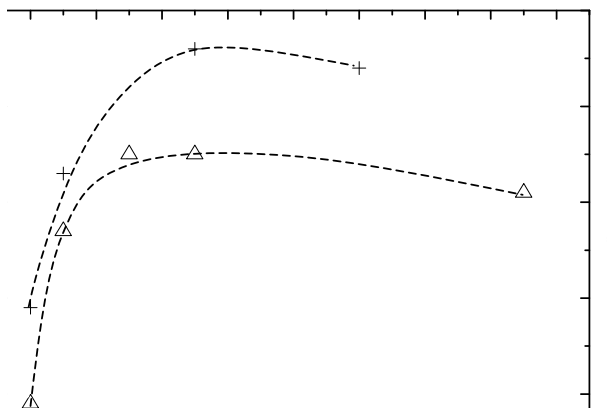


Figure 99. Comparison of the CO_2 selectivity obtained for different Au content in-situ Au/MWCNTs (---+) and ex-situ ncAu/CB catalysts (---Δ).

These results are very promising and clearly show how Au affects the thermal stability of model soot (CB). Indeed, the effect of these Au clusters in decreasing the combustion temperature of CB was recently patented in collaboration with a private company (*Goldemar Solutions*) in 2013 and will be published in 2014^[11]. In this context, the ability of Au clusters in decreasing the soot oxidation temperature under unfavourable contact conditions was then investigated.

5.2.3 SOOT OXIDATION

Usually, soot oxidation measures are carried out using tight contact (Chapter 1, Section 1.6.2). This type of contact, although not real, leads to higher activities and to reproducible values due to the best contact between the catalyst and soot. For the evaluation of intrinsic reaction mechanisms, physical phenomena such as mass and heat transfer limitations must be minimised. This study is necessary for a future industrial catalyst design^[12]. Nonetheless, despite decreasing the reaction rate due to the importance of physical phenomena

loose contact is the type of contact that represents more realistic conditions. Thus, in this study it was decided to study the intrinsic catalyst activity of in-situ Au/CeO₂ catalysts in soot oxidation under loose contact conditions.

The support was chosen to be CeO₂ due to its oxidative properties crucial for this reaction as discussed in Chapter 1 (Section 1.6.2). Indeed, a study about the soot catalytic activity dependence with the support showed that CeO₂ is one of the best supports for this reaction (Chapter 1, Section 1.6.2, Figure 19). Two gold contents were tested (0.5 wt% and 3 wt%). When using the Au/CeO₂-soot mixtures, almost symmetric TPO peaks were obtained, i.e. $T_{50} \sim T_m$ indicating that the diffusion limitations were not significant in this catalytic reaction (Table 31).

Table 31. Temperatures of maximum combustion rate and where 50% of soot is converted obtained for the catalysts used.

Catalyst	T _m (°C)	T ₅₀ (°C)
soot	590	556
CeO ₂ -soot	520	513
Au(0.5wt%)/CeO ₂ -soot	428	426
Au(3wt%)/CeO ₂ -soot	456	443

Results showed that bare CeO₂ is able to decrease the soot combustion temperature in 43 °C (Figure 100). Then the addition of Au leads to a higher decrease of this variable. The lowest gold content catalyst achieved the highest decrease in respect to pure soot ($\Delta T_{50} = 130$ °C) (Figure 100). The Au(3wt%)/CeO₂ showed a slightly decrease of activity when compared to the Au(0.5wt%)/CeO₂ catalyst ($\Delta T_{50} = 113$ °C). The decrease of activity for the higher Au content catalyst is not in accordance with the observations of the Au/MWCNTs combustion (Section 5.2.1). Nevertheless, this decrease is due to the Au aggregation into larger nanoparticles at high temperatures when supported in CeO₂. CeO₂ has a surface area approximately five times lower than MWCNTs (375.3 m²/g vs 74.0 m²/g) and for this reason Au will aggregate easier, faster and at lower temperature than when supported on MWCNTs.

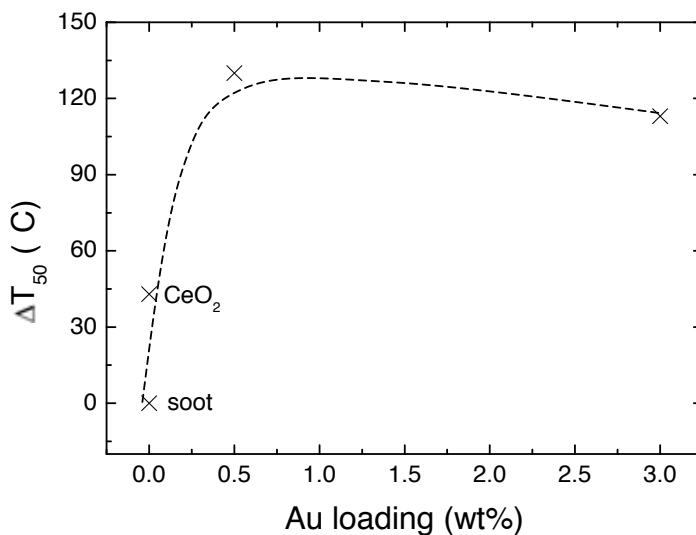


Figure 100. Dependence of the soot ΔT_{50} with the Au loading using in-situ Au/CeO₂ catalysts mixed with soot under loose contact conditions.

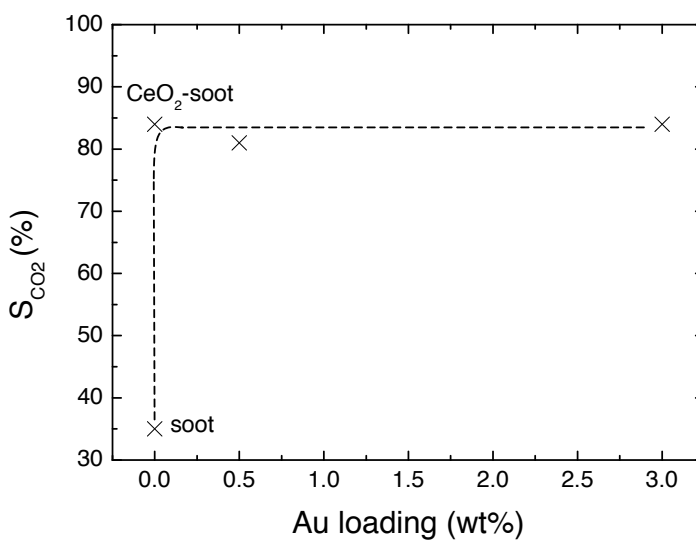


Figure 101. Effect of the Au loading in CO₂ selectivity using in-situ Au/CeO₂ catalysts mixed with soot under loose contact conditions.

Nevertheless, in terms of the in-situ Au/CeO₂ catalysts CO₂ selectivity a similar value for bare CeO₂ and both Au/CeO₂ catalysts was obtained (Figure 101). This result is similar to the one observed for CO oxidation using these catalysts (Chapter 3, Section 3.6.2) indicating once again that in-situ synthesised

catalysts are not the most adequate to CO oxidation. Even though the ability of these Au nanoclusters to decompose soot under unfavourable contact conditions and the proximity of the liberated CO to Au clusters these are still not be able to convert CO into CO₂.

Despite the low CO₂ selectivity, these results are very promising once that when using real conditions (loose contact) these catalysts are able to reduce the soot combustion temperature up to 426 °C which is close to the temperature required by an engine (300 °C – 400 °C) to perform this reaction^[13]. The use of ex-situ ncAu/CeO₂ instead in-situ Au/CeO₂ catalysts would probably improve the CO conversion as it was observed for CO oxidation performed under a gas flow (Chapter 4, Section 4.4).

The catalytic activity of the in-situ synthesised Au/CeO₂ catalysts was compared with the Au catalysts reported in literature for soot combustion under loose contact conditions. A list of the Au catalysts used for soot oxidation under loose contact conditions until now is presented in Table 32. The catalysts activity is compared in terms of ΔT_{50} , i.e. difference between the combustion temperatures at which 50% of the soot is converted using bare soot and catalyst-soot catalytic systems. Some authors report the activity of the catalyst-soot systems in terms of the temperature of maximum combustion rate (T_m). Despite the temperature profiles most of the times are not presented, it was considered that $T_m = T_{50}$ in order to compare literature data with the results obtained in this work. As explained (Section 5.2.1), it was considered that these temperatures are coincidental in approximation, since this would only happen if there is only one type of active site and diffusion limitations do not occur during the catalytic process affecting the reaction rate. Additionally, also, the comparison of activities is made taking into account the atmosphere used to carry out the reaction since the use of NO in the gases flows might improve the soot oxidation by the formation of strong oxidant species.

Table 32. Activity of different Au-based catalysts for soot oxidation under loose contact conditions.

Catalyst	ID	wt% Au	d (nm)	Soot/catalyst ratio	T ₅₀ (°C)	ΔT ₅₀ (°C)
Au/SiO ₂ [7]	CAu1	1.5	n.a.	1:10	590 (a), (b)	0
Au/ZrO ₂ [13]	CAu2	3.0	~ 2 (1.5-5)	1:2	511 (a), (b)	21
Au/TiO ₂ [13]	CAu3	3.0	~ 2 (1.5-5)	1:2	490 (a), (b)	42
Au-V/ZrO ₂ [13]	CAu4	3.0	~ 2 (1.5-5)	1:2	478 (a), (b)	54
Au-V/TiO ₂ [13]	CAu5	3.0	~ 2 (1.5-5)	1:2	419 (b)	113
Au/SiO ₂ -CsNO ₃ [7]	CAu6	1.0	n.a.	1:10	467 (a), (b)	123
Au/(3DOM ZrO ₂)[14]	CAu7	1.2	1.2	1:10	430 (c)	155
Au/(3DOM LaFeO ₃)[15]	CAu8	n.a.	~ 3	1:10	368 (a), (c)	217
Au/(3DOM Ce _{0.9} Zr _{0.1} O ₂)[14]	CAu9	1.3	3.3	1:10	361 (c)	224
Au/ZrO ₂ -CsNO ₃ [7]	CAu10	0.8	n.a.	1:10	360 (a), (b)	230
Au/(3DOM CeO ₂)[14]	CAu11	1.3	3.4	1:10	349 (c)	236

(a) Temperature of the maximum combustion rate

(b) Atmosphere: air

(c) Atmosphere: 5 v/v% O₂ and 0.2 v/v% NO balanced with Ar.

ID – catalyst nomenclature.

When comparing the activity of the in-situ Au/CeO₂ catalysts with those Au catalysts presented in literature for soot oxidation interesting results are obtained. In this comparison the catalysts with ΔT₅₀ < 20 °C (first catalyst in Table 32) was excluded. Figure 102 shows the activity of Au catalysts reported in literature for soot oxidation grouped by approximately the same Au loading.

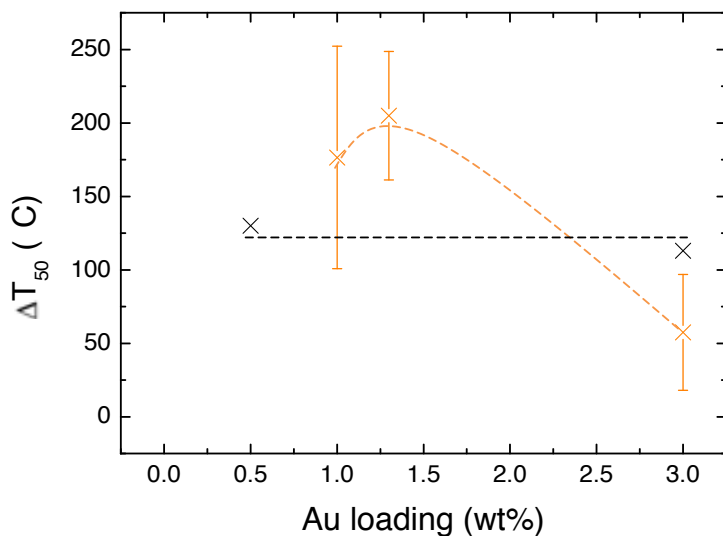


Figure 102. Catalytic activity comparison of in-situ Au/CeO₂ catalysts (--x--) and literature reported Au catalysts (--x--) for soot oxidation under loose contact conditions.

The combustion temperature of bare soot particles used in each experiment is similar. A difference of $\sim \pm 30$ °C exists between T_{50} of bare soot used in this work ($T_{50} = 556$ °C) and the bare soot of the catalysts described in literature ($T_{50} = 532$ °C - 590 °C).

By Figure 102 it can be seen that the literature Au catalysts prepared with Au loadings of 1 wt% and 1.3 wt% are in general slightly more active than the in-situ Au/CeO₂ catalysts, even though the soot mixed with the catalysts grouped in these Au loadings is slightly more difficult to oxidise ($T_{50, \text{bare soot-literature}} \sim 590$ °C) than the one used in this work ($T_{50, \text{bare soot-Au/CeO}_2} = 556$ °C). These higher activities result from the type of supports used in the different reported Au catalysts and the type of atmosphere used to carry out the reaction. For example, the 1 wt% catalysts described in literature (CAu6 and CAu10) have CsNO₃. It has been demonstrated that nitrates favour the soot oxidation reaction^[7, 16]. Indeed, the catalysts promoted with CsNO₃ higher activity results from their ability to oxidise soot. The reaction mechanism of CsNO₃ catalysts involves a first step of soot oxidation by nitrate ion reduction and a second step

of nitrate regeneration with oxygen from the gaseous phase^[7]. Despite this advantage, one of this CsNO₃ catalysts (CAu6) has shown lower activity than the in-situ Au(0.5wt%)/CeO₂ catalyst.

Also, the catalysts prepared with approximately 1.3 wt% Au content (CAu7, CAu9, CAu11) are the most active. The higher activities obtained for these catalysts presented in literature can be explained by the use of 3DOM supports and the fact that reactions were carried out in an atmosphere containing NO. On the one hand, the 3DOM support significantly increases the activity for soot oxidation due to the better contact between the catalyst and the soot particle. The bigger pore sizes (> 100 nm) allow the soot particle (> 20 nm) to enter the inner pores of the catalyst and to easily transport and diffuse^[17, 18]. On the other hand Au is able to adsorb the NO from the gas flow and generate superficial NO₂ which is more oxidising than oxygen increasing therefore the catalytic activity^[7]. Thus, despite the larger Au particle size (~ 3 nm) of some of the 1.3 wt% catalysts (CAu9, CAu11), these are more active than the in-situ Au/CeO₂ catalysts.

Finally, all the catalysts prepared with a Au loading of 3 wt% (CAu2, CAu3, CAu4, CAu5) show a lower activity than both Au(0.5wt%)/CeO₂ and Au(3wt%)/CeO₂ catalysts. The in-situ Au/CeO₂ catalysts, unlike the similar size Au supported catalysts reported (Au/ZrO₂ – CAu2, Au/TiO₂ – CAu3, Au-V/ZrO₂ – CAu4 and Au-V/TiO₂ – CAu5), showed a high activity for soot oxidation being able to reduce the T₅₀ soot combustion temperature in 130 °C when using a Au(0.5wt%)/CeO₂ catalyst. This result is extremely positive. Firstly, because the soot used in this work is more difficult to oxidise than the one mixed with 3 wt% Au literature catalysts (T_{50, bare soot-literature} = 532 °C vs T_{50, bare soot-Au/CeO2} = 556 °C), and secondly, because the Au literature catalysts mean particle diameter (d ~ 2 nm) is close to the in-situ Au mean particle diameter of the Au(3wt%)/CeO₂ catalyst (d ~ 1.2 nm). Nevertheless, the co-existence of gold nanoparticles with a size range between 1.5 nm and 5 nm in the CAu2, CAu3, CAu4 and CAu5 catalysts can explain their lowest activity. Larger gold nanoparticles will be less

active for this reaction and, therefore, the existence of a higher quantity of small Au clusters will favour the reaction due to the existence of more Au active sites.

All in all, these results are extremely satisfactory. The in-situ Au/CeO₂ catalysts are more active for soot oxidation than Au/supported similar sized catalysts and with a similar gold content when using supports with similar characteristics under the same atmosphere. The higher activities observed under the same atmosphere were only due to the presence of nitrates in the catalyst support. Additionally, Au/(3DOM support) catalysts in a NO atmosphere also showed a higher catalytic activity.

Regarding CO conversion the authors that studied the soot oxidation using Au catalysts refer CO₂ selectivities of the order of 97.8 % using Au/(3DOM ZrO₂) catalysts to 99.7 % using Au/(3DOM LaFeO₃) catalysts^[14, 15]. The selectivity obtained with the in-situ Au/CeO₂ catalysts is slightly lower (around 80%) since the effect of Au in CO oxidation using these catalysts was not observed (Figure 101).

Then, the in-situ synthesised Au/CeO₂ catalysts activity for soot oxidation was also compared with a compilation of the most common used catalysts described in literature for this reaction (Table 33). All the literature comparison was made for catalysts mixed by loose contact and taking into account the different atmospheres used to carry out the reaction (containing or non-containing NO atmosphere).

Table 33. Activity of different catalysts formulations for soot oxidation under loose contact conditions.

Catalyst	Soot/catalyst ratio	T ₅₀ (°C)	ΔT ₅₀ (°C)
4.5wt%Ag/TiO ₂ ^[19]	5:95	549 ^{(a), (b)}	11
V/ZrO ₂ ^[20]	1:2	597 ^{(a), (b)}	24
4.5wt%K/TiO ₂ ^[19]	5:95	536 ^{(a), (b)}	24
CeO ₂ ^[21]	1:19	590 ^{(a), (b)}	50
K/ZrO ₂ ^[20]	1:2	569 ^{(a), (b)}	52
10wt%K/CeO ₂ ^[19]	5:95	497 ^{(a), (b)}	63
5mol%Ru-Co/ZrO ₂ ^[22]	5:95	460 ^(b)	100
KOH/MgO ^[12]	1:4	545 ^{(a), (b)}	112
Mo/ZrO ₂ ^[20]	1:2	501 ^{(a), (b)}	120
Sr _{0.8} Ce _{0.2} CoO ₃ ^[23]	5:95	420 ^(b)	130
LaMnO ₃ ^[24]	1:10	432 ^{(a), (c)}	180
La _{0.65} K _{0.35} MnO ₃ ^[24]	1:10	356 ^{(a), (c)}	256
CeO ₂ -Ag ^[21]	1:19	376 ^{(a), (b)}	264
Pt/SiO ₂ ^[25]	1:100	312 ^{(a), (d)}	~ 349

^(a)Temperature of the maximum combustion rate.

^(b)Atmosphere: air

^(c)Atmosphere: 5% O₂ + 2000 ppm NO in He.

^(d)Atmosphere: 10% O₂ + 7% H₂O + 1000 ppm NO +100 ppm SO₂ in N₂.

The most active catalyst of this work – Au(0.5wt%)/CeO₂ – achieved a decrease of 130 °C in relation to the bare soot T₅₀ combustion temperature. This value puts this catalyst in a very good position in relation to the several types of groups of catalysts studied for this reaction. From the collected reported catalysts only, perovskites, CeO₂-Ag and Pt/SiO₂ catalysts show a higher activity than the in-situ Au(0.5wt%)/CeO₂ catalyst. However, to attain a correct comparison of activities it is necessary to take into account the type of atmosphere where the reaction was carried out.

Under an air atmosphere, this in-situ catalyst show a similar activity to that of the Sr_{0.8}Ce_{0.2}CoO₃ type perovskite catalyst (the activity of this perovskite type catalyst is, besides its intrinsic properties, attributed to the presence of Ce.

Apparently Ce contributes to the reaction by enhancing the redox properties of the catalyst.). Moreover, from the rest of collected catalysts only the CeO₂-Ag catalyst is more active under an air atmosphere. The activity of the CeO₂-Ag catalyst with a “rice-ball” morphology (Ag particles surrounded by fine CeO₂ particles) has been attributed to the formation of O_n^{x-} species. The oxygen species adsorbed on the Ag surface migrate to the CeO₂ surface by the Ag/CeO₂ interface to form these species. These oxidising species migrate then to the soot particles thus decreasing their combustion temperature^[21].

Furthermore, under an NO containing atmosphere, perovskites catalysts (LaMnO₃ and La_{0.65}K_{0.35}MnO₃) and the Pt/SiO₂ catalyst are more active than the in-situ Au(0.5wt%)/CeO₂ catalyst. Nevertheless, when comparing these catalysts activity it is necessary to take into account that their reaction atmosphere contained NO that will favour the reaction and therefore lead to higher activities. The activity of perovskite catalysts is related to its good stability and ability to deliver oxygen species that will assist the soot oxidation. Moreover, the addition of a metal like K increases its intrinsic activity, which can be explained by different possibilities: La³⁺ is partially replaced by K⁺ and consequently a part of Mn³⁺ changed to Mn⁴⁺ that has a better catalytic oxidation activity than Mn³⁺^[24]; the addition of K will lead to an increase of oxygen vacancies which consequently increases the adsorption and oxygen activation at the catalyst surface. Another possible explanation is that La_{1-x}K_xMnO₃ nanoparticle perovskite-type will be formed. The particles on the surface of these nanoparticles will be smaller and surface atoms on the nanoparticle surface have a high mobility^[24]. For these reasons the contact between the soot and the catalyst is still good even under loose contact conditions. Besides, the soot used in the perovskites reaction requires a higher temperature to achieve 50% of conversion than the soot used in this work ($T_{50, \text{bare soot-perovskites}} = 612 \text{ }^\circ\text{C}$ vs $T_{50, \text{bare soot-Au/CeO}_2} = 556 \text{ }^\circ\text{C}$). Moreover, Pt catalysts are one of the best catalytic systems known for soot combustion under loose contact conditions^[15, 24, 25]. Indeed, the Pt/SiO₂ catalyst in a NO atmosphere is able to decrease the soot combustion temperature in approximately 219 °C

($\Delta T_{50, \text{Pt/SiO}_2} - \Delta T_{50, \text{Au(0.5wt\%)/CeO}_2} = 219 \text{ }^\circ\text{C}$) more than the Au(0.5wt%)/CeO₂ catalyst.

It has been observed that in loose contact conditions the results obtained using in-situ synthesised Au/CeO₂ catalysts for soot oxidation are very promising. These catalysts are able to decrease significantly the soot oxidation temperature and show a higher activity than several reported gold or other metal catalysts for the reaction carried out under the same atmosphere. Due to the catalytic results obtained for CO oxidation (Chapter 4, Section 4.4), it is believed that ex-situ Au catalysts would be even more efficient. A higher CO₂ selectivity than when using in-situ catalysts would be probably obtained. Moreover, carrying out experiments using tight contact also would increase significantly the catalytic activity, as demonstrated by several authors^[12, 20, 26, 27]. Modifications of the support with other elements such as transition or rare earth metals in order to decrease the thermal deactivation of CeO₂ at high temperatures (stabilises the CeO₂ surface area) and to improve the CeO₂ redox properties or the use of supports with higher pore sizes would also increase significantly the Au/CeO₂ catalytic activity in soot oxidation as discussed for literature reported catalysts.

5.3 CONCLUSIONS

In this chapter, how Au affects the thermal stability of carbonaceous materials was investigated for what might be the first time. Until now this field of investigation has been explored very little.

It was concluded that MWCNTs oxidation temperature is significantly decreased when these are decorated with gold (in-situ synthesis method). Increasing the Au content up to 23 wt%, a decrease of the temperature at which 50% of MWCNTs are converted of 246 °C is obtained. Furthermore, the in-situ Au/MWCNTs catalyst with a gold loading of 0.5 wt% is the most selective to

CO₂. Thus, it was concluded that in order to have a compromise between a good activity and selectivity, gold clusters catalysts must be used in this reaction. Additionally, SEM characterisation corroborated the effect of Au in decreasing the oxidation temperature of MWCNTs. By this technique it was noticed that, when using a Au/MWCNTs catalyst, all the MWCNTs are decomposed at 400 °C, unlike undecorated MWCNTs which oxidation only starts at 460 °C and therefore their complete oxidation was only observed at 500 °C. Comparing these results with literature it was concluded that a stronger decrease of the initial combustion temperature of MWCNTs was obtained using in-situ Au/MWCNTs catalysts rather than the ~ 5.8 nm Au-MWCNTs catalyst (Au-MWC-5.8) reported by Lorençon *et al.* In-situ Au/MWCNTs catalysts also showed a higher ability to decrease the initial combustion temperature of MWCNTs than other similar sized metal catalysts such as Pt or Pd. A slightly lower activity was obtained only when compared to a Co(a)-MWC catalyst.

Furthermore, using a model soot (CB) decorated with Au nanoclusters (ex-situ synthesis method), the ability of Au to decrease the combustion temperature of soot was verified. The higher ncAu/CB catalyst activity and selectivity was noticed for the catalyst with a gold content of 0.5 wt% ($\Delta T_{50} = 292$ °C). It has been noticed that low Au loadings are preferential to avoid Au agglomeration. Importantly these results were patented in collaboration with a private company (*Goldemar Solutions*) in 2013 and will be published in 2014. Moreover, the most active catalyst - ncAu(0.5wt%)/CB - showed a higher decrease of the carbon oxidation initial temperature than the catalyst of soot decorated with 3.7 nm Au nanoparticles (Au-soot-3.7) studied by Lorençon *et al.*

Finally, soot oxidation combustion using in-situ Au/CeO₂ catalysts under loose contact conditions revealed a high activity of these catalysts. A Au(0.5wt%)/CeO₂ catalyst was able to decrease the soot combustion temperature up to 426 °C ($\Delta T_{50} = 130$ °C), although it is not selective to CO₂. This catalyst has a higher activity than other Au/supported catalysts and than almost all of the collected catalysts used in soot oxidation under loose contact

conditions. A lower activity was observed only when compared to gold catalysts promoted with CsNO_3 and to the CeO_2 -Ag catalyst (NO non-containing atmosphere) and to the Au/(3DOM support), to perovskites catalysts or to the Pt/ SiO_2 catalyst (NO containing atmosphere).

Overall, the results obtained are very promising and lead to a new field of investigation, about the effect of Au in the thermal stability of carbonaceous materials, which has been until now hardly investigated.

5.4 REFERENCES

- [1] J. Turkevich, P. C. Stevenson, J. Hillier, *Discussions of the Faraday Society* **1951**, 11, 55-75.
- [2] J. L. Figueiredo, F. R. Ribeiro, *Catálise Heterogênea*, Lisboa, Fundação Calouste Gulbenkian **1989**.
- [3] F. V. Caldas, R. R. de Cassia Moreira da Silva, A. de Almeida Rocha, *Engevista* **2009**, 11, 117-126.
- [4] L. Alves, B. Ballesteros, M. Boronat, J. R. Cabrero-Antonino, P. Concepción, A. Corma, M. A. Correa-Duarte, E. Mendoza *Journal of the American Chemical Society* **2011**, 133 (26), 10251-10261.
- [5] E. Lorençon, R. G. Lacerda, L. O. Ladeira, R. R. Resende, A. S. Ferlauto, U. Schuchardt, R. M. Lago, *Journal of Thermal Analysis and Calorimetry* **2011**, 105, 953-959.
- [6] A.-R. Leino, M. Mohl, J. Kikkola, P. Maki-Arvela, T. Kokkonen, A. Schukarev, K. Kordas, *Carbon* **2013**, 57, 99-107.
- [7] M. L. Ruiz, I. D. Lick, M. I. Ponzi, E. Rodriguez-Castellón, A. Jiménez-Lopez, E. N. Ponzi, *Applied Catalysis A: General* **2011**, 392, 45-56.
- [8] A. Bredin, A. V. Larcher, B. J. Mullins, *Tribology International* **2011**, 44, 1642-1650.
- [9] H. N. Sharma, L. Pahalagedara, A. Joshi, S. L. Suib, A. B. Mhadeshwar, *Energy Fuels* **2012**, 26, 5613-5625.
- [10] M. Dhakad, S. Rayalu, J. Subrt, S. Bakardjieva, T. Mitsuhashi, H. Haneda, S. Devotta, N. Labhsetwar, *Current Science* **2007**, 92, 1125-1128.
- [11] E. Mendoza Gómez, J. Llorca Piqué, L. Rodrigues Alves, E. Galindo, M. Santiago Redondo, *Patent submitted* **2013**, European Patent Application No: 12382137.1.
- [12] R. Jiménez, X. García, C. Cellier, P. Ruiz, A. L. Gordón, *Applied Catalysis A: General* **2006**, 297, 125-134.
- [13] J. V. Craenenbroeck, D. Andreeva, T. Tabakova, K. V. Werde, J. Mullens, F. Verpoort, *Journal of Catalysis* **2002**, 209, 515-527.

- [14] Y. Wei, J. Liu, Z. Zhao, A. Duan, G. Jiang, *Journal of Catalysis* **2012**, 287, 13-29.
- [15] Y. Wei, J. Liu, Z. Zhao, Y. Chen, C. Xu, A. Duan, G. Jiang, H. He, *Angewandte Chemie International Edition* **2011**, 50, 2326-2329.
- [16] M. L. Ruiz I. D. Lick, M. S. L. Aparicio, M. I. Ponzi, E. Rodriguez-Castellón, E. N. Ponzi, *Industrial & Engineering Chemistry Research* **2012**, 51, 1150-1157.
- [17] M. Sadakane, T. Horiuchi, N. Kato, C. Takahashi, W. Ueda, *Chemistry of Materials* **2007**, 19, 5779-5785.
- [18] G. Zhang, Z. Zhao, J. Liu, G. Jiang, A. Duan, J. Zheng, S. Chen, R. Zhou, *Chemical Communications* **2010**, 46, 457-459.
- [19] H. Shimokawa, Y. Kurihara, H. Kusaba, H. Einaga, Y. Teraoka, *Catalysis Today* **2012**, 185, 99-103.
- [20] J. P. A. Neeft, M. Makkee, J. A. Moulijn, *Applied Catalysis B: Environmental* **1996**, 8, 57-58.
- [21] K. Yamazaki, T. Kayama, F. Dong, H. Shinjoh, *Journal of Catalysis* **2011**, 282, 289-298.
- [22] M. Dhakad, D. Fino, S. S. Rayalu, R. Kumar, A. Watanabe, H. Haneda, S. Devotta, T. Mitsunashi, N. Labhsetwar, *Topics in Catalysis* **2007**, 42-43, 273-276.
- [23] M. Chakad, S. S. Rayalu, R. Kumar, P. Doggali, S. Bakardjieva, J. Subrt, T. Mitsunashi, H. Haneda, N. Labhsetwar, *Catalysis Letters* **2008**, 121, 137-143.
- [24] H. Wang, Z. Zhao, C.-m. Xu, J. Liu, *Catalysis Letters* **2005**, 102, 3-4, 251-256.
- [25] J. O. Uchisawa, A. Obuchi, Z. Zhao, S. Kushiyama, *Applied Catalysis B: Environmental* **1998**, 18, L183-L187.
- [26] E. Aneggi, J. Llorca, C. de Leitenburg, G. Dolcetti, A. Trovarelli, *Applied Catalysis B* **2009**, 489-498.
- [27] K. Yamazaki, T. Kayama, F. Dong, H. Shinjoh, *Journal of Catalysis* **2011**, 282, 289-298.

CHAPTER 6:

GENERAL CONCLUSIONS

This thesis contributes to the field of development of new simple, reproducible and environmentally friendly synthetic protocols which allow us to obtain uniform stable populations of Au nanoclusters ($d < 2$ nm) or single Au atoms deposited on nanostructured surfaces. Two different synthesis methods were presented. The first (in-situ) was developed starting with a patented method from our group to obtain Au clusters on amine surfaces. The second (ex-situ) was newly developed for the first time based on a synthetic protocol utilised for the sonochemical synthesis of Ag nanoclusters.

In this thesis a thorough characterisation of the prepared catalysts was carried out. Thus the optimisation and understanding of how the Au mean diameter might vary with different variables was achieved. The ability of these catalysts to oxidise CO was investigated. Finally, the Au clusters contribution in decreasing the combustion temperature of carbonaceous materials and their activity for soot oxidation was also investigated.

This investigation presents the successful synthesis of in-situ Au clusters in three different surfaces, namely MWCNTs-PAH, CeO₂-PAH and TiO₂-PAH hybrids demonstrating the ability of this method to be further explored using other supports covered with amine groups. Additionally, the synthesis of a unique population of single Au atoms, until now scarcely reported, was achieved by this in-situ protocol using Au loadings lower than 0.5 wt%. This opens then a new field of investigation about these Au atoms activity in different chemical reactions. Moreover, by aberration-corrected HRTEM it was concluded that higher in-situ Au content catalysts (> 3 wt%) are not composed by a unique population of Au clusters but by the coexistence of single Au atoms, very small Au clusters (Au_n, $n = 2-3$) or Au clusters ($d \sim 1.1$ nm). The quantity of the lower sized species is decreased with the increase of the Au content. Furthermore, HRTEM characterisation revealed that the mean Au particle size of the in-situ synthesised catalysts is easily varied by simply changing the nominal Au content. The Au mean diameter is increased for higher Au loadings. Agglomeration of Au clusters was not observed up to a nominal Au content of

13 wt% but in-situ Au catalysts with a loading of 50 wt% showed the coexistence of Au nanoclusters with large Au nanoparticles. It was also observed that the support surface area also affects the Au particle size. Lower support surface areas lead to an increase of the Au particle size when using the same Au content. Thus, using the same Au content, the Au particle size decreases in the following order: $\text{TiO}_2 > \text{CeO}_2 > \text{MWCNTs}$. XPS characterisation revealed that in-situ Au/MWCNTs, independently of the Au content (up to 3 wt%), are composed only by positively charged Au ($\text{Au}^{\delta+}$). This positive charge was attributed to oxygen species bonded to the Au surface. In-situ Au/ CeO_2 and Au/ TiO_2 catalysts are composed by both cationic ($\text{Au}^{\delta+}$) and metallic (Au^0) gold species. It was noticed that the quantity of metallic Au species rises with the increase of the Au particle size. Finally, it was concluded that the in-situ protocol is not the most adequate to prepare active CO oxidation catalysts. The surface of both CeO_2 and gold is covered by intermediate species of the gold synthesis reaction. This limits dramatically the catalytic activity of the material, specially at low temperature. Thus, another synthetic protocol (ex-situ) to obtain Au clusters catalysts was developed.

Using a new clean sonochemical synthetic protocol (ex-situ) an uniform population of Au nanoclusters ($d < 2 \text{ nm}$) was obtained. The polymer PMAA acted as reducing and capping agent. Au nanoclusters with a mean diameter of 1.3 nm were obtained using a concentration of Au of 0.02 mg/mL and a RCO_2^-/Au molar ratio of 0.5. By AFM characterisation an increase of the Au nanoparticles ($d > 2 \text{ nm}$) in solution for higher RCO_2^-/Au molar ratios was noticed. Furthermore, ex-situ gold catalysts were for the first time successfully prepared by anchoring these pre-synthesised Au nanoclusters to MWCNTs-PAH, CeO_2 -PAH or TiO_2 -PAH surfaces by a simple 15 minutes ultrasonication. Ex-situ ncAu/support catalysts with a mean diameter of approximately $1.4 \pm 0.4 \text{ nm}$ were obtained. XPS characterisation revealed that ex-situ ncAu/ CeO_2 catalysts are composed only by metallic gold (Au^0). Additionally, for the first time the activity of supported sonochemical prepared Au nanoclusters catalysts was reported. It was observed that ex-situ ncAu/ CeO_2

catalysts are active for CO oxidation. These catalysts showed a lower activity than the Au/CeO₂ catalysts usually prepared by deposition-precipitation but a similar activity to the ones prepared by co-precipitation. Thus, based on the CO oxidation activity results of the ex-situ ncAu/CeO₂ catalysts, it was verified that the presence of metallic Au is essential for this reaction.

Additionally, it was concluded that Au clusters synthesised by both in-situ or ex-situ protocols decrease the thermal stability of carbon materials such as MWCNTs or CB. By SEM characterisation, it was noticed that MWCNTs doped with 3 wt% of Au (in-situ) were all decomposed at 400 °C while bare MWCNTs were only decomposed at 500 °C. It was observed that Au clusters are the most active species in the combustion reaction of carbonaceous materials and that higher CO₂ selectivities were obtained for lower gold contents (lower Au particle size).

Finally, it was demonstrated that in-situ Au/CeO₂ catalysts mixed by loose contact with soot were able to decrease the soot oxidation temperature although they were not selective to CO₂. A Au(0.5wt%)/CeO₂ catalyst decreased this temperature down to 426 °C ($\Delta T_{50} = 130$ °C). These results were comparable to or even better than most of other common used catalysts for this reaction. Prior to this study, Au catalysts had been scarcely used for soot oxidation reaction thus opening a new field of investigation. In order to achieve both good activity and CO₂ selectivity, the use of ex-situ instead of in-situ Au clusters can be a good alternative.

ANNEXES

A.1 DETERMINATION OF THE NOMINAL NUMBER OF Au CLUSTERS PER MWCNT

The nominal number of Au clusters per MWCNT presented in Chapter 3 (Section 3.3.2, Figure 40) was determined considering a nanotube with 100 nm of length and 10 nm of diameter in accordance with Equations 18 to 24.

$$\text{Number of Au clusters per MWCNT} = \frac{\text{nr. Au clusters}}{\text{nr. MWCNTs}} \quad (18)$$

where,

Number of Au clusters per MWCNT – nominal number of Au clusters per MWCNT.

nr. Au clusters – number of Au clusters in the catalyst.

nr. MWCNTs – number of MWCNTs in the catalyst.

$$\text{nr. Au clusters} = \frac{m_{Au}}{m_{Au \text{ cluster}}} \quad (19)$$

where,

m_{Au} – total mass of Au in the catalyst, in mg.

$m_{Au \text{ cluster}}$ – mass of a Au cluster, in mg.

$$m_{Au} = \frac{\text{Au loading}}{100} \times m_{catalyst} \quad (20)$$

where,

Au loading – nominal Au loading in wt%.

$m_{catalyst}$ – total catalyst mass, in mg.

$$m_{Au\ cluster} = n_{at.Au} \times m_{at.Au} \quad (21)$$

where,

$n_{at.Au}$ – number of Au atoms of a Au cluster ($d = 1.1\text{ nm}$ - $n_{at.Au} = 40$ ^[1]).

$m_{at.Au}$ – mass of a Au atom in mg ($m_{at.Au} = \frac{MW_{Au}}{N_A} \times 1000 = \frac{196.97}{6 \times 10^{23}} \times 1000$).

$$nr.MWCNTs = \frac{m_{MWCNTs}}{m_{MWCNT}} \quad (22)$$

where,

m_{MWCNTs} – total mass of MWCNTs in the catalyst, in mg ($m_{MWCNTs} = 50\text{ mg}$).

m_{MWCNT} – mass of a MWCNT in mg.

$$m_{MWCNT} = V_{MWCNT} \times \rho_{MWCNT} \quad (23)$$

where,

V_{MWCNT} – volume of a MWCNT in cm^3 .

ρ_{MWCNT} – density of a MWCNT in g/cm^3 ($\rho_{MWCNT} = 2\text{ g}/\text{cm}^3$ ^[2]).

$$V_{MWCNT} = \pi \times r^2 \times L \quad (24)$$

where,

r – MWCNT radius in cm ($r = 5 \times 10^{-7}\text{ cm}$).

L – MWCNT length in cm ($L = 1 \times 10^{-5}\text{ cm}$).

A.2 IN-SITU CATALYSTS ACTIVITY: CO OXIDATION - EXPERIMENTAL PROTOCOL

The CO oxidation reaction of in-situ Au/CeO₂ catalysts (Chapter 3, Section 3.6.2) was carried out in a *Microactivity-Reference* reactor using 50 mg of the solid catalyst^[3]. A simplified chemical engineering draw and description of the reaction system is presented in Chapter 2 (Section 2.10.2, Figure 27).

For the catalytic activity tests the catalysts were prepared with a molar ratio of sodium citrate/Au of 1. Before reaction the catalysts were calcined at 300 °C during three hours (ramp temperature: 2 °C/min) in order to eliminate the major part of the agents used in the synthesis that could decrease the catalytic activity by covering the active sites. Once placed in the reactor the catalysts were firstly pre-treated at 300 °C (ramp temperature: 5 °C/min) during 1 hour under a N₂ atmosphere using a flow of 50 mL/min (Figure 103). This pre-treatment was carried out in order to clean the surface of remaining impurities. After this pre-treatment the reactor was cooled to approximately 25 °C under the same flow. Then, a first cycle using a flow of 50 mL/min (96 v/v% N₂; 2 v/v% O₂; 2 v/v% CO) was carried out up to 600 °C (Figure 103). A ramp of 5 °C/min was used and temperatures levels were left during 30 minutes. Between each temperature, in order to calculate correctly the reaction conversion, at each temperature a 20 minute by-pass (analysis of the gases flow that enters in the reactor) was carried out. Finally, the reactor was cooled to 50 °C under a flow of 10 mL/min of N₂. As before, the temperature was then raised under a flow of 50 mL/min (96 v/v% N₂; 2 v/v% O₂; 2 v/v% CO) from 50 °C up to 400 °C (second cycle, Figure 104) in order to investigate the catalysts activity after being at 600 °C. The conditions used to carry out this activity test are summarised in Table 34.

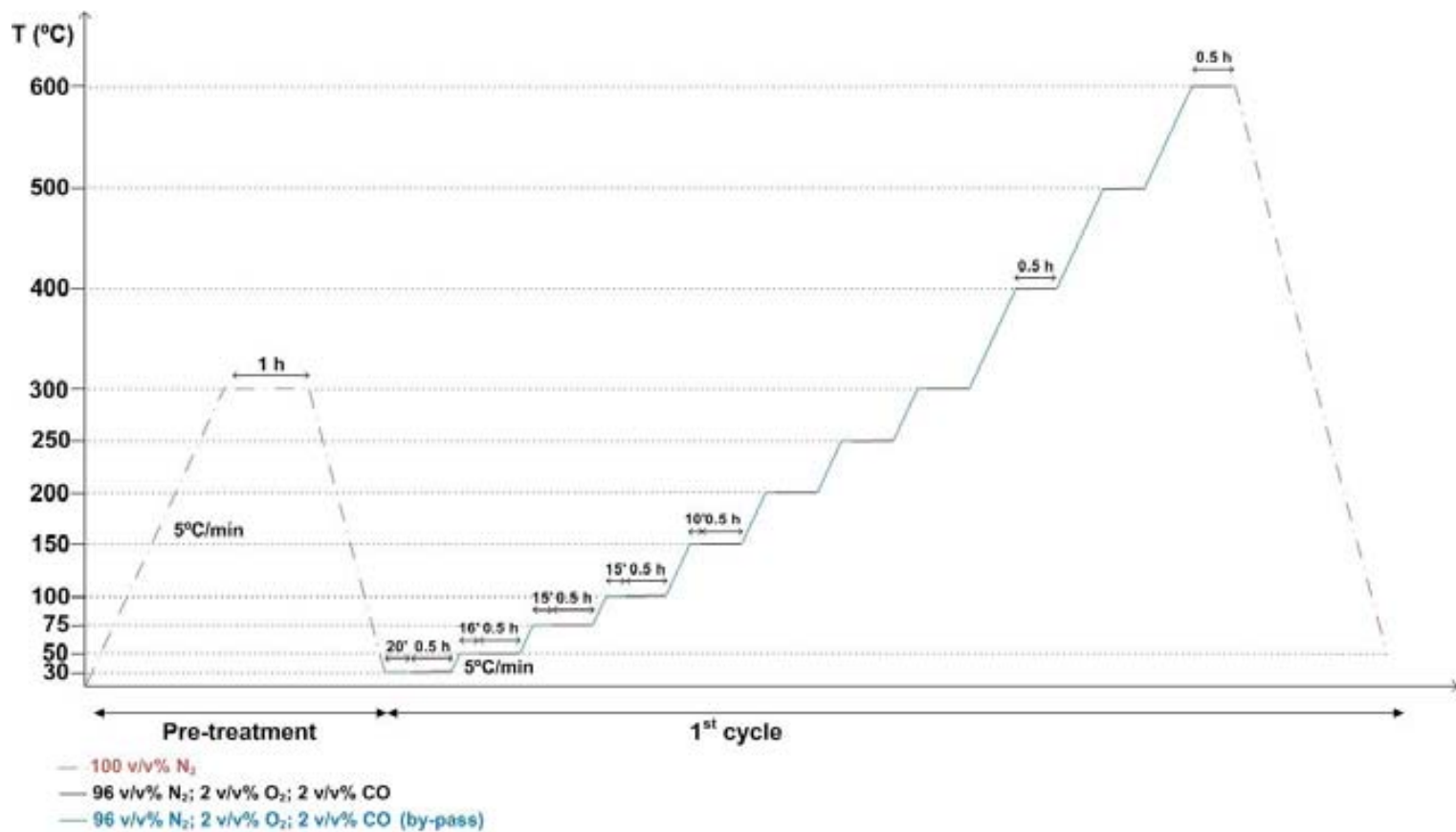


Figure 103. Schematic representation of the CO oxidation catalytic activity test for in-situ Au/CeO₂ catalysts (pre-treatment and 1st cycle).

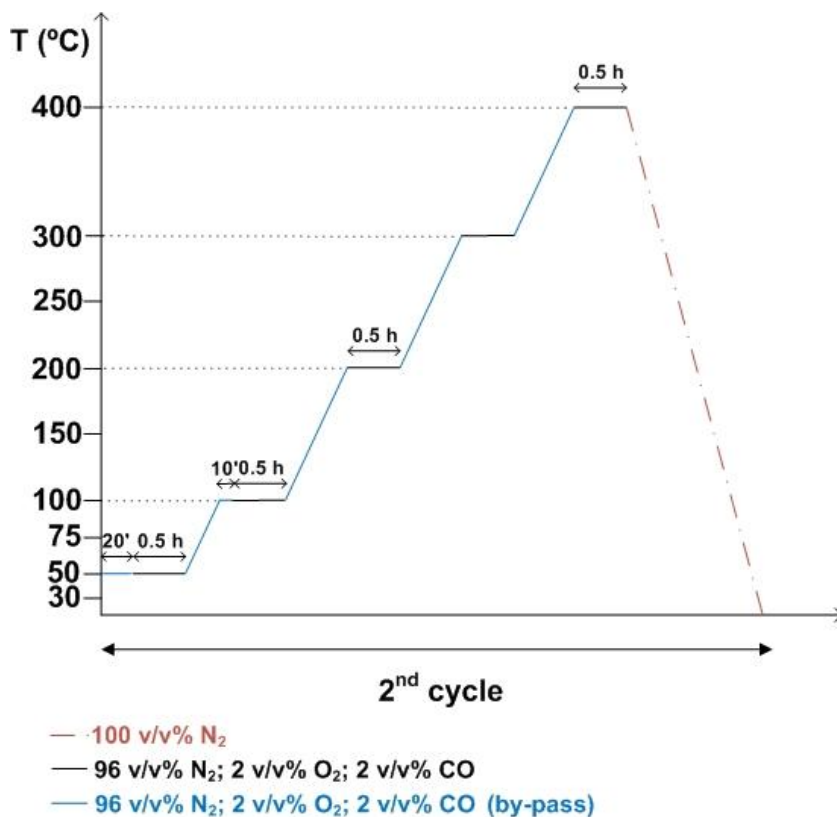


Figure 104. Schematic representation of the CO oxidation catalytic activity test for in-situ Au/CeO₂ catalysts (2nd cycle).

Table 34. CO oxidation reaction conditions for in-situ Au/CeO₂ catalysts.

Catalyst mass (mg)	50
Flow (mL/min)	50
WHSV (mL.h ⁻¹ .g _{cat.} ⁻¹)	60 000
Contact time (s)	0.08

The values of weight hourly space velocity (WHSV) and contact time, presented in Table 34, were determined according to Equations 25 and 26.

$$WHSV = \frac{F}{m_{catalyst}} \quad (25)$$

where,

WHSV - weight hourly space velocity in mL.h⁻¹.g⁻¹.

F - total gases flow fed to the reactor in mL/h (*F* = 3000 mL/h).

m_{catalyst} - catalyst mass in g (*m_{catalyst}* = 0.05 g).

$$Contact\ time = \frac{\pi.R^2.L}{F} \quad (26)$$

where,

Contact time - contact time in seconds.

R - ratio of the quartz tube in cm (*R* = 0.46 cm).

L - height of the catalytic bed in cm (*L* ~ 0.1 cm).

F - total gases flow fed to the reactor in mL/s (*F* = 0.8 mL/s).

The comparison of the catalytic activities observed with the documented values is difficult due to the different conditions used to carry out the reaction, namely catalyst weight, CO/O₂ ratio, flow-rate etc.. Along these lines, in this work the catalytic activity is measured and compared in terms of reaction rate, i.e. all the conversion values experimentally obtained were normalised to mol of CO converted per unit of second and square meter of gold. In this way, the values of CO conversion were firstly determined (Equation 27) and then normalised according to Equation 28. The value of the Au area was determined by Equation 29 considering that all the gold was on the support surface available for reaction. The diameter of the Au catalysts used to determine the catalytic activity in terms of reaction rate was that obtained by HRTEM for the Au(3wt%)/CeO₂ catalyst (*d* = 1.2 nm). The diameter of a single Au atom (0.1 wt% and 0.5 wt% catalysts) was considered to be 0.27 nm as reported by Slater^[4].

$$CO_{conversion} = \frac{CO^{in} - CO^{out}}{CO^{in}} \times 100 \quad (27)$$

where,

$CO_{conversion}$ - carbon monoxide conversion in %.

CO^{in} - CO quantity that enters in the reactor.

CO^{out} - CO quantity that exists the reactor.

$$Reaction\ rate = \frac{F \times \frac{\%CO^{in}}{100} \times \frac{CO_{conversion}}{100}}{V_m} \times \frac{1}{A_{Au}} \quad (28)$$

where,

Reaction rate - molar quantity of CO converted per second and square meter of gold in $mol.s^{-1}.m_{Au}^{-2}$.

F - total gases flow fed to the reactor in mL/s ($F = 0.8$ mL/s).

$\%CO^{in}$ - percentage of CO in volume in the feed mixture ($\%CO^{in} = 2v/v\%$).

$CO_{conversion}$ - carbon monoxide conversion in %.

V_m - molar volume of an ideal gas at 1 atmosphere of pressure and 0 °C

($V_m = 22400$ mL/mol).

A_{Au} - area of Au on the surface of the support in m^2 .

$$A_{Au} = \frac{m_{Au}}{d_{Au}} \times \frac{3}{r} \quad (29)$$

where,

A_{Au} - area of Au on the surface of the support in m^2 .

m_{Au} - mass of Au in the catalyst in g (determined by Equation 20).

d_{Au} - density of Au ($d_{Au} = 19.3 \times 10^6$ g/ m^3).

r - the radius of the mean Au cluster diameter in m.

A.3 EX-SITU CATALYSTS ACTIVITY: CO OXIDATION – EXPERIMENTAL PROTOCOL

The CO oxidation reaction of the ex-situ Au/CeO₂ catalysts (Chapter 4, Section 4.4) was carried out in the same reaction system as the in-situ catalysts presented and described in Chapter 2 (Section 2.10.2, Figure 27). In these experiments 100 mg of powder catalyst were used. Activity tests were carried out using the conditions registered in Table 35. The values of weight hourly space velocity (WHSV) and contact time were determined by Equations 25 and 26 respectively (Section A.2). For these catalysts, the height of the catalytic bed (L) was approximately 0.3 cm.

Table 35. CO oxidation reaction conditions for ex-situ nAu/CeO₂ catalysts.

Catalyst mass (mg)	100
Flow (mL/min)	100
WHSV (mL.h ⁻¹ .g _{cat} ⁻¹)	60 000
Contact time (s)	0.1

Before entering the reactor, in order to increase the catalytic activity, the catalysts were calcined during three hours at 300 °C (ramp: 2 °C/min). In this way, the major part of the reagents used during the synthesis were eliminated, leading to the increase of the number of the active sites available to reaction.

Once placed in the quartz reactor, the catalysts were firstly pre-treated for one hour at 300 °C (ramp: 3 °C/min) under a 100 mL/min N₂ flow in order to remove any remaining impurities from the catalyst surface (Figure 105). Then, the cooling of the reactor down to approximately 30 °C was followed by a consequent increase of temperature up to 350 °C under the 100 mL/min reaction flow (96 v/v% N₂; 2 v/v% O₂; 2 v/v% CO) (first cycle) (Figure 105). A ramp of 5 °C/min was used and each temperature analysed was left stable for 30 minutes. Between each temperature, a 20 minute by-pass analysis was carried out in order to measure the gases quantities that enter in the reactor.

After this first cycle, the temperature was again decreased down to 50 °C under a flow of 100 mL/min of N₂. Then, a second temperature increase cycle using the reaction flow (96 v/v% N₂; 2 v/v% O₂; 2 v/v% CO) was made up to 400 °C (second cycle) (Figure 106).

The catalytic activity experimentally obtained was compared in terms of reaction rate, i.e. number of moles of CO converted per second and square meter of gold. This value was determined according to Equation 28 (Section A.2) taking into account the total flow used in the tests registered in Table 35. The CO conversion was determined by Equation 27 (Section A.2) using the values obtained by the gas chromatograph. Finally, the area of gold was obtained by Equation 29 (Section A.2) taking into account the catalysts gold loading and the mean Au nanocluster diameter obtained by HRTEM and AFM characterisation. It was considered a mean diameter of 1.3 nm since the HRTEM size distributions of Au nanoclusters in the different supports had mean values between 1.3 nm and 1.4 nm and by AFM characterisation the mean Au diameter is 1.2 nm (Section 4.2 and 4.3.1).

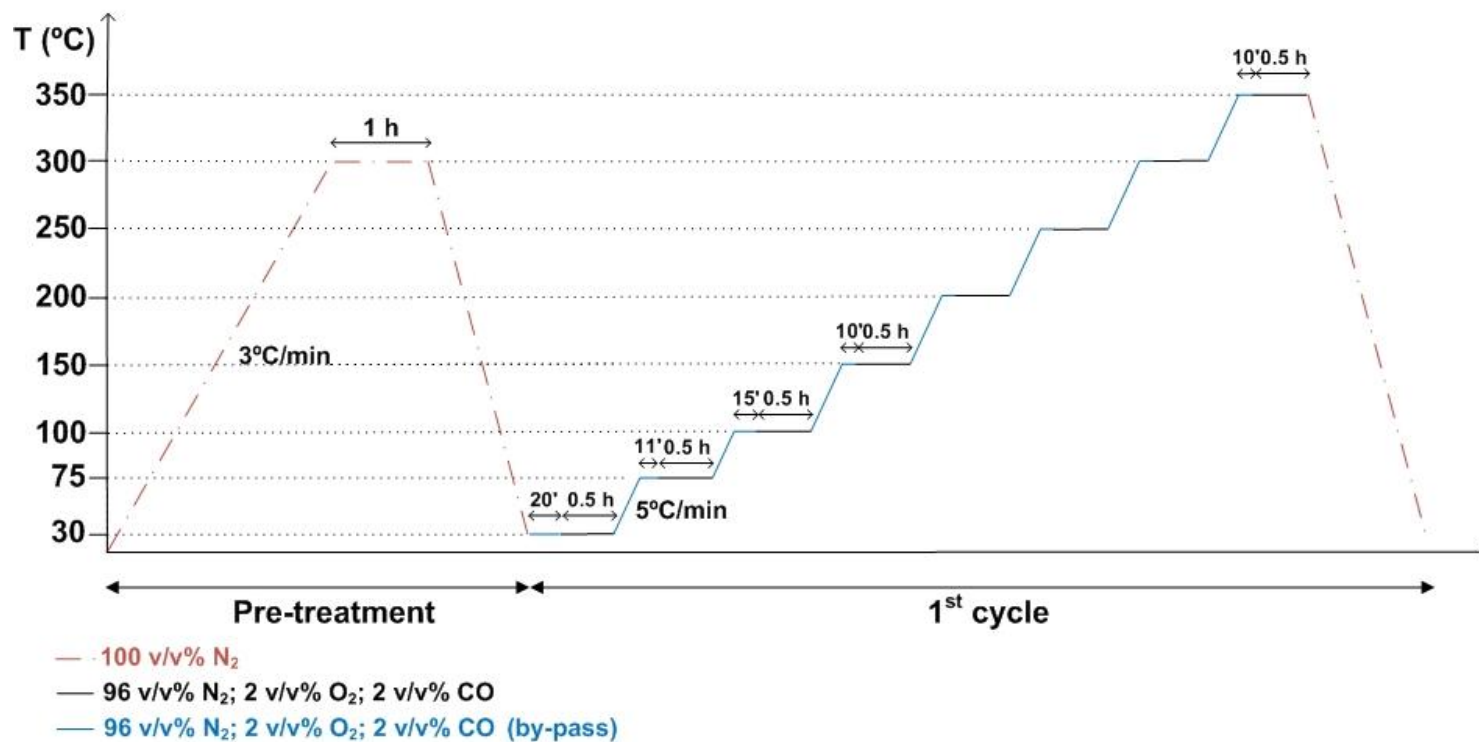


Figure 105. Schematic representation of the CO oxidation catalytic activity test for ex-situ ncAu/CeO₂ catalysts (pre-treatment and 1st cycle).

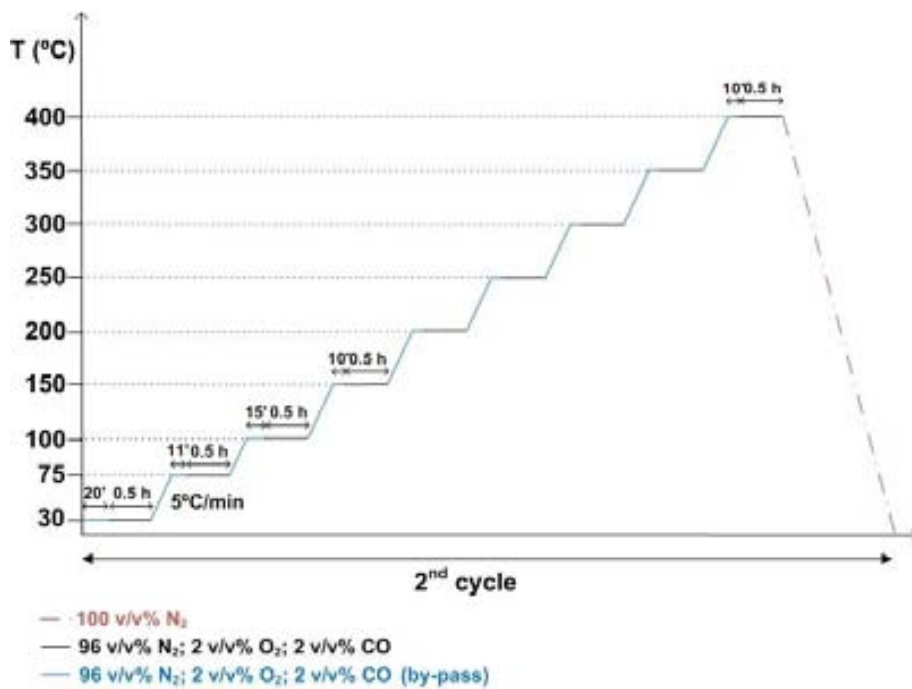


Figure 106. Schematic representation of the CO oxidation catalytic activity test for ex-situ ncAu/CeO₂ catalysts (2nd cycle).

A.4 REFERENCES

- [1] T. G. Schaaff, M. N. Shafigullin, J. T. Khoury, I. Vezmar, R. L. Whetten, W. G. Cullen, P. N. First, *J. Phys. Chem. B* **1997**, 101, 7885-7891.
- [2] <http://www.nanocyl.com/en/CNT-Expertise-Centre/Carbon-Nanotubes>, consulted 07/01/2014.
- [3] <http://www.pidengtech.com/thereference.html>, consulted 12/02/2014.
- [4] J. C. Slater, *The Journal of Chemical Physics* **1964**, 41, 3199-3203.

This doctoral thesis is about the synthesis and the catalytic activity study of gold particles with a diameter lower than 2 nm, gold nanoclusters. The interest is due to the catalytic activity that gold has at room temperature when its size is less than approximately 5 nm.

In this thesis, two distinct synthesis' methods that allow stable gold clusters with a well defined particle size to be obtained have been developed. In one method, gold clusters with a narrow size distribution and a particle diameter less than 2 nm are firstly synthesised and then deposited on a support. In the other method, gold clusters are directly synthesised on the selected support. In the latter method, the size of gold can be easily varied by simply altering the gold precursor quantity during the synthesis process. Thus, uniformly dispersed isolated gold atoms, 2 nm Au clusters or nanoparticles larger than 10 nm can be obtained on the material support surface.

The synthesised catalysts were characterised using distinct physico-chemical techniques: HRTEM, SEM, AFM, XPS and XAS. Additionally, their catalytic activity was investigated for the oxidation of CO and carbonaceous materials. Finally, the particle size was related with the catalytic activity of the material.